UCL SCHOOL OF PHARMACY

Development and characterisation of nanocarrier systems of hydrophobic drugs for pulmonary delivery

Nattika Nimmano

Thesis submitted in accordance with the requirements of UCL for the degree of Doctor of Philosophy

February 2019

UCL School of Pharmacy
29-39 Brunswick square
London WC1N 1AX
United Kingdom

Declaration

This thesis describes research conducted in the School of Pharmacy, University College London between November 2014 and October 2018, under the supervision of Professor Kevin M.G. Taylor and Dr. Satyanarayana Somavarapu.

I, Nattika Nimmano, certify that the research described is original. I also confirm that I have written all the text herein. All source materials that have already appeared in the publication have been clearly indicated by suitable citations.

Signature:_____ Date:_____

Acknowledgements

I would like to express my deep and sincere gratitude to my primary supervisor, Professor Kevin M.G. Taylor for his scientific vision, experienced guidance, kindness, and willingness to develop my knowledge in pulmonary delivery as well as my writing skill. Apart from academic aspect, he is very optimistic person and he has constantly supported me throughout this PhD, which made me feel motivated every time I meet him. I am sincerely grateful to him since he was the most important person giving me this valuable opportunity to do my PhD in University College London.

I would also like to thank my second supervisor, Dr. Satyanarayana Somavarapu for contributing many ideas during my PhD and giving me a great chance to do research in the Lab 402.

I wish to express my appreciation to my advisor at Chulalongkorn University, Dr. Jittima Chatchawansaisin and Dr. Pongsakornpat Arunothayanunt for inspiring me to do PhD in abroad. I am especially thankful to Dr. Jittima for contacting Prof. Taylor and believing in my ability.

I am extremely grateful to all my labmates (Lab 402), Dr. Zahra, Dr. Norhayati, Dr. Atiqah, Acom for sharing the ideas, their care, valuable friendship and emotional support. This made my PhD life so memorable and joyful. I am very lucky to meet these people who are always being by my side in every single moment.

Also, I would like to thank my Thai friends, Dr. Wunlapa, Dr, Varin, Dr. Natchagorn, Dr. Ukrit, Dr. Piyaphong, Dr. Supathep, Mr. Pongsakorn, Mr. Nat, Mrs. Supanan, Mr. Akkapon, Mr.Nuphak, Mr. Wishchapol, Mr. Patchara, Mr. Autthaporn and my closed office mates, Miss Yanling, Mr. Chin Ping and Miss Pamela for their encouragement.

I would also like to thank to all staff of UCL School of Pharmacy, especially to Ms. Catherine, Mr. David, Dr. Sunny, Mr. John, Mr. Chris, Ms. Isabel, Ms. Kate

for their kindly technical assistance. I would like to convey my gratitude to Dr.Asma for helping me with DSC techniques.

I would like to thank my friends from Goodenough College especially Miss Keting, Mr.Siong Kie and Miss Florence for their amazing friendship and warm support. Thanks to running club and zumba society for giving me strength, energy and mental and physical well-being.

Last but not least, I would like to express my truly appreciation to my parents and brother for their unconditional love, care and endless support, all of which have given me the power to pursue my study. My PhD would not have come this far without their support and faith in me.

Abstract

Background: The bioavailability of BCS class II drugs used in non-small cell lung cancer (NSCLC) treatment is limited by low water solubility. Also, current therapies for NSCLC cause systemic side effects and sub-therapeutic levels of drugs at the target sites. Colloidal systems administered by the pulmonary route may overcome these problems.

Method: A genistein-mPEG conjugate was synthesised and characterised for delivering erlotinib or curcumin in micelles. Liposomes co-loaded with genistein and erlotinib were developed as an alternative formulation approach and studies using DSC and HPLC analysis. The aerosol properties of micelles and liposomes were measured using the Next Generation Impactor (NGI). The Fast Screening Impactor (FSI) was investigated as an alternative to the NGI for aerosol characterisation of nebulised liposomes. Three parameters (nebuliser types, impactor operating conditions and liposome size reduction methods) were studied using the FSI.

Results: Successful conjugation was confirmed by FT-IR, NMR and MS. Curcumin loading into conjugate micelles had mean size < 200nm, with ≈ 50% encapsulation efficiency (EE). However, the genistein conjugate was not appropriate for erlotinib delivery, having low EE (<3%). For liposomes, the mean size was ≈130 nm, with 10% EE (erlotinib) and 100% EE (genistein). DSC results showed incorporation of both drugs into the bilayer, giving a broadening of the main phase transition of DPPC with a decreased main phase temperature. The air-jet nebuliser was superior to the vibrating-mesh device in terms of significantly higher fine particle dose (FPD) and fine particle fraction (FPF). The FSI (5± 3 ºC), with modification operated at 15 L/min, was found to be simple to use and labour-saving for simple aerosol characterisation, giving comparable results to the NGI for FPD and FPF. Extruded liposomes showed greater size stability than sonicated vesicles during preparation and nebulisation.

Conclusions: Optimised micelles and liposomes with desired mean size and drug entrapments have the potential for nebuliser delivery of genistein, erlotinib and curcumin, and may be suitable for delivering other hydrophobic drugs.

Research Impact Statement

Lung cancer accounts for almost 20% of total cancer-related deaths worldwide in both men and women. 85% of all lung cancer cases are classified as non-small cell lung cancer (NSCLC). The majority of NSCLC patients have experienced advanced local invasion and metastatic disease, as current therapies including chemotherapy are not sufficiently curative. Currently, chemotherapeutic molecules are administered via the oral or parenteral routes, causing systemic side effects and sub-therapeutic doses at the target sites. Thus, this study aimed to develop drug-carriers capable of pulmonary delivery, which may achieve the effective localised treatment of NSCLC.

This study helps in our understanding of the potential of polymeric micelles and liposomes for the co-delivery of hydrophobic anti-cancer molecules by the pulmonary route. Since this delivery route allows the avoidance of first-pass metabolism and drug is administered at the target site, lower doses can be considered compared with oral route. Such a formulation approach may be beneficial for NSCLC patients, improving their survival rate and quality of life, and this can be a platform for other drugs used in the treatment of respiratory diseases.

The findings indicate that an abbreviated impactor using the Fast Screening Impactor (FSI) may be a useful alternative tool compared to a full-cascade impactor (Next Generation Impactor, NGI) for simple aerosol characterisation of nebulised formulations for routine quality control of large-scale production, or in pharmaceutical development studies. The concept of abbreviated impactor measurement (AIM) using Efficient Data Analysis (EDA) is receiving with attention from medicine regulators and world pharmacopoeias for routine quality control of inhaled products. This study presents key data informing the development of this new methodology.

Table of Contents

List of Tables

List of Figures

List of Abbreviations

ACI:	Andersen cascade impactor
AIM:	Abbreviated impactor measurement
AKT:	Serine/threonine kinase
APSD:	Aerodynamic particle size distribution
BCS:	Biopharmaceuticals Classification System
DCC:	N, N-dicyclohexylcarbodiimide
DL:	Drug loading
DMAP:	4-dimethylaminopyridine
DMF:	N, N-dimethylformamide anhydrous
DMSO:	Dimethyl sulfoxide
DOPE:	Dioleoylphosphatidylethanolamine
DPI:	Dry powder inhaler
DPPC:	Dipalmitoylphosphatidylcholine
DSC:	Differential Scanning Calorimetry
ED:	Emitted dose
EE:	Encapsulation efficiency
EGFR:	Epidermal growth factor receptor
EGFR-TKIs:	Epidermal growth factor receptor- tyrosine kinase inhibitors
FDA:	US Food and Drug Administration
FPD:	Fine Particle Dose

FPF:	Fine Particle Fraction
FSA:	Fast Screeing Andersen
FSI:	Fast Screening Impactor
FT-IR:	Fourier transform infrared spectroscopy
Gen-mPEG:	Genistein-methoxy poly (ethylene glycol)
GSD:	Geometric standard deviation
HHW:	Half-height width
HSDSC:	High sensitive differential scanning calorimetry
HPLC:	High performance liquid chromatography
HSPC:	Hydrogenated soybean phosphatidylcholine
ICH:	International Council for Harmonisation
LOD:	Limit of detection
LOQ:	Limit of quantification
MLV:	Multilamellar vesicle
MMAD:	Mass median aerodynamic diameter
MOC:	Micro-orifice collector
mPEG:	Methoxy poly (ethylene glycol)
mPEG-COOH:	Methoxy poly (ethylene glycol) carboxyl
NF-kB:	Nuclear factor kappa-light-chain-enhancer of activated B cells

NGI:	Next Generation Impactor
NMR:	Nuclear magnetic resonance
NSCLC:	Non-small cell lung cancer
PDI:	Polydispersity index
pMDI:	Pressurised metered-dose inhaler
RE:	Relative error
rNGI:	Reduced Next Generation Impactor
RSD:	Relative standard deviation
SCLC:	Small cell lung cancer
SUV:	Small unilamellar vesicle
TFA:	Trifluoracetic acid
TLC:	Thin layer chromatography
TSI:	Two-stage impactor
UV:	Ultraviolet
VMD:	Volume median diameter

Chapter 1 Introduction

1.1 Lung cancer

1.1.1 Background

Lung cancer causes the most cancer-related deaths (more than 1.69 million deaths, 19.20%) in both men and women worldwide (Zarogoulidis et al., 2013; Siegel et al., 2014). Lung cancer is divided into two types: 85% of all lung cancer cases are classified as non-small cell lung cancer (NSCLC), whereas small-cell lung cancer (SCLC) accounts for 15% of total cases (Babu et al., 2013; Goel et al., 2013). NSCLC is classified into three main types: squamous-cell carcinoma (25-30% of all cases), adrenocarcinoma (40% of the cases) and large-cell carcinoma (5-10% of lung cancers) (Zarogoulidis et al., 2013; Zappa and Mousa, 2016). The common signs and symptoms of NSCLC are cough, wheezing, breathlessness, loss of appetite and chest pain. However, most patients are asymptomatic. When the cancer spreads to other organs, it may affect bones, liver and nervous systems, causing bone pain, jaundice and fatigue. Patients who experience the common symptoms of NSCLC are generally referred for a chest x-ray and/or CT scan to determine whether the cancer has spreads beyond the lungs (Kayser et al., 2017; Grapatsas et al., 2017). More than 70% of patients with NSCLC are diagnosed with metastatic and locally advanced disease, while those having a localised cancer account for only about 20% of NSCLC cases at the initial diagnosis (Grapatsas et al., 2017; Rudokas et al., 2016). There are a number of risk factors associated with lung cancers, such as smoking, alcohol, air pollution, occupational exposure and genes. More than 80% of lung cancer deaths are attributed to cigarette smoking (Molina et al., 2008; Zappa and Mousa, 2016).

1.1.2 Current treatment options

The treatment options for NSCLC are primarily based on the stage of the lung cancer. Surgery is the most successful and consistent therapy to remove the tumour for patients with early stages (stage I and stage II NSCLC), whereas those who are diagnosed with locally advanced (stage III NSCLCL) or metastatic (stage IV NSCLC) (approximately 70%) benefit better from cisplatin-based chemotherapy or targeted therapy (personalised medicine) (Molina et al., 2008;

Reck et al., 2013; Zarogoulidis et al., 2013). Radiation treatment is beneficial for those who do not respond to surgery or chemotherapy (Molina et al., 2008; Zappa and Mousa, 2016). The combination of chemotherapy, surgery and/or radiation therapy or adjuvant therapy is used as the standard treatment to reduce the risk of lung cancer relapse and to increase overall survival. However, this regimen is suitable only for certain patients with early-stage NSCLC (Schettino et al., 2008; Sangha et al., 2010; Zarogoulidis et al., 2013).

1.1.3 **Targeted therapy**

Targeted therapy for NSCLC has been developed to treat specific molecular targets by altering major cell-signaling and regulatory pathways (Molina et al., 2008). The epidermal growth factor receptor (EGFR), a tyrosine kinase receptor, plays an important role in the development and progression of NSCLC (Zarogoulidis et al., 2013; Zappa and Mousa, 2016) and overexpresses in various epithelial tumours including NSCLC (40- 80%) (Schettino et al., 2008). Inhibitors of EGFR including tyrosine kinase inhibitors (TKIs) such as erlotinib and gefitinib as well as anti-EGFR antibodies such as cetuximab and panitumumab have shown clinical benefit in patients with NSCLC. However, TKIs are the most promising therapy for NSCLC due to a significant response for patients with lung adenocarcinoma (Riely and Ladanyi, 2008; Zappa and Mousa, 2016). EGFR gene mutations, which account for 10-15% of European and Asian patients with adrenoma carcinoma, can cause uncontrolled cell division (Zappa and Mousa, 2016; Liao et al., 2017). These mutations are sensitive to EGFR tyrosine kinase inhibitors (EGFR-TKIs) which exhibited a good response rate of 70%, with significantly improved overall survival for patients who received erlotinib compared with a placebo (Zappa and Mousa, 2016). However, there was no difference in overall survival between gefitinib and placebo groups (Nurwidya et al., 2016; Chang et al., 2017).

The first-generation EGFR-TKIs such as erlotinib (Tarveca®, 150 mg orally daily) and gefitinib (Iressa®, 250 mg orally daily) and the second-generation EGFR-TKIs such as afatinib (Gilotrif®, 40 mg orally daily) have all been approved by the US FDA as standard first-line treatment for advanced EGFR

mutant NSCLC (Liao et al., 2017). Among the three approved drugs, gefitinib is limited to use in a subgroup of patients with NSCLC, while afatinib has not improved the overall survival as compared to gefitinib and erlotinib treatment (Nurwidya et al., 2016; Yang et al., 2017a). The next section will further discuss erlotinib, EGFR –TKI, used in this study. The third-generation EGFR-TKIs such as osimertinib, olmutinib and rociletinib have been developed with activity against EGFR mutations, but with less skin rash and diarrhea adverse effect than first and second-generation EGFR-TKIs agents. However, these drugs are still in the trial phase (Liao et al., 2017; Yang et al., 2017a).

According to the UK National Institute for Health and Care Excellence (NICE) and the US Food and Drug Administration (USFDA), erlotinib is approved as a first-line treatment for initial treatment of patients with NSCLC whose cancer has spread to other parts of the body and who have certain types of EGFR mutations, and as second or third line treatment for maintenance treatment of advanced-stage NSCLC (Zarogoulidis et al., 2013). However, erlotinib is associated with dermatological toxicities through the mechanism of EGFR-associated cutaneous toxicity, which is not completely understand since there are several steps involved in the inhibition of EGFR-mediated signaling pathways, including premature differentiation and stimulation of inflammation (Thatcher et al., 2009).

Erlotinib is currently marketed for the treatment of locally advanced or metastatic NSCLC in film-coated oral tablet under the trade names of Erlocip® (Cipla), Tarceva® (Roche) and Erloshil® (Raichem). The usual clinical oral dose of erlotinib is 150 mg/day, which is its maximum tolerated dose (MTD) (Yeo et al., 2010b, BNF, 2018). The mechanism of action, chemical structure as well as formulation approaches for erlotinib will be further described in Section 1.8.1.

1.2 Pulmonary drug delivery

Approximately 70% of patients with NSCLC suffer from advanced local invasion and/or distant metastasis stage at the time of diagnosis, meaning that surgery is not sufficiently curative treatment for these patients (Reck et al., 2013; Rudokas et al., 2016). Moreover, current oral drug delivery of cytotoxic drugs may cause

systemic side effects and sub-therapeutic doses at the target sites (Hu et al., 2013; Rudokas et al., 2016). Pulmonary delivery may reduce the side effects of systemic administration and enhance therapeutic efficacy by delivering a chemotherapeutic agent directly to its site of action in order to achieve the most effective localised treatment (Patil and Sarasija, 2012). Therefore, strategies for targeting lung cancer locally (pulmonary drug delivery) have been considered not only for possible remission of cancer but also for the control of lung cancer metastases. Such local delivery can possibly enhance the effectiveness of surgery and/or radiotherapy (Hu et al., 2013; Rudokas et al., 2016).

Pulmonary drug delivery is an attractive delivery approach as it can produce a rapid onset of drug action, is non-invasive and is an effective route of administration for drugs having local and systemic effects (Pilcer and Amighi, 2010). Furthermore, lower dosages can be delivered since this delivery system allows the avoidance of first-pass metabolism and drug degradation compared with oral route. Further, unwanted side effects and drug interactions when more than one medication is administered concurrently can be minimised (Timsina et al., 1994). The physiology of lung ensures it is an attractive target for drug delivery. It provides a large absorptive surface area (approximately 70-140 m^2) and a highly permeable membrane (0.2-0.7 μm thickness) especially in the alveolar region, the absorption site for most drugs and various macromolecules. Furthermore, the lung has a rich blood supply and low enzymatic activity compared to the gastrointestinal tract (GI) and liver. The pulmonary route thus offers efficient drug absorption to the systemic circulation (Labiris and Dolovich, 2003; Patil and Sarasija, 2012). However, deposition of inhaled drugs within the airways and the effectiveness of the inhalation route are still challenging for multifunctional reasons including the physicochemical properties of drugs, the characteristic properties of formulations and the types of inhaled devices available (Rudokas et al., 2016). Adrenocarcinoma cells (40% of NSCLC cases) are found in small peripheral airways (bronchioles and alveoli) and type II aveolar cell, these regions are therefore major targets for NSCLC treatment (Zappa and Mousa, 2016; Gazdar et al., 1990), with delivery approaches targeting these lung regions being be particularly appropriate.

1.2.1 Lung physiology

The respiratory tract is predominantly involved in the oxygenation of blood and the elimination of carbon dioxide. The respiratory tract starts from the nose and extends to the alveolar sacs. There are several ways of classifying the different regions of the respiratory airway; upper and lower respiratory tract is one of the most common ways. The upper respiratory tract comprises nose, nasal cavity, throat, pharynx and larynx, whereas the lower respiratory airway includes trachea, bronchi, terminal bronchioles, respiratory bronchioles, alveolar ducts and alveolar sacs.

Another classification divides the airways into two main regions: the conducting region (the first 16 generations of the respiratory tract; from trachea to terminal bronchioles) and the respiratory region (including generations 17 to 23, between respiratory bronchioles and alveolar sacs), where gases are exchanged between blood and inhaled air (Kleinstreuer and Zhang, 2010). Aerosol flow and deposition differ in different regions of the respiratory tree (Figure 1-1), such that this model is commonly used in considerations of particle deposition in the human airways.

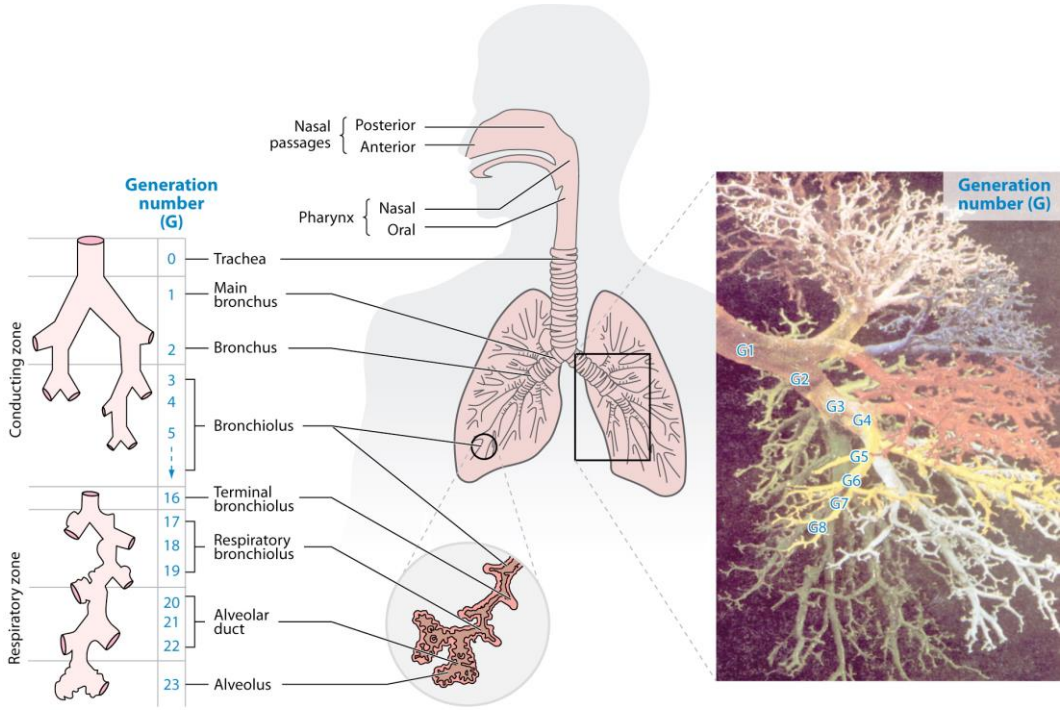

Figure 1-1 The human airways (Kleinstreuer and Zhang, 2010)

1.2.2 Inhalation aerosols and aerodynamic diameter

In order to deliver medication to the deep lung region, certain parameters should be considered. The most critical parameter determining the site of aerosol deposition and distribution within the airways is particle size and this term is normally standardised to aerodynamic diameter (d_a, Eq.1-1). The aerodynamic diameter (d_a) is the diameter of a sphere of unit density that reaches the same terminal settling velocity in an air stream as the particle in question. This parameter depends on the particulate properties such as geometric size, shape and density and can be calculated using Eq. 1-1 (Chow et al., 2007).

$$d_a = d_{geo} * \sqrt{\frac{\rho}{\chi \rho_o}} \qquad \text{Eq. 1-1}$$

where d_{geo} is the physical diameter of particle, ρ is the density of particle, χ is the dynamic shape factor and ρ_0 is unit density. Since shape can influence the motion of the particles in the airsteam for non-spherical particles, the relationship between d_a and d_{geo} can be complexed in these cases. The dynamic shape factor

is expressed as the ratio of the drag force on a non-sphere particle to the drag force of a sphere with the same volume at the same velocity (Chow et al., 2007).

Most inhalation systems are polydispersed, containing a range of particle sizes. Mass median aerodynamic diameter (MMAD), which refers to the particle diameter that has 50% of cumulative mass above and below it, is generally presented. The distribution of sizes or the variability of the particle diameters within the aerosol is expressed as the geometric standard deviation (GSD) for log normal distributions. This parameter is calculated from the ratio of the particle diameter at 84.13% and 15.87% on the cumulative distribution curve. A GSD equivalent to 1 indicates a monodisperse system, whilst, a GSD of > 1.2 indicates a polydispersed system (Colombo, 2013).

1.2.3 Mechanisms of aerosol deposition in the airways

The particle size of an aerosol is a major factor determining the efficacy of a therapeutic aerosol, determining airways penetration, deposition, dissolution and clearance. More specifically, an aerosol size below approximately 5 μm is required to penetrate to the respiratory region. In order to reach alveolar regions, an aerosol size smaller than 2 μm is preferable. Particles with diameter less than 1 μm may be exhaled during normal tidal breathing. On the other hand, larger droplets are deposited in the upper respiratory airways and quickly eliminated by mucociliary clearance mechanism (Chow et al., 2007) Thus, most inhalation products are formulated in the aerodynamic diameter range between 1 and 5 μm (Colombo, 2013).

Three mechanisms, namely inertial impaction, gravitational sedimentation and Brownian diffusion, are predominantly responsible for particle deposition in the lung. All of these depend on particle diameter. Particle deposition can also occur by other mechanisms including interception and electrostatic precipitation (Figure 1-2).

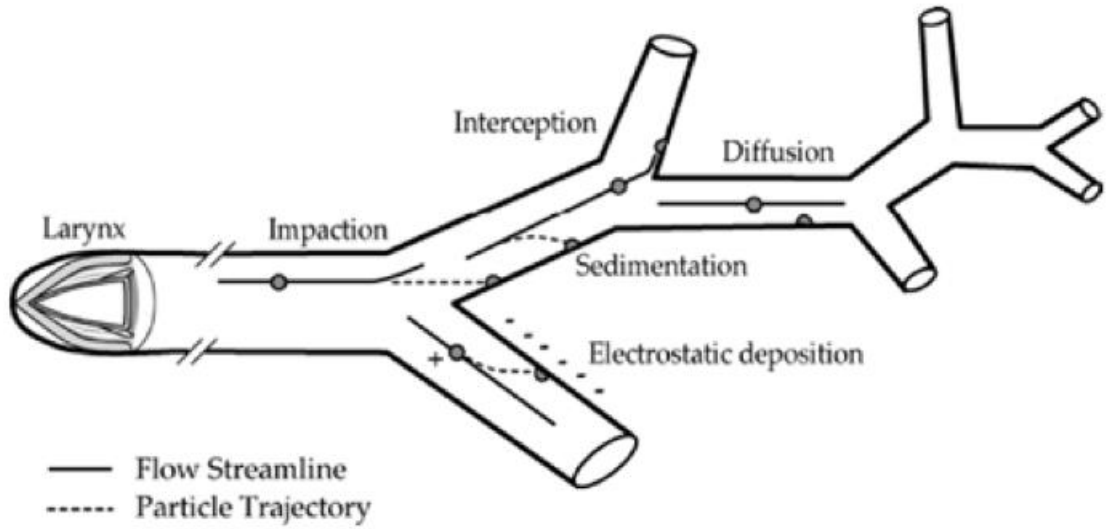

Figure 1-2 Particle deposition in the respiratory tract (Mossman et al., 2011)

In the upper respiratory tract and at the conducting airway bifurcations, inertial impaction is the most important deposition mechanism for particles greater than 5 μm and particular larger than 10 μm. The change in airflow direction causes particles having a large momentum to impact on the airway's walls since their momentum tends to keep them on their original trajectories instead of following the air streamline. Hence, impaction normally occurs in the first 10 airways generations or near the sharp-angled bifurcations, where the velocity of airflow is high and airstream is turbulent. Particles in the size range 0.5 to 5 μm, which escape impaction, are largely deposited by gravitational sedimentation. This mechanism, resulting from the gravitational force, occurs in the last 5 or 6 generation of airways (bronchioles and alveolar region), where the air velocity is low. Brownian diffusion is the most prevalent deposition mechanism for particles with diameter smaller than approximately 0.5 μm, where airstream velocity is near zero or absent (alveolar region). Deposition by this mechanism is caused by the random bombardment of gas molecules against the particles. This effect can result in an irregular motion of the particles from high to low concentrations, causing them to diffuse from the aerosol cloud to the airways' walls and thus to deposit.

1.3 Challenges in pulmonary delivery

According to Eq.1-1, particles with smaller size, lower particle density and/or higher dynamic shape factor will have smaller aerodynamic diameter. One approach to enhance alveolar deposition is to create large porous hollow particles (LPHPs). This design is to lower the density of particles to achieve a small aerodynamic diameter. Previous studies have shown that larger porous particles have higher dispersibility from a delivery device and improved fine particle fraction as compared to smaller non-porous particles. This possibly due to their smaller surface-to-volume ratio, resulting in easier deagglomeration upon inhalation (Gharse and Fiegel, 2016). Larger particles with low density can lower the probability of inhaled drug losses before particles enter the airways, leading to a better systemic bioavailability as seen in the case of insulin in vivo (Edwards et al., 1997).

Particle interactions including particle-particle and particle-surface interactions are another crucial factor for deep lung deposition. This is associated with van der Waals forces, which are related to particle shape, surface properties, size, hygroscopicity and electrostatic properties. For example, particles having lower van der Waals force (attractive force) and lower contact surface show less aggregation during aerosolisation, resulting in better flowability, aerosolisation and deposition (emitted dose and fine particle fraction) properties. This can be seen in a comparison of pollen-shaped particles and other particle shapes such as needles, cubes and plates (Hassan and Lau, 2009).

When the aerodynamic diameter of the particles is very small compared with the dimensions of the airways, the centre of mass remains in a mainstream flow, while the distal ends of the particles may come into contact with an airway or alveolar wall, giving high interception deposition due to their large attractive forces. This can be seen in the case of elongated or needled-like particles such as fibres (Hassan and Lau, 2009; Cheng, 2014).

Nanocarriers smaller than 200 nm have been demonstrated to escape macrophage phagocytosis. Hence, nanomaterials may remain longer in the lung fluid compared

to those in micrometre size range (Pardeike et al., 2011). As compared to microparticulate suspensions, nanoparticulate formulations have shown a smaller and more uniform droplet size, resulting in a better dose uniformity (Pardeike et al., 2011). In aspects of regional deposition in the lungs, particle size with the most efficient deposition in deep lung regions should be ideally in the range 0.5- 5 μm (Pilcer and Amighi, 2010). However, the relationship between particle size and regional lung deposition of nanometre aerosol size has not been widely investigated.

Conventionally, particles smaller than 1 μm considered to be easily exhaled. However, nanoparticles may have higher deep lung deposition in accordance with Brownian diffusion (Jabbal et al., 2017). Previously, Stahlhofen and his colleagues have investigated the influence of particle size on lung deposition (Stahlhofen et al., 1989). The findings have shown that the total lung deposition decreased with reducing particle size until 0.5 μm, where the total lung deposition troughed. Further decrease in particle size resulted in increasing total lung deposition, with equivalent or higher level as shown in Figure 1-3 (Carvalho et al., 2011). Recently, the relationship between MMAD, total lung deposition and exhaled fraction was evaluated and the findings demonstrated that extra-fine particles (< 2 μm) were not related to a noticeably higher exhaled fraction (Jabbal et al., 2017). These observations possibly due to the different mechanisms of deposition predominantly for particles of different size with particle ≈ 0.5 μm not depositing well by diffusion, impaction or sedimentation.

Few in vivo studies of nanoparticles administered by the pulmonary route have been assessed. Nebulisation of poly (DL-lactideco-glycolide) nanoparticles containing the anti-tuberculosis drug (rifampicin or isoniazid or pyrazinamide) improved drug bioavailability and decreased drug dosing in guinea pigs (Pandey et al., 2003; Lu et al., 2014). For lung cancer treatment, inhaled doxorubicin-loaded nanoparticles resulted in significantly reduced tumours as compared to the control groups as in vivo study in mice (Roa et al., 2011; Lu et al., 2014). These findings support the potential of nanoparticles in pulmonary delivery.

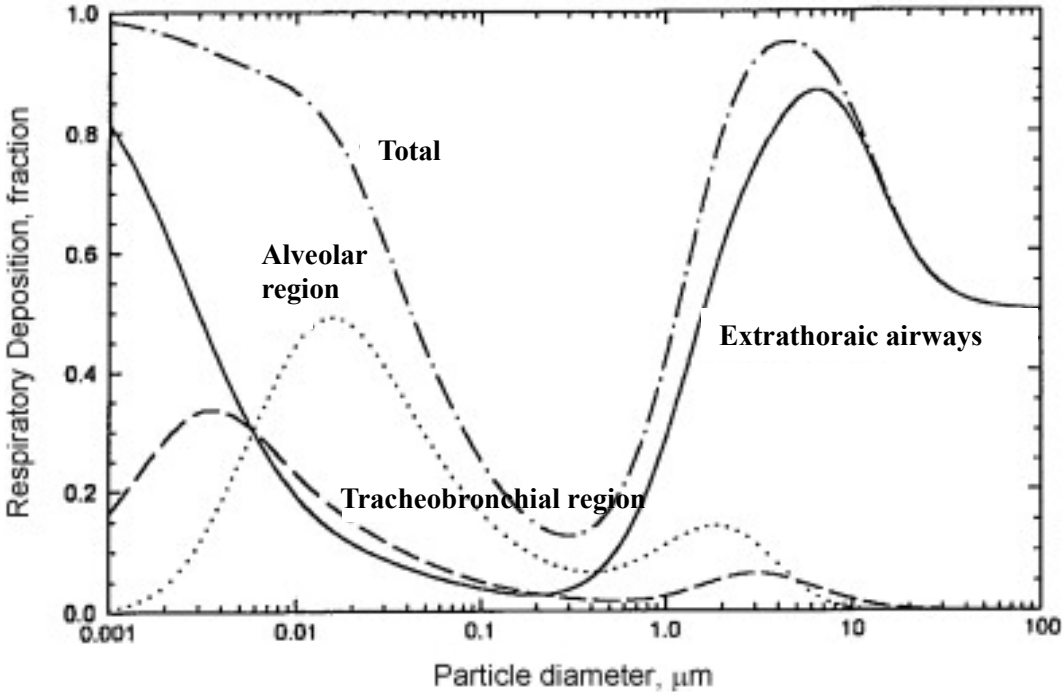

Figure 1-3 The relationship of particle size and respiratory deposition fraction of inhaled product (Carvalho et al., 2011)

1.4 Inhalation devices for pulmonary delivery

Currently, there are four main types of delivery devices for inhalation commercially available, which are pressurised metered-dose inhalers (pMDIs), dry powder inhalers (DPIs), soft-mist inhalers and nebulisers.

1.4.1 Pressurised metered- dose inhalers (pMDIs)

Pressurised metered- dose inhalers (pMDIs) are the most common multi-dose devices used for pulmonary delivery (Dolovich and Dhand, 2011; Lavorini et al., 2017). Their portability, disposability, relatively low cost, multidose convenience, and reproducible dose delivery has led to their popularity for the treatment of COPD and asthma (Newman, 2005; Stein et al., 2014; Taylor, 2018). Formulations for pMDIs can be as solutions or suspensions in liquefied propellant together with other excipients such as surfactants, co-solvents, and solubilising agents to solubilise and stabilise drug in the formulations (Newman, 2005; Ibrahim et al., 2015). Traditional chlorofluorocarbon (CFC) propellants are no longer used and have been replaced by non-ozone-depleting propellants,

hydrofluoroalkanes (HFAs) namely heptafluoropropane (HFA-227) and tetrafluoroethane (HFA-134a) (Ibrahim et al., 2015; Taylor, 2018).

A major drawback of pMDIs is the low fraction of drug delivered (not more than 20% of the stated emitted dose) to the lung attributed to high particle exit velocity and poor actuation and inhalation coordination by patients (Newman, 2005; Pilcer and Amighi, 2010; Lavorini et al., 2017). Spacer attachments (AeroChamber Plus®), valve holding chambers (Autohaler®) and breath-actuated pMDIs (Syncroner®, Easi-breathe®) have been developed in order to overcome problems with inhalation-actuation coordination since the devices can fire the dose automatically through a spring mechanism when the patients inhale. Also, these inhalation aids may slow down the velocity of the emitted aerosol cloud and allow efficient propellant evaporation, causing a relatively smaller size slowly moving, with improved potential for deep lung deposition and lower throat impaction (Ibrahim et al., 2015). However, spacer devices are not convenient to use. In addition, the static charge on the internal walls can occur with some models of plastic spacers, thereby decreasing the emitted dose to the patients (Newman, 2014).

1.4.2 **Dry powder inhalers (DPIs)**

Dry powder inhalers (DPIs) are convenient and simple-to use devices, with various advantages over pMDIs (Atkins, 2005; Pilcer and Amighi, 2010; Dolovich and Dhand, 2011). DPI formulations are propellant-free and do not require any excipients except sometimes a carrier (e.g. lactose). Moreover, DPI dosage forms generally have better chemical and physical stability than liquid formulations (Pilcer and Amighi, 2010). These inhaler devices can deliver larger drug doses than pMDIs, which are limited by the volume of the metering valve and the highest concentration of suspension that can be employed without valve clogging. DPIs require less coordination of breathing and actuation as compared to pMDIs since they are generally breath-actuated devices (Ibrahim et al., 2015; Taylor, 2018).

Based on the mechanism for powder aerosolisation, DPIs can be divided into two types; passively- (relying on the patient inspiration's effort) and actively- DPIs (containing energy source) (Ibrahim et al., 2015). Active DPIs seem simpler to operate than the passive devices, though none of such advanced inhalers are currently available in the market. DPIs can also be classified into three types by the number of doses; single-unit dose, multi-unit dose and multi-dose reservoirs (Figure 1-4). In unit dose inhalers such as Aerolizer®, Cyclohaler® and Handihaler® (Figure 1-4a and 1-4b), drug dose is pre-metered in a single hard gelatin capsule which is discarded after use. This device requires the patients to insert a new capsule before each use. Multi-unit dose inhalers (Figure 1-4c) contain multiple pre-metered individual doses in replaceable foil blisters (Ellipta® and Diskhaler®). Multi-dose devices (Figure 1-4d) comprise a reservoir of drug powder (Easyhaler® and Turbuhaler®), from which the device-metered dose will be delivered upon each inhalation (Pilcer and Amighi, 2010; Ibrahim et al., 2015; Lavorini et al., 2017).

However, the multitude of DPIs having unit-dose and multi-dose design, which may be complex and confusing for patients resulting in inhalation errors, and errors in device preparation, handling with a negative effect on adherence (Newman, 2014).

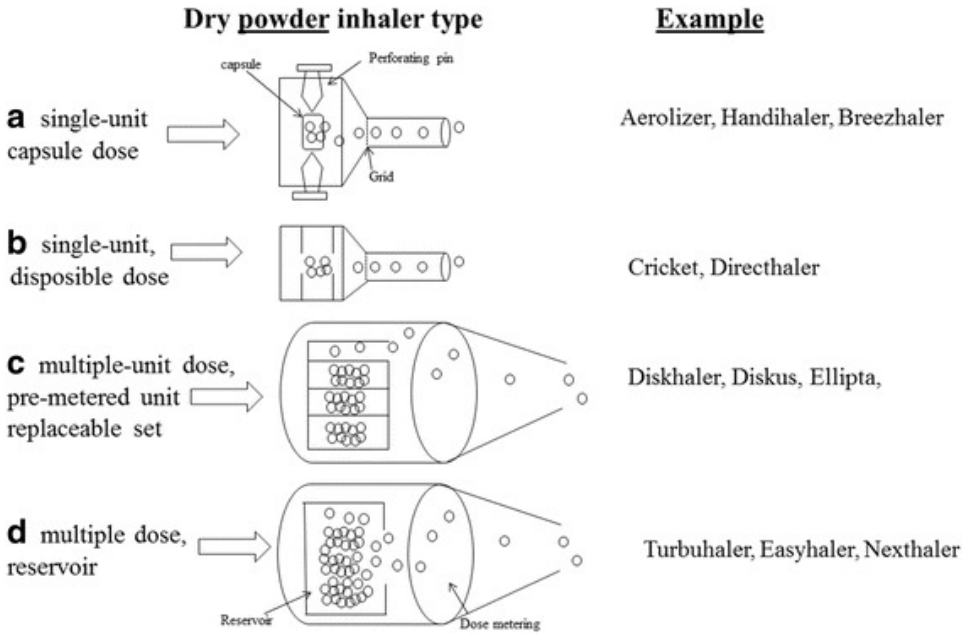

Figure 1-4 Dry powder inhaler devices; a) single-unit capsule dose, b) multiple-unit dose and c) multiple dose inhalers (Lavorini et al., 2017)

1.4.3 **Soft-mist inhalers (SMIs)**

The soft-mist inhalers (Spiriva Respimat® and AERx®) also called metered-dose liquid inhalers and non-pressurised metered-dose inhalers are a new novel type of multiple-dose, propellant-free, hand-held liquid inhaler device (Hira et al., 2018). These are designed to produce a fine mist in a single breath from a solution within a pocket size device using a patient-independent and environmentally friendly energy source. As compared to pMDIs and DPIs, these devices generate a slow-moving aerosol cloud with longer time for aerosol generation, leading to a higher fraction of emitted dose being deposited in the deep lungs. Thus, these innovative devices are superior to the pMDIs and the DPIs with respect to the ease of use, environmentally friendly, higher dose of drug deposition in the lungs, lower oropharyngeal deposition and no requirement for spacer devices (Dalby et al., 2011).

For the mechanism of aerosol generation, these devices contain a spring to force a metered-dose of solution through two-channel nozzles, generating two fine jets of liquid and the soft mist (Dalby et al., 2004; Bohr and Beck-Broichsitter, 2015).

Drug solutions can be formulated in either water or ethanol. Ethanol can be used as a solvent and preservative. Soft-mist inhalers are beneficial for patients who have difficulty in coordinating inhalation and actuation may represent in the future direction of novel delivery devices (Watts et al., 2008; Dalby et al., 2011; De Pablo et al., 2017).

Until now, all the aforementioned devices (pMDIs, DPIs and SMIs) can deliver only small doses of the therapeutic agent (i.e. asthma) and thus may not be appropriate for the treatment of many diseases which large doses are needed including cancer and infectious diseases (Rudokas et al., 2016).

1.4.4 **Nebulisers**

Nebulisers are devices which are used for converting liquid formulations (an aqueous solution or suspension) into an aerosol where most of the drug released is in droplets having an aerodynamic diameter of 1-5 μm (O'Callaghan and Barry, 1997). Nebulisers have several advantages over pMDIs, DPIs and SMIs in that larger doses/volumes can be delivered over an extended period, requiring minimal processing of formulations (e.g. lack of organic solvents and drying stages) (Rudokas et al., 2016). Patients can inhale medication fluid through a facemask or mouthpiece during a normal tidal breathing, and thus these devices can be used for any patient groups and/or clinical conditions. They are alternative devices for patients who cannot coordinate actuation and inhalation for pMDIs and/or those who experience difficulties with the inspiration flow required by DPIs (Ibrahim et al., 2015). Nebulisers are useful for drugs that cannot be readily formulated for pMDIs and DPIs or where the therapeutic dose is too high for delivery by those devices. Moreover, different compatible solutions can be concurrently nebulised (Taylor and McCallion, 1997; Ari, 2014).

There are some disadvantages of nebulisers; for example, a longer administration time is required, they have reduced portability, and there is a requirement for an external power source such as battery or main electric supply and compressed air for air-jet devices (Cipolla et al., 2013).

Commercially available nebulisers are divided into three categories depending on their operating principle: ultrasonic, air-jet, and vibrating-mesh nebulisers.

1.4.4.1 Ultrasonic nebulisers

Ultrasonic nebulisers produce aerosol droplets at high frequency (1-3 MHz) using a vibrating piezoelectric crystal at the base of the device. The vibrations are transmitted directly to the surface of a drug solution, resulting in a fountain of liquid on the surface in a nebuliser chamber. The size distribution of aerosols is determined by baffles, which recycle large droplets and allow the smaller ones to be delivered for inhalation (Elhissi et al., 2012).

During operation, heat is generated in the fluid being aerosolised which can denature heat-sensitive materials such as proteins (Ari, 2014). These devices are not suitable for delivering viscous liquids and suspensions, probably due to a reduced force used to atomise the fluid (Hess, 2008; Ibrahim et al., 2015). Also, increasing temperatures during operation may impact delicate formulations particularly liposomes, resulting in fusion and drug loss (Elhissi et al., 2012). Consequently, the popularity of this type of device has decreased in recent years particular with the advent of vibrating-mesh devices (Le Brun et al., 2000; Yeo et al., 2010a; Ari, 2014).

1.4.4.2 Air-jet nebulisers

Air-jet nebulisers are the most commonly used nebulisers due to ease of use, convenience and relatively low cost (Hess, 2008). The driving gas passes through a narrow aperture (Venturi nozzle) from the compressor. At the aperture, the pressure decreases and the gas velocity increases, leading to a production of a cone shape. Due to a negative pressure, fluid is drawn up the feeding tube system into fine ligaments. The fine ligaments collapse into droplets due to the liquid's surface tension (O'Callaghan and Barry, 1997; Lavorini, 2013; Taylor, 2018).

During atomisation of liquid, coarse aerosol droplets that are the majority of liquid mass impact on baffles and the nebuliser works depending on the design of

air-jet devices. The large droplets will return to the fluid reservoir, while small droplets are emitted from the nebulisers. The design of the nebuliser device is critical, affecting droplet size and particle deposition (Hess, 2008). Other parameters including the characteristics of the fluid (density, viscosity, surface tension), the velocity and the flow rate of gas and fluid also determine the droplet size produced by nebulisers (Hess, 2000). For example, an increase in gas velocity can reduce droplet size (Hess, 2008; Lavorini, 2013; Ibrahim et al., 2015).

Another crucial consideration relating particularly to the nebuliser design, in the use of air-jet nebulisers is the dead or residual volume. This parameter represents the volume that is trapped within the nebuliser and thus will not be successfully delivered from the device. The medication loss due to dead volumes can be minimised by optimising the internal design of the nebulisers and/or the operation by the patients during the treatment. Using a conical shaped reservoir can reduce the residual volume since this design decreases the surface area of the internal surface of the nebulisers. In addition, patients and clinicians may tap the devices to increase the aerosol and/or drug output (Hess, 2000; Lavorini, 2013). Also, adding diluent or more medical fluid may increase the amount of therapeutic agents delivered. However, this will prolong the administration time, potentially causing difficulties in maintaining good inhalation technique and a reduction of patient adherence during therapy (Rubin and Williams, 2014).

There are many designs of jet nebulisers. This may cause variations in clinical outcomes between air-jet nebulisers combined with different flow rates, compressors and fill volumes (Abdelrahim et al., 2010; Saeed et al., 2017). Other drawbacks with the use of air-jet nebulisers are the noise from the compressor, a drop in the temperature of nebuliser fluid during use, limited portability and the requirement for a compressor (Waldrep and Dhand, 2008; Ibrahim et al., 2015). Consequently, nebuliser design has been developed to overcome some of the aforementioned problems. Air-jet nebulisers can be divided into three classes: constant output jet nebulisers, breath-enhanced jet nebulisers and breath-actuated jet nebulisers as described below.

1.4.4.2.1 Constant output jet nebulisers

Constant output jet nebulisers such as Misty-Neb® and SideStream® are conventional constant-output devices producing aerosol during a patient's inspiration, expiration and breath- holding (L Rau et al., 2004). They are easy to handle and use, with good patient compliance (Ari, 2014). However, aerosol and/or drug loss during the expiration phase and a large dead volume in the reservoir are serious problems, leading to relatively poor patient dosing and the variability of drug dose (Chatburn and McPeck, 2007).

These problems have led to developments in air-jet nebuliser design in order to minimise the drug wastage and enhance drug output.

1.4.4.2.2 Breath-enhanced jet nebulisers

Breath-enhanced jet nebulisers such as the PARI LC® Sprint, PARI LCD® and NebuTech® generate aerosol droplets using a negative pressure from the patient's inspiratory effort. Such devices are modified conventional air-jet devices, using two one-way valves. Figure 1-5 shows that the inspiratory valve opens and allows additional ambient air to be entrained into the nebuliser when the patient's inhaled airflow is greater than the driving flow of the device. This results in higher aerosol output compared with conventional designs. By contrast, exhaled gas passes through an expiratory valve in the mouthpiece and the aerosol returns to the chamber for renebulisation. This can cause less aerosol/drug wastage to the surroundings (Ho et al., 2001; Lavorini, 2013; Ari, 2014).

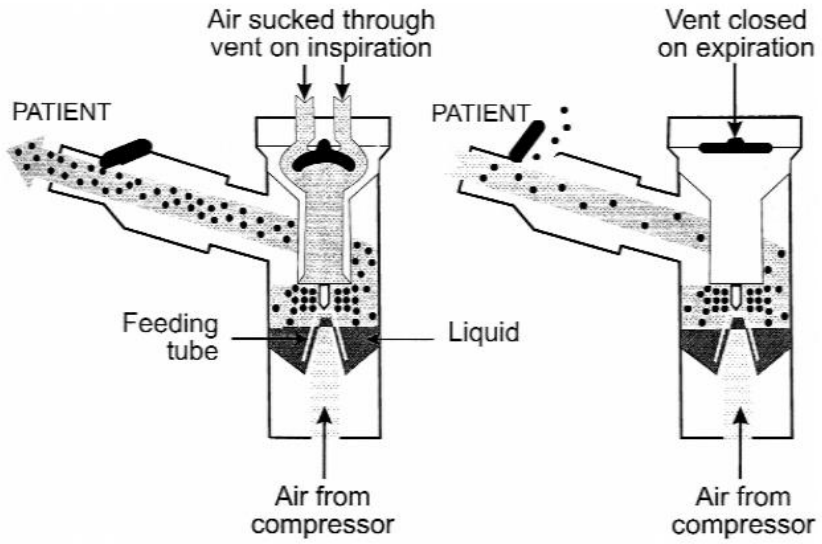

Figure 1-5 Operating principle of breath-enhanced jet nebulisers (Coates and Ho, 1998)

1.4.4.2.3 Breath-actuated jet nebulisers

Breath-actuated jet devices are designed to generate aerosol only on inspiration, thereby decreasing drug waste to the atmosphere (Muchão and Silva Filho, 2010). These delivery systems can also adapt aerosol delivery in accordance with an individual patient's breathing pattern. For instance, the HaloLite® analyzes the patient's breathing pattern and then determines the precise dose delivered to each patient (Leung et al., 2004; Van Dyke and Nikander, 2007; Muchao and Filho, 2010; Lavorini, 2013). Consequently, this type of nebuliser can reduce the variability in the delivered dose and drug waste, and enhance the amount of inspired aerosol as well as patient compliance (Lavorini, 2013; Ari, 2014). However, the drawbacks of this technology are loud noise in operation and high price (Muchao and Filho, 2010).

1.4.4.3 Vibrating-mesh nebulisers

Vibrating-mesh nebulisers have shown numerous advantages over other nebuliser systems; in particular they are small and portable nebulisers, with quiet operation, short administration times, improved drug/aerosol output efficiency, precise and consistent drug delivery, low residual volume and the capability to deliver small drug volumes. Additionally, these devices efficiently deliver a wide range of heat-

sensitive substances including insulin, nucleic acids and other proteins and peptides since they do not significantly heat up the fluid during nebulisation as the case of ultrasonic devices (Ghazanfari et al., 2007; Lavorini, 2013; Ari, 2014; Choi et al., 2018).

However, there are several disadvantages with these devices. For example, they are not suitable for delivering viscous liquids or those that can crystallise on drying. Furthermore, some models are only available for specific drugs (drug-device combinations) (Pritchard et al., 2018). Vibrating-mesh nebulisers are a relatively recent development in nebuliser technology, therefore they are expensive compared to ultrasonic and air-jet nebulisers (Lavorini, 2013; Ari, 2014). It has been suggested that the biological safety and durability of these devices should be taken into considerations since the mesh metal can possibly be broken into small pieces after repeated use (Choi et al., 2018).

Vibrating-mesh nebulisers can be divided into two main types according to their designs: actively vibrating and passively vibrating devices. However, aerosol production of both types is based on the same mechanism. Overall, fluid is forced through multiple micrometre-sized apertures in a mesh or aperture plate to generate the aerosol (Elhissi et al., 2012).

Passively vibrating-mesh devices

Passively vibrating-mesh nebulisers; for example, the Omron MicroAir NEU22®, consist of three main parts: 1) a piezoelectric crystal 2) a transducer horn and 3) a mesh plate containing 6000 tapered holes (3 µm in diameter). The piezoelectric crystal transmits high frequency vibrations via a transducer horn, which induces ‘passive’ vibrations in the perforated plate, resulting in upwards and downwards movements of the plate to extrude the fluid through the mesh apertures and generate aerosol droplets (as Figure 1-6; Ghazanfari et al., 2007; Elhissi et al., 2012; Lavorini, 2013).

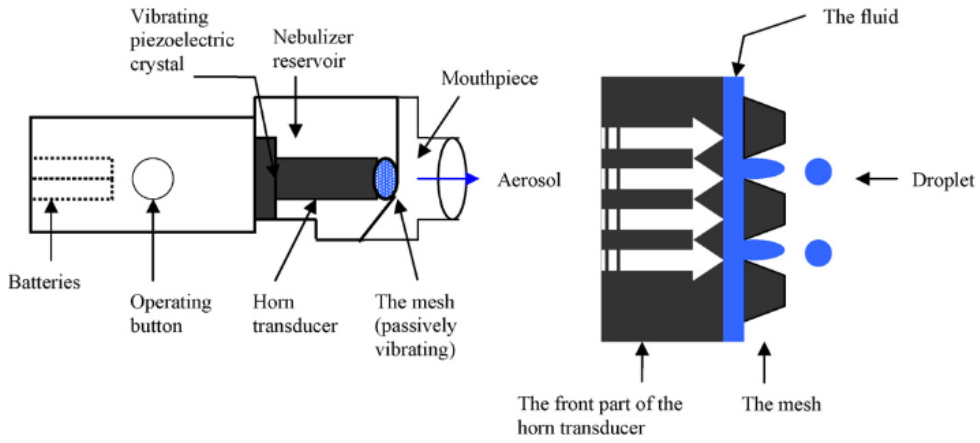

Figure 1-6 Operating principle of passively vibrating-mesh nebulisers (Ghazanfari et al., 2007)

Actively vibrating-mesh devices

Aeroneb®, eFlow® and Velox® are examples of actively vibrating-mesh nebulisers. These contain an aerosol generator comprising 1000 electroformed dome-shaped apertures in a plate and a vibrational element. The vibrating element creates micropump effect by contracting and expanding on application of an electrical current, this leads to vibration of the plate, consequently producing a slowly moving aerosol as liquids is drawn through the mesh apertures (Figure 1-7) (Ghazanfari et al., 2007; Elhissi et al., 2011a; Elhissi et al., 2012; Ari, 2014).

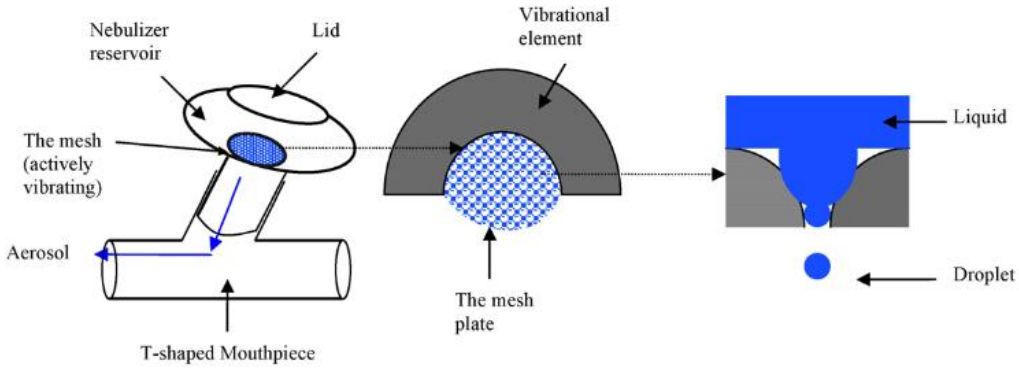

Figure 1-7 Operating principle of actively vibrating-mesh nebulisers (Ghazanfari et al., 2007)

Although vibrating-mesh nebulisers improve the efficiency of aerosol delivery due to their lower residual volume, drug waste on exhalation is still major issue due to continuous drug delivery without any adaptation of output to the patient's breathing pattern (Denyer and Dyche, 2010). Adaptive aerosol delivery (AAD) technology such as the I-neb AAD System nebuliser determines the pattern of patient's breathing so as to tailor the duration of aerosol production and improve the precision and reproducibility of drug dosing. These devices have been designed to pulse aerosol only during inhalation using one of two different breathing patterns (the Tidal Breathing Mode and the Target Inhalation Mode), thereby reducing drug waste on exhalation, and are thus particularly suitable for the delivery of expensive or potent drugs (Dhand, 2010; Nikander et al., 2010; Ari, 2014; Pritchard et al., 2018). Furthermore, patients are guided to inhale slowly and deeply for 8 s, while aerosol is pulsed for up to 7 s when using the current version of the Target Inhalation Mode. This allows 1 s to enhance deposition in the deep lung, and decreases particle impaction in the upper airways by promoting slow and deep inhalation (Denyer and Dyche, 2010; Geller et al., 2010; Nikander et al., 2010).

The I-neb AAD shows better performance in terms of outcomes, patient acceptance and adherence. However the high cost is a major drawback with the I-neb AAD system. Also, healthcare staff, carers and patients need to be trained properly about how to clean and use these devices (Dhand, 2010).

1.5 Effect of fluid physicochemical properties on nebuliser performance

In general, the vehicle in nebuliser formulations is water, often with the inclusion of other excipients such as a co-solvent, surfactant and stabiliser. Since both hypotonic and hypertonic solutions may produce bronchoconstriction, isotonic solutions with a pH in the range 3-10 are usually recommended (Beasley et al., 1988; Kwong et al., 1990; Taylor, 2018). Studies have shown that isotonic solutions may become hypertonic during nebulisation in the case of air-jet nebuliser, though this osmolality change does not cause any adverse reactions in the airways. Preparations may be diluted with water or more usually normal saline before administration (Beasley et al., 1988).

Nebulisation is the process of converting bulk liquid into an aerosol. The relationship between the properties of liquid formulations and the operating principle of the device plays an important role in determining nebuliser performance (Carvalho and McConville, 2016). In order to assess the effectiveness of aerosol delivery, characteristic properties of disperse phase for formulations such as viscosity, surface tension, and ion concentration should be evaluated to determine whether these factors have an impact on aerosol size and output characteristics; for instance, on the proportion of aerosol droplets smaller than 5 μm and the total output (McCallion et al., 1995; Ghazanfari et al., 2007; Bohr and Beck-Broichsitter, 2015).

It has been previously reported that droplet size is inversely proportional to fluid viscosity for air-jet nebulisers and vibrating-mesh nebulisers (Najlah et al., 2013). By contrast, a direct relationship between droplet size and fluid viscosity has been reported for ultrasonic devices (McCallion et al., 1995; Najlah et al., 2013). The viscosity and surface tension of nebuliser fluid also affect total drug/aerosol output of nebulisers since both parameters require energy to generate a new surface. For example, higher viscosity fluids result in aerosols having a smaller droplet size and a subsequent increase in FPF and FPD in the case of air-jet and vibrating-mesh nebulisers, but require a longer nebulisation time and are associated with lower output and output rate (Ghazanfari et al., 2007). Ultrasonic devices are not suitable to nebulise high viscosity (McCallion et al., 1995), whilst for both passively and actively vibrating-mesh nebulisers, aerosol generation ceases or becomes intermittent at higher viscosities (> 1.92cP). Consequently, air-jet nebulisers are the most effective devices for generating aerosols from highly viscous preparations (Ghazanfari et al., 2007; Chan et al., 2011; Najlah et al., 2013).

The correlation between surface tension and aerosol size and/or aerosol output is complex. However, studies have demonstrated that an increased total drug output results for lower surface tension delivered by air-jet and ultrasonic devices for salbutamol sulfate solutions when surface-active agent is included (Arzhavitina and Steckel, 2010; Carvalho and McConville, 2016).

For vibrating-mesh nebuliser, the presence of ions at increasing concentration has been shown to cause a reduction in droplet VMD, thereby increasing FPF and FPD in vibrating-mesh nebulisers. It is proposed that the inclusion of ions in solutions can reduce water adhesion to the internal wall and mesh pores of the devices, leading to an earlier detachment of droplets from bulk solutions, a decrease in the variability of aerosol size, aerosol output rate, nebulisation time and increasing aerosol output. Therefore, the effective performance of vibrating-mesh nebulisers may require the inclusion of electrolyte particularly halide ions (Ghazanfari et al., 2007).

A recent study has reported that there was an inverse relationship between aerosol output and halide concentration for fluoride, bromide and chloride, while aerosol output was proportional to iodide concentration (Najlah et al., 2013). This may be because iodide ions have the greatest polarizing ability at the air-water interface compared to the other three ions, thereby modulating electrostatic repulsion within the aerosol cloud. This effect may lead to the finest aerosol, resulting in the highest aerosol output and FPF. On the other hand, other three ions are likely to be present in bulk fluid due to their less polarizing properties at the interface. All observations indicated that different types of halide ions affected the performance of vibrating-mesh nebuliser (Najlah et al., 2013; Bohr and Beck-Broichsitter, 2015). Thus, the effect of various types of ion (cations and anions) requires further work for the better understanding of the correlation between ion presence in solutions and nebulisation performance.

1.6 Delivery of advanced formulations

In nebulisers, the main operating principle of nebulisation is based on the atomisation of liquid into fine droplets; however, there are significant differences in the mechanism of aerosol generation, which impacts the formulation. Ultrasonic devices are generally considered not suitable for delivering high viscosity fluids (greater than 6cP), microparticulate dispersions, suspension, liposomes and thermolabile peptides or DNA (Hess, 2008; Ibrahim et al., 2015). However, these devices seem to have applications for aerosol delivery when the disperse phase is very small since it can be entrained into droplets, with examples

of radiolabelled solid lipid nanoparticles (200 nm) and itraconazole-loaded nanostructured lipid carriers (≈100 nm) being successfully delivered (Videira et al., 2002; Pardeike et al., 2011).

Various formulations such as protein solutions (rhDNase I), suspensions (Pulmicort Respules®, budesonide suspensions), nanoemulsions, nanoparticles, polymeric micelles in the nanosize range and liposomal formulations can be effectively aerosolised using air-jet nebulisers (Moazeni et al., 2012; Carvalho and McConville, 2016). Aerosol generation of suspensions using this type of devices is dependent on the characteristic properties of formulation including particle size distribution of the dispersed phase in the presence of different excipients (Tadros, 2008; Amani et al., 2010). The aggregation of nanoparticles may be observed during aerosolisation from these devices (Dailey et al., 2003; Carvalho and McConville, 2016). Several studies have shown partial protein degradation and some large aggregation with and without excipients at the air-water interface, attributed to the shear force during jet-nebulisation (Niven et al., 1996; Respaud et al., 2014; Hertel et al., 2015).

Vibrating-mesh nebulisers have been demonstrated to be the most effective device for delivering a number of liquid formulations with better stability during aerosolisation (Respaud et al., 2014; Bohr and Beck-Broichsitter, 2015; Carvalho and McConville, 2016). Vibrating-mesh nebulisers are considered preferable to deliver protein than air-jet and ultrasonic devices since they do not significantly generate changes in temperature and minimise recycling processes, resulting in small changes to protein integrity (Bohr and Beck-Broichsitter, 2015).

Among a large number of drug-carriers, liposomes (bilayered phospholipid vesicles) have shown potential to improve inhalation treatment regimens (Bohr and Beck-Broichsitter, 2015). Several studies of liposomal formulations delivered by these devices have shown that different device designs, lipid concentrations and types of lipid affect the properties of nebulised liposomes and the efficiency of delivery (Carvalho and McConville, 2016). For example, unilamellar liposomes smaller than 200 nm are suggested as an optimal system since they can be easily incorporated into aerosol droplets with minimal drug losses (Lehofer et

al., 2014). Moreover, incorporating cholesterol to make fluid state bilayers more rigid can reduce drug leakage during nebulisation (Lehofer et al., 2014; Cipolla et al., 2016). Delivery of liposomes using air-jet and vibrating-mesh nebulisers is more successful than with ultrasonic devices, as these less damage to liposome bilayers during aerosolisation (Elhissi et al., 2013). Recently, two liposomal formulations; Arikace® and Pulmaquin® have been studied in phase II/III clinical trials for the treatment of pulmonary infections (Paranjpe and Müller-Goymann, 2014; Bohr and Beck-Broichsitter, 2015).

In conclusion, critical formulation parameters including particle size, surface alteration, morphology, rigidity of nanocarriers as well as type of nebuliser need to be considered to achieve the most effective nanoparticle-based approach for pulmonary delivery.

1.7 Methods of aerosol particle size analysis

Nebulised formulations need to be assessed for aerodynamic particle size, fine particle dose (mass), fine particle fraction and the emitted dose in order to compare nebulised systems and possibly to predict the clinical responses (Abdelrahim et al., 2010). It should be noted that the properties of the aerosol are a function of both the formulation and the particular device used for aerosolisation. The fundamental approaches that have been used for aerosol size analysis are microscopy, laser diffraction, particle time of flight (TOF), phase-Doppler particle size analysis (PDA) and cascade impaction.

For routine measurements, laser diffraction has been commonly used for particle size distribution (PSD) of aerosols to estimate the deposition characteristic in the lung particularly in the case of nebulised aerosols (Clark, 1995). However, laser diffraction measures geometrical particle dimensions instead of aerodynamic particle size distribution based on volume, surface and number basis (Pilcer et al., 2008). Volume median diameter (VMD) with the span value (distribution width) are commonly reported for particle size analysis (De Boer et al., 2002). Since the nebulised cloud can be sized when it emits from the mouthpiece before evaporation occurs, this technique is recommended by Ph. Eur. to use for rapid

size-distribution measurement of nebulised aerosol (Ziegler and Wachtel, 2005; Martin et al., 2006). Among all techniques, cascade impactors are the most widely method used for measurement of the particle size distribution by mass of inhalation products based on impaction.

1.7.1 Cascade impactors and impingers

The inertial size-separation of particles in a cascade impactor depends on the aerodynamic diameter, a key parameter determining particle deposition in the lung during inhalation (Section 1.2.2). Cascade impactors allow calculation of FPF and other size fractions of the active pharmaceutical ingredient (API) as well as non-active ingredients in the formulations following chemical analysis (usually high performance liquid chromatography). Other methods cannot readily differentiate between active and non-active components in the formulation as they measure overall particle size distribution in the absence of chemical assay (Martin et al., 2006). Moreover, a fine particle mass corresponding to a particle size distribution of less than 5 µm is the key quality parameters for inhaled aerosol drug product specifications in accordance with European Medicines Agency guidelines (EMA, 2006). Cascade impactors provide the greatest information concerning aerodynamic particle size distribution (APSD) for aerosolised products with particles in the range of 0.5 to 5 µm and are therefore well suited for inhalation aerosol characterisation. For these reasons, cascade impaction is the standard method for characterisation of inhalation aerosols, including nebulisers and is included in United States Pharmacopoeia, European Pharmacopeia and British Pharmacopeia (Marple et al., 2003; Majoral et al., 2006; Taylor, 2018; Fishler and Sznitman, 2017).

There are a number of impactors available; the two most widely employed are 1) the Andersen Cascade Impactor (ACI; Ph. Eur. Apparatus D) and 2) the Next Generation Impactor (NGI; Ph. Eur. Apparatus E). Both the ACI and NGI comprise a series of stages each made up of a plate, with specific nozzle size. Aerosolised particles are fractionated on the basis of inertial impaction according to their aerodynamic size distribution, when the aerosol is drawn into the device at a fixed flow rate. It should be noted that the cascade impactor is not a lung

simulator due to a numerous factors including the geometry at the point of impact, the hardness of the collection surface, coatings and a constant flow rate. Moreover, each collection stage throughout the impactor does not represent any specific deposition sites in the lung (Marple et al., 2003). However, the data obtained from the impactors allows prediction of the probability of an aerosol cloud's deposition to the lower lung according to the airborne particle's behavior in turbulent airsteams and they are rounetinely used in the pharmaceutical development and quality control of inhalation products.

When aerosol droplets pass through the nozzles, large/dense particles will deposit on the collecting plate by impaction. Smaller/less-dense particles will follow the airstream, which is directed at a right angle to the exit of the nozzle, and they will impact on the subsequent collecting plate if they have been given sufficient momentum under high jet velocities (Figure 1-8).

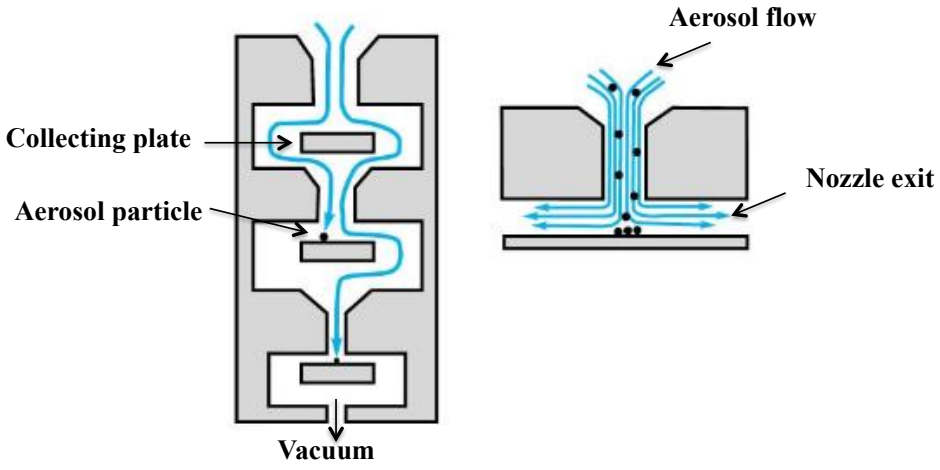

Figure 1-8 Airflow and particle in a cascade impactor (adapted from Copley, 2008)

Deposited aerosol on each stage of the impactor is usually collected and assayed by high performance liquid chromatography (HPLC). Mass Median Aerodynamic Diameter (MMAD) and Geometric Standard Deviation (GSD), are calculated from a plot of cumulative fraction of active substance on each stage versus the cut-off diameter for that stage plotted on a log scale (Figure 1-9). MMAD is determined as the particle size at 50% of cumulative fraction by mass for the

deposited particles or droplets. GSD is calculated from the same plot as for MMAD determination as mentioned using the equation below:

$$GSD = \sqrt{\frac{Size\ X(D84.13\%)}{Size\ Y(D15.87\%)}}$$

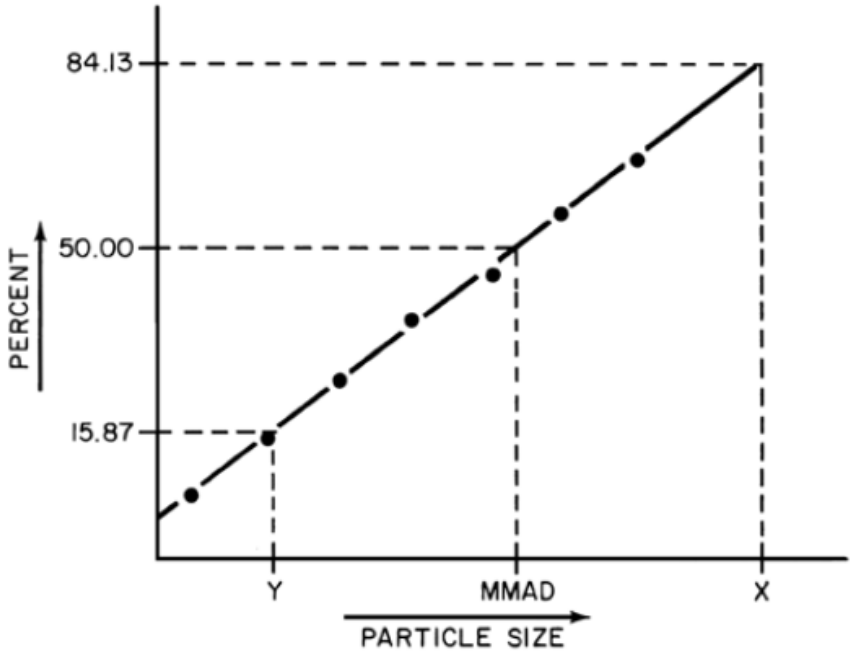

Figure 1-9 The cumulative percentage of mass less than the stated aerodynamic diameters versus the cut-off diameter; log-probability plot (USP29 NF40)

The ACI (Figure 1-10) and NGI (Figure 1-11) have been used for the determination of the fine particle dose and the aerodynamic particle size distribution of aerosols delivered by pMDIs and DPIs. The multistage liquid impinger (Ph. Eur. Apparatus C) also works on the principle of cascade impaction, and consists of five stages, with wet sintered glass collection plates followed by a terminal filter. The European Pharmacopoeia indicates the NGI is also appropriate for the evaluation of nebuliser performance by measuring the mass of active ingredient as a function of aerodynamic diameter.

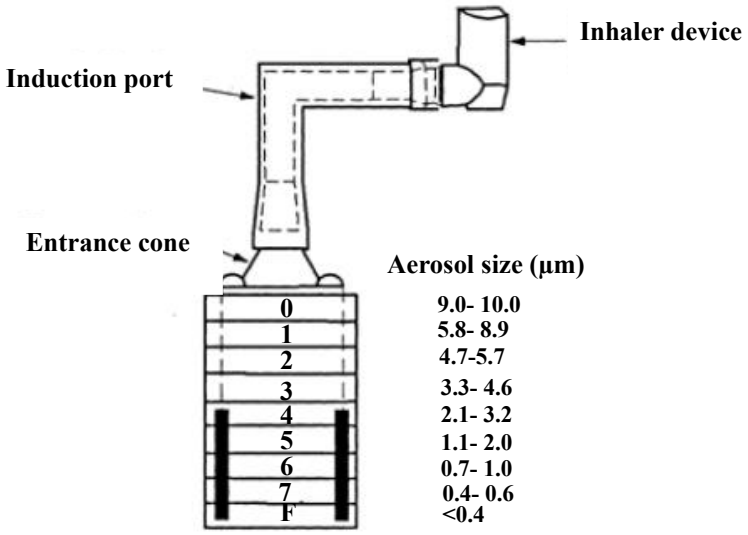

Figure 1-10 Andersen cascade impactor (USP29 NF40)

The NGI (Figure 1-11) used in this study is used with a 90º bend 'induction port' to mimic the human throat, followed by seven compaction stages and the micro-orifice collector (MOC). A back-up filter after the MOC is used to ensure quantitative recovery of the extra-fine particles from small aerosol droplets (Berg et al., 2007b; Abdelrahim et al., 2010). This impactor has been calibrated at 15 L/min for characterising the aerosol particle size distribution of nebulised aerosols between 0.5 and 5 µm with five stages having cut-off diameter in the appropriate range. This flow rate represents a good approximation to the midpoint flow rate achieved by a tidally breathing healthy adult (Abdelrahim and Chrystyn, 2009).

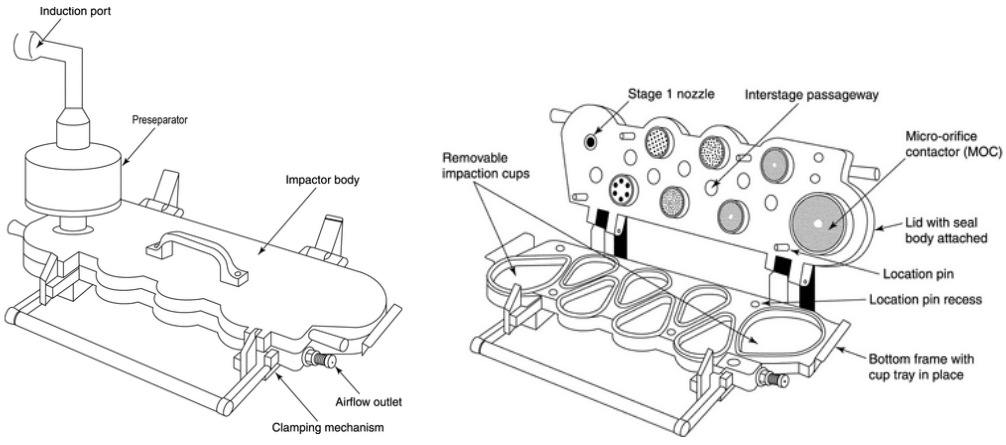

Figure 1-11 Next Generation Impactor (Ph. Eur., 2017)

The Ph. Eur. requires cooling of the NGI at 5 ºC for at least 90 min before use in order to minimise evaporation effects and limit changes in droplet size during the assessment process. Some studies have reported that the MMAD of aerosol droplets determined with the impactor at lower temperature was larger than that determined using a non-cooled impactor (Finlay and Stapleton, 1999; Zhou et al., 2005). This may be explained by differences in temperature between the aerosol exiting the nebuliser and the body of the impactor, resulting in significant droplet shrinkage by evaporation (Finlay and Stapleton, 1999).

At 15 L/min, the cut-off diameters for each stage of the NGI are shown in Table 1-1.

Table 1-1 Cut-off diameters for the NGI stages when operated at a flow rate of 15 L/min

Stage	**Cut-off diameter (µm)**
1	14.1
2	8.61
3	5.39
4	3.30
5	2.08
6	1.36
7	0.98

The United States and European pharmacopoeias recommend that collecting plates of the NGI are coated with silicone oil or high viscosity coatings to reduce particle bounce-off, particle re-entrainment and inter-stage loss of particles during aerosolisation for DPI-based formulations, since these effects can lead to a reduction of the collection efficiency of impactor stages, causing unreliable and distorted APSDs data. The collecting plates do not require coating with such materials for aerosol characterisation of nebulised products as these are no shifts in measured size distributions when uncoated and coated collecting plates were

investigated (Berg et al., 2007a; Berg et al., 2008; Abdelrahim and Chrystyn, 2009).

1.7.2 Abbreviated Impactor Measurement (AIM)

The aerodynamic particle size distribution (ASPD) of inhaled medicinal products is a critical quality attribute obtained with a full-cascade impactor. This parameter is closely linked with the location of drug deposition in the human lung (Nichols et al., 2016). Despites their advantages, cascade impactors are labour intensive and time-consuming to use. Consequently, a traditional cascade impactor-based analysis is not well suited for high throughput applications such as routine product quality testing, product development and comprehensive stability studies (Mitchell et al., 2010; Fishler and Sznitman, 2017; Mohan et al., 2017). Furthermore, drug deposited across the eight stages of the extended impactors may cause analytical quantification problems for formulations with low drug concentration such as potent drugs or low dose medications (Mitchell et al., 2009a). Therefore, the development of simpler, rapid, accurate and precise technique has gained in the importance for product development and quality control of orally inhaled products.

The glass/two-stage impinger (TSI; Ph. Eur.; Apparatus A; Figure 1-12) can be employed as an alternative to a full-stage impactor. Aerosol droplets are nebulised in the two stages of the impinger representing coarse aerosol (stage 1) and fine particle dose (stage 2), suggesting therapeutically useful aerosol (Hallworth and Westmoreland, 1987). The TSI has a number of drawbacks, particularly, the cut-off diameter for the lower stage (stage 2) is 6.4 µm (Miller et al., 1992; Holzner and Müller, 1995), rather than 5 µm, as required for determining the fine particle dose (FPD) and fine particle fraction (FPF) (EMA, 2006). In addition, the high flow rate of 60 L/min employed may cause solvent/water evaporation, resulting in inaccurate measurement of aerosol size. Thus, the TSI provides less information about aerodynamic particle size distribution than a full cascade impactor/impinger, plus presents concerns regarding the suitability of the cut-off diameter for routine analysis.

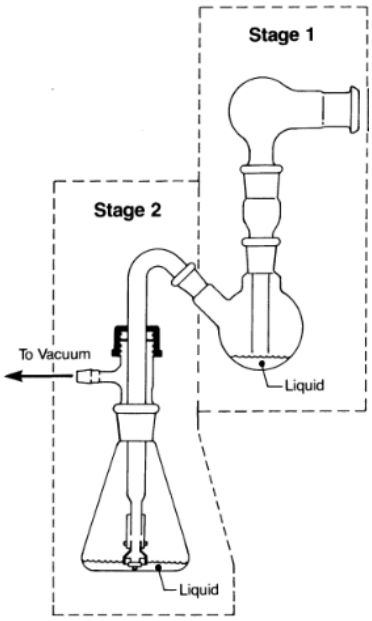

Figure 1-12 Two-stage impinger (Miller et al., 1992)

Whilst the two-stage impinger has been available for many years, it has largely fallen into disuse. Abbreviated Impactor Measurement (AIM), has not yet been included in international pharmacopoeias nor is it considered suitable by regulatory agencies. It is currently being researched as a relatively simple and quick method for aerosol analysis with improved productivity for the quality control of inhalation products. The AIM concept has commonly employed an abbreviated version of a full-stage NGI or ACI with two-size-fractionating stages of the cascade impactor and a final filter for assessing aerodynamic particle size distribution and fine particle dose of pMDIs and DPIs (Mitchell et al., 2009b; Nichols et al., 2016; Mohan et al., 2017). Currently, three abbreviated cascade impactors are available; Fast Screening Andersen (C- FSA; Copley Scientific Ltd., and T-FSA; Trudell Medical International), Reduced Next Generation Impactor (rNGI; Copley Scientific Ltd.) and Fast Screening Impactor (FSI; Copley Scientific Ltd. and MSP Corporation). All have been used to obtain APSD measurements and other quality attributes for marketed pMDIs and DPIs.

The stainless steel Fast Screening Andersen impactor (FSA, Figure 1-13) is an abbreviated version of the standard full-resolution Andersen Cascade Impactor (ACI) used for quality control and product development for pMDI and DPI

formulations. The FSA consists of two inertial size-fractionation stages (with or without internal dead space), followed by a final filter. These stages represent coarse, fine and extra-fine particle fractions. The FPD collected from the FSA is the summation of drug mass on the surface of the size-fractionation stage and those deposited on the back-up filter (Mitchell et al., 2009a; Nichols et al., 2016).

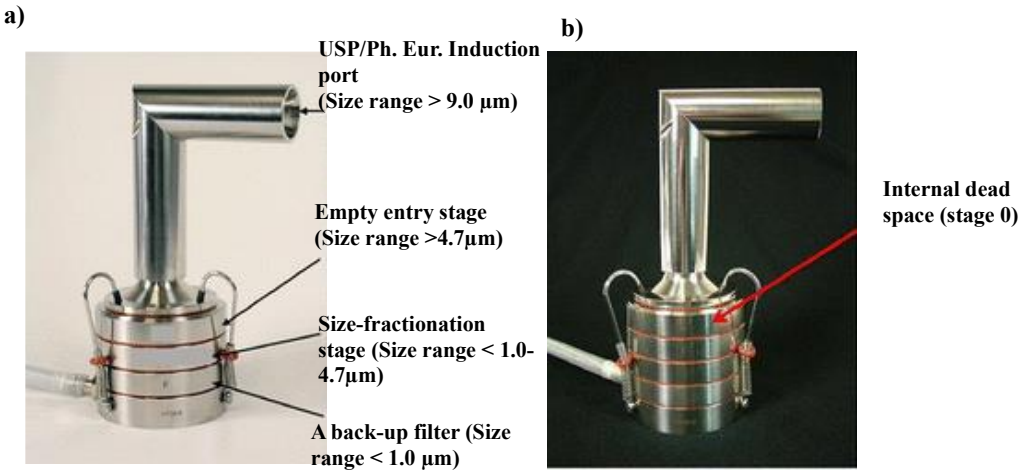

Figure 1-13 The Fast Andersen impactor a) C-FSA (without dead space) b) T-FSA (with dead space) (Nichols et al., 2016)

The reduced Next Generation Impactor (rNGI), which is an abbreviated configuration of the NGI, can be divided into two types; the-filter-only configuration (rNGI-f; Figure 1-14a) and the modified-cup configuration (rNGI-mc; Figure 1-14b). The rNGI-f employs the total internal volume of the conventional NGI, with all collecting plates in place connected to the vacuum pump. The rNGI-mc, employs a modified cup with an outlet tube attached directly to the vacuum pump, thus reducing the entire NGI internal volume. A filter is placed with a special rNGI filter holder on the top of the chosen stage for both configurations. The mass of drug deposited on all collecting plates above the chosen stage is defined as the coarse particle mass, while the mass of drug collected from the filter (i.e. on stage 3 or 4) is considered as the fine particle mass (Mohan et al., 2017).

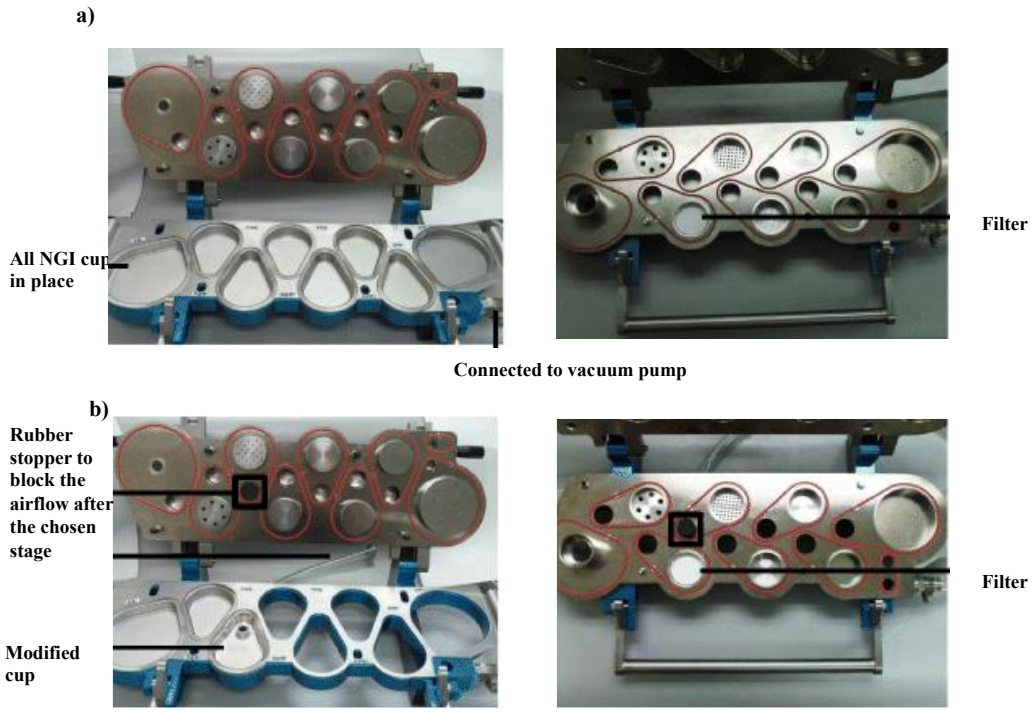

Figure 1-14 The Reduced Next Generation Impactor a) rNGI-f b) rNGI-mc (Mohan et al., 2017)

The Fast Screening Impactor (FSI, Figure 1-15), a two-stage abbreviated impactor with a cut-off diameter of 5 µm between stages and equipped with the USP induction port and a pre-separator, collects coarse particle mass or non-inhalable mass (in a pre-separator chamber) and the fine particle mass (filter). A range of inserts (Figure 1-15b) allows a 5µm cut-off diameter with flow rates between 30 and 100 L/min, allowing characterisation of DPIs and pMDIs (El-Gendy et al., 2012). It should be noted that abbreviated impactors usually use the same components as their parent-full resolution impactors. The FSI does not have a parent-full cascade apparatus; however the NGI has been previously used as the reference impactor for comparisons based on the pre-separator (Mitchell et al., 2012b).

Figure 1-15 Fast Screening Impactor (FSI), a) components of the FSI, b) additional insert and c) assembled FSI (Nichols et al., 2016)

The AIM concept which employs impactors with 2 or 3 stages may improve overall method precision by eliminating impaction stages on which small amounts of active pharmaceutical ingredient (API) which are hard to assay or on which no drug is deposited (Mitchell et al., 2009a; Mitchell et al., 2010; Guo et al., 2013). Sampling errors may be decreased by summing data from several collecting plates, particularly where the mass of active substance recovered on some stages is near to the lower limit of quantification. However, the removal of some stages from a full-cascade impactor may produce changes in APSD metrics, resulting from particle bounce, internal losses and differences in evaporation behaviour in the abbreviated impactor as demonstrated for pMDIs and DPIs (Mitchell et al., 2008). Moreover, key parameters of aerosolisation such as MMAD and GSD cannot be calculated using an abbreviated impactor (Guo et al., 2013). However, it is possible to use the relatively limited data; coarse, fine and/or extra-fine particle mass obtained using AIM apparatus (Mitchell et al., 2009a).

In terms of critical quality attributes for aerosolisation, the coarse particle mass (particle > 5µm) represents particle deposition in the throat and upper airways. The fine particle mass (particle <5 µm) represents drug particles that potentially penetrate into deep lung region, while particles smaller than 1 µm (extra-fine particle dose) have the possibility to reach the alveoli or be exhaled (Guo et al., 2013). Two metrics: the ratio of coarse particle mass and fine particle mass and the total amount of particles sized within the impactor (impactor-sized mass; ISM)

are employed in what is termed 'Efficient Data Analysis (EDA)'. The concept of EDA has been proposed as beneficial for routine quality control, allowing better decisions with respect to APSD determinations of inhaled products for quality control and batch release (Tougas et al., 2011a; Mitchell et al., 2012b; Mohan et al., 2017). However, this abbreviated apparatus should be validated on a product-by-product basis to demonstrate an equivalent performance before applying an AIM approach for routinely characterisation of inhaler product (Tougas et al., 2011a; Guo et al., 2013).

The AIM-based systems have received attention from the pharmaceutical industry and instrument manufacturers in aspects of the design of AIM-based apparatus for evaluating specific type/drug product of DPIs, pMDIs and nebulisers (Tougas et al., 2011b). For example, the stage '0' was included for T-FSA to mimic the internal dead volume of the ACI, when pMDIs containing low volatile solvents (ethanol) were characterised (Mitchell et al., 2009a; Tougas et al., 2011b). Moreover, there are few studies comparing the performance of abbreviated and their full-resolution cascade impactors for characterising inhalation products particularly pMDIs and DPIs. For example, the ability of two abbreviated CIs (C-FSA and T-FSA) was investigated for characterising pMDIs. The findings show equivalent values of coarse particle fraction (CPF), fine particle fraction (FPF) and extra-fine particle fraction (EPF) compared to a full-resolution ACI when collecting stages were coated (Mitchell et al., 2009a; Mitchell et al., 2009b). When looking at the performance of the rNGI (rNGI-mc and rNGI-f) and the full-resolution NGI for evaluating DPIs, significant differences in FPD, FPF and EDA metrics were observed for Foradil® and Relenza®. Whilst, Spiriva® yielded statistically similar data of those key parameters of aerosolisation for all three NGI configurations. Moreover, there were statistically differences in FPD for Foradil® and Relenza® obtained using the FSI and the NGI. However, FPF values for the three DPIs collected from both impactors were similar (Mohan et al., 2017). These observations were possibly due to different products and/or device resistance. Further studies are required for a better understanding of these differences.

Among three available AIM-based apparatus, FSI with the cut-off diameter of 5 µm between coarse and fine particle fractions can be used to demonstrate compliance with the EMA guideline for quality of orally inhaled products, reflecting directly to FPD and FPF calculations (5 µm). It should be noted that the use of the FSI for characterising the properties of nebulised formulations has received very little attention. Consequently, the FSI was the focus in this thesis.

1.8 Therapeutic agents used in this study and their formulation approaches

1.8.1 Erlotinib

Erlotinib, an EGFR-TKI, inhibits tyrosine kinase activity on EGFR by completing with ATP at the ATP binding site. There are three pathways downstream of EGFR involving cell regulations (Schettino et al., 2008). Thus, the blockage of EGFR signaling pathways promotes cell cycle arrest and apoptosis, and leads to the inhibition of angiogenesis and cell invasion as shown in Figure 1-16.

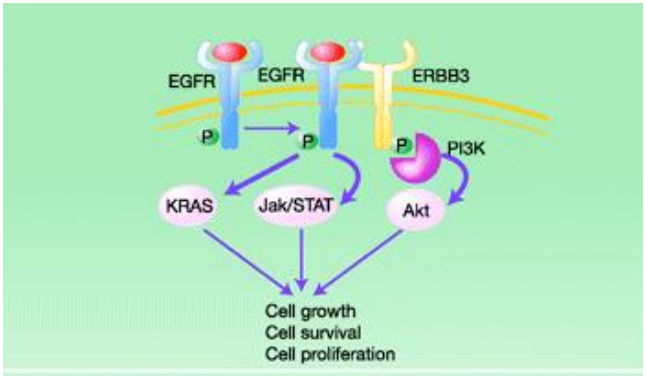

Figure 1-16 The mechanism of action of erlotinib (Hammerman et al., 2009)

Erlotinib or N-(3-ethynylphenyl)-6,7-bis(2-methoxyethoxy)quinazolin-4-amine, has low aqueous solubility and high permeability and therefore it is classified as class II in the Biopharmaceutics Classification System (BCS). Previous reports have shown that erlotinib has a pH-dependent solubility and its solubility increases with decreasing pH. The drug molecule is completely non-ionised and ionised at the pH values of 11 and 2, respectively (Tóth et al., 2016). Other physicochemical properties of erlotinib including molecular structure, molecular weight, molecular formula and log P are shown in Table 1-2.

Table 1-2 Physicochemical properties of erlotinib

Molecular structure	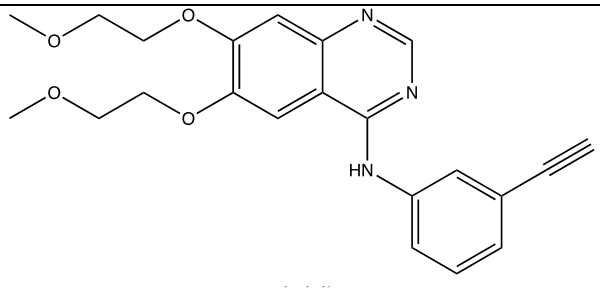
Molecular weight	393.43572 g/mol
Molecular formula	$C_{22}H_{23}N_3O_4$
Log P (octanol/water)	2.75 (Tóth et al., 2016)
pK_a	5.18 (benzylimine)
Aqueous solubility (µg/mL) at pH 6.8	3-6 (Tóth et al., 2016; Truong et al., 2016)

Erlotinib has been approved by the FDA and is available as a film-coated tablet (Tarceva®), with 60% bioavailability (Vrignaud et al., 2012). The oral absorption of erlotinib may increase when administered with food. However, food has an impact on the variability in absorption and potential side effects and thus, erlotinib is recommended to be taken on an empty stomach (Yang et al., 2017b). Erlotinib's poor solubility limits bioavailability and hence, pharmaceutical technology has been employed to improve the solubility delivery of erlotinib using various formulation strategies as shown in Table 1-3.

Table 1-3 Formulation studies for erlotinib

Delivery System	Description	Treatment	Route	Study
Lipid-based nanocarriers	Reverse micelle-loaded lipid nanocarriers containing erlotinib hydrochloride	Pancreatic cancer	-	(Vrignaud et al., 2012)
	Liposomes co-loaded with erlotinib and doxorubicin	Lung and breast cancer	Intravenous	(Morton et al., 2014)
	Erlotinib-loaded core-shell type lipid-polymer hybrid nanoparticles	NSCLC	-	(Mandal et al., 2016)
	Microparticles containing erlotinib-loaded solid lipid nanoparticles	NSCLC	Pulmonary	(Bakhtiary et al., 2017)
	Co-delivery of erlotinib and IL36 siRNA in amphiphilic lipid nanocarriers	Psoriasis	Topical	(Boakye et al., 2017)
	Erlotinib-loaded solid lipid nanoparticles	Lung cancer	Pulmonary	(Naseri et al., 2017)
	Erlotinib-loaded liposomes modified with galactosylated lipid	Lung cancer	Intravenous	(Xu et al., 2017)
	Erlotinib-loaded nanoliposomal formulation	NSCLC	Intravenous	(Zhou et al., 2018)

Table 1-3 (Cont) Formulation studies for erlotinib

Non-lipid based nanocarriers	Erlotinib-loaded poly caprolactone-polyethylene glycol-polycaprolactone PCEC) nanoparticles	NSCLC	-	(Barghi et al., 2014)
	Inclusion of erlotinib in cyclodextrin nanosponge complex	Pancreatic cancer	Oral	(Dora et al., 2016)
	Solid self-emulsifying system containing erlotinib	-	Oral	(Truong et al., 2016)
	Erlotinib-conjugated dextran-coated monocrystalline iron oxide nanoparticles	Cancer	Intravenous	(Ali et al., 2016)
	Poly (D,L-lactic-co-glycolic acid)(PLGA) nanoparticles co-loaded with erlotinib and paclitaxel	Breast Cancer	Oral	(Khuroo et al., 2018)

1.8.2 **Genistein**

Phytochemicals present in fruits and vegetables have been studied for their role in the prevention and cancer treatment in various lung cancer cell lines. In-vitro and in-vivo studies have demonstrated that the bioactive compounds present in the diet, including genistein (soybean), curcumin (turmeric) and fisetin (fruit and vegetables) produce alterations of cell cycle control, induce apoptosis, and inhibit angiogenesis and metastasis (Russo et al., 2010; Khan and Mukhtar, 2015). Consequently, the use of these dietary agents in monotherapy or in combination with chemotherapy has been gaining in interest. In the next section, the physicochemical properties of phytochemicals used in this study namely genistein and curcumin as well as their pharmaceutical formulations will be discussed.

Flavonoids, chemically classified as compounds containing a phenylchromanone structure (C_6-C_3-C_6) with at least one hydroxyl substituent, are especially promising candidates for cancer prevention (Yao et al., 2011). Genistein, the major flavonoid isolated from soybeans, has attracted a great deal attentions as an anticancer, antioxidant, antiinflammatory and antiproliferative agent (Danciu et al., 2012; Andrade et al., 2014). Genistein can modify cancer progression by increasing apoptosis through the inactivation of the Akt signaling pathway. As seen from Figure 1-17, this pathway activates NF-kB, which transcribes genes important for cell survival, invasion and metastasis. The inhibition of NF-kB also partially explains the effects of genistein on cell cycle progression and apoptosis (Kumi-Diaka et al., 2010; Shukla et al., 2015; Cai et al., 2017).

Genistein, through inhibition of the Akt pathway, has been shown to potentiate the activity of EGFR-TKIs; for example, erlotinib and gefitinib in NSCLCs. Consequently, down-regulation of Akt and NF-kB appears to correlate with the antitumour activity of EGFR-TKIs (Gadgeel et al., 2009; Li et al., 2012a; Li et al., 2012b). Genistein has therefore been used to concomitantly decrease the toxicity of chemotherapeutic agents since a lower dose of cytotoxic drug is required when used in combination.

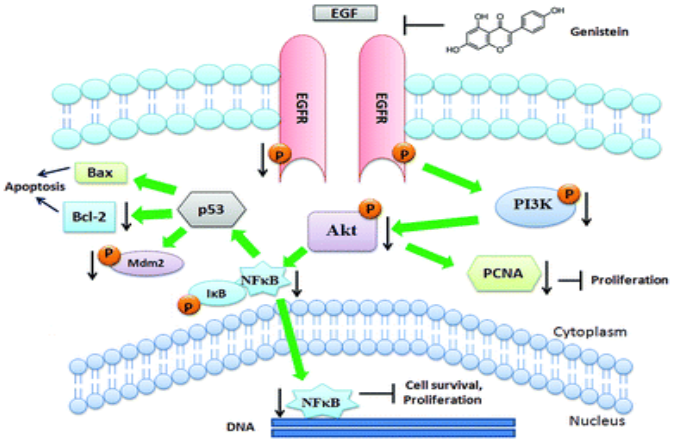

Figure 1-17 Schematic representation of the action of genistein on inhibition of EGFR signaling (Niero et al., 2014; Shukla et al., 2015)

Genistein or 5,7-dihydroxy-3-(4-hydroxyphenyl)chromen-4-one is a hydrophobic BCS class II molecule (Chen et al., 2013), having low aqueous solubility and high permeability as shown in Table 1-4.

Table 1-4 Physicochemical properties of genistein

Molecular structure	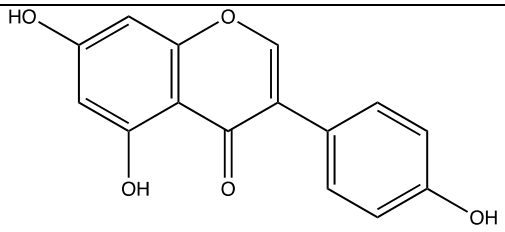
Molecular weight	270.24 g/mol
Molecular formula	$C_{15}H_{10}O_5$
Log P (octanol/ water)	2.84 (Aditya et al., 2013)
pKa	7.63, 9.67 and 10.83
Aqueous solubility (µg/mL) at pH ≈7	0.9-1.4 (Phan et al., 2013; Cai et al., 2017)

Despite its attractive therapeutic properties, the low aqueous solubility of genistein limits its potential applications (Kim et al., 2017). Pharmaceutical technology has thus been employed for the delivery of genistein, using diverse pharmaceutical formulations to improve its dissolution profile and bioavailability as shown in Table 1-5.

Table 1-5 Formulation studies for genistein

Delivery System	Description	Treatment	Route	Study
Lipid-based nanocarriers	Nanostructured lipid carriers co-loaded with genistein and curcumin	Prostate cancer	Oral	(Aditya et al., 2013)
	Genistein-loaded nanoliposomal formulation	Breast, ovarian and prostate cancers	Oral	(Phan et al., 2013)
	Genistein-loaded lipid nanocarriers	Skin cancer	Dermal	(Andrade et al., 2014)
	Genistein incorporated into nanostructured lipid carriers coated with a cationic Eudragit	Precorneal retention	Ocular	(Zhang et al., 2014b)
	Genistein-loaded solid lipid nanoparticles	-	Oral	(Kim et al., 2017)
Non-lipid based nanocarriers	Genistein-loaded pluronic micelles	-	Oral	(Kwon et al., 2007)
	Folic acid-conjugated genistein-loaded chitosan nanoparticles	Cervical cancer	-	(Cai et al., 2017)
	Genistein-conjugated gold nanoparticles	Lung cancer	-	(Stolarczyk et al., 2017)
	Genistein incorporated into beta-cyclodextrin derivatives	Anti-inflammatory	Topical	(Danciu et al., 2012)

1.8.3 **Curcumin**

Curcumin (diferuloylmethane), a natural compound extracted from the rhizome of turmeric (*Curcuma longa*), has been used in a wide range of therapeutic applications; for example, it has been shown to have antimicrobial, antioxidant, antiparasitic, antimutagenic and anticancer activity (Anand et al., 2010; Khan and Mukhtar, 2015; Tsai et al., 2015). In this research, the anticancer activity on non-small cell lung cancer was the interest. Although the mechanism of action in NSCLC is still not completely clear (Chen et al., 2016a; Shindikar et al., 2016), studies have shown that curcumin inhibits cell proliferation and induces cell apoptosis of human NSCLC through the suppression of the PI3K/Akt pathway (Jin et al., 2015; Tsai et al., 2015). Curcumin has been reported to significantly increase the cytotoxicity of erlotinib, thereby enhancing erlotinib-induced apoptosis, decreasing the expression of EGFR and inhibiting NF-kB signaling pathway in NSCLC cells (Khan and Mukhtar, 2015). In addition, this molecule has demonstrated synergistic antitumour activity in NSCLC when used with other chemotherapeutic agents such as cisplatin and adiponectin. Consequently, curcumin is one of the plant-based medicines used as an adjuvant agent in the lung cancer treatment and was chosen for investigation in this study.

Curcumin or (1E, 6E)-1,7-bis (4-hydroxy-3-methoxyphenyl)- 1,6-heptadiene-3,5-dione is considered a hydrophobic BCS class II drug (Hu et al., 2015), characterised by low solubility and high permeability (Table 1-6).

Table 1-6 Physicochemical properties of curcumin

Molecular structure	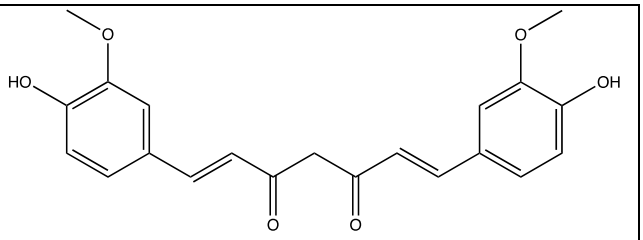
Molecular weight	368.39
Molecular formula	$C_{21}H_{20}O_6$
Log P	3.29 (Aditya et al., 2013)
pKa	8.5, 10 and 10.5 (Lee et al., 2013)
Aqueous solubility (μg/mL) at pH 7.4	0.6 (Shin et al., 2016)

Nanotechnology has been employed to produce curcumin delivery systems to improve the water solubility, absorption rate and oral bioavailability of curcumin (Table 1-7).

Table 1-7 Formulation studies for curcumin

Delivery System	**Description**	**Treatment**	**Route**	**Study**
Lipid-based nanocarriers	Curcumin-loaded nanoemulsions	Malignant glioma	Oral	(Kumar et al., 2016)
	Curcumin-loaded nanostructured lipid carriers	Anti-inflammatory	Dermal	(Chen et al., 2016b)
	Curcumin-loaded solid lipid nanoparticles	NSCLC	-	(Jiang et al., 2017)
	Curcumin-loaded liposomes	Anti-inflammatory	-	(Ng et al., 2018)
	Curcumin-loaded liposomes in liquid and dry powder form	NSCLC	Pulmonary	(Zhang et al., 2018)
Non-lipid based nanocarriers	Curcumin-cyclodextrin complexes	Lung cancer	Oral, intraperitoneal	(Rocks et al., 2012)
	Poly(amidoamine) dendrimer containing curcumin	NSCLC	-	(Wang et al., 2013)
	Curcumin-loaded methoxy polyethylene glycol-polylactide (mPEG/PLA) micelles	NSCLC	-	(Zhu et al., 2017)
	Co-encapsulation of curcumin and doxorubicin in pH-sensitive nanoparticles	Breast cancer	Intravenous	(Cui et al., 2017)

1.9 Thesis overview

Erlotinib, genistein and curcumin, all classified as BCS class II drugs, were used as therapeutic agents in this study. The therapeutic application of the three active compounds, which may be used in the treatment of non-small cell lung cancer (NSCLC), is limited due to their poor aqueous solubility. In order to overcome this, nanocarriers may be employed to improve the water solubility. No study has previously investigated the nanocarriers co-loaded with erlotinib and genistein for potential synergistic antitumour activity. Although the co-delivery of curcumin and genistein has been previously reported, the route of administration and formulation approach is different from this study. Hence, this research describes studies to explore a strategy for delivering hydrophobic anticancer drugs using polymeric micelles, by synthesizing a novel micelle-forming genistein-mPEG conjugate for the delivery of either erlotinib or curcumin. Liposomes were also investigated for the co-delivery of erlotinib and genistein by pulmonary route as an alternative formulation approach. Lipid-based nanocarriers were chosen in this study since lipid-based nanocarriers administered by pulmonary route have previously shown high accumulation and long retention time in the lungs (Garbuzenko et al., 2014).

Nebulised drug delivery has some advantages over pressurised metered-dose inhalers (pMDIs) and dry powder inhalers (DPIs), in terms of delivering large doses of drugs in an aqueous vehicle. The nebulised aerosols generated from the novel lipid-based aerosols were characterised using cascade impactor. An advantage of Abbreviated Impactor Measurement (AIM), which has been proposed for the routine quality control of inhaler products as an alternative to full impactors, is that it employs only 2 or 3 stages, representing coarse and fine particle fractions. This permits rapid, accurate quantification for low dose formulations. In this study, the Fast Screening Impactor (FSI), a two-stage abbreviated impactor with a cut-off diameter of 5 µm between stages was investigated as an alternative to the Next Generation Impactor (NGI) for in-vitro studies of nebulised liposomes. This investigation was anticipated to overcome the analytical quantification problem of drug-loaded liposomes. The properties of aerosols generated from micelles and liposomes by air-jet and vibrating-mesh

nebulisers were studied and compared using the same operating conditions using the NGI and FSI.

Ultimately, formulation strategies explored in this thesis for co-delivery of therapeutic agents may overcome some of the problems associated with hydrophobicity of drug molecules while reducing the use of excipients, and be suitable for local treatment of NSCLC via nebulisation with potential for synergistic therapeutic activity. Moreover, the use of an abbreviated apparatus will hopefully contribute to a simpler and more rapid, accurate and precise technique for aerosol characterisation of both formulations during product development, whilst the data will help inform current databases about the usefulness of AIM for characterisation of inhaler products.

1.10 Aims and Objectives

The aim of this study is to investigate new formulation approaches for the co-delivery of genistein and curcumin, and genistein and erlotinib. Determining the aerosol properties of the final formulations delivered by air-jet and vibrating-mesh nebulisers is important for demonstrating future potential therapeutic applications. To achieve these aims, the study was conducted with the following objectives:

1) To synthesise and characterise a novel genistein-methoxy poly(ethylene glycol) conjugate
2) To develop and optimise formulations of curcumin and/or erlotinib-loaded genistein-methoxy poly (ethylene glycol) micelles with potential for pulmonary delivery
3) To produce, characterise and optimise liposomes co-loaded with erlotinib and genistein with potential for pulmonary delivery
4) To investigate the FSI as an alternative impactor to the NGI for aerosol characterisation of nebulised co-loaded liposomes using the same operating conditions.
5) To investigate the effects of operating parameters on aerosol properties demonstrated using the FSI:
    I. Type of nebulisers (air-jet and vibrating-mesh nebulisers)

II. Impactor operating conditions
    - Impactor temperature (cooled and non-cooled FSI)
    - Flow rates (15 and 30 L/min)

III. Liposome size reduction methods (probe-sonication and membrane-extrusion)

Figure 1-18 outlines the flow of the research described in this PhD thesis. The project started with the synthesis and characterisation of genistein-methoxy poly (ethylene glycol) conjugate (Chapter 2). This was followed by the preparation of micellar formulations using this conjugate containing curcumin and/or erlotinib. The aerosol characteristics of these micellar systems following delivery using air-jet and vibrating-mesh nebulisers were determined using the NGI (Chapter 3). Novel erlotinib and genistein co-loaded liposomes were prepared, characterised and optimised (Chapter 4). The drug-drug and drug-lipid interaction in these systems were studied using thermal analysis (Chapter 4). The FSI as an alternative impactor to the NGI was investigated and the aerosol properties of the optimised co-loaded liposomes size reduced by probe-sonication or extrusion delivered using air-jet and vibrating-mesh nebulisers were subsequently characterised using the FSI (Chapter 5).

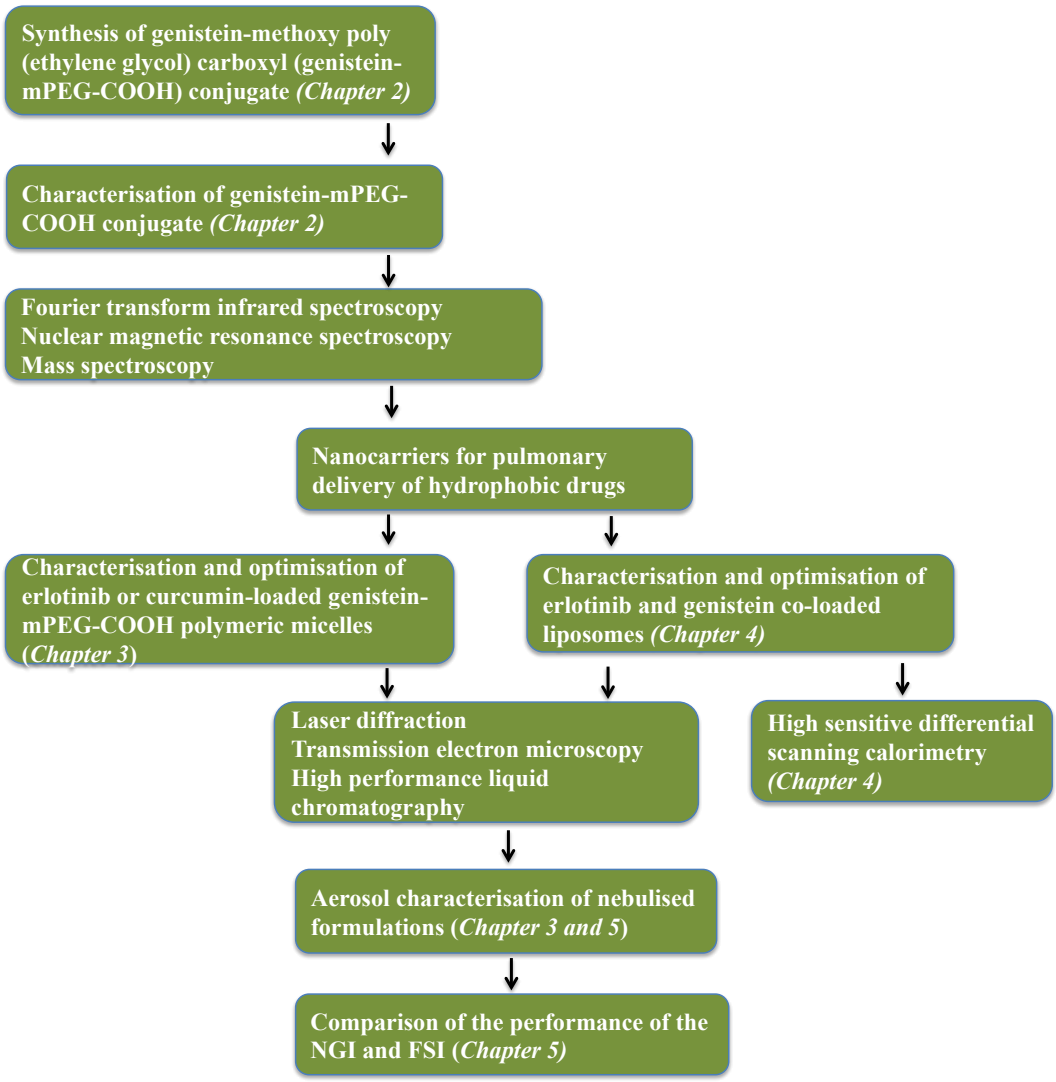

Figure 1-18 Thesis overview describing preparation, characterisation and in vitro studies of optimised micelles and liposomes prepared for pulmonary delivery of genistein, erlotinib and curcumin

Chapter 2 Synthesis of genistein-methoxy poly (ethylene glycol) conjugate

Chapter 2 Synthesis of genistein-methoxy poly (ethylene glycol) conjugate

2.1 Introduction

Previous reports have demonstrated that the conjugation of chemotherapeutic agents; for example, paclitaxel, methotrexate, doxorubicin, camptothecin and small hydrophobic drug molecules, to water-soluble polymers to form drug–polymer conjugates, provides a useful method for formulating these hydrophobic drugs (Qiu et al., 2010). Drug-polymer conjugates provide a potential strategy for improving the aqueous solubility of hydrophobic drugs, protecting the activity of drugs from metabolism or deactivation during systemic circulation, reducing the systemic side effects of potent drugs, and also enhancing passive or active targeting to the site of a drug's pharmacological action (Hans et al., 2005; Khandare and Minko, 2006). The chemical and physical properties of polymers used in conjugation should be taken into consideration in order to modify and enhance the pharmacokinetic and bio-distribution profiles compared with traditional small molecular or macromolecular drugs (Larson and Ghandehari, 2012).

A number of polymers have been studied as hydrophilic drug carriers. Methoxy poly(ethylene) glycol (mPEG) is one of the most common candidates because it is hydrophilic, non-immunogenic, biodegradable, biocompatible and non-toxic. mPEG-drug conjugates have been reported to enhance the aqueous solubility of water-insoluble drugs, improve the efficacy of therapeutic agents through the enhanced permeability and retention effect and minimise the systemic side effects by reducing non-specific cell uptake (Hans et al., 2005; Xie et al., 2009; Banerjee et al., 2012).

There are a numerous factors; for example, chemical structure, molecular weight, reactive functional group and steric hindrance that influence the outcome of conjugation of mPEG with bioactive molecules (Banerjee et al., 2012; Zhang et al., 2014d). mPEG, with molecular weight 5kDa, has been widely used for conjugation (Danafar et al., 2017) and consequently was chosen in this study.

In order to synthesize genistein-mPEG conjugate, the terminal hydroxyl group (-OH) of mPEG was converted to a carboxyl group (-COOH) via oxidation and was then attached to the –OH group of genistein through esterification.

2.2 Aims

To synthesize and characterise a novel amphiphilic polymer that might be considered as a promising compound for producing carriers for hydrophobic drugs in further studies, by conjugation of a small hydrophobic drug to a hydrophilic polymer (genistein-mPEG conjugate) through an ester linkage.

2.3 Materials

Genistein (4',5,7-trihydroxyisoflavone) (GEN, LC Laboratories, USA) and poly (ethylene glycol) methyl ether with molecular weight 5 kDa, (mPEG, Sigma-Aldrich, UK) were used as the main materials for the synthesis of the amphiphilic polymer conjugate. The following reagents and solvents were obtained from Sigma-Aldrich (UK): erbium (III) trifluoromethanesulfonate 98%, 4-dimethylaminopyridine (DMAP, 99%), N, N-dicyclohexylcarbodiimide (DCC, 99%), N, N-dimethylformamide anhydrous (DMF, 99.8%), dimethyl sulfoxide (DMSO, >99.7%, gradient grade for HPLC), anhydrous dichloromethane (DCM, 99.8%), magnesium sulphate ($MgSO_4$, >99 %), triethylamine (TEA, >99.5%), chloroform (99.8%, analytical grade), methanol (99.9%, HPLC gradient grade) and ethyl acetate (99.8%). Acetronitrile (HPLC gradient grade) acquired from Fisher Scientific (UK) and succinic anhydride (SA) supplied by Merck (Germany) were used as the solvent and the reagent in polymer synthesis. Deionised water was produced by Purelab® Ultrapure Water Purification Systems (Thermo Fisher Scientific, UK).

Silica gel 60 (0.040-0.063 mm, 99.5%) purchased from Alfa Aesar (USA) and a column with Rotaflo™ stopcock (40 mm diameter x 400 mm length) obtained from Fisher Scientific (UK) were used for the synthesized compound separation.

Deuterated chloroform ($CDCl_3$) and dimethyl sulfoxide-d_6 99.9% for ^{1}H NMR and ^{13}C NMR structural analysis were obtained from Cambridge Isotope Laboratories (USA).

2.4 Methods

2.4.1 Synthesis of methoxypoly (ethylene glycol)-carboxyl (mPEG-COOH)

Carboxylic acid end-group methoxypoly (ethylene glycol) (mPEG-COOH) was synthesized according to the method previously described (Jeon et al., 2003; Wang and Hsiue, 2005; Jeong et al., 2008; Xie et al., 2009; Xiang et al., 2011; Zhang et al., 2014a) with slight modification. Firstly, mPEG 5KDa (10 g, 2 mmol) was dissolved in acetronitrile (20 mL) with magnetic stirring at room temperature. Meanwhile, succinic anhydride (0.1480 g, 1.4790 mmol) and erbium trifluoromethanesulfonate (0.0909 g, 0.1479 mmol) as shown in Table 2-1 were dissolved separately in acetronitrile (10 mL) and added dropwise in the flask of mPEG solution. Then, the mixture solution was refluxed for 2 h at 85°C and the progress of the chemical reaction monitored by thin layer chromatography (TLC) eluted with a mixture of mobile phase as described in Section 2.4.3.1.

After the reaction was complete, the solvent was removed by rotary evaporation (RC 900, Knf Neuberger GmbH, Germany) under vacuum at 60°C for 10 min. The product, by-product, and unreacted reagents in the flask were rinsed with deionised water and transferred to a separating funnel to extract the product. After separation, the desired product was washed 3 times with a mixture of ethyl acetate and deionised water (50:50 %v/v). The separated product in an ethyl acetate layer was collected into a round-bottomed flask and all traces of water were then eliminated using magnesium sulphate ($MgSO_4$). The ethyl acetate solution was afterwards passed through filter paper (110 mm diameter, Whatman®) to remove all $MgSO_4$ clumps, and the filtrate was subsequently evaporated once by rotary evaporation at 60°C for 5 min. The mPEG-COOH product was then obtained and dried in a desiccator overnight.

Table 2-1 Components used in mPEG-COOH synthesis

Material	**Molecular weight (g/mole)**	**Molar ratio**
mPEG 5K Da	5000	1
Succinic anhydride	100.07	0.7395
Erbium triflouromethanesulfonate 10% mole	614.47	0.07395

2.4.2 Synthesis of genistein-mPEG conjugate

For the mechanism of esterification in the presence of DCC and DMAP, DCC (dicyclohexylcarbodiimide) initially reacted with mPEG-COOH. This resulted in an *O*-acylisourea intermediate. Genistein, which contains 3 –OH groups, was then added to activate –COOH group to form an ester linkage and yielded the genistein-mPEG product together with the stable dicyclohexylurea (DCU). However, DMAP, which is a comparatively stronger nucleophile than genistein, also reacted with O-acylisourea and yielded a reactive amide or active ester. This intermediate side product rapidly reacted with genistein and also produced genistein-mPEG conjugate (Gilles et al., 2015) as shown in Figure 2-1**.**

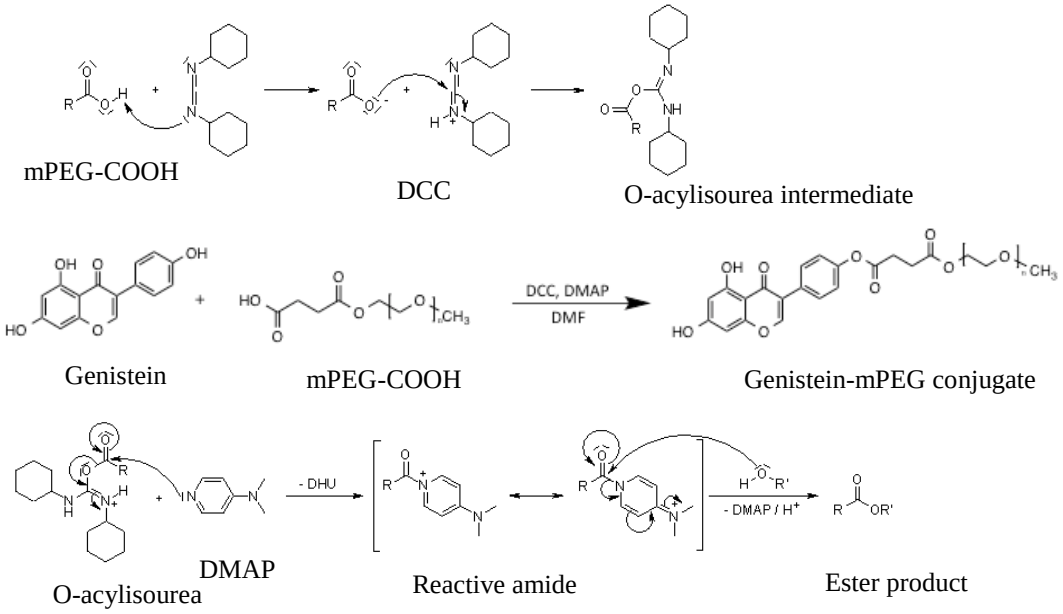

Figure 2-1 The reaction scheme for esterification in the presence of DCC and DMAP to produce the genistein-mPEG conjugate

2.4.2.1 **Development of the genistein-mPEG conjugate synthesis**

Genistein-mPEG synthesis was undertaken according to the method previously described (Jiang and Kuang, 2009; Qiu et al., 2010; Soto-Castro et al., 2010; Yeap et al., 2012; Cholkar et al., 2014) with slight modification. The synthesis of genistein-mPEG conjugate was developed by varying two main factors such as the type of solvent and the composition of genistein and mPEG-COOH in terms of mole ratio. Anhydrous dichloromethane (DCM), anhydrous dimethylsulfoxide (DMSO) and anhydrous dimethylformamide (DMF) normally used for esterification reactions in the presence of DCC and DMAP were investigated using 1:1 mole ratio of genistein and mPEG-COOH, to obtain the suitable solvent for this reaction (Jiang and Kuang, 2009; Soto-Castro et al., 2010; Yeap et al., 2012; Cholkar et al., 2014). Based on the preliminary data (Section 2.5.2.5), anhydrous DMF was the most suitable solvent and was then required for further optimisation. The mole ratio of genistein and mPEG-COOH was compared between 1:1 and 1:3 and the final ratio of 1:3 was chosen for the revised methodology of the genistein-mPEG conjugate synthesis as described in Section 2.4.2.2.

2.4.2.2 Optimised methodology of the genistein-mPEG conjugate synthesis

Briefly, mPEG-COOH (5 g, 1.0 mmol), DMAP (12.2 mg, 0.1 mmol) and DCC (247.6 mg, 1.2 mmol) were dissolved in anhydrous DMF (40 mL) with magnetic stirring for 1 h. Genistein (90 mg, 0.33 mmol) was dissolved in anhydrous DMF (10 mL) and then added to the previous solution under nitrogen with stirring for 48 h and the progress of the chemical reaction monitored by thin layer chromatography (TLC) as explained in Section 2.4.3.1. After the reaction was complete, the solvent was removed under vacuum by rotary evaporation at 60 °C in a water bath for 20 min and the product was further purified by column chromatography on a silica gel-packed column (40 mm diameter x 400 mm length) eluted with chloroform and methanol starting from 100% v/v chloroform to 80:20 % v/v chloroform: methanol.

2.4.3 Characterisation of the synthesized compound

2.4.3.1 Thin layer chromatography (TLC)

For mPEG-COOH synthesis, the solvent system for TLC using TLC plates (5x10 cm, coated with silica gel, Merck, USA) was chloroform/ methanol (70:30, %v/v) and the spray reagent consisted of sulfuric acid (Sigma-Aldrich, UK)/ethanol (VWR International Ltd., UK) (80:20, % v/v) and succinic vanillin (0.05% w/v, Sigma-Aldrich, UK).

For genistein-mPEG synthesis, the solvent system for TLC was chloroform/ methanol (90:10, % v/v) using TLC plates explained above.

2.4.3.2 Fourier transform infrared (FT-IR) spectroscopy

2 mg of mPEG, succinic acid, mPEG-COOH, genistein and genistein-mPEG were each analysed by a Perkin-Elmer Spectrum 100 FT-IR Spectrometer (Perkin-Elmer, USA) using a KBr disk for preparation of samples. Data in the wavenumber range of 400-4,000 cm^{-1} were collected at a resolution of 4 cm^{-1} with

the number of scans at 4, and presented using the Perkin-Elmer Express software (Perkin Elmer, USA).

2.4.3.3 Nuclear magnetic resonance (NMR) spectroscopy

10 mg samples of mPEG and mPEG-COOH were dissolved in 0.6 mL $CDCl_3$, and 10 mg samples of succinic acid, genistein, and genistein-mPEG were dissolved in 0.6 mL of DMSO-d_6. The spectra were obtained using an 500 MHz NMR spectrometer and data were processed using TopSpin^{TM} software 4.0 (Bruker Ltd., UK).

2.4.3.4 Matrix-Assisted Laser Desorption-Time of Flight (MALDI-TOF) mass spectrometry

MALDI-TOF mass analysis was performed using a Voyager-DE Pro mass spectrometer (Applied Biosystem, UK) equipped with a nitrogen laser (337nm, 3-ns pulse width) and time-delayed extraction ion source. 5mg samples of mPEG-COOH and genistein-mPEG were dissolved in alpha-cyno-4-hydroxycinnamic acid. The analysis was measured in positive linear mode using an accelerating voltage of 25 kV.

2.5 Results and discussion

2.5.1 Synthesis of methoxypoly(ethylene glycol)-carboxyl (mPEG-COOH)

2.5.1.1 TLC

Thin-layer chromatography (TLC) is a rapid analytical technique and commonly used in synthetic chemistry and pharmaceutical analysis, e.g. for isolating the impurities of samples, identifying individual components in a given sample, and monitoring the progress of a reaction (Khale, 2010). Different compounds in the sample move up a TLC plate by capillary action from its original spot at different rates due to two main considerations, the differences in their attraction to the stationary phase normally silica gel and differences in solubility in the mixture of eluting solvents. The mobile phase, which is a mixture of co-solvents, has less

polarity than silicon oxide (silica) due to the Si-O-H bond at the surface of the silica gel on the TLC plate. Hence, different compounds are separated due to these two main factors and reported as the total distance travelled by a component divided by the distance travelled by solvent from the original point (R_f value) (Meyers and Meyers, 2001). In general, more polar substances have stronger interaction with the silica and are adsorbed tightly on to the TLC plate, and this thus contributes to a lower R_f value compared with less polar components.

The compounds separated using TLC can be identified by several techniques; for example, physical (individual colour of compound or fluorescence of substance in short or long wavelength UV light), chemical (visualising agent needed) and biological (biodetector needed) methods (Pyka, 2014). As mPEG-COOH does not have any aromatic rings, it would not be directly detected on a TLC plate in UV light. Therefore, the spray reagent, vanillin in hot sulfuric acid, was prepared to detect the structure of hydroxyl or carbonyl or polyester compounds. The mechanism of visualisation can be explained by the electrophilic aromatic substitution of a phenol group of vanillin in the presence of sulfuric acid, resulting in the formation of a coloured compound (Johnson et al., 1977). As seen from Figure 2-2, the spot of the product, mPEG-COOH appeared at a lower position (R_f value = 0.24) compared with the starting material, mPEG (R_f value = 0.60). This suggests mPEG-COOH was more polar than mPEG due to the attachment of carboxylic group, resulting in greater retention at the silica binding sites. TLC technique was used in this study as a screening tool, the reaction was further confirmed using FT-IR and NMR (Zhang et al., 2007b).

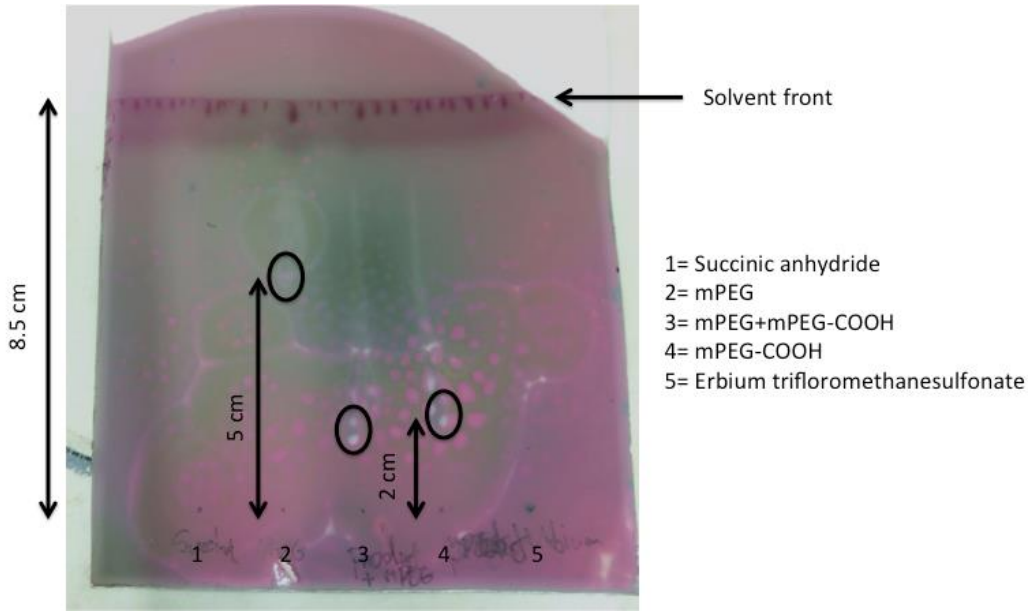

Figure 2-2 TLC plate of starting materials and product of mPEG-COOH synthesis

2.5.1.2 **FT-IR**

mPEG-COOH synthesis was confirmed using FT-IR analysis (Figure 2-3a -2-3c). The absorption bands of methylene units (-CH_2-) and ether links (C-O-C) with stretching and asymmetrical stretching vibration, which appeared at approximately 2,880 cm^{-1} and 1,100 cm^{-1}, respectively, could be observed in spectra of both mPEG and mPEG-COOH (Zhang et al., 2007b; Castillo et al., 2014; Gao et al., 2016). Furthermore, the sharp peaks at approximately 1,470, 960 and 840 cm^{-1} also demonstrated the essential polyethylene oxide backbone of mPEG and mPEG-COOH as expected (Zhang et al., 2007b; Jeong et al., 2008; Castillo et al., 2014; Danafar et al., 2017). The FT-IR data for the mPEG-COOH product exhibited all mPEG bands, whereas the FT-IR spectrum of mPEG did not show any absorption peaks in the range of 1,750-1,700 cm^{-1}. This indicated the absence of carbonyl group (C=O) in mPEG (Sant and Nagarsenker, 2011).

The FT-IR spectrum for succinic acid (Figure 2-3b) showed distinctive bands with scissoring vibration at 1,410 cm^{-1} and stretching vibration at 1,685 cm^{-1}, corresponding to the skeleton carbon (-CH_2-) and carbonyl group of carboxylic acid, respectively (Castillo et al., 2014). The characteristic carbonyl peak of succinic acid disappeared; meanwhile, a new absorption peak was detected at 1,737 cm^{-1} in mPEG-COOH. This new band, which appeared in three batches of

mPEG-COOH product, indicated the presence of the carbonyl group (C=O) of carboxylic acid with stretching vibration. Furthermore, a significant shift of 52 cm^{-1} (from 1,685 to 1,737 cm^{-1}) implied the effect of the carboxylic acid functional group being introduced to the end-hydroxyl group of mPEG due to ring-opening of succinic anhydride. The IR data were in agreement with previously reported values, supporting successful synthesis of the mPEG-COOH (Zhang et al., 2007b; Zhang et al., 2009; Zhang et al., 2014a).

Two broad peaks for the –OH groups of alcohol and carboxylic acid molecule were also expected to be present, ranging from 3,550 to 3,200 cm^{-1} (mPEG) and 3,000 to 2,500 cm^{-1} (mPEG-COOH), respectively. However, these were not detected using FT-IR. This might be because the intensity of vibrational frequencies of the 1 terminal –OH group was comparatively weaker than that of over 100 repeating units of ethylene oxide in the same IR spectrum for both polymers. Moreover, a KBr disk might not be translucent, possibly due to water in the disk and/or poorly dispersed sample. Therefore, the structure of this synthesized polymer was then further confirmed by ^{1}H- and ^{13}C-NMR.

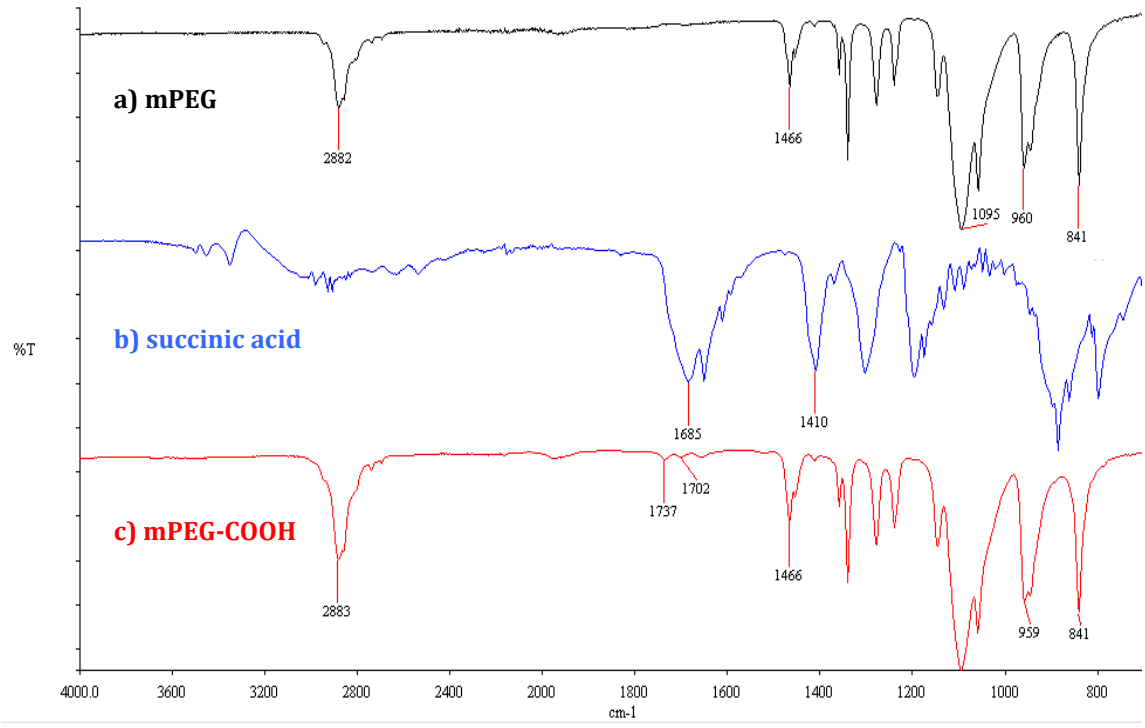

Figure 2-3 FT-IR of spectra of a) mPEG, b) succinic acid and c) mPEG-COOH

2.5.1.3 NMR

H-NMR

From Figure 2-4a - 2-4b, ^{1}H NMR spectra of mPEG and mPEG-COOH in $CDCl_3$ showed multiple peaks in the range of 3.60-3.67 ppm, corresponding to the protons of repeating units (–OC**H**$_2$-C**H**$_2$O-)$_n$. A single peak at 3.37 ppm was ascribed to the protons of the terminal methyl group (O-C**H**$_3$). The characteristic mPEG-COOH peak at 4.26 ppm was assigned to the methylene protons in mPEG adjacent to the succinyl group ($CH_2C(=O)OC$**H**$_2CH_2$) and the multiple peaks at 2.64 ppm came from the methylene proton of the succinyl group (CH_2-C**H**$_2$-COOH). A signal at 12.14 ppm in the ^{1}H-NMR spectrum of succinic acid (Figure 2-4c), which represented the protons of –COO**H**, disappeared in mPEG-COOH. All these results confirmed the existence of a carboxyl group in mPEG-COOH due to ring-opening of succinic anhydride upon reaction, and this was in agreement with the IR data (Section 2.5.1.2).

In order to determine the degree of conversion of hydroxyl group to carboxyl group, the hydroxyl moiety peak area was measured and directly compared with the areas of other peaks in the same ^{1}H-NMR spectrum (Dust et al., 1990). In this study, the integration ratio of peak area of the protons from the terminal mPEG methyl group (3.37 ppm) to the methylene protons adjacent to succinyl group (4.26 ppm) was 3:2, indicating the complete conversion of the end-hydroxyl group of mPEG into carboxyl group with the mole ratio of 1:1 (Zhang et al., 2007b; Zhang et al., 2009). This result was also in agreement with previously reported values (Ishii et al., 2005; Zhang et al., 2007b; Jeong et al., 2008; Zhang et al., 2009; Qiu et al., 2010; Wu et al., 2010; Sant and Nagarsenker, 2011; Du et al., 2012; Liu et al., 2014a; Zhang et al., 2014a; Gao et al., 2016).

a)

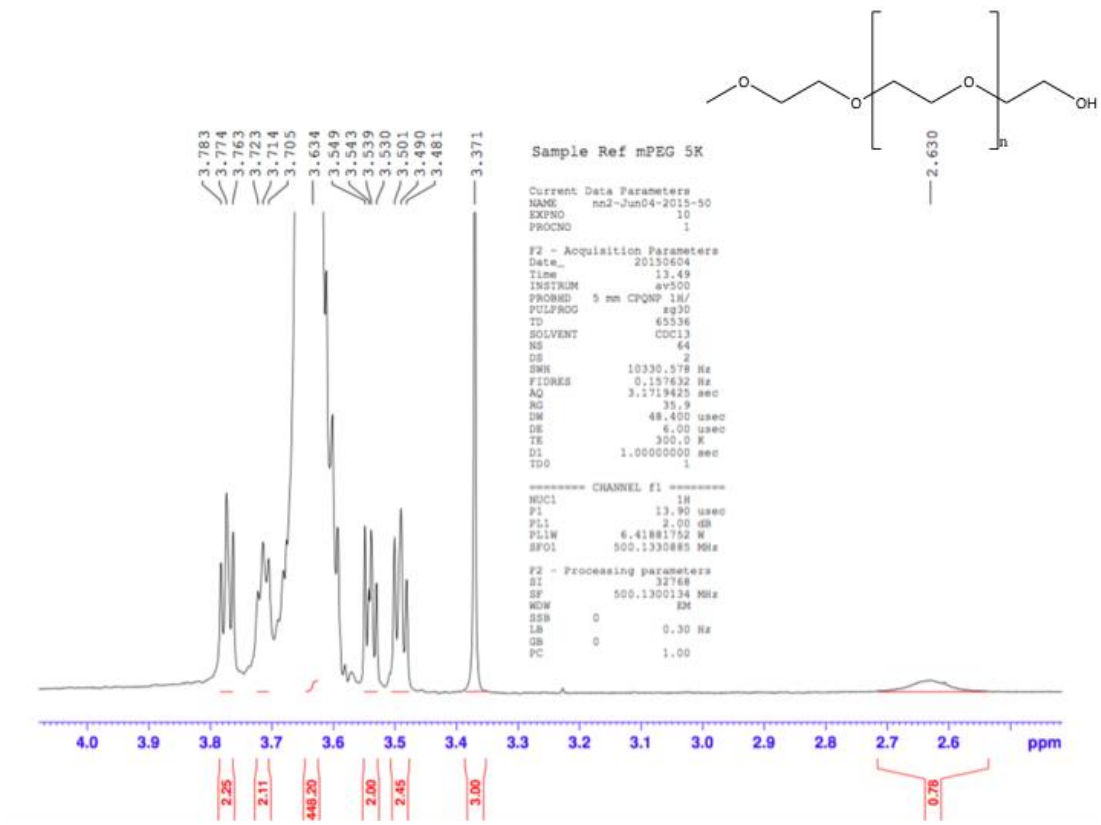

b)

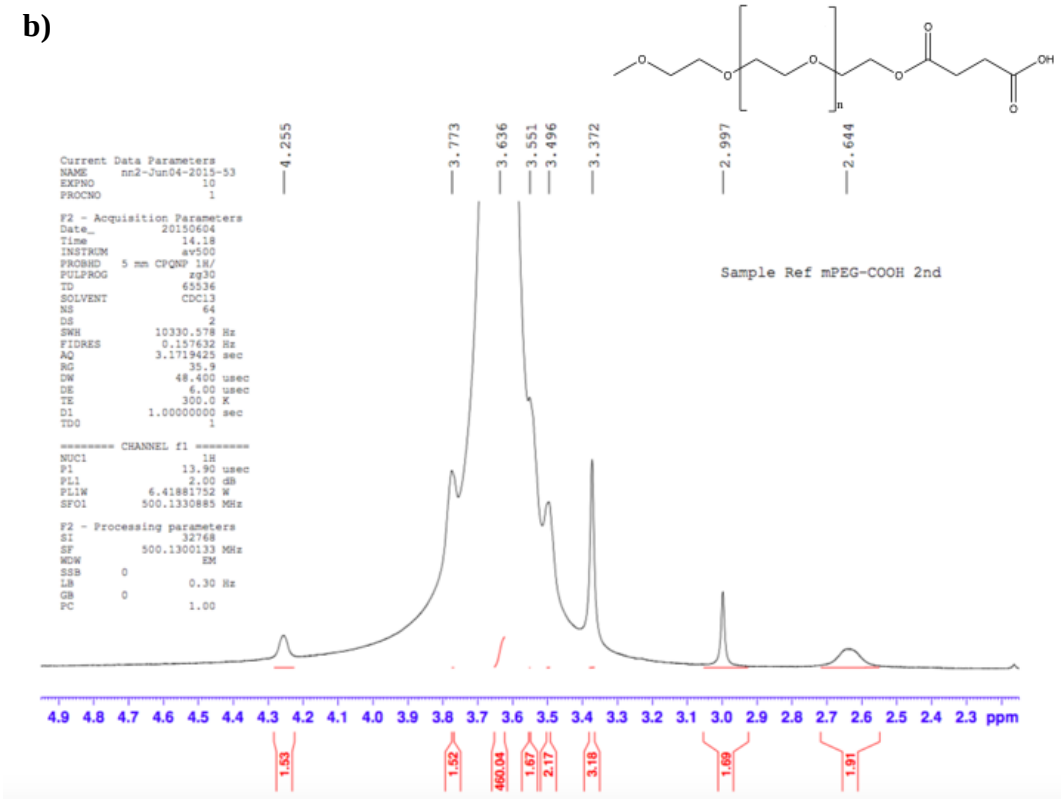

Figure 2-4 H-NMR spectra of a) mPEG, b) mPEG-COOH and c) succinic acid

c)

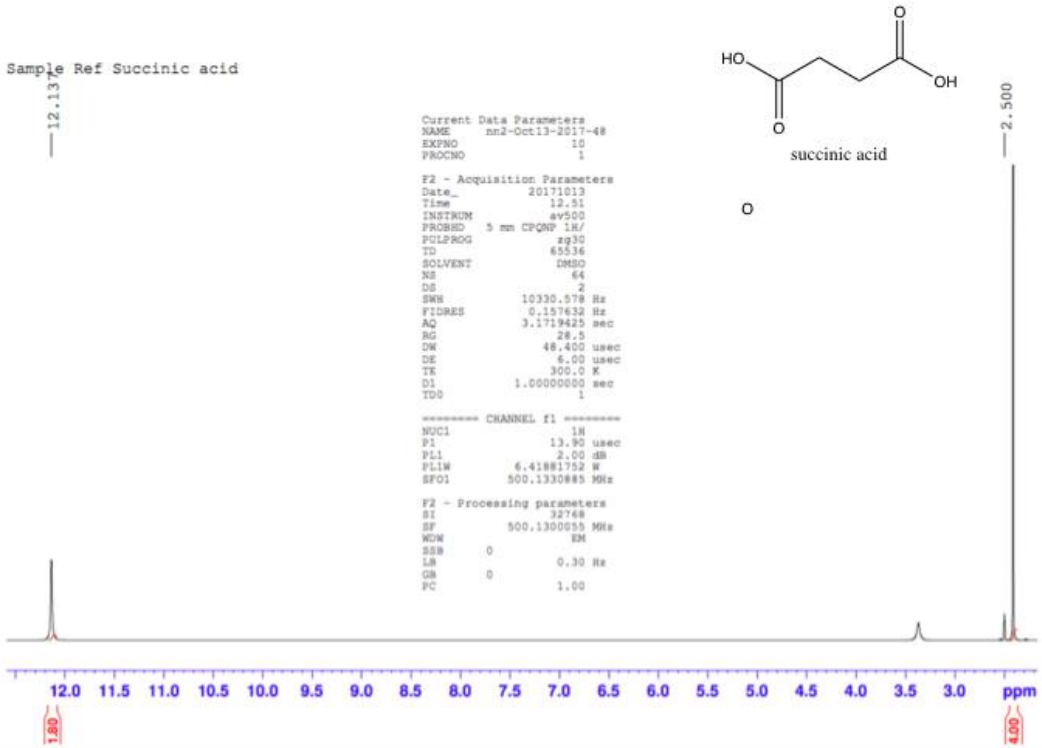

Figure 2-4 (Cont.) H-NMR spectra of a) mPEG, b) mPEG-COOH and c) succinic acid

C-NMR

As shown in Figure 2-5a, the ^{13}C-NMR spectrum of mPEG exhibited a peak at 59.21 ppm corresponding to the –O-**C**H_3 group, and a distinctive sharp peak around 70.73 ppm due to repeating units (–OC**H**$_2$-C**H**$_2$O-)$_n$. The ^{13}C-NMR spectrum of mPEG-COOH (Figure 2-5b) had a peak at 28.52 ppm ascribed to -COO**C**H_2**C**H_2COOH-. A peak, which implied the existence of the carboxyl group (-**C**OOH), appeared at 170.71 ppm in mPEG-COOH. Furthermore, there was an obvious shift in the terminal C in mPEG adjacent to –OH group (-**C**H_2OH) from 61.89 to 63.97 after succinic acid was introduced to its molecule. These values were in agreement with previous reports (Jeong et al., 2008; Zhang et al., 2009). All these combined results confirmed that a new functional group (-COOH) was successfully attached to the terminal part of mPEG.

a)

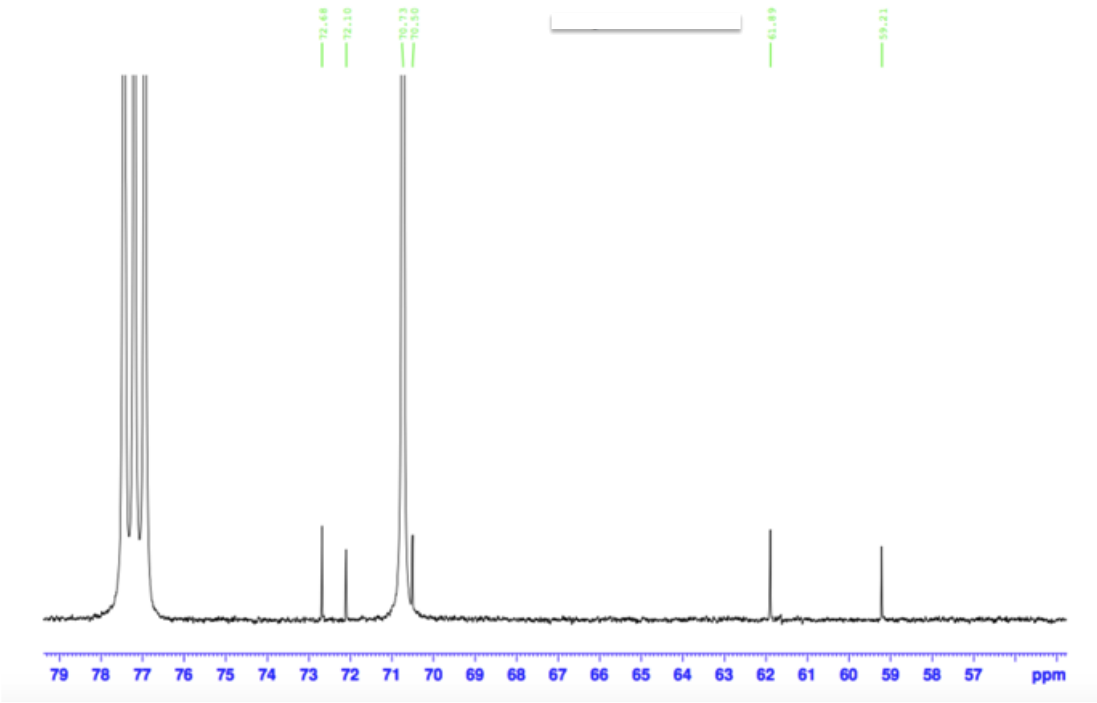

b)

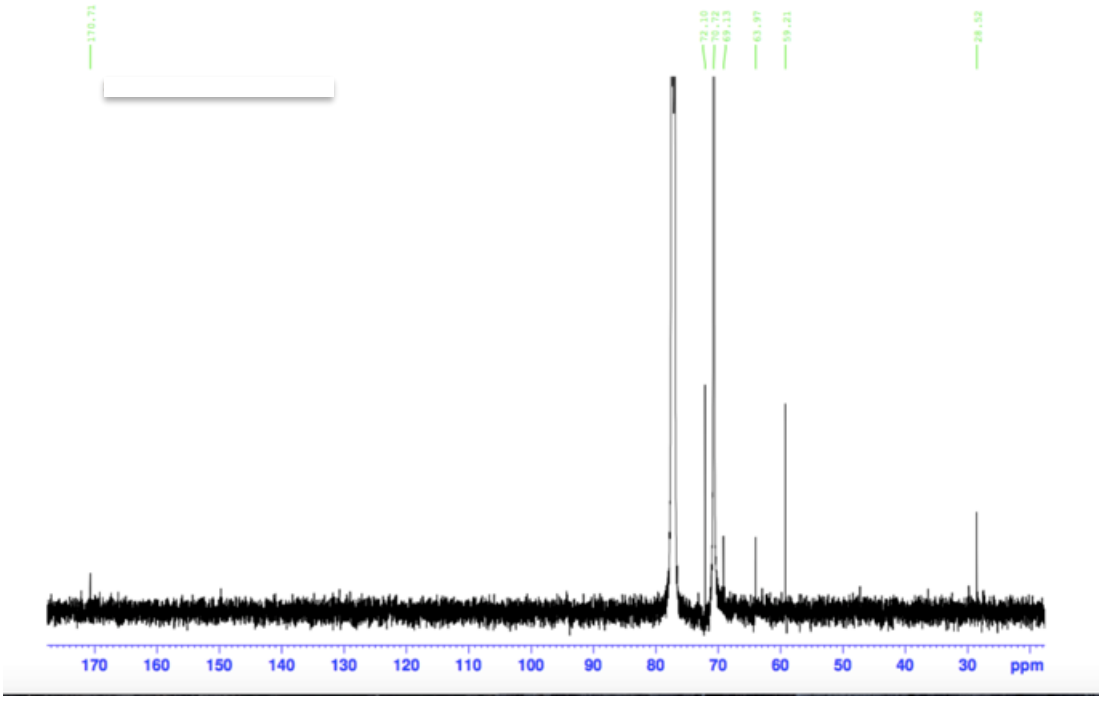

Figure 2-5 C-NMR spectra of a) mPEG and b) mPEG-COOH

2.5.1.4 Development of the mPEG-COOH synthesis

According to the procedure previously described (Jeon et al., 2003; Wang and Hsiue, 2005; Jeong et al., 2008; Xie et al., 2009; Xiang et al., 2011; Zhang et al., 2014a), mPEG-COOH can be synthesized using different methods based on the same chemical reaction, shown in Figure 2-6. The ring of succinic anhydride is opened and then introduced into the end- hydroxyl group of mPEG by a substitution and elimination reaction. The combined results of the NMR analysis demonstrated the existence of –COOH at the end of the mPEG molecule.

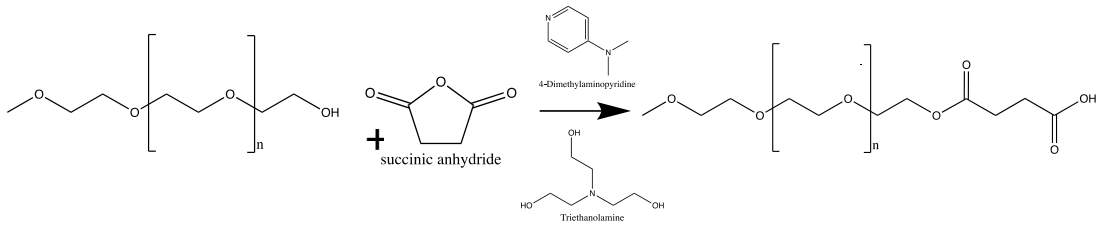

Figure 2-6 Scheme of mPEG-COOH synthesis

In general, acylation of the mPEG with excess succinic anhydride results from the presence of 4-(dimethylamino)pyridine (DMAP) and triethylamine (TEA) in an anhydrous non-polar solvent (Jeon et al., 2003; Xie et al., 2009; Chen et al., 2011; Zhang et al., 2014a; Karolina et al 2016).

1,4 dioxane and pyridine are normally used as anhydrous non-polar solvents. These are not environmental friendly and are harmful for operators. Therefore, other solvents, which are more environmental friendly, should be used as alternatives where possible. Additionally, humidity has to be strictly controlled during reactions because moisture can interfere with the reaction progress. Moreover, mPEG-COOH, which is the intermediate product for a further synthesis step, takes at least 24 h to produce by the conventional synthesis process. Hence, it would be useful to find other procedures that take a shorter time to obtain this intermediate product.

Erbium trifluromethanesulfonate ($Er(OTf)_3$ has been reported to be an efficient, non-toxic, and recyclable catalyst in several organic reactions. This effective, rapid, and waste-free method yields good results and can be done in a short

reaction time with minimal amounts of waste under almost neutral conditions, with no further requirement for a purification process (Antonio et al., 2004; Renato et al., 2009; Tran et al., 2015; Herrera Cano et al., 2016). In this study, $Er(OTf)_3$ was chosen as the catalyst to investigate the transformation of the end-hydroxyl group of mPEG to carboxylic acid. The reaction mixture was heated at reflux for 2 h at 85°C in order to reduce the reaction time compared with other conventional methods (Antonio et al., 2004). Therefore, the use of TEA and 10% mole DMAP were replaced with 10% mole of erbium trifluoromethanesulfonate in the studied reaction.

In this revised synthesis, mPEG-COOH was prepared with modifications by using mPEG, succinic anhydride and erbium trifluromethanesulfonate in the presence of acetronitrile with the lowest molar ratio (1:0.7350:0.0735) (Xie et al., 2009) to lessen the unreacted succinic anhydride which would affect the subsequent reaction step as illustrated in Figure 2-7.

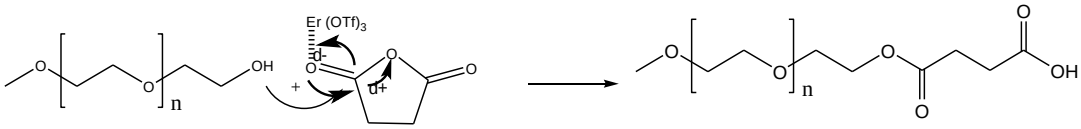

Figure 2-7 The scheme of mPEG synthesis in the presence of erbium trifluoromethanesulfonate and succinic anhydride

Over all, all the results from TLC, FT-IR, ^{1}H-NMR and ^{13}C-NMR demonstrated that mPEG-COOH was synthesized successfully using this revised methodology. This product, then, had been transferred to the subsequent reaction step.

2.5.2 **Synthesis of genistein-mPEG**

2.5.2.1 **TLC**

TLC was used to monitor and assess the completion of reactions. From the TLC plate (Figure 2-8), it can be seen that the spot produced by the product, genistein-mPEG appeared in three positions compared with all starting materials, mPEG-COOH, DCC and DMAP. This means that the product of this reaction was a mixture and required purified to obtain the final product.

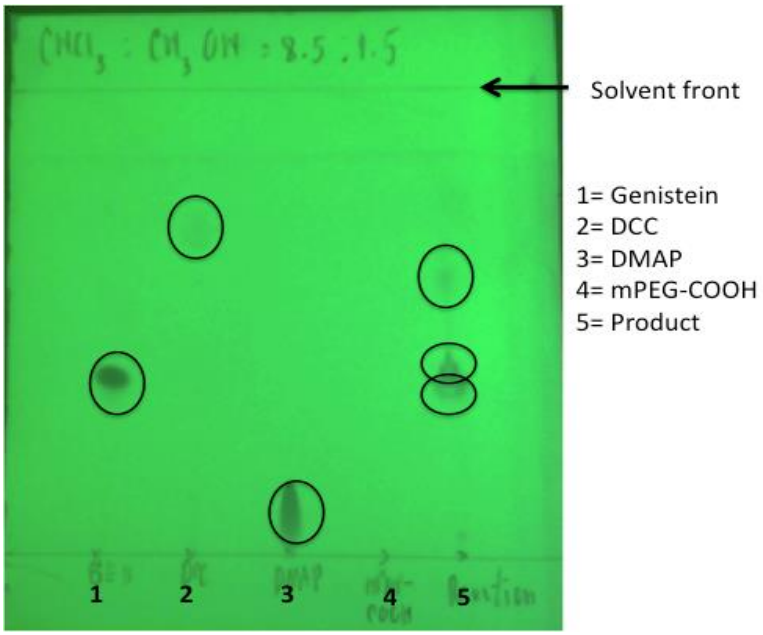

Figure 2-8 TLC of starting materials and product of genistein-mPEG synthesis

2.5.2.2 **FT-IR**

The synthesis of genistein-mPEG (Figure 2-9) was confirmed using FT-IR. The IR spectrum of genistein (Figure 2-10a) exhibited two broad bands at 3,403 cm^{-1} and 3,086 cm^{-1} due to the phenolic –OH and C-H stretching vibration, respectively. The presence of carbonyl (C=O), C-O and aromatic C=C stretching bands appeared in the range of 1,660-1,640 cm^{-1}, 1,260-1,000 cm^{-1} and 1,600-1,400 cm^{-1}, respectively**.** IR data for genistein were in agreement with previous reports (Usha et al., 2005; Crupi et al., 2007; Almahy and Alhassan, 2011; Pandit and Patravale, 2011). The FT-IR spectrum of mPEG-COOH (Figure 2-10b) showed characteristic absorption peaks at approximately 1,780 cm^{-1} corresponding to C=O, and at 2,880, 1,470, 1,100, 950 and 840 cm^{-1} ascribed to the essential polyether backbone as outlined in Section 2.5.1.2.

The absorption peaks of phenolic –OH at 3,403 cm^{-1} disappeared in the spectrum for genistein-mPEG conjugate (Figure 2-10c), implying the conjugation of the phenolic -OH group of genistein (Sojitra et al., 2010). However, the IR spectrum of mPEG-COOH also did not show any broad bands of –OH of free –COOH in that region. Thus, the attachment of –OH group of genistein to the –COOH group of mPEG-COOH could not be confirmed from this absorption peak.

Although most of the characteristic bands of genistein-mPEG conjugate (Figure 2-10c) were almost the same as those of mPEG-COOH (Figure 2-10b), there were two new absorption bands at 1,654 cm^{-1} and in the region 1,600-1,400 cm^{-1}. These two bands, which were characteristic of genistein, indicated the existence of a C=O group and the attachment of the C=C aromatic ring of genistein to mPEG-COOH upon an esterification reaction. However, the intensity of the IR absorption of these two bands was weaker than those for genistein. This might be because there was less genistein in the drug-polymer conjugate compared with a raw material of genistein. Also, the stronger absorption of mPEG-COOH could comparatively decrease the signal of genistein in the conjugate due to numerous repeating units of ethylene oxide.

Many peaks appeared in the range 1,500 – 800 cm^{-1} in the IR spectra of genistein (Figure 2-10a) and mPEG-COOH (Figure 2.10b). This would be likely to lead to either an overlap or an elimination of these functional vibrations merging into boarder bands and decreased signals for genistein-mPEG conjugate, as can be seen in the case of methotrexate in methotrexate-PEG-PAMAM conjugate (Noorzidah et al., 2012) and naproxen conjugated mPEG-PCL (Karami et al., 2016).

All these bands in FT-IR spectrum, which showed the characteristic mPEG-COOH and genistein bands together with a new peak of C=O, provide evidence of the successful conjugation of genistein to mPEG-COOH polymer. However, ^{1}H-NMR was also employed further to confirm the structure of the final product of the synthesis.

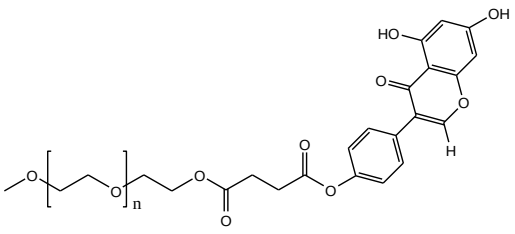

Figure 2-9 The structure of genistein-mPEG

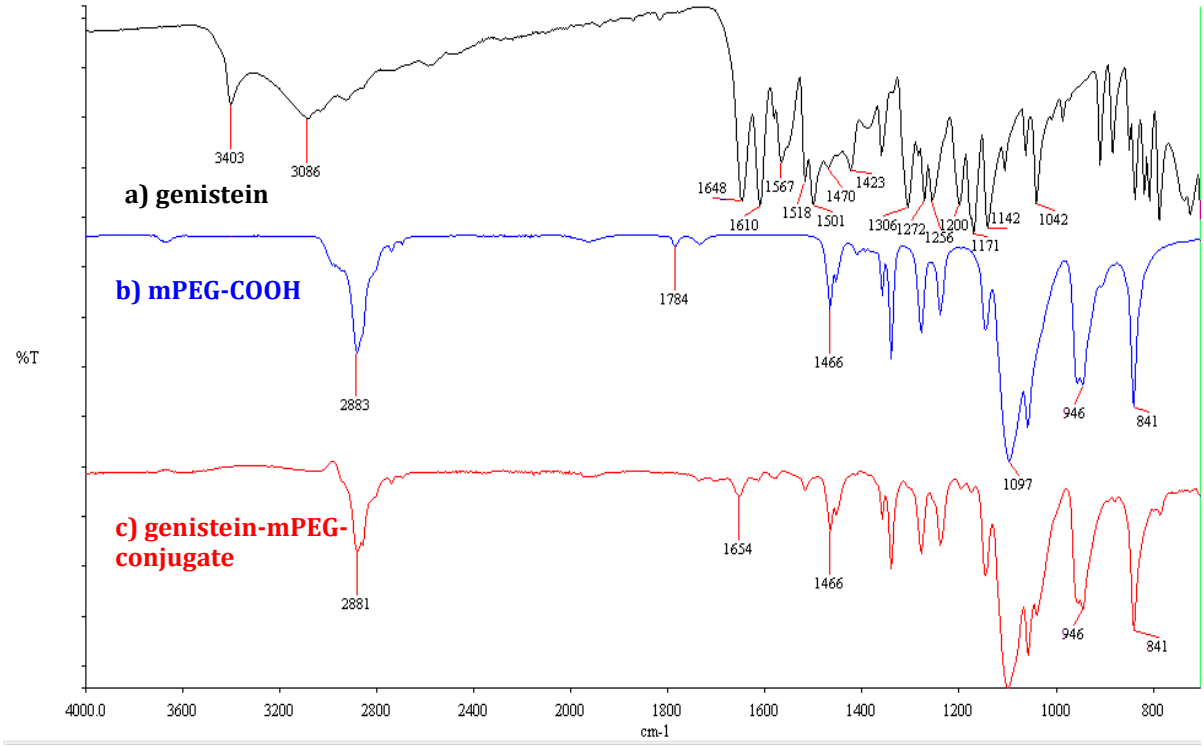

Figure 2-10 FT-IR spectra of a) genistein, b) mPEG-COOH and c) genistein-mPEG

2.5.2.3 **NMR**

H-NMR

The ^{1}H NMR spectrum of the genistein-mPEG conjugate in $DMSO_{d6}$ showed a singlet peak at 3.24 ppm due to the –O-C**H**$_3$ group and multiple peaks in the range of 3.41-3.43, 3.57-3.59 and 3.63-3.65 ppm attributed to the C**H**$_2$O unit of the mPEG-COOH molecule (Figure 2.11a -2.11b). The poly (ethylene) oxide repeating units (–OC**H**$_2$-C**H**$_2$O-)$_n$ of mPEG-COOH produced multiple bands around 3.50 ppm. The peak in the region 4.09-4.11 ppm was attributed to 2H from the $CH_2C(=O)OC\mathbf{H}_2CH_2$ group of the mPEG-COOH molecule.

Additionally, the characteristic peaks at 6.21, 6.37 and 8.31 ppm were due to 1H on the aromatic ring and the duplex peaks between 6.81-6.83 ppm and 7.36-7.38 were due to 2H on the benzene ring of genistein (Figure 2-12a - 2.12b). There were 2 singlet peaks at 9.59 and 12.95 ppm presenting the –OH groups of the genistein molecule. ^{1}H-NMR results were in agreement with previous reports for genistein molecule (Hassan and Nafisa, 2011; Pandit and Patravale, 2011; Stolarczyk et al., 2017).

When the NMR signals of genistein and genistein conjugate were compared (Figure 2-12a- 2-12b), there were slight chemical shifts corresponding to 1H and 2H on the benzene rings in the range of 6.21-8.32 ppm. Also, the characteristic –OH peak on the phenol ring at 10.87 ppm was absent in the spectrum of the conjugate, confirming the formation of the chemical bond. In addition, the integration ratio of peak area of the protons from the terminal methyl group of mPEG-COOH (3.24 ppm) to the protons from the hydroxyl group of genistein (12.95 ppm) was 3:1, indicating the complete formation of an ester linkage between genistein and mPEG-COOH. These findings allow the conclusion that genistein was successfully conjugated with mPEG-COOH with a mole ratio of 1:1 using ^{1}H-NMR analysis.

a)

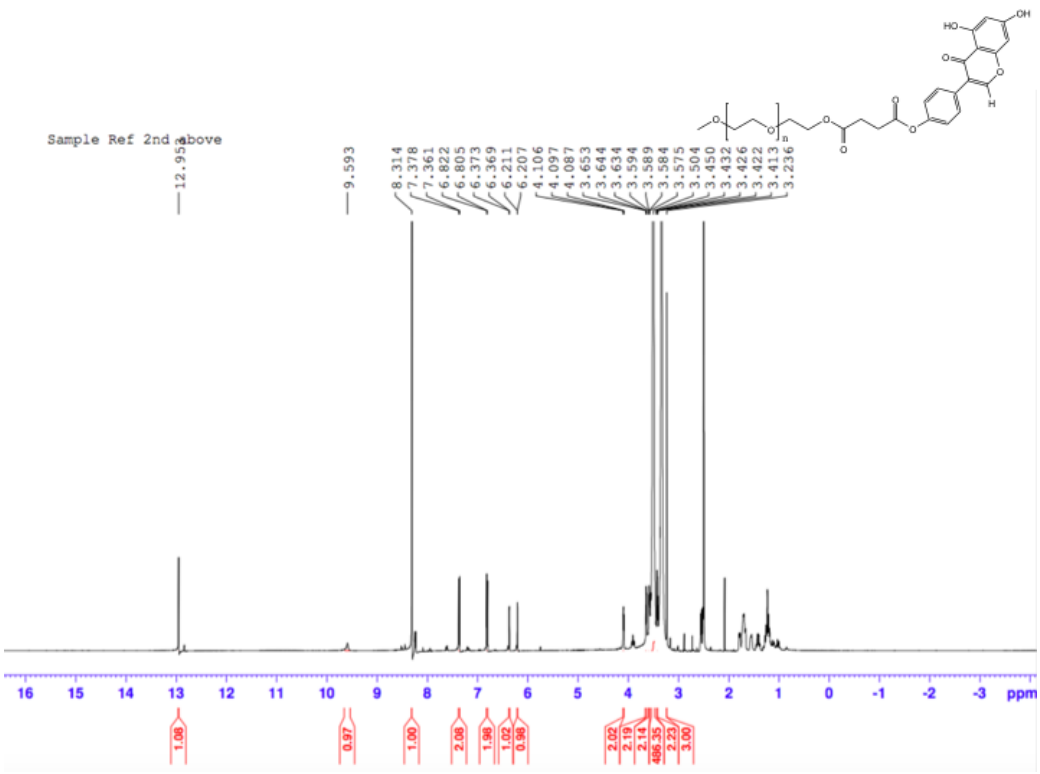

b)

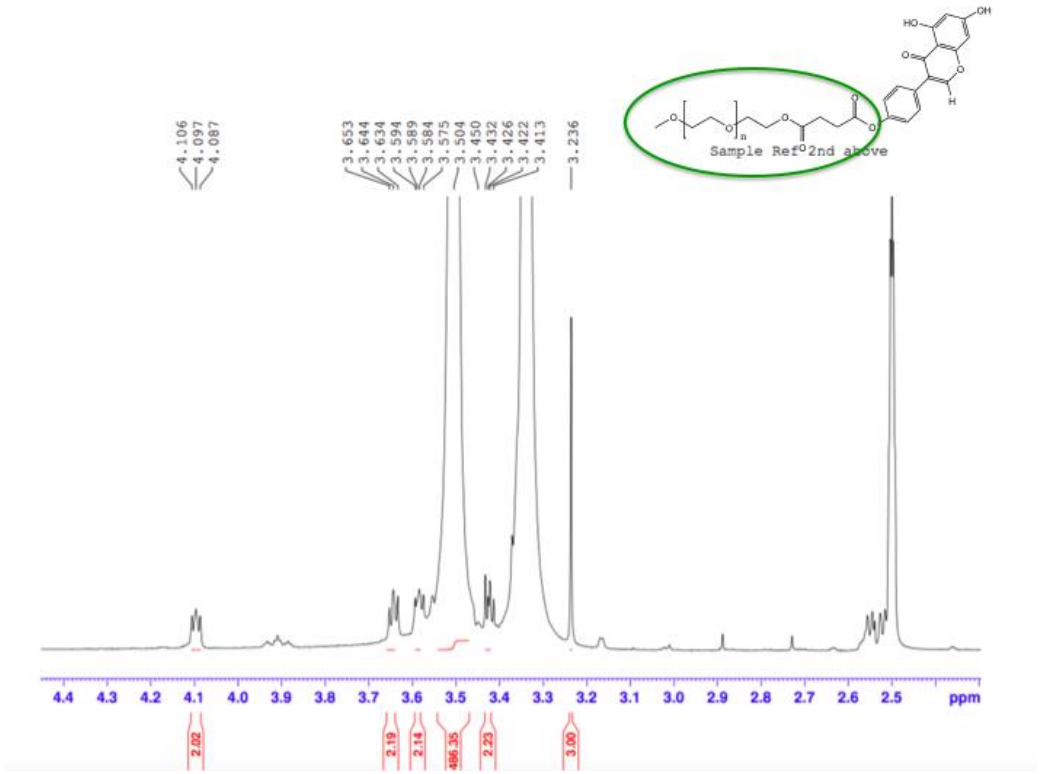

Figure 2-11 H-NMR of a) genistein-mPEG synthesis and b) mPEG-COOH component of genistein-mPEG conjugate

a)

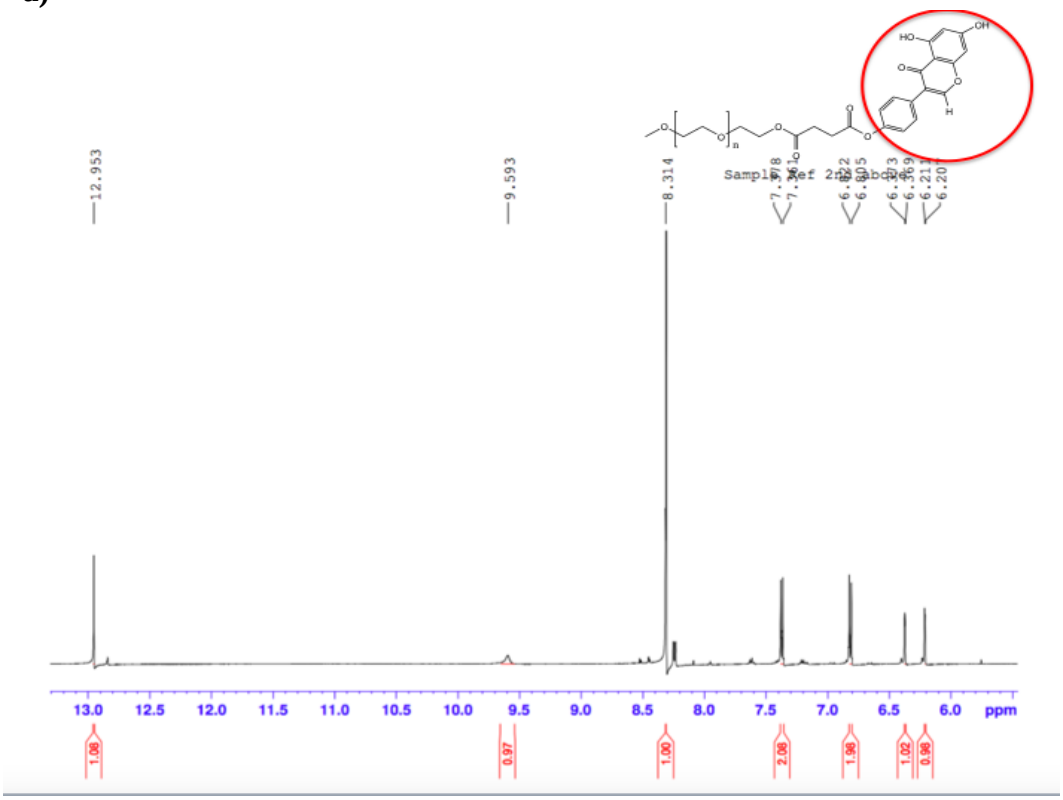

b)

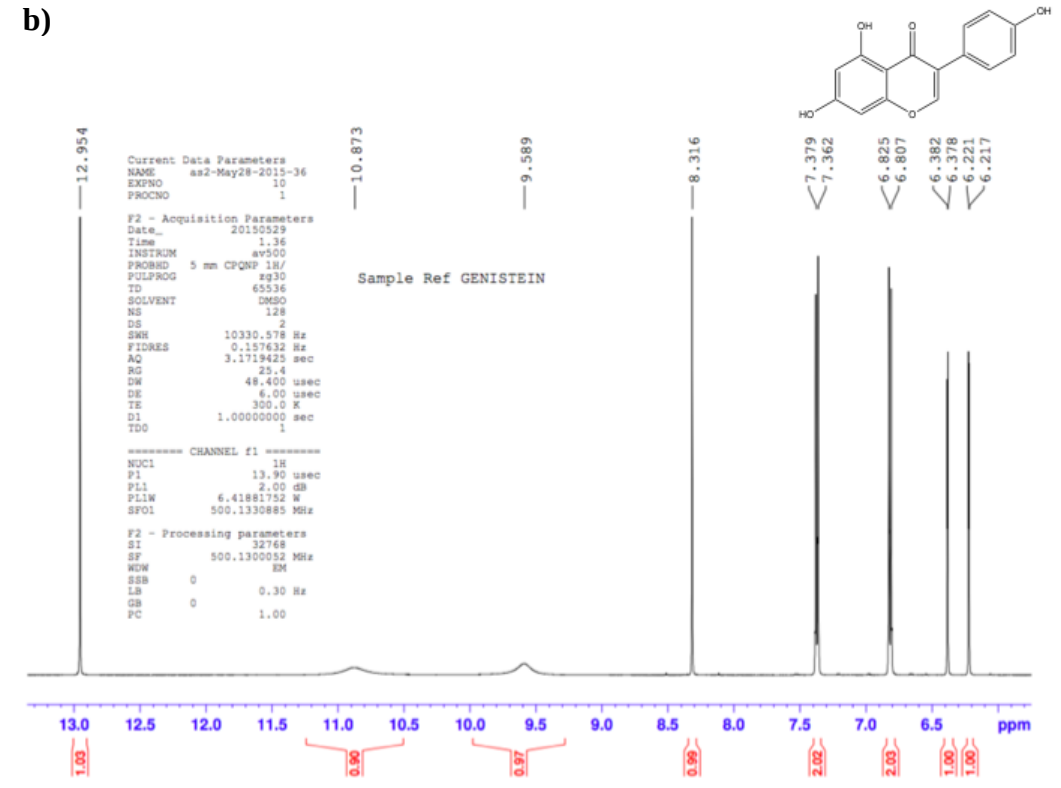

Figure 2-12 H-NMR of a) genistein component of genistein-mPEG conjugate and b) genistein

2.5.2.4 **Mass spectroscopy**

MALDI TOF analysis is one of the most useful techniques to identify molecules which have molecular weights lower than 10 KDa and for polymer analysis, allowing determination of chemical structure by analyzing the mass and the charge of ions (Riebeseel et al., 2002; Qiu et al., 2010). In this research, based on the molecular weight of the starting materials, the average molecular weight of genistein-mPEG conjugate was expected to be in the range 5,200-5,400 Da. MALDI TOF analysis showed a shift in the average mass distribution of the drug-polymer to the higher masses compared with mPEG-COOH, from 5,004.25 to 5,276.30 Da (Figure 2-13a- 2-13b**)**. The mass distribution shift of 272.05 Da, which was very close to the reported molecular weight of genistein (270.24 Da), indicated that one mPEG-COOH molecule carried exactly one genistein molecule. Thus, MALDI TOF analysis can reflect the degree of ligand loading as report previously (Ajazuddin et al., 2013; Heath et al., 2016). All the combined results from TLC, FT-IR, NMR and mass spectrometry have demonstrated that the conjugation of genistein and mPEG-COOH was successful with a mole ratio of 1:1.

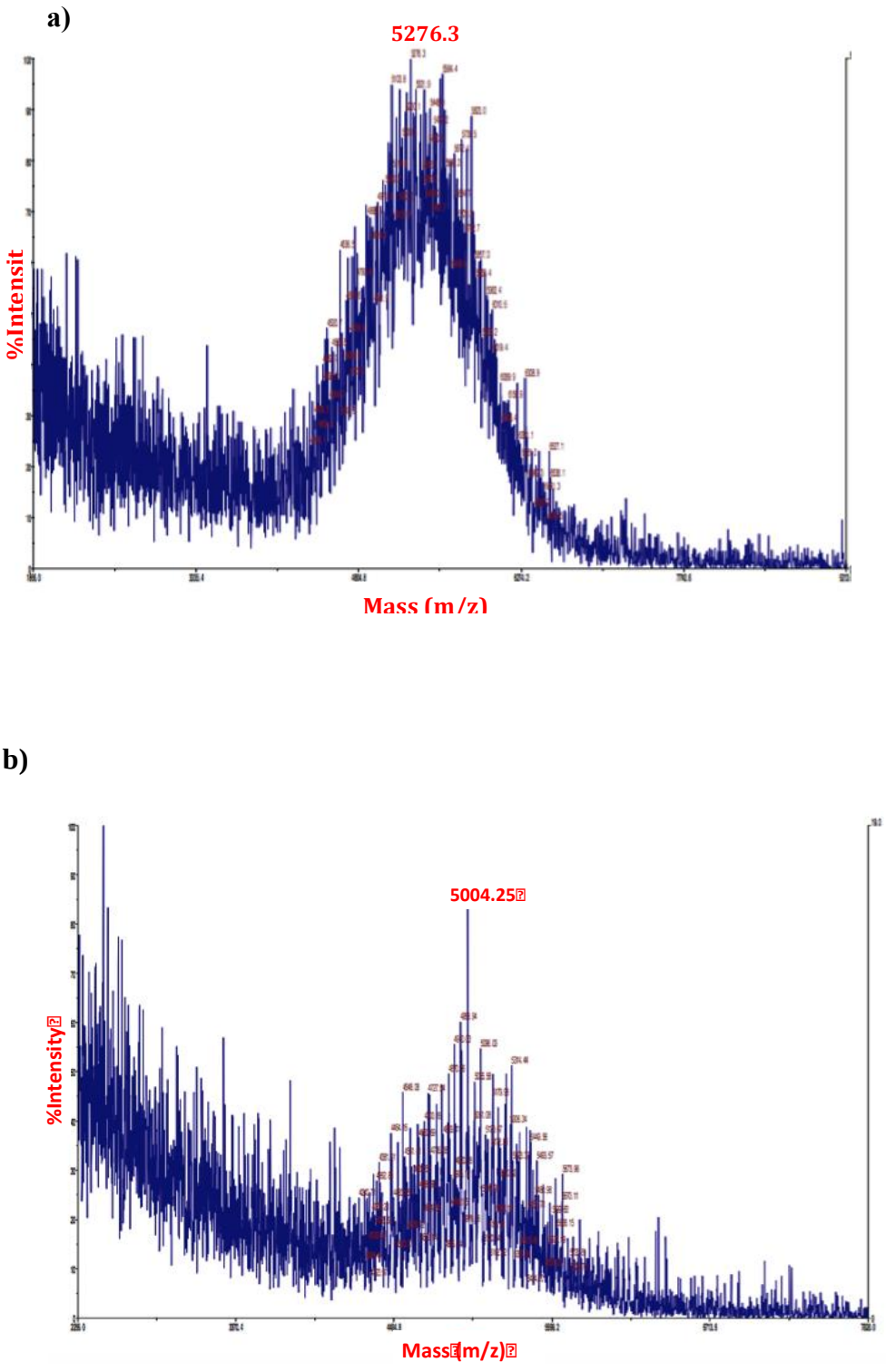

Figure 2-13 Mass spectra of a) mPEG-COOH and b) genistein-mPEG-

2.5.2.5 Development of the genistein-mPEG conjugate synthesis

For anhydrous DCM, mPEG-COOH, DCC and DMAP could be dissolved freely. However, genistein is sparingly soluble in this solvent, suggesting that anhydrous DCM might not be a suitable solvent in this case.

Anhydrous DMSO, all reagents were freely soluble, and the solution was clear before purifying the product. The boiling point of DMSO is 180°C. It, thus, cannot be removed by rotary evaporation, even when using very low pressure, indicating that this solvent was not suitable and practical for the synthesis of this conjugate. Therefore, anhydrous DMF was the next solvent investigated.

Anhydrous DMF was chosen for this reaction for two main reasons. First, all reagents dissolved freely, except mPEG-COOH, which needed heat to facilitate dissolution. Second, the boiling point of DMF is lower than DMSO and therefore, it was easier and more convenient to remove DMF by rotary evaporation. Therefore, DMF was used for the further step to obtain the optimal mole ratio of genistein and mPEG-COOH.

In terms of the molar ratio between genistein and mPEG-COOH, a ratio of 1:1 for acidic and hydroxyl compound is usually employed (Liu et al., 2014a). Initially, genistein and mPEG-COOH in the ratio of 1:1 was investigated, with TLC used to monitor the progress of the reaction. Genistein attached to at least one mPEG-COOH molecule was aimed in this study. However, there was a spot for genistein, indicating that not all of genistein molecules were incorporated into mPEG-COOH and the amount of drug used was excessive at this ratio. Due to the fact that genistein contains three hydroxyl groups (–OH) and each group can possibly carry one mPEG-COOH molecule through an ester bond, this factor may result in an insufficient quantity of mPEG-COOH in the reaction. These observations consequently led to a decrease in molar ratio of genistein and mPEG-COOH and 1:3 mole ratio of drug and polymer was subsequently further investigated.

1:1 and 1:3 ratios of genistein and mPEG-COOH were compared by the size of the genistein spot on the TLC plate. The larger the spot, the more incomplete the

reaction was. From the TLC plate, both ratios showed the spot of genistein, indicating there was still genistein residue and the reaction was incomplete. Increasing amount of mPEG-COOH was consequently suggested for further optimisation. This could be because mPEG-COOH in the first step had not yet been purified and possibly still contained a mixture of unreacted mPEG. Therefore, adding a higher amount of mPEG-COOH or reducing the mole ratio of genistein and mPEG-COOH in further studies was expected to be one of the solutions to compensate for the actual required amount of mPEG-COOH, minimise an excessive of genistein in this reaction and improve a yield of 43.7%.

2.6 Conclusion

A novel amphiphilic genistein-mPEG conjugate was synthesized via two main reaction steps: (1) the terminal hydroxyl group of mPEG was converted into a carboxylic group by reacting with succinic anhydride in the presence of erbium trifluoromethanesulfonate; (2) the end-carboxyl group of mPEG-COOH was reacted with hydroxyl group of genistein by esterification condensation with 1:3 mole ratio of genistein and mPEG-COOH through an ester linkage in the presence of DCC and DMAP.

The production of this drug-polymer conjugate obtained as a light yellow powder, was confirmed using TLC, FT-IR, ^{1}H-NMR and mass spectrometry. Consequently, this compound was then studied further for erlotinib, curcumin and other hydrophobic drugs as new nanocarriers as outlined in Chapter 3.

Chapter 3 Hydrophobic drug-loaded genistein-mPEG micelles

3.1 Introduction

The bioavailability of hydrophobic drugs used in the treatment of non-small-cell lung cancer (NSCLC) is limited by their aqueous solubility. Erlotinib has been extensively studied in patients with NSCLC, though problems with toxicity, stability and sub-therapeutic drug levels remain (Wang et al., 2012; Truong et al., 2016). Curcumin, a hydrophobic polyphenol extracted from *Curcuma longa*, has several pharmacological applications including for the treatment of NSCLC (Aditya et al., 2013; Tsai et al., 2015). Genistein, the major isoflavone isolated from soybeans, has attracted a great deal of attention as a chemo-preventive agent and has also shown synergistic activity with erlotinib in three separate NSCLC cell lines (Gadgeel et al., 2009; Tang et al., 2011). Genistein and curcumin, are both commonly used as major ingredients in Asian foods, and have been previously studied in combination for their potentiation effects including anti-cancer activity (Aditya et al., 2013). Therefore, combinations of a herbal substance and a cytotoxic drug (genistein+ erlotinib) and of two herbal substances (genistein+curcumin) were investigated in this study.

The therapeutic applications of these three compounds (all BCS class II; poorly water- soluble but highly permeable) are limited due to their low aqueous solubility (Chen et al., 2013; Hu et al., 2015; Yang et al., 2017b), consequently formulation approaches have been investigated to overcome these problems to enhance their therapeutic applications.

The treatment of lung cancer is impeded due to systemic side effects associated with current oral and injected therapies and sub-therapeutic levels of drugs at the target site. Colloidal drug delivery systems; for example, liposomes, polymeric nanoparticles and micelles, have been used as drug carriers for pulmonary delivery to improve the solubility of hydrophobic drugs, prolong their circulation time and reduce drug toxicity (Yang et al., 2015). In this chapter, the amphiphilic drug-polymer conjugate (genistein-mPEG) described in Chapter 2 will be further assessed to determine whether it forms self-assembled polymeric micelles suitable for the delivery of erlotinib or curcumin by the pulmonary route. Polymeric micelles incorporating either erlotinib or curcumin were prepared and

characterised for drug entrapment to obtain the optimal drug/polymer mass ratio and to study the effect of physicochemical properties such as the partition coefficient (log P), water solubility, melting point, molecular structure and molecular weight on the properties of the polymeric micelles formed.

Nebulised drug delivery has the advantages of delivering large doses of drugs and nano-sized delivery systems with minimal processing compared to pressurised metered-dose inhalers (pMDIs) and dry powder inhalers (DPIs). Therefore, the aerosol properties of optimised formulation delivered by two nebuliser types (air-jet and vibrating-mesh nebulisers) were determined using the Next Generation Impactor (NGI).

3.2 Aims

1. To measure the critical micelle concentration (CMC) of genistein-mPEG conjugate using dynamic light scattering (DLS) analysis

2. To study the incorporation of the hydrophobic drugs, erlotinib and curcumin, into genistein-mPEG polymeric micelles

3. To characterise and optimise curcumin-loaded genistein-mPEG polymeric micelles for potential delivery to the lung

4. To assess the aerodynamic characteristics of nebulised micelles delivered by air-jet and vibrating-mesh nebulisers using the Next Generation Impactor (NGI)

3.3 Materials

Erlotinib 99% (LC Laboratories, USA) and curcumin 95% (Alfa Aesar, USA) were used as hydrophobic drugs for solubilisation in genistein-mPEG polymeric micelles. Methanol (99.9%, HPLC gradient grade), absolute ethanol (99.8%, analytical grade) and HPLC grade water purchased from Sigma Aldrich (Poole, UK) were used as solvents in the preparation of formulations.

The following reagents and solvents obtained from Sigma Aldrich (Poole, UK): methanol (99.9%, HPLC gradient grade), dimethyl sulfoxide (DMSO, >99.7%, HPLC gradient grade), acetronitrile (ACN, 99.9%, HPLC gradient grade), HPLC grade water and trifluoroacetic acid (TFA, >99.0%) were used for the quantitative HPLC determination of curcumin and erlotinib.

3.4 Methods

3.4.1 High performance liquid chromatography (HPLC) methods for assay of erlotinib and curcumin

3.4.1.1 Chromatographic conditions for HPLC analysis of erlotinib

The analysis was conducted using a high performance liquid chromatography (HPLC) system equipped with an auto sampler and UV/Vis detector (Agilent 1100 Series, USA). A Synergi 4 µm Polar-RP 80 ºA HPLC column (250 x 4.6 mm x 4 µm) was used as the stationary phase for drug separation.

For erlotinib, isocratic elution was carried out with the mobile phase comprising a mixture of ACN and 0.1% v/v TFA in HPLC grade water (50:50 %v/v). The eluents were degassed before pumping through the column at a flow rate of 1 mL/min. The column temperature was maintained at 25 °C and the sample injection volume was 10 µL, with a run time of 10 min. The UV wavelength was set at 246 nm throughout the entire experiment. To determine the quantity of erlotinib in the genistein-mPEG micelles, it was assayed using HPLC chromatographic parameters as present in Table 3-1. The validation of the high performance liquid chromatography (HPLC method) for erlotinib according to ICH Q2 (ICH Guideline, 2005) will be described in Section 3.4.1.5.

Table 3-1 HPLC chromatographic conditions for assay of erlotinib

HPLC parameters	
Injection volume (µL)	10
UV/Vis detector wavelength (nm)	246
Mobile phase (ACN: 0.1% v/v TFA in HPLC grade water)	50:50
Column temperature (°C)	25
Flow rate (mL/min)	1
Run time (min)	10

3.4.1.2 Chromatographic conditions for HPLC analysis of curcumin

The HPLC method for assay of curcumin was developed and previously validated in our laboratory (Merchant, 2017). HPLC chromatographic parameters such as composition of the mobile phase, flow rate of the eluents and sample injection volume were the same as those used in the erlotinib HPLC assay. However, the column temperature was set at 40ºC and the UV wavelength was fixed at 420 nm, with the run time was 15 min period.

To determine the content of curcumin in the genistein-mPEG polymeric micelles, the HPLC conditions shown in Table 3-2 were employed.

Table 3-2 HPLC chromatographic conditions for assay of curcumin

HPLC parameters	
Injection volume (μL)	10
UV/Vis detector wavelength (nm)	420
Mobile phase (ACN: 0.1% v/v TFA in HPLC grade water)	50:50
Column temperature (°C)	40
Flow rate (mL/min)	1
Run time (min)	15

3.4.1.3 Preparation of HPLC calibration curve for erlotinib

A standard stock solution of erlotinib 1000 μg/mL was prepared by dissolving 10 mg of erlotinib in 5 mL of DMSO in a 10 mL volumetric flask. The sample was bath-sonicated for a few min and the volume was made up to the final volume of 10 mL. To study the linearity, serial dilutions of the stock solution were made in the range of 1- 70 μg/mL; 1, 2, 3, 4, 5, 10, 20, 30, 40, 50, 60 and 70 μg/mL.

3.4.1.4 Preparation of HPLC calibration curve for curcumin

A standard stock solution of curcumin 1000 μg/mL was prepared by dissolving 25 mg of curcumin in 20 mL of methanol in a 25 mL volumetric flask. The sample was subjected to bath sonication and diluted with the same solvent to the final volume of 25 mL. Serial dilutions of stock solution were prepared in the range of 3- 50 μg/mL; 3, 4, 5, 10, 20, 30, 40 and 50 μg/mL in order to study the linearity.

Calibration curves for erlotinib and curcumin were obtained by plotting peak area on the Y-axis against concentration of assay solution on the X-axis.

3.4.1.5 Analytical method validation of erlotinib

The HPLC method for erlotinib was validated for linearity, precision, accuracy, limit of detection and limit of quantification following the International Conference on Harmonisation (ICH Q2) guidelines.

3.4.1.5.1 Linearity

Linearity in this study was performed by taking four samples of all serial dilutions of 1, 2, 3, 4, 5, 10, 20, 30, 40, 50, 60, 70 μg/ mL from the stock solution and then injecting 10 μL of each concentration into the HPLC chromatographic system and recording the response. The degree of linearity was then determined by calculating the correlation coefficient. The slope, intercept and correlation coefficient of erlotinib were determined from the equation describing the response.

3.4.1.5.2 Precision

Precision is an expression of the closeness of individual measurement to each other or the degree of scatter. In this study, two parameters; namely the inter-day and intraday precisions were assessed. Intraday precision was performed by injecting three concentrations (8, 35 and 55 μg/mL) in triplicate per concentration onto the chromatographic system on the same day. Meanwhile, the inter-day precision was determined with those concentrations on three consecutive days. The repeatability study was undertaken by injecting the chosen concentration of 35 μg/mL 9 times to obtain the relative standard deviation (%RSD) calculated using equation Eq.3-1.

$$Precision\ (\%RSD) = \frac{Standard\ deviation}{Mean\ value} \text{ x } 100 \qquad \text{Eq. 3-1}$$

where; %RSD- percent relative standard deviation

3.4.1.5.3 Accuracy

Accuracy measures the closeness of agreement between the actual value and the value found. The accuracy study was determined by the recovery method, using a series of concentrations between 3 and 70 μg/mL for erlotinib. This analysis was

performed in triplicate for the quantification of erlotinib. Then, the percentage recovery was calculated following equation Eq. 3-2.

$$\text{Accuracy (\%RE)} = 100 - \frac{(Reference\ value - measured\ value)}{Reference\ value} \text{x}100 \qquad \text{Eq. 3- 2}$$

where; %RE- relative error

3.4.1.5.4 Limit of detection

The limit of detection (LOD) is defined as the lowest concentration of an analyte that can be detected under the prescribed conditions, but not quantified. It can be calculated using the following equation Eq. 3-3 according to ICH guidelines:

$$LOD = \frac{3.3\,\sigma}{S} \qquad \text{Eq. 3- 3}$$

where; σ = the standard deviation of the response

S = the slope of the calibration curve estimated from calibration curve

3.4.1.5.5 Limit of quantification

The limit of quantification (LOQ) is the lowest concentration of substance in a sample that can be determined with acceptable precision and accuracy under the stated operational conditions of the method. It can be calculated using the following equation Eq. 3-4 according to ICH guidelines:

$$LOQ = \frac{10\,\sigma}{S} \qquad \text{Eq. 3- 4}$$

3.4.2 Critical micelle concentration of genistein-mPEG conjugate

A stock solution of polymeric micelles was prepared by the thin-film hydration method. 50 mg of genistein-mPEG was dissolved in 20 mL of methanol in a 250 mL round-bottomed flask and then a rotary evaporator (RC 900, Knf Neuberger GmbH, Germany) was used to remove the solvent under low pressure at 150 bars for 20 min at 70 ºC, with a rotation speed of 150 rpm to produce a thin film of polymer. The resultant film was flushed with nitrogen gas to remove residual

solvent and then hydrated with 5 mL of HPLC grade water with vigorous hand-shaking and rotated on the rotary evaporator at 250 rpm for 10 min at 60 ºC in a water bath to obtain a micellar solution of 10 mg/mL genistein-mPEG. To determine the critical micelle concentration (CMC) of the conjugate, serial dilutions of the stock solution were made in the range of 10-0.078 mg/mL; 10, 5, 2.5, 1.25, 0.625, 0.3125, 0.156, 0.078 mg/mL.

The CMC was determined from the linear relationship between the intensity of scattered light and concentration (Topel et al., 2013), using the Malvern Nano ZS Zetasizer (Malvern Instruments Ltd, UK) containing a 4mW He-Ne laser, operating at 633 nm. 1.0 mL of each diluted solution was placed without further dilution into the zeta potential DTS1070 folded capillary cell (Malvern, UK), and light scattering measured at 25°C by non-invasive back scatter (NIBS) optics, at an angle of 173º, for high sensitivity and good quality of signal.

The data were plotted as scattered light intensity (the derived count rate in kilo counts per second, kcps) on the Y-axis against concentration of genistein-mPEG conjugate in HPLC grade water (in a logarithmic scale) on the X-axis. The intersection of two linearly extrapolated lines yielded the CMC value of genistein-mPEG conjugate in mg/mL.

3.4.3 Preparation of drug-loaded genistein-mPEG polymeric micelles

3.4.3.1 Preparation of erlotinib-loaded genistein-mPEG polymeric micelles

A stock solution of erlotinib (1.25 mg/mL) was prepared in a 28 mL glass vial by dissolving 25 mg of erlotinib in 20 mL of absolute ethanol. Erlotinib-loaded genistein-mPEG polymeric micelles were prepared by the thin-film hydration method as shown in Figure 3-1.

2 mL of stock solution was added to 50 mg of genistein-mPEG dissolved in 20 mL of absolute ethanol in a 250 mL round-bottomed flask. The mixture was subjected to bath sonication (Ultrawave U95 Ultrasonic Cleaner, Ultrawave Precision Ultrasonic Cleaning Equipment, UK) to ensure the complete dissolution

of drug and polymer, and solvent was subsequently removed by rotary evaporation using the conditions described in Section 3.4.2. The resultant film was flushed with nitrogen and then hydrated with 10 mL of HPLC grade water to form polymeric micelles having polymer concentration of 5 mg/mL. Freshly prepared micelles were bath-sonicated for a few minutes to aid dispersion. Then, non-incorporated drug was removed by passing once through a 0.45 μm cellulose acetate syringe filter membrane (Merck Millipore Ltd., UK), to give a filtrate of a drug-loaded micellar solution (Moazeni et al., 2012).

Empty (drug-free) micelles were also prepared using the same method in the absence of drug for comparative purposes to study the effect of drug incorporation on the properties of the polymeric micelles.

All formulations were characterised (Section 3.4.4) for mean hydrodynamic diameter, size distribution (polydispersity index, PDI), zeta potential and drug entrapment (entrapment efficiency and drug loading). The data are presented as mean values± standard deviation for triplicate experiments using three different batches.

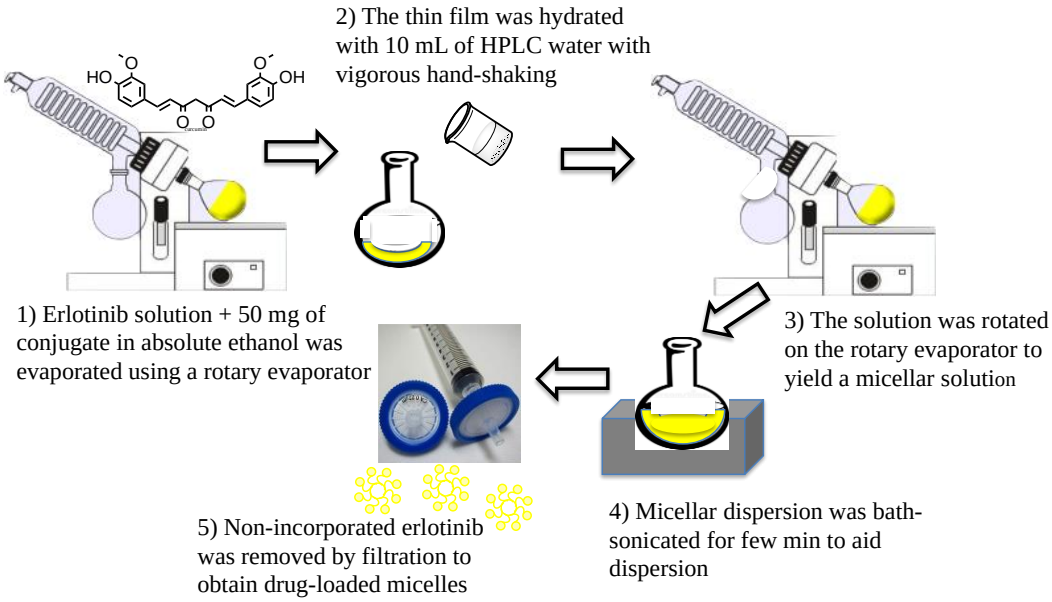

Figure 3-1 Preparation of erlotinib-loaded genistein-mPEG micelles

3.4.3.2 Preparation of curcumin-loaded genistein-mPEG polymeric micelles

A stock solution of curcumin (1.25 mg/mL) was prepared in a 28 mL glass vial by dissolving 25 mg of curcumin in 20 mL of methanol. Curcumin-loaded genistein-mPEG polymeric micelles were prepared by the thin-film hydration method under the operating conditions outlined in Section 3.4.3.1.

3.4.4 Characterisation of micellar formulations

3.4.4.1 Particle size distribution

The hydrodynamic diameter (expressed as Z-average value) and the particle size distribution (polydispersity index, PDI) were measured using the Malvern Nano ZS Zetasizer (Malvern Instruments Ltd, UK) by dynamic light scattering (DLS). 1.0 mL of drug-loaded micelles was placed undiluted into the zeta potential DTS1070 folded capillary cell (Malvern Instrument Ltd, UK), and then the hydrodynamic diameter and the size distribution of micelles undergoing Brownian motion within the aqueous dispersion were determined at 25°C in triplicate.

A PDI value < 0.1 indicates a monodispersed sample, < 0.3 is typically considered a relatively monodispersed system, whereas > 0.7 is determined as a polydispersed system (ISO-22412, 2008).

3.4.4.2 Surface charge of empty and erlotinib or curcumin-loaded genistein-mPEG polymeric micelles

For zeta potential measurements, 1.0 mL of hydrophobic drug-loaded polymeric micelles and empty micelles was measured using the Malvern Nano ZS Zetasizer and zeta potential determined based on electrophoretic mobility using the Helmholtz- Smoluchowski equation.

3.4.4.3 Drug -loading and entrapment efficiency

The content of erlotinib in micelle formulations was determined using HPLC. 1 mL of micelle solutions was diluted with DMSO to a final volume of 10 mL prior to quantification using the HPLC conditions shown in Table 3-1.

For curcumin, 1 mL of formulations was diluted with methanol to a final volume of 10 mL prior to determination by the HPLC chromatographic parameters presented in Table 3-2.

The entrapment efficiency (%EE) and drug loading (%DL) were calculated using the following equations:

$$\text{Encapsulation efficiency (\%EE)} = \frac{\text{mass of drug in micelles}}{\text{mass of drug available for encapsulation}} \times 100 \qquad \text{Eq. 3-5}$$

$$\text{Drug loading (\%DL)} = \frac{\text{mass of drug in micelles}}{\text{mass of polymer and drug}} \times 100 \qquad \text{Eq. 3-6}$$

3.4.4.4 Transmission electron microscopy

The morphology and aggregation behaviour of empty and curcumin-loaded genistein-mPEG micelles were observed using a transmission electron microscope (TEM; Philips Electron Optics BV, Netherlands). To prepare the samples for TEM, a drop of micelle solution was placed on a copper grid and the excess fluid removed with filter paper. The sample was negatively stained with a drop of uranyl acetate (1%, w/v), and left in place 2 min. The sample was then dried under ambient conditions prior to loading into the TEM.

3.4.5 Optimisation of curcumin-loaded genistein-mPEG micelles

The incorporation of curcumin into genistein-mPEG polymeric micelles was varied to identify the optimal drug/polymer concentration (as % w/w). To prepare different initial concentrations of curcumin-loaded micelles (2.5%, 5%, 10% and 20% w/w drug in polymer); 1, 2, 4 and 8 mL of stock solution of curcumin (1.25 mg/mL) were directly pipetted into 50 mg of genistein-mPEG dissolved in 20 mL of methanol. The method for preparing polymeric micelles having polymer

concentration of 5 mg/mL was as described in Sections 3.4.2 and 3.4.3. The final preparations were characterised for mean hydrodynamic diameter and polydispersity index (Section 3.4.4.1), zeta potential (Section 3.4.4.2) and drug entrapment (Section 3.4.4.3) in each experiment making three independent measurements.

3.4.6 Mass output and time to dryness for various fill volumes delivered from air-jet and vibrating-mesh nebulisers

2, 4 and 8 mL of HPLC grade water were directly pipetted into a pre-weighed air-jet nebuliser (Pari LC® Sprint Reusable nebuliser, PARI Medical Ltd, UK). The compressor (Pari TurboBoy, PARI Medical Ltd, UK) produced a medium flow rate of 4.0-6.0 L/min through the air-jet nebuliser reservoir (Kendrick et al., 1997; Dennis et al., 2008). Fluid was nebulised to dryness, with hand tapping of the nebuliser to maximise the mass output.

For the vibrating-mesh nebuliser (Pari Velox®, PARI Medical Ltd, UK), 2, 4 and 6 mL of HPLC water were placed in the reservoir and nebulisation was commenced and continued to dryness. The differing fill volumes of water for these two devices were based on their minimum and maximum fill volumes.

The nebulisation time to dryness (min) for both nebulisers was recorded after aerosol generation ceased completely. After that, the nebuliser was weighed to determine the weight or mass of residual volume. Aerosol mass output (%) was calculated for the different fill volumes using Equation 3-7.

$$\text{Aerosol mass output} = \frac{\text{Weight difference of nebuliser before and after nebulisation}}{\text{Weight of fluid placed into the nebuliser reservoir}} \text{x}100\% \quad \text{Eq. 3-7}$$

3.4.7 Comparison of aerosol properties of nebulised curcumin micelles using the Next Generation Impactor (NGI)

The NGI (Copley Scientific, UK) was set up according to the requirements of European Pharmacopoeia (Ph. Eur. 9.0, 2017, *Section 2.9.44 Preparations for nebulization characterization*), after cooling the impactor at 2-8ºC for at least 90

min to prevent water evaporation during use. The air-jet and vibrating-mesh nebulisers with mouthpiece adapter were connected to the induction port, and the NGI was attached to the vacuum pump (Copley Scientific, UK). The air-flow rate generated by the Pari TurboBoy compressor was monitored using flow meter (Copley Scientific, UK) at 15 L/min which represents the midpoint flow of tidal breathing for adult (Abdelrahim and Chrystyn, 2009). The removable cups of the NGI did not require coating with silicone as for dry powder inhaler characterisation (Abdelrahim and Chrystyn, 2009). A microfibre back-up filter (7 mm diameter Grade GF/D, Whatman®, UK), recommended by previous studies, was placed after the Micro Orifice Collector (MOC, which is the final stage in the NGI), to retain the smallest aerosol droplets when the NGI is operated at 15 L/min (Abdelrahim and Chrystyn, 2009). 4 mL of optimised curcumin-loaded micelles (containing curcumin at a concentration of 114.01 µg/mL, based on encapsulation efficiency of curcumin-loaded polymeric micelles at 5% w/w drug in total conjugate (45.60% EE; Table 3-5)) was placed in both nebuliser reservoirs and nebulisation continued for 10 min based on the results of time to dryness for 4 mL fill volume of water using an air-jet nebuliser. This was to compare the performance of these two devices for delivering curcumin-loaded micelles under the same operating conditions.

Deposited material was collected by rinsing with methanol from the nebuliser reservoir, induction port, NGI collection cups and the back-up filter. All collected samples were made up to fixed volumes for HPLC assay. The curcumin deposited on the induction port, all NGI stages, internal filter and that still remaining in the nebuliser was quantified by HPLC analysis (Section 3.4.1.2). Mass balance, Emitted Dose (ED), Fine Particle Dose (FPD) and Fine Particle Fraction (FPF) were calculated as follows:

$$\text{Mass balance (\%)} = \frac{\text{Mass of drug from nebuliser to filter}}{\text{Mass of drug initially placed into the nebuliser}} \text{x } 100 \qquad \text{Eq. 3-8}$$

$$\text{Emitted Dose (\%ED)} = \frac{\text{Mass of drug from induction port to filter}}{\text{Mass of drug from nebuliser to filter}} \text{x } 100 \qquad \text{Eq. 3-9}$$

Fine Particle Dose (FPD) = Drug mass less than 5 µm determined from the plot of cumulative mass of active substance versus cut-off diameter.

Fine Particle Fraction (FPF) = Percentage cumulative fraction of drug less than 5 µm from the plot of cumulative fraction of active substance versus cut-off diameter.

3.4.8 Statistical analysis

All measurements were carried out in triplicate and the data are presented as the mean ± standard deviation. Comparison of the data from two groups or more was statistically analysed by Student's t-test and analysis of variance (ANOVA) followed by Tukey's post hoc test, using SPSS Statistic 22 Software. A *p* value of < 0.05 was considered significant.

3.5 Results and discussion

3.5.1 HPLC assay for the quantification of erlotinib and curcumin

3.5.1.1 HPLC chromatogram of erlotinib and erlotinib-loaded genistein-mPEG polymeric micelles

Figure 3-2 and 3-3, show the chromatograms of erlotinib and erlotinib-loaded genistein-mPEG micelles in DMSO using the erlotinib HPLC assay. The peak for DMSO (solvent font) occurred at a retention time of approximately 3 min for both chromatograms. For erlotinib, the symmetrical chromatogram appeared at the retention time of 4.57 min (Figure 3-2). Two peaks appeared at different retention times of approximately 4.57 and 5.79 min were due to erlotinib and genistein-mPEG, respectively (Figure 3-3). This indicated that neither the drug-polymer conjugate nor DMSO would interfere with quantification of erlotinib. The run time for the HPLC analysis of erlotinib was set at 10 min based on these HPLC chromatograms.

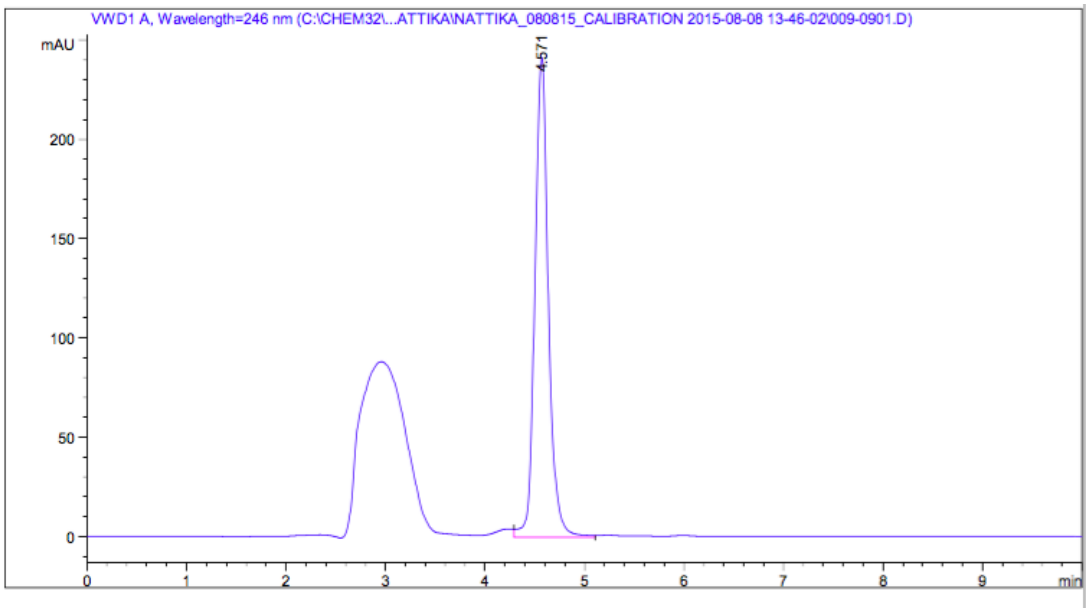

Figure 3-2 HPLC chromatogram of erlotinib in DMSO

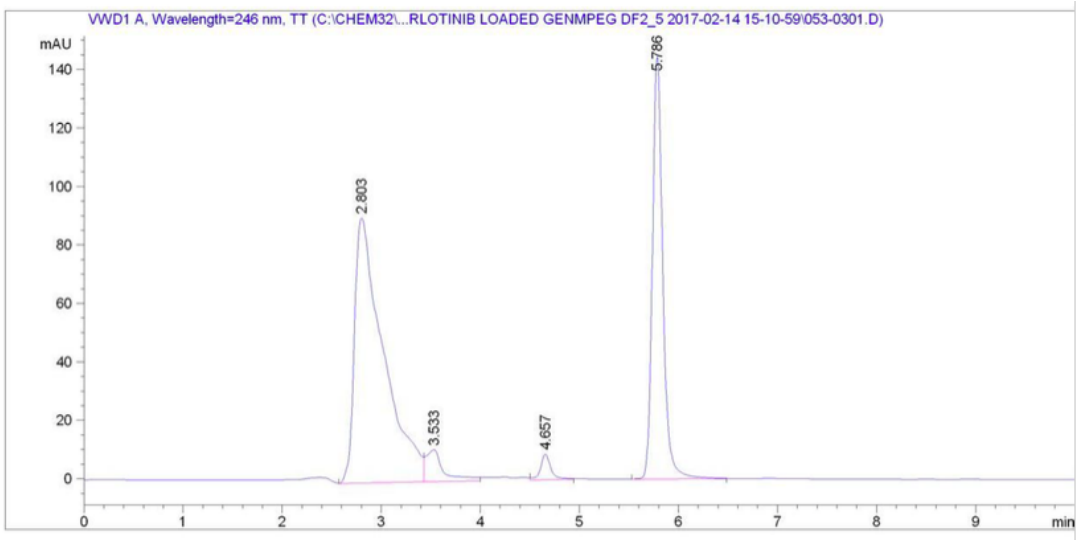

Figure 3-3 HPLC chromatogram of erlotinib-loaded genistein-mPEG polymeric micelles dissolved in DMSO

3.5.1.2 HPLC chromatograms of curcumin and curcumin-loaded genistein-mPEG polymeric micelles

Commercial grade curcumin contains not only curcumin, but also approximately 10-20% of desmethoxycurcumin and less than 5% of bisdesmethoxycurcumin as shown in Figure 3-4 (Sharma et al., 2005). The HPLC chromatogram of curcumin

(Figure 3-5) exhibited three peaks comprising curcumin and its derivatives with good peak resolutions. The major peak appeared at a retention time of approximately 10.54 min was ascribed to curcumin, whereas the two minor peaks corresponding to bisdemethoxycurcumin and demethoxycurcumin presented at retention times of approximately 8.99 and 9.73 min, respectively. A solvent peak of methanol was detected at approximately 2.95 min. This was in a good agreement with previous reports; using similar conditions for the HPLC analysis of curcumin (Mollaei et al., 2013; Fonseca-Santos et al., 2016). Genistein-mPEG was not detected under the same HPLC conditions (Figure 3-5 and 3-6), ensuring that genistein-mPEG conjugate will not interfere the quantitative result of curcumin throughout the further studies.

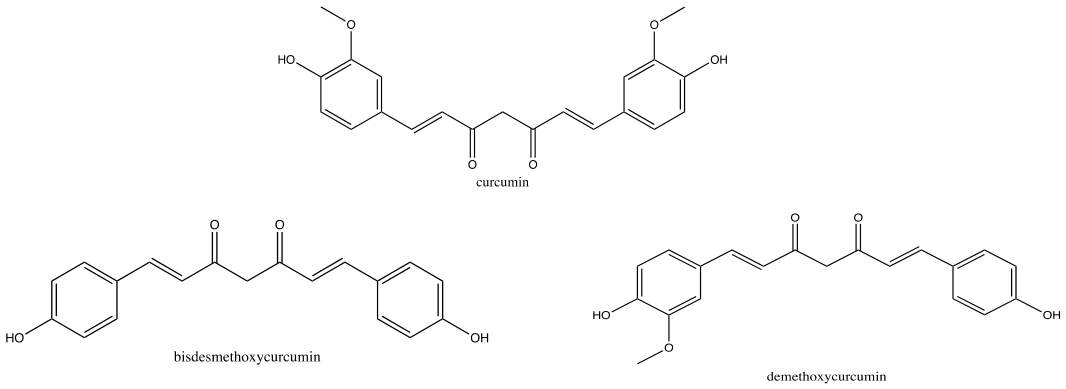

Figure 3-4 The structure of curcumin and its derivatives

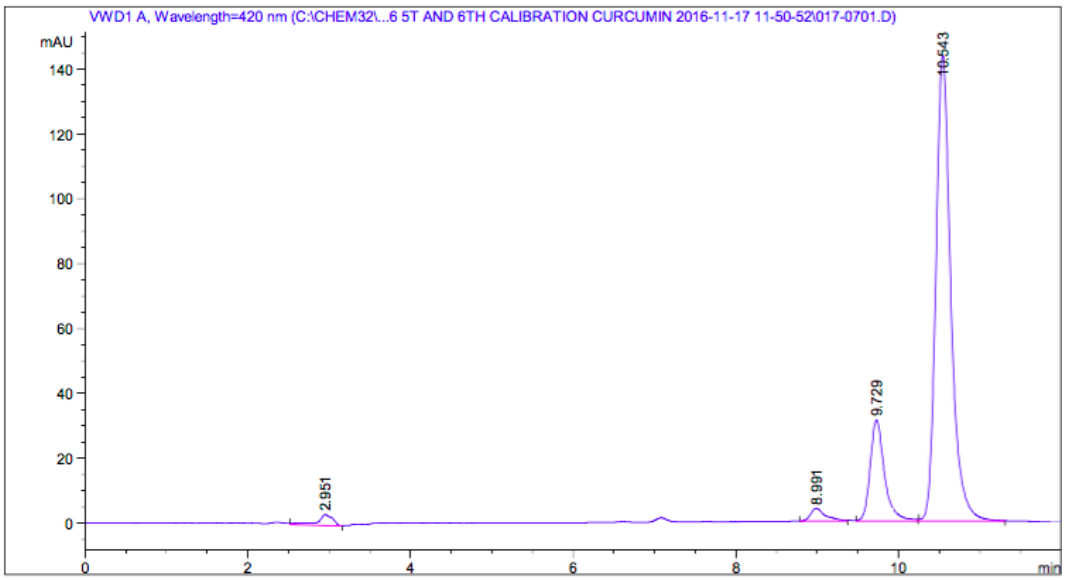

Figure 3-5 HPLC chromatogram of curcumin and its derivatives in methanol

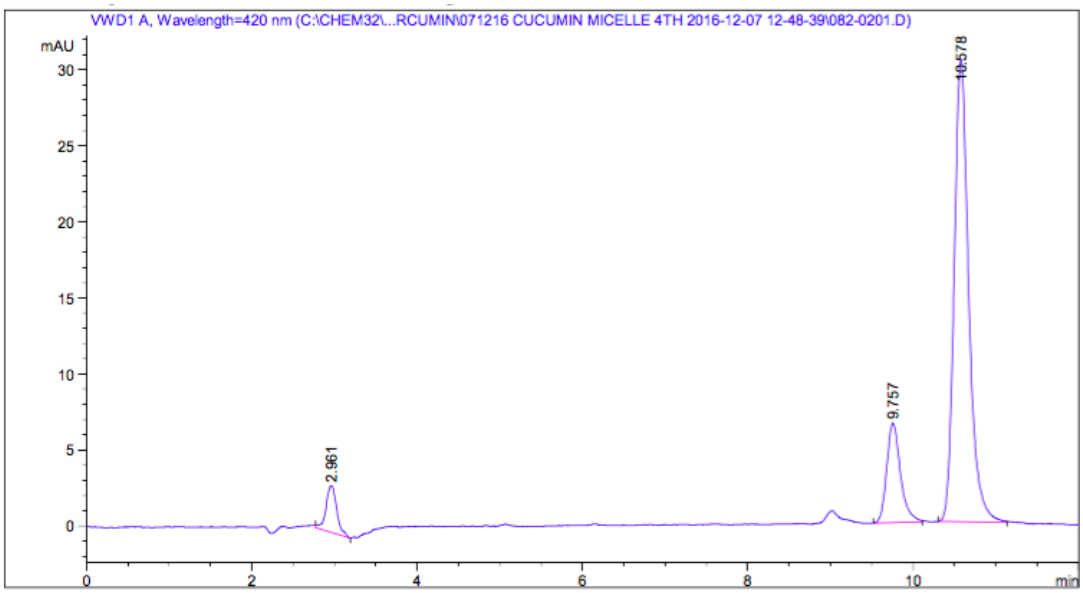

Figure 3-6 HPLC chromatogram of curcumin loaded genistein-mPEG micelles dissolved in methanol

3.5.1.3 **Calibration curve for erlotinib**

To study the linearity of erlotinib, dilutions were made in the range of 1-70 µg/ mL. A plot of erlotinib concentration against peak area response was linear over this concentration range (Figure 3-7).

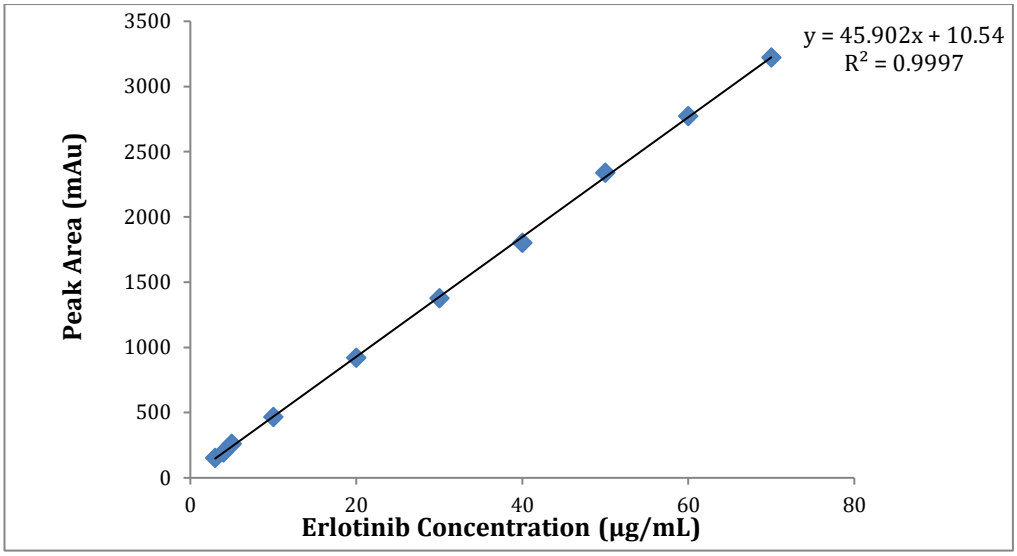

Figure 3-7 Calibration curve of erlotinib using HPLC analysis (n=3)

3.5.1.4 Calibration curve for curcumin

A plot of curcumin concentration against peak area was found to be linear over the range of 3-50 µg/mL (Figure 3-8).

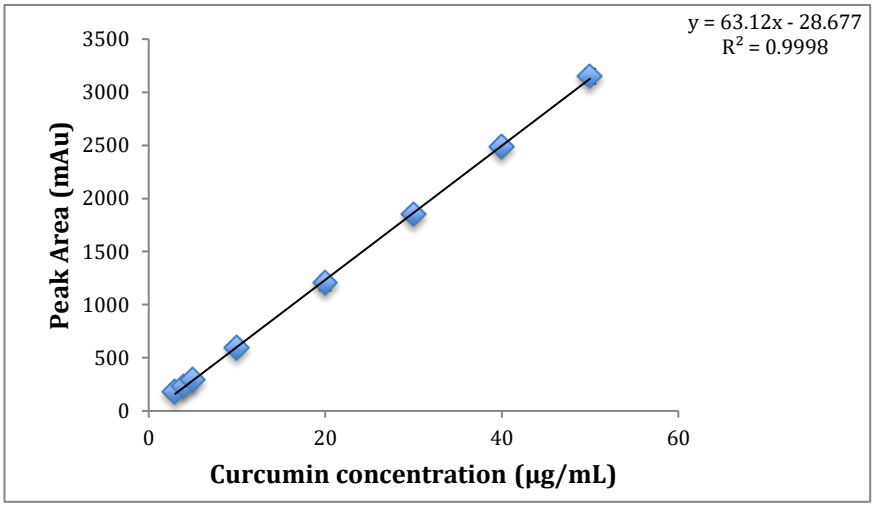

Figure 3-8 Calibration curve of curcumin using HPLC analysis (n=3)

3.5.1.5 Analytical method validation

The results of analytical method validation including linearity, precision, accuracy, limit of detection and limit of quantification were shown the acceptable values following ICH guidelines in Table 3-3.

The developed reverse phase high performance liquid chromatography (RP-HPLC) for the determination of erlotinib does not require any buffer solutions throughout the analysis compared with the reported methods (Latha et al. 2017; Faivre et al., 2011; Bolandnazar et al., 2013). However, erlotinib was still eluted in the short running time with the good result of precision, accuracy and linearity. These validation results were achieved using ICH guidelines in the term of validation of analytical procedures; therefore, this novel method can be used to determine the amount of erlotinib in laboratories through at the remaining studies.

Table 3-3 Regression characteristics, validation and system suitability for the analysis of erlotinib (n=4)

Parameters	
Retention time (min)	4.6
Linearity range (µg/ mL)	3-70
Number of samples per curve	10
Limit of detection (µg/ mL)	0.78
Limit of quantification (µg/ mL)	3.00
Accuracy (%)	97.60 – 108.69
Precision (%RSD, n=3)	1.89- 7.52
Repeatability (%RSD) at 35 µg/mL (n=9)	2.70

3.5.2 Critical micelle concentration of genistein-mPEG conjugate

The critical micelle concentration (CMC), which is the minimum concentration of surfactants and/or polymers required for micelle formation, is an important parameters to define the characteristics of surface active agents and micelles (Owen et al., 2012). A number of direct and indirect methodologies are available

for its measurement; for example, fluorescence intensity, electrical conductivity, surface tension, UV absorbance, and scattered light intensity have been used to determine the CMC value based on a sudden change in physical properties upon micelle formation. Fluorescence spectroscopy and light scattering are the two most commonly employed techniques due to their high precision and sensitivity to the thermodynamic properties of micelles (Torchilin, 2001; Topel et al., 2013; Fu et al., 2015).

Compared to fluorescence spectroscopy, DLS has shown equivalent performance in terms of its sensitivity, but is more practical for routine use. Three main parameters: the intensity of scattered light, correlation function of scattering intensity and measured size changed were determined by DLS in this study, in order to confirm micelles were formed from the conjugate in an aqueous medium, and to measure the CMC of genisten-mPEG-COOH (Topel et al., 2013).

Figure 3-9 shows that there were two distinct slopes from the plot of the average intensity of scattered light (Derived Count Rate, in kilo counts per second, kcps) against various concentrations of genistein-mPEG (mg/mL, on a logarithmic scale). The intensity of scattered light remained at the same level for the polymer concentrations between 0.08 and 0.83 mg/mL. This was due to the background scattering from either monomers of drug-polymer conjugate or HPLC grade water in the preparations (Davis et al., 2011; Topel et al., 2013). However, there was an increase in scattering intensity with increasing polymer concentration from 1.25 to 10 mg/mL, resulting from the self-aggregation of monomer/surfactant molecules or micelles.

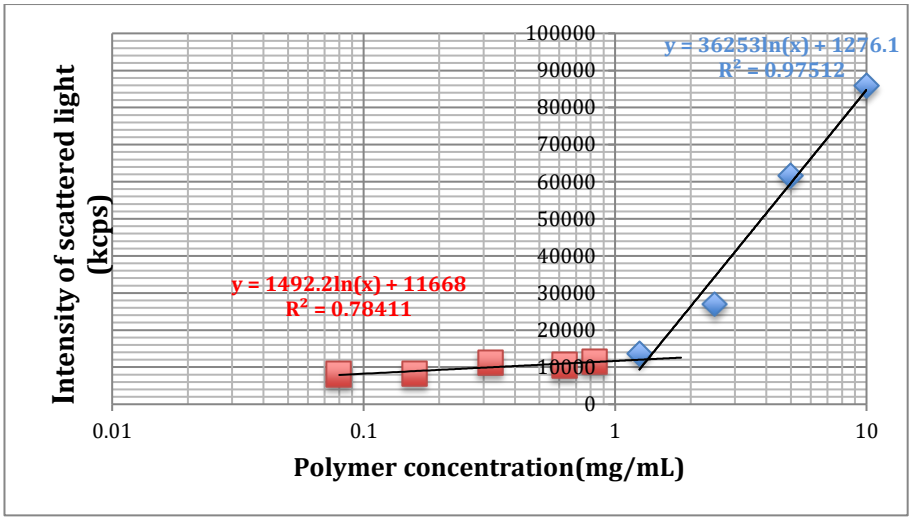

Figure 3-9 Effect of increasing concentration on scattered light intensity for genistein-mPEG solutions (n=3, mean± S.D.)

In theory, at low concentrations (below CMC), there are single polymer chains/ monomers dispersed insufficiently in the bulk solution and at the interface of air-water phase. As the polymer concentration reaches the CMC, both polymer chains and micellar aggregates are saturated in an aqueous environment and at the interface (Owen et al., 2012). To determine the CMC, best curve fitting was employed to obtain the intersection of two lines drawn through all data points. In this work, the intersection of two straight lines corresponding to the CMC of genistein-mPEG conjugate was 1.35 mg/mL (2.56 x 10^{-4} M).

The correlation function curve indicates the formation of micelles. Figure 3-10 shows that there were poor signal to noise ratios when very low concentrations were studied. This means that hydrodynamic diameter of very diluted micelles could not be detected since the time-dependent correlation function of the scattering intensity was not reproducible, being similar to water (Ogino et al., 1988; Topel et al., 2013). However, the intercepts of correlation functions increased markedly when the polymer concentrations were above the CMC, suggesting the presence of micelles (Topel et al., 2013). The measured size was determined and the results demonstrate that there was a rapid change in size around the CMC (Figure 3-11), in good agreement with a previous report using the DLS technique (Topel et al., 2013)

Thus, changes in the intensity of scattered light, measured size and correlation function depended on the concentration of amphiphilic polymer. This confirms that genistein was successfully attached to mPEG and that this conjugate self-assembled into micelles.

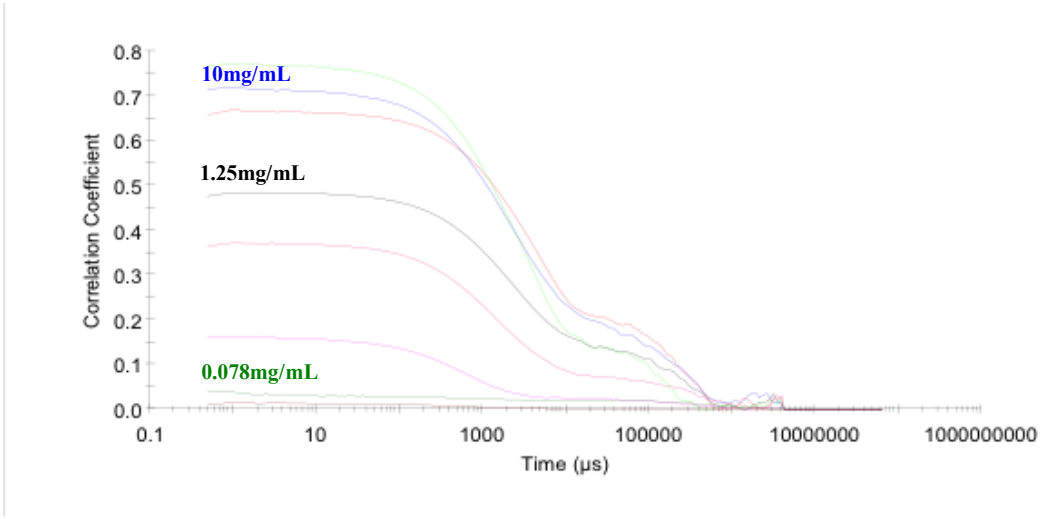

Figure 3-10 Effect of increasing concentration on correlation function (signal intensity to baseline noise ratio) (n=3, mean± S.D.)

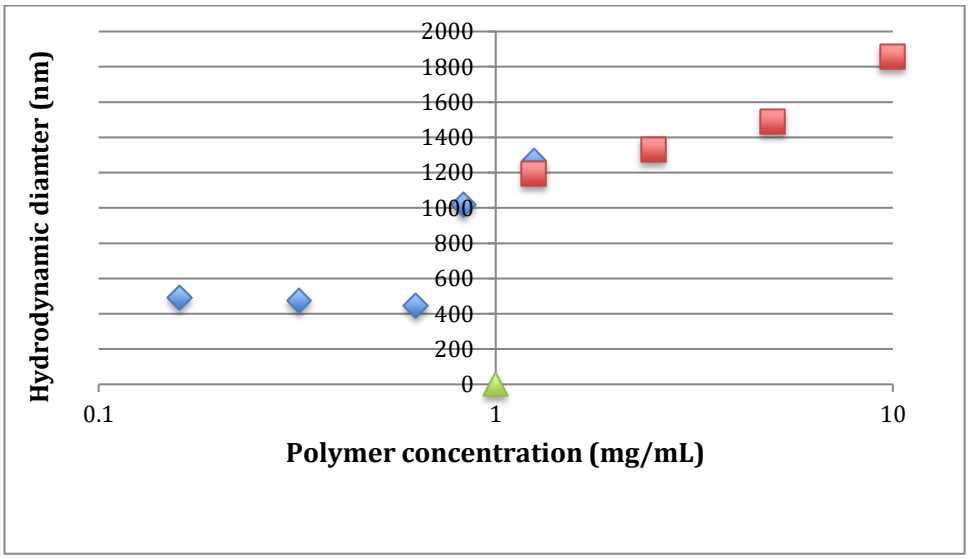

Figure 3-11 Effect of increasing concentration on mean hydrodynamic diameter of genistein-mPEG solutions (n=3, mean± S.D.)

3.5.3 Characterisation of drug-loaded genistein-mPEG micelles

3.5.3.1 Size distribution, surface charge and drug entrapment of erlotinib-loaded micelles

Erlotinib at 5%, 10% and 20% w/w drug in total conjugate was incorporated into polymeric micelles, prepared above the CMC of genistein-mPEG-COOH (1.35 mg/mL). From preliminary studies, %EE could not be accurately determined because drug concentrations for all formulations were lower than the LOD (0.78 µg/mL) and LOQ (3.00 µg/mL) of HPLC determination, being approximately 3%, 1% and less than 1% for 5%, 10% and 20% w/w drug in polymer, respectively. Moreover, a turbid white suspension due to the colour of erlotinib powder was seen during preparation, suggesting that this polymer conjugate was not appropriate for a micelle formulation of erlotinib, in terms of the ability to accommodate erlotinib and the stability.

3.5.3.2 Size distribution, surface charge and drug entrapment of curcumin-loaded micelles

A transparent yellowish micellar solution of curcumin with no precipitation was formed in which curcumin could be accurately quantified by HPLC analysis in the desired concentration range. This indicates the successful incorporation of curcumin into genistein-mPEG polymeric micelles.

Physical entrapment of drug is generally considered to dominate for micelles formed from drug-polymer conjugates, especially for hydrophobic drugs (Batrakova et al., 2006). Previous studies have shown that physical entrapment depends on a number of factors; for example, solubility of the drug in water (hydrophilicity/ hydrophobicity); the preparation method (dialysis, oil-in-water emulsification, solvent evaporation, etc.); and the interrelations of drug and the core-forming block of polymeric micelle including the steric properties, the block length of hydrophobic and hydrophilic segments of polymer and the physical properties of inner core segment (crystallinity, glass transition temperature, etc.) (Batrakova et al., 2006; Raval et al., 2012; Takahashi et al., 2014; Rao et al.,

2015). It is noted that parameters such as the preparation method for loading drugs into polymeric micelles and the amount as well as the type of polymer used were constant for the two drugs studied here. Thus, the physicochemical properties of erlotinib and curcumin are likely to affect drug entrapment, and hence micellisation may not be suitable for incorporating all drugs as discussed below.

The partition coefficient (log P value) or the octanol/water coefficient (K_{ow}) expresses the ratio of concentrations of a compound in a mixture of organic and aqueous phases. The solubility of a solid compound depends on the energy required to break its crystal lattice. Curcumin has a higher log P value (respectively; 3.29 and 2.75 for curcumin and erlotinib) but lower water solubility (respectively; 0.6 and 3-6 μg/mL for curcumin and erlotinib) compared to erlotinib; these factors are likely to lead to the differences in drug incorporation. Curcumin molecules are more likely to reside within the hydrophobic core of the micelles than erlotinib based on their physicochemical properties, resulting in a significantly higher in drug entrapment (Table 3-4).

Table 3-4 Properties of erlotinib and curcumin and their incorporations into genistein-mPEG polymeric micelles (n=3, mean± S.D.)

Hydrophobic drugs	**Erlotinib**	**Curcumin**
Molecular structure	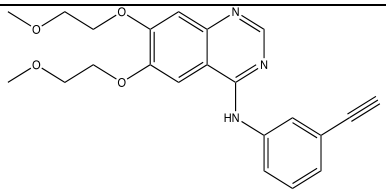	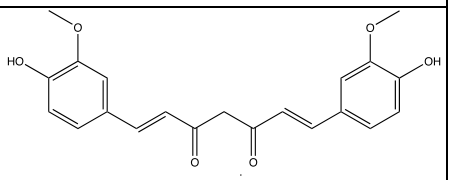
Entrapment efficiency (%EE)	N/A	45.60± 6.19
Drug loading (%DL)	N/A	2.17± 0.29

*5% w/w drug in polymer; drug and polymer concentrations were 0.25 and 5 mg/mL in water, respectively

Considering the chemical structures of these two hydrophobic drugs, nitrogen atoms from the quinazolinamine ring and oxygen from methoxyethoxy chains of the erlotinib molecule may form weak electrostatic bonding with the carboxylic group (-COOH) of genistein-mPEG conjugates at the surface of micelles. Furthermore, the rigid structure and the steric hindrance of erlotinib comprising three benzene rings attached to alkyne (C ≡ C; Triple bond) could limit the rotation of the erlotinib molecule to penetrate and align into the hydrocarbon region and inner core of micelles. These effects may result in weakening of van der Waals' force, π-π stacking interaction and H-bonding with genistein within the hydrophobic core, such that, the entrapment efficiency was very low.

For curcumin, the molecular structure is more flexible; there are fewer aromatic rings, and the molecule is smaller than erlotinib, with no bulky aliphatic side chains, so that it may pack more easily into the polymeric micelles. Hydrophobic interaction (van der Waals's force) and/or π-π stacking interaction and H-bonding between curcumin and genistein within the hydrophobic core can enhance the encapsulation of curcumin, due to the two benzene rings of curcumin. Furthermore, the two hydroxyl groups (-OH group) on the benzene rings of curcumin are easier to protonate and have stronger ionic interaction and H-bonding with the carboxylic group (-COOH) of genistein-mPEG. This can ensure higher entrapment efficiency as compared to erlotinib, being approximately 45.6%.

Overall, the results demonstrate that the amphiphilic drug-polymer conjugate can self-assemble to form micelles. This synthetic polymer seems unsuitable for erlotinib delivery possibly due to its molecular structure limiting micellar incorporation. However, it has shown that genistein-mPEG can be considered a promising compound for producing drug-carriers for curcumin, and may be the applicable for other hydrophobic drugs. Therefore, curcumin-loaded genistein-mPEG polymeric micelles were studied further for potential pulmonary delivery.

3.5.4 Characterisation and development of curcumin-loaded micelles

The aim of this study was to investigate whether the synthesis of genistein-mPEG conjugate would improve the water solubility of curcumin by including the drug molecule in the hydrophobic core of micelles. As seen from Figure 3-12, curcumin-incorporated into genistein-mPEG-COOH micelles after passage through a 0.45µm membrane filter were transparent yellow, suggesting curcumin is well-dispersed in an aqueous solution (Yang et al., 2015). This can be attributed to the structure of amphiphilic micelles, allowing PEG segments to serve as hydrophilic shell in water. Meanwhile, the genistein components of the conjugate were packed in the hydrophobic core of the micelle, serving as a binding site for curcumin (Danafar et al., 2014). Figure 3-12 demonstrates that this amphiphilic drug-polymer conjugate could serve as a carrier for curcumin, and curcumin-loaded genistein-mPEG micelles were consequently characterised for further studies.

Figure 3-12 Appearance of curcumin dispersed in genistein-mPEG micelles (a) pre-filtration (b) post-filtration

3.5.4.1 Effect of curcumin concentration on size distribution, surface charge, entrapment efficiency and drug loading of micellar formulations

3.5.4.1.1 Effect of curcumin concentration on micelle size distribution

Particle of size larger than about 200 nm can be easily recognised and phagocytosed by alveolar macrophage within the alveolar airspace, resulting in an

insufficient concentration of drug at the tumour site and the failure of treatment (Menon et al., 2014; Lee et al., 2015b; Nakamura et al., 2016).

Considering delivery to the lungs, nanocarriers in the range 50 -200 nm, achieve alveolar deposition, as reported for nanosuspensions (Dandekar et al., 2010; Amini et al., 2014; Menon et al., 2014), and can be readily incorporated into the droplets during aerosol generation from nebulisers (Kamali et al., 2016). Polydispersity Index (PDI), which is a measure of the size distribution or the size uniformity in the sample, can be a measure of physical stability of nanoparticles, indicating particle aggregation (Masarudin et al., 2015; Clayton et al., 2016). Therefore, the mean size of the genistein-mPEG polymeric micelles produced in this study was considered ideally to be approximately 200 nm or smaller, with a PDI <0.3 representing a stable micelle formulation, suitable for nebulised delivery to the airways.

The DLS results showed that mean diameter of curcumin-loaded micelles was approximately 200 nm with one peak of narrow size distribution (PDI<0.2) for all drug concentrations, representing as a relatively monodispersed system of appropriate size (Table 3-5, Figure 3-13). When curcumin concentration was increased from 2.5% to 20% w/w drug in conjugate, a significant increase in hydrodynamic diameter from 173.62 to 215.18 nm ($p<0.05$) was observed. These results were in agreement with previous reports, suggesting that physically-encapsulated curcumin could expand the inner core and the space within the micelles, contributing to a larger measured size (Song et al., 2014; Gao et al., 2015).

Table 3-5 Characterisation of curcumin-loaded genistein-mPEG micelles at different drug concentrations (n=3, mean ± S.D.)

Curcumin concentration	**Hydrodynamic diameter (nm)**	**Polydispersity Index**	**Zeta Potential (mV)**	**Entrapment Efficiency (%)**	**Drug Loading (%)**
2.5%	173.62± 2.16	0.08± 0.03	-14.52± 2.81	43.36± 3.67	1.06± 0.09
5%	197.54± 2.27	0.07± 0.04	-15.88± 0.86	45.60± 6.19	2.17± 0.29
10%	211.80± 1.65	0.06± 0.02	-16.70± 1.49	32.48± 9.67	2.95± 0.88
20%	215.18± 5.12	0.18± 0.14	-16.72± 0.99	10.20± 3.85	1.69± 0.65

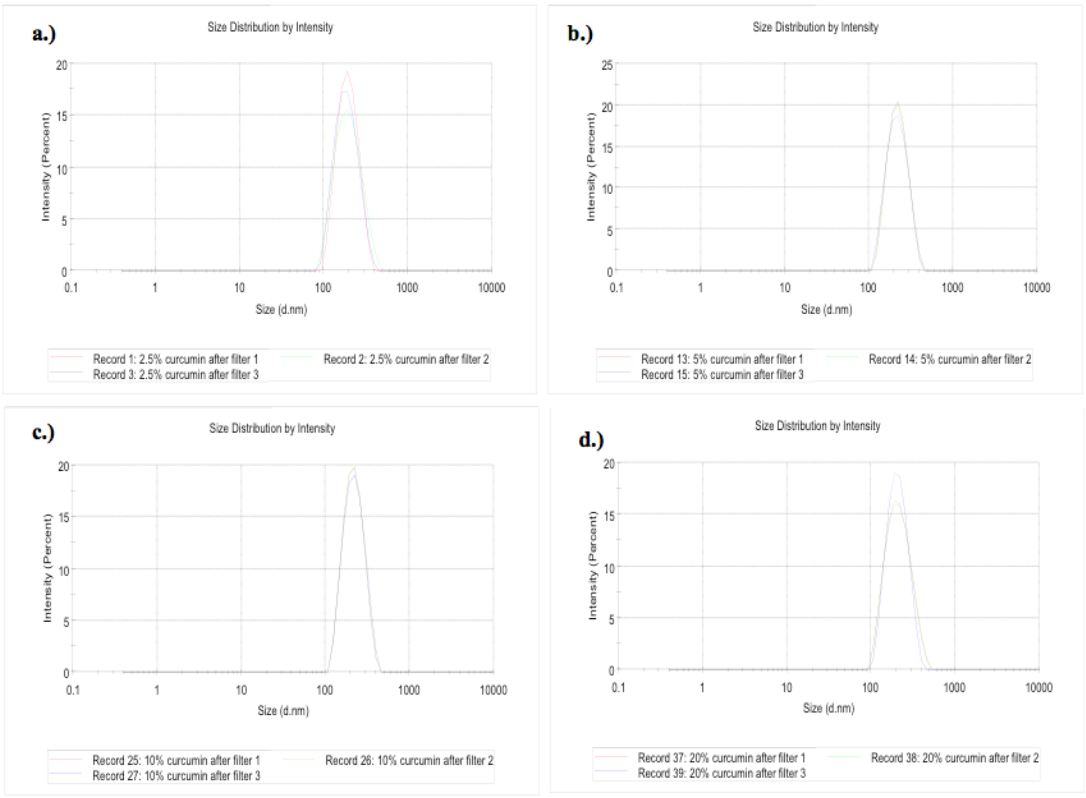

Figure 3-13 Size distribution of curcumin-loaded genistein-mPEG polymeric micelles at concentrations of a) 2.5%, b) 5%, c) 10% and d) 20% (w/w drug in polymer)

3.5.4.1.2 Effect of curcumin concentration on the surface charge of micelles

Surface charge is an important factor determining whether the nanocarriers will adhere to cells having opposite charge and also impacts the physical stability of colloids (Danafar et al., 2014); a high value of zeta potential either negative or positive is recommended for long-term stability (Mahajan and Mahajan, 2016). Nanocarriers with positive charge interact through electro-static forces with negatively-charged cell membranes, resulting in highly effective internalisation (Wang et al., 2011). On the other hand, nanoparticles with negative charge; for instance, PLGA and gold nanoparticles, have been described as penetrating cell membranes through caveolae-mediated pathways (Wang et al., 2011).

The surface modification of nanocarriers using PEG has been demonstrated to enhance passive targeting through a stealth effect, due to a protective barrier against the adherence of serum proteins. This can contribute to a reduction of nanocarriers being taken by macrophages (Iyer et al., 2015; Hassanzadeh et al., 2017). In this study, all curcumin-loaded genistein-mPEG formulations were

negatively charged; between -14 and -16 mV as shown in Table 3-5. This value was in agreement with previous reports using mPEG 5kDa in conjugates (Yin et al., 2013; Danafar et al., 2014; Gao et al., 2015). The negative-charge may possibly be due to protonation of the carboxylic group (–COOH) from the presence of residual mPEG-COOH in genistein conjugate in deionised water (pH values between 5.5 and 6.5), resulting in the COO^- ion.

Overall, the conjugate of genistein and mPEG was likely to be suitable for forming polymeric micelles for cancer delivery, due to the small hydrodynamic diameter (< 200 nm), narrow size distribution, and high negative charge (ranging from -14 to -16 mV) of the micelles. However, in order to achieve optimal therapy, drug entrapment was further considered.

3.5.4.1.3 Effect of curcumin concentration on drug entrapment in genistein-mPEG micelles

Drug entrapment of hydrophobic drugs in micelles may be attributed to chemical conjugation or physical entrapment. Physical entrapment was expected to be the main factor in this study (Mahajan and Mahajan, 2016). There was a marked increase in drug loading between 2.5% and 5% w/w curcumin-encapsulated genistein-mPEG micelles ($p<0.05$), being approximately 1.06 % and 2.17%, respectively (Table 3-5). However, entrapment efficiency for both formulations was similar ($p>0.05$). When 5% and 10% w/w curcumin-loaded micelles were compared, entrapment efficiency and drug loading for both preparations showed no significant differences ($p>0.05$), suggesting that 5% curcumin is the optimal content for efficient entrapment. Interestingly, there was a noticeable drop in entrapment efficiency and drug loading ($p<0.05$) for 20% w/w curcumin. This might be because micelles were saturated with curcumin at high concentration, with no available space to accommodate further molecules of curcumin. Therefore, higher amounts of curcumin in the initial formulation used to generate micelles resulted in the lower drug entrapments calculated according to Equations 3-1 and 3-2.

Higher concentrations of curcumin in curcumin-loaded polymeric micelles significantly increased the mean hydrodynamic diameter (Table 3-5; $p<0.05$).

However, changes in PDI and surface charge were not evident ($p>0.05$). The initial weight ratio between curcumin and the synthesized conjugate of 1:20 (5% w/w) was chosen for further characterisation as due to the maximum solubilisation of curcumin in the conjugate, with mean micelle size < 200nm.

3.5.4.1.4 Effect of curcumin incorporation on the size distribution of genistein-mPEG micelles

When empty micelles (drug-free) and the 5% w/w curcumin-loaded genistein-mPEG micelles were compared, the mean diameter of blank micelles was considerably larger than those in the presence of drug ($p<0.05$; Table 3-6). This may be attributed to the intermolecular forces between curcumin and genistein in the conjugate. It is possible that encapsulated curcumin molecule caused stronger van der Waal's interactions and/or electrostatic forces with genistein compared with empty micelles. Furthermore, the phenyl groups of curcumin could possibly also have hydrophobic-hydrophobic interaction with alkyl chain of mPEG-COOH as seen in the case of the incorporation of meso- tetraphenyl porphine into polyethylene glycol – distearoyl phosphatidyl ethanolamine and the incorporation of norcantharidin into poly (ethylene glycol) -poly (caprolactone) polymeric micelles (Ahmad et al., 2014). All of these factors result in a more tightly packed micelle core as in previously reported (Chen et al., 2012; Scarano et al., 2014; Li et al., 2016; Gong et al., 2017).

The size distribution was also affected by the incorporation of curcumin. The value of PDI was significantly lower ($p<0.05$) and the size distribution curve showed only one peak for drug-loaded micelles, indicating a relatively uniformly dispersed or more homogeneous population compared to empty self-assembled micelles as shown in Figure 3-14. Whereas empty micelles show broader size distribution peak, possibly indicating aggregation.

The data suggest that the strong physical interactions consisting of hydrophobic-hydrophobic interactions, H-bonding and π-π stacking between curcumin and genistein-mPEG conjugate contributed to a reduced mean size of the carriers and relatively lower PDI for curcumin-encapsulated micelles compared with blank micelles ($p<0.05$).

Table 3-6 Size distribution of empty and curcumin-loaded genistein-mPEG micelles (n=3, mean ± S.D.)

Formulations[a]	**Hydrodynamic diameter (nm)**[a]	**Polydispersity Index (PDI)**
Empty genistein-mPEG-micelles	274.48± 27.41	0.38± 0.05
5% curcumin-loaded genistein-mPEG micelles	197.54± 2.27	0.07± 0.04

[a] Polymer concentration = 5 mg/mL

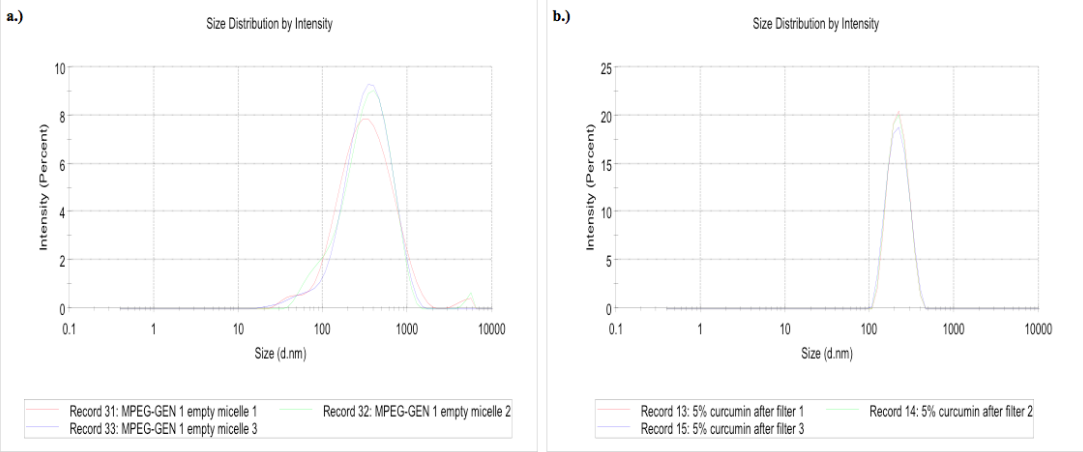

Figure 3-14 Size distribution of a) empty genistein-mPEG polymeric micelles and b) curcumin-loaded genistein-mPEG polymeric micelles

3.5.4.2 Transmission electron microscopy of empty and curcumin-loaded genistein-mPEG polymeric micelles

TEM images of empty genistein-mPEG micelles (Figure 3-15a) and curcumin-containing genistein-mPEG micelles (Figure 3-15b) demonstrate that micelles for both preparations were well-dispersed in aqueous medium as individual spherical micelles with narrow size distribution. The sizes of both formulations observed under TEM were smaller as compared to those measured by DLS, being approximately 140 nm and 190 nm for curcumin-loaded micelles, and 30 nm and 250 nm for empty micelles, respectively. This is in agreement with previous

reports and may be explained by the different techniques and physical conditions of TEM and DLS for measuring particle size (Qiu et al., 2009; Gao et al., 2013).

The combined results of the morphology, mean particle size and size distribution of blank and curcumin-loaded micelles determined by TEM and DLS confirm the molecular self-association of genistein-mPEG conjugate into polymeric micelles, into which curcumin can be incorporated.

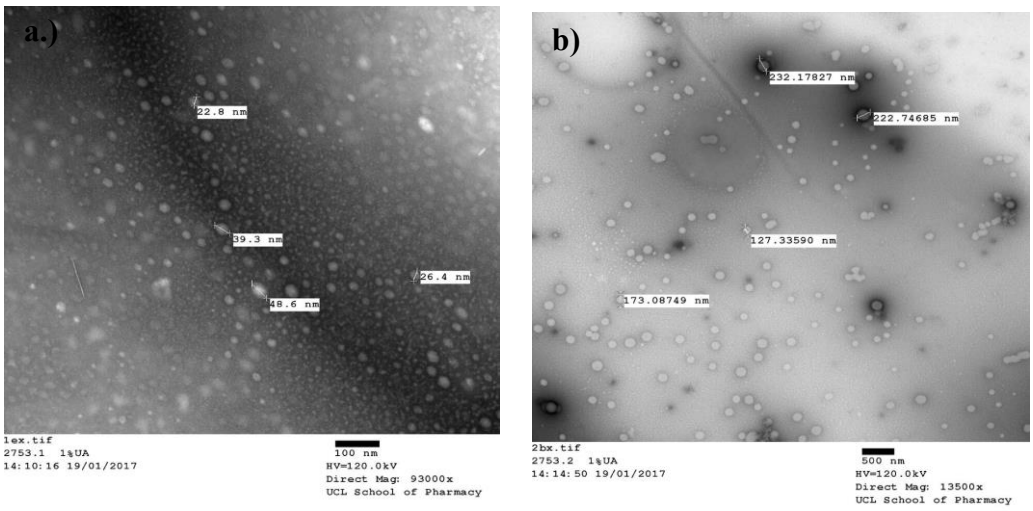

Figure 3-15 TEM images of a) empty micelles and b) curcumin-loaded genistein-mPEG micelles after filtration

3.5.5 Effect of nebuliser fill volume on time to nebulise to dryness and aerosol output for air-jet and vibrating-mesh nebulisers

In general, nebulisers do not release all of the fluid-loaded into the nebuliser chamber as an aerosol. The amount of liquid that remains in the device at the end of nebulisation is referred to as 'the residual volume' or 'dead volume' (Elhissi et al., 2013). The weight output or aerosol mass output, represents the weight of product successfully delivered by the nebuliser, and depends on a combination of factors; including the fill volume of fluid at the beginning of nebulisation, the efficiency of device, the nebulisation time, the design of the nebuliser reservoir, and the physicochemical properties of the formulation such as the viscosity, the surface tension, the concentration of drug solution and sometimes ion content (Kendrick et al., 1997; Ghazanfari et al., 2007). It is noted that drug output, which

expresses the percentage of drug or active ingredient emitted from the nebuliser, considered a critical factor for clinical outcomes, is not necessarily the same as aerosol mass output (Kendrick et al., 1997; Elhissi et al., 2013). The aim of this study was to measure the time taken to nebulise 2, 4 and 8 mL of HPLC grade water to 'dryness' i.e. the point at which aerosol output ceased and to determine the percentage nebulised at a specific time, in order to establish the suitable nebuliser fill volume before micellar aerosols were characterised.

From previous literature, the suitable fill volume should be at least twice the residual volume and sufficient to deliver a therapeutic dose of medicine with minimal drug loss (Kendrick et al., 1997). A large residual volume indicates that a large amount of drug remains in the nebuliser and cannot be inhaled, and thus in practice, adding a diluent to small fill volumes is recommended in order to maximise drug delivery over the nebulisation period (Rubin and Williams, 2014)). However, larger volumes of medical fluid increase administration time (Rubin and Williams, 2014). A period of nebulisation in the range of 5-10 min is recommended, as a prolonged nebulisation time may affect patience adherence (Kendrick et al., 1997; Jevon and Ewens, 2001; Chan et al., 2011).

There are various types of air-jet nebuliser designs as mentioned in Chapter 1; for example, constant output, breath-actuated and breath-enhanced air-jet nebulisers which have different output rates due to the design of the device and the positioning of internal baffles (Lavorini, 2013; Ibrahim et al., 2015). For all designs, the driving pressure or driving gas flow is the major determinant of output (O'Callaghan and Barry, 1997). The Pari® LC Sprint jet nebuliser used in this study is a breath-enhanced jet nebuliser, that is modified from a conventional device to increase the output rate, and decrease the nebulisation time and aerosol waste (Lavorini, 2013).

Increasing in fill volumes of water from the minimum of 2 mL to the maximum volume of 8 mL in the Pari air-jet nebuliser reservoir based on manufacturer' s literature required a longer time for nebulisation to dryness, from approximately 3 min to 20 min (Figure3-16a). A shorter time is usually preferable for patient

convenience; however, the percentage aerosolised in specific time should also be considered, so as to achieve the most effective localised treatment.

Figure 3-16b shows that greater than 50 % of water in the reservoir was nebulised for all fill volumes. A fill volume of at least 2 mL in an air-jet nebuliser is usually recommended by manufacturers (Clay et al., 1983); however, only 56.19 % released as aerosol in this study. In order to increase the proportion of water emitted from an air-jet device, increasing the fill volume was required. Increasing the fill volume to 4 and 8 mL considerably enhanced the percentage nebulised, being 78.34% and 87.12%, respectively. The time taken to nebulise 8 mL was approximately double as that for a 4 mL fill (respectively; 20 min and 9 min) (Figure 3-16a).

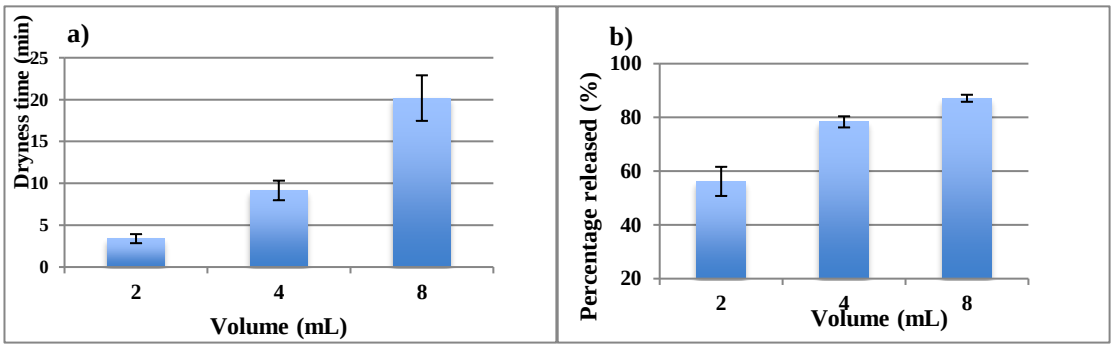

Figure 3-16 Effect of fill volumes of water on (a) time to nebulise to dryness and (b) percentage nebulised at dryness using an air-jet nebuliser (n=3, mean± S.D.)

Vibrating-mesh nebulisers are more efficient and provides more consistent and higher doses of drug to patients with smaller residual volume than air-jet devices (Ari, 2014; Pritchard et al., 2018). However, these devices are more expensive due to the increased number of tolerance critical components that associated with the electronic control circuit as well as the material used in the mesh manufacture (i.e. platinum, palladium, nickel and stainless steel) and require thorough cleaning (Ghazanfari et al., 2007; Ari, 2014; Pritchard et al., 2018). A vibrating-mesh nebuliser was used as the alternative device in this study to improve output efficiency. In these devices, vibration of a perforated plate results in extrusion of liquid through the mesh pores, causing aerosol generation as described in Chapter 1 (Figure 1-7). The times taken to nebulise defined volumes of water to 'dryness' for the vibrating-mesh nebuliser (Pari Velox®) was studied and compared with

the air-jet nebuliser (Figure 3-17). For 2 and 4 mL fill volumes, it took less time ($p<0.05$) for the vibrating-mesh nebuliser (respectively; 2.23 and 6.41 min) compared to the air-jet nebuliser (respectively; 3.39 and 9.15 min).

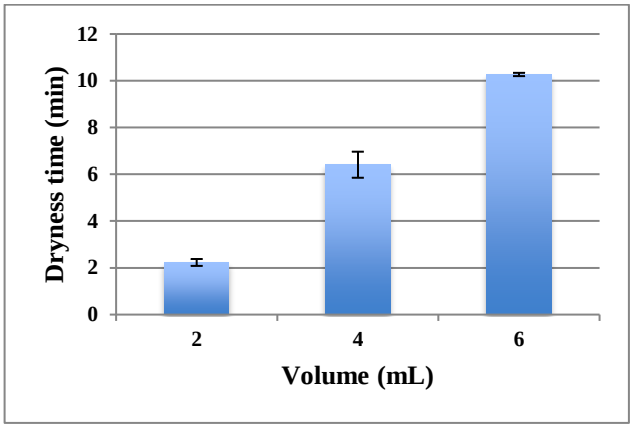

Figure 3-17 Effect of fill volumes of water on time to nebulise to dryness for the vibrating-mesh nebuliser (n=3, mean± S.D.)

All fill required less than 10 min to reach dryness state with the vibrating-mesh device. However, the percentage aerosolised could not be measured for the vibrating-mesh device due to the mechanism of aerosol generation, which leads to the deposition of most of the aerosol at the base of the device housing, resulting in high residual volume (Chan et al., 2011) unless the aerosol is drawn from the device by patient breaths. For air-jet nebulisers, the compressed air produces the aerosol droplets and directs them towards the patient for inhalation. By contrast, the direction of the aerosol stream is directed downwards for vibrating-mesh nebuliser as demonstrated in Figure 3-18 (Ghazanfari et al., 2007).

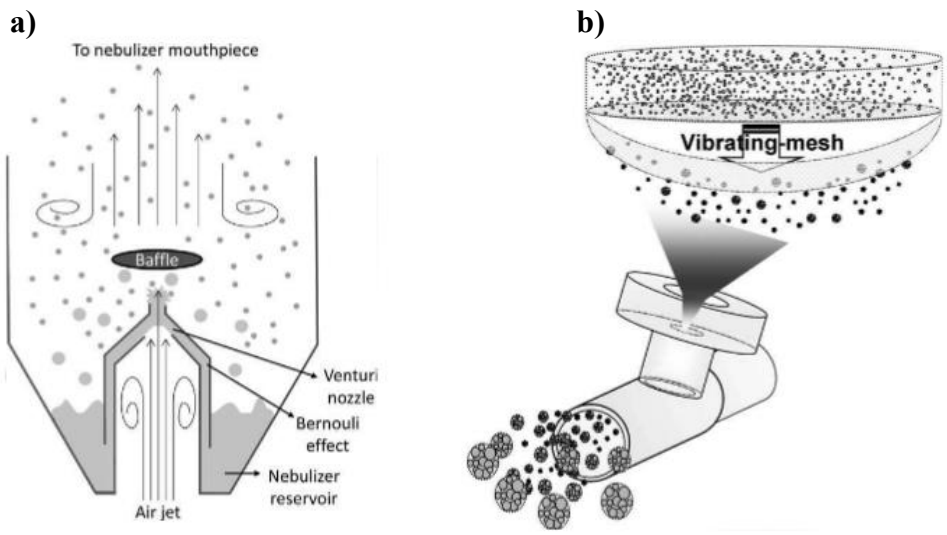

Figure 3-18 Schematic diagram of the mechanism of a) air-jet and b) vibrating-mesh nebulisers (Carvalho et al., 2016)

Based on these results, 4 mL was considered an appropriate fill volume for further studies. This allows complete delivery of aerosol (to dryness) and would represent an acceptable time to nebulise a suitable volume of fluid for clinical applications. For further studies, the dispersant used in the optimised micelles was also HPLC grade water. It is noted that in practice, solutions should be isotonic to avoid bronchospasm. However, water was used in this study to keep formulations as simple as possible, so as to understand the impact of key formulation variables. Hence, 4 mL of curcumin-loaded genistein-mPEG micelles delivered by both nebulisers for 10 min was initially employed for the aerodynamic assessment of nebulised micellar aerosols using a cascade impactor.

3.5.6 Assessment of aerosol properties of curcumin-loaded genistein-mPEG micelles delivered from air-jet and vibrating-mesh nebulisers using the Next Generation Impactor (NGI)

The Next Generation Impactor (NGI) was set up for aerosol characterisation of optimised curcumin-loaded genistein-mPEG micelles according to the requirements of the Ph. Eur. as described in Section 3.4.7. 4 mL of micellar solution was nebulised at a flow rate of 15L/min for 10 min using air-jet and vibrating-mesh nebulisers under the same operating conditions. Then, the aerosolisation parameters: Emitted Dose (ED), Fine Particle Mass or Fine particle

Dose (FPD), Fine Particle Fraction (FPF), Mass Median Aerodynamic Diameter (MMAD) and Geometric Standard Deviation (GSD) delivered for both nebulisers were determined and compared as shown in Table 3-7.

Table 3-7 Aerosol parameters of curcumin-loaded genistein-mPEG micellar aerosols delivered from air-jet and vibrating-mesh nebulisers into the cooled NGI at a flow rate of 15L/min (n=3, mean± S.D.)

Type of nebulisers	**Air-jet (Pari LC® Sprint nebuliser)**	**Vibrating-mesh (Pari Velox®)**
Mass balance (%)	88.16± 0.80 %	89.19± 2.11 %
Emitted Dose (ED)	60.79± 0.19 %	50.83± 1.38 %
Fine Particle Dose (μg)	123.00± 13.11	88.33± 15.28
Fine Particle Fraction (%)	47.00± 1.00 %	36.33± 2.89 %
MMAD (μm)	5.24± 0.09	6.09± 0.21
GSD	1.96± 0.02	1.65± 0.02

The mass balances for both air-jet and vibrating-mesh devices were within European Pharmacopeia acceptance limits. Therefore, the NGI can be used to compare these two nebulisers in order to assess the suitable device for delivering curcumin-loaded micelles. Emitted Dose, which represents the dose of drug emitted from the nebuliser, was considerably higher for the air-jet nebuliser ($p<0.05$) compared with vibrating-mesh nebuliser. The MMAD for the air-jet device was smaller than vibrating-mesh device ($p<0.05$), whereas the GSD values were similar, being in the range of 1.65-1.96, indicating a polydispersed aerosol. Moreover, the air-jet nebuliser produced significantly higher FPD and FPF ($p<0.05$) compared to the vibrating-mesh nebuliser, as expected based on the MMAD values for both nebulisers.

The lower efficiency of the vibrating-mesh device in this study was at variance with other reports. In previous studies, vibrating-mesh nebulisers were more efficient than air-jet nebulisers in terms of shorter time to complete nebulisation and/or yielding higher output rate (Ghazanfari et al., 2007; Elhissi et al., 2012; Ari,

2014). However, the performance of vibrating-mesh devices is highly affected by the physicochemical properties of the fluid being nebulised, particularly viscosity, surface tension, drug concentration and ion content (Zhang et al., 2007a; Chan et al., 2011; Elhissi et al., 2011a). The less efficient output of vibrating-mesh nebuliser could be due to the high negative surface charge of curcumin-loaded micelles (-18 mV), or drug crystallisation with particles adhering to and blocking the mesh apertures during aerosol generation. Furthermore, high electrostatic charge has been previously reported to inhibit the flow of fluid through mesh pores and/or the detachment of aerosol droplet, and also to increase the aerosol deposition on the wall of nebuliser (Manunta et al., 2011). These factors could possibly cause the lower energy input for atomisation and output rate as reported in the case of the delivery of receptor-targeted nanocomplexes with high surface charge by a vibrating-mesh nebuliser for gene therapy (Manunta et al., 2011).

According to Poiseuille's law (Equation 3-10), the performance of vibrating-mesh nebuliser depends on fluid properties. A higher density and lower viscosity of solution result in higher liquid flow through the mesh pores and greater aerosol output (Zhang et al., 2007a). Therefore, the inclusion of viscosity reducing agents may alter fluid output as seen in the reports for solutions and liposomes (Ghazanfari et al., 2007; Zhang et al., 2007a; Elhissi et al., 2011a; Elhissi et al., 2012).

$$Q = \pi\rho \, \Delta \, \mathrm{P}R^2/4\mathfrak{y}L \qquad \text{Eq. 3-10}$$

where ρ= the density, *R*= the radius of aperture, ∆ P= the pressure drop across aperture, *L*= the length of solution pumped through aperture, η= the fluid viscosity and Q= liquid flow

Previous studies have also shown that the inclusion of electrolyte or surfactant can reduce water adhesion to the internal structure of reservoir surfaces and mesh pores of the mesh nebuliser by increasing the electrical conductivity and the repulsive force towards the bulk solution and decreasing the droplet surface charge (Ghazanfari et al., 2007). These effects lead to an earlier detachment of droplets from the bulk solution and consequently decrease the nebulised aerosol

size, resulting in an enhanced emitted dose and drug output (Deshpande et al., 2002; Ghazanfari et al., 2007; Chan et al., 2011). Furthermore, the presence of ion in solution (especially halide ions; for example NaCl solution) can reduce the droplet size and cause an increase in output rate, FPF and FPD (Ghazanfari et al., 2007).

The lack of excipients in this study may result in non-ideal properties of fluid, reflected in the lower efficiency of vibrating-mesh nebuliser as compared to air-jet nebuliser (Beck-Broichsitter and Oesterheld, 2017). Further formulation development would be appropriate to enhance the delivery of a micelle solution from these devices.

Overall, the curcumin-encapsulated genistein-mPEG micelles were effectively delivered by an air-jet nebuliser with satisfactory values for the key aerosol quality parameters (Kendrick et al., 1997). However, the characteristic properties of the formulation are likely to be the predominant reason for an unexpected performance of vibrating-mesh nebuliser. Thus, further investigations of nebuliser performance for micelle delivery should be conducted to determine the effect of physicochemical properties of medical fluids in the presence of suitable types and concentrations of surfactants, electrolytes and viscosity modifying agents during aerosol generation to achieve the specific requirements for lung delivery.

3.6 Conclusions

The incorporation of curcumin into genistein-mPEG micelles was successfully achieved using the thin-film hydration method. This synthesized conjugate was not suitable for the delivery of erlotinib due to its molecular structure limited micellar incorporation. However, curcumin-encapsulated micelles with desired mean size and drug entrapment have shown the potential for pulmonary delivery, performed by air-jet and vibrating-mesh nebulisers as demonstrated using the NGI. The results showed that the performance of the air-jet device was superior to vibrating-mesh device in terms of higher %ED, FPD and FPF for this formulation (5% w/w curcumin-loaded genistein-mPEG micelles), which are the key parameters of aerosolisation. However, further studies on physicochemical

properties of micellar formulations in the presence of surfactants, electrolytes and viscosity agents during nebulisation are required for the better understanding of the differences in nebuliser performance.

Chapter 4 Liposomes loaded with erlotinib and genistein

4.1 Introduction

In Chapter 3, curcumin was successfully incorporated into genistein-mPEG polymeric micelles, though these nanocarriers could not adequately incorporate erlotinib. Liposomes are considered safe, biocompatible and biodegradable lipid-based drug carriers, which have previously been proposed for pulmonary delivery, for various applications including cancer treatment (Elhissi et al., 2011a; Sercombe et al., 2015; Rudokas et al., 2016). Liposomes consist of one or more bilayers of amphiphilic molecules that have a hydrophilic head and two hydrophobic chains (Bozzuto and Molinari, 2015).

The degree of drug loading into liposomes depends on various factors including the physicochemical properties of drugs, the nature of the lipid membrane, the composition of the formulations (type of lipid, lipid-to-cholesterol ratio, drug-to-lipid ratio) as well as the method of preparation (Pattni et al., 2015; Chountoulesi et al., 2017). Liposomes can be classified on the basis of their lamellarity, namely uni-, oligo- and multilamellar vesicles, which depends on the method used for their preparation and post-formation processing (Bozzuto and Molinari, 2015; Pattni et al., 2015).

Dipalmitoylphosphatidylcholine (DPPC) was chosen as the major component of the liposome formulation in this study as it is the predominant constituent of lung surfactant (Kaviratna and Banerjee, 2012; Joshi et al., 2014). DPPC liposomes containing erlotinib and genistein individually or together were prepared by thin-film hydration to obtain multilamellar vesicles (MLVs). This classical manufacturing technique is suggested for hydrophobic drugs since those molecules become incorporated in the phospholipid bilayer upon the formation of self-assembled liposomes (Pattni et al., 2015). Multilamellar vesicles were then reduced in size by probe-sonication to yield unilamellar vesicles. Unilamellar liposomes are ideal since they can easily fit into smaller aerosol, with minimal drug leakage during nebulisation (Lehofer et al., 2014; Cipolla et al., 2016). Cholesterol and DOPE used as stabiliser and helper lipid respectively were also included to obtain the desired characteristics of liposomes co-loaded with erlotinib and genistein, in terms of vesicle size, surface charge, encapsulation

efficiency and the stability of liposomes. Furthermore, the incorporation of cholesterol into liposomes may improve stability during aerosolisation (Cipolla et al., 2016).

Hydrophobic molecules are incorporated into liposomal bilayers (Figure 4-1). Cholesterol as well DOPE and hydrophobic drugs used in the formulation may complete for the same region within the DPPC bilayer. Therefore, an understanding of the effect of drugs and excipients on the properties of the lipid bilayer is important with respect to drug entrapment efficiency, drug release and in-vitro stability (Budai et al., 2003; Wu et al., 2012).

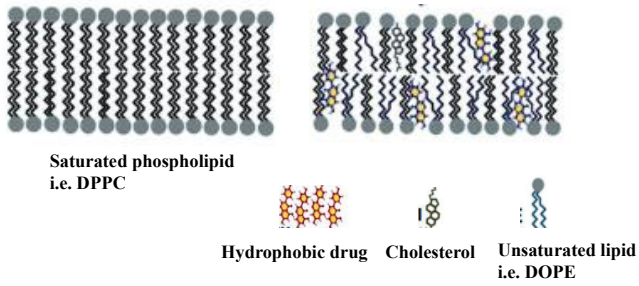

Figure 4-1 The structure of liposomes containing hydrophobic drug, cholesterol and DOPE within lipid bilayer (Phan et al., 2013; Monteiro et al., 2014)

The mobility of the molecules within and across the lipid bilayer is dependent on the temperature. The DPPC bilayer undergoes a pre-transition (transformations in the orientation of the polar head groups of DPPC) and a main phase transition (transformations in the orientation of acyl chains of hydrophobic region) when increasing the temperature. These thermotropic behaviours play an important role in bilayer fluidity, permeability and stability (Gardikis et al., 2006; Wu et al., 2012; Monteiro et al., 2014). Specifically, the DPPC bilayer has low fluidity and permeability to encapsulated exogenous compounds at a temperature below the main gel phase to the liquid-crystalline phase transition (T_c = 41 °C). However, DPPC bilayers have high fluidity at a temperature above the T_c (Monteiro et al., 2014).

The T_c of phospholipids depends on a number of factors; for example, the degree of saturation of the acyl chains, the length of the hydrocarbon chains and the type

of the polar head group (Monteiro et al., 2014). Figure 4-2 shows the effect of cholesterol incorporation into the bilayer of a saturated PC such as DPPC on the bilayer properties. As results of the addition of cholesterol, the fluidity and permeability of DPPC bilayer decrease in a fluid state as compared to DPPC bilayer at above the T_c. By contrast, the bilayer becomes less condensed but more fluidity and permeable when compared with the pure DPPC at below the T_c. The inclusion of unsaturated lipids (DOPE), cholesterol and biomolecules, which affect bilayer packing may have a significant impact on the thermal properties and permeability of DPPC-based bilayer.

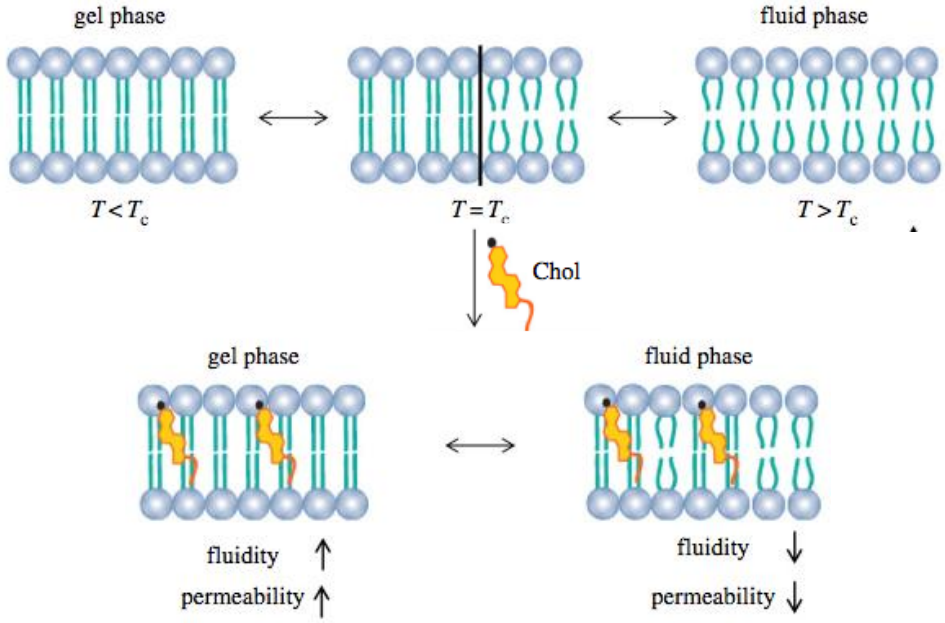

Figure 4-2 Influence of temperature and cholesterol on the DPPC phospholipid bilayer (Monteiro et al., 2014)

Differential Scanning Calorimetry (DSC) has proved a valuable thermal analytical approach for investigating the thermodynamic lipid phase transition and the interaction of agents with saturated lipid such as DPPC by measuring thermal changes of the lipid bilayer. Multichannel Differential Scanning Calorimetry (MCDSC) was therefore used in this study to investigate drug interactions with the phospholipid bilayer membrane and to determine maximum drug incorporation (drug/lipid ratio) for a better understanding of the co-loaded liposomal formulation during pre-formulation studies.

4.2 Aims

4.2.1 To develop and validate a reversed-phase high-performance liquid chromatography (RP-HPLC) method for quantification and co-quantification of erlotinib and genistein in accordance with International Conference on Harmonisation (ICH) guidelines.

4.2.2 To investigate the lipid composition of DPPC-based liposomes for the delivery of erlotinib and genistein as individual and co-loaded formulations and to characterise the properties of liposomes in terms of particle size distribution, surface charge and encapsulation efficiencies of both drugs.

4.2.3 To characterise individual and co-loaded liposomal formulations using two methodologies (HPLC and MCDSC analysis) that may be useful to estimate the maximum incorporation and to understand bilayer interactions of erlotinib and genistein in DPPC-based liposomes.

4.3 Materials

Erlotinib >99% (N-(3-ethynylphenyl)-6,7-bis(2-methoxyethoxy)quinazolin-4-amine) and genistein >99% (4',5,7-trihydroxyisoflavone) (LC Laboratories, USA) were used as hydrophobic drugs in the liposomal formulations. The phospholipids, hydrogenated soy phosphatidylcholine (HSPC, L-α-phosphatidylcholine, hydrogenated (Soy)), DPPC (1,2- dipalmitoyl- sn- glycerol- 3- phosphocholine) and DOPE (1,2-dioleyl- sn- glycerol- 3- phosphoethanolemine), supplied by Lipoid (Ludwigshafen, Germany), were used without further purification as the major and helper lipids, respectively. Cholesterol (Sigma-Aldrich; Poole, UK) was used as the bilayer stabiliser in the liposomes. Absolute ethanol (99.8%, analytical grade), chloroform (99.8%, analytical grade) and HPLC grade water acquired from Sigma-Aldrich (Poole, UK) were used as solvents and a diluent in liposomes. The following reagents and solvents were obtained from Sigma-Aldrich (Poole, UK): dimethyl sulfoxide (DMSO, >99.7%, HPLC gradient grade), acetonitrile (99.9%, HPLC gradient grade), trifluoroacetic acid (TFA, >99.0%) and HPLC grade water, and used for a validated HPLC method for the

quantitative determination of genistein and erlotinib, and simultaneous analysis of the drugs in combination.

4.4 Methods

4.4.1 Validation of HPLC analytical method for erlotinib and genistein

4.4.1.1 Chromatographic conditions for HPLC analysis of erlotinib and genistein

A validated HPLC analysis was developed for the quantitative determination of erlotinib and genistein individually and for co-quantification of the two drugs in combination, to allow calculation of entrapment efficiency for individually load and co-loaded liposomes. Preliminary studies on the UV absorbance of erlotinib and genistein performed by UV-Vis Spectrophotometer (Agilent Cary 100, UK), gave the λ_{max} values for erlotinib and genistein as 246 and 260 nm, respectively. Quantification was carried out using an HPLC system equipped with an auto sampler and UV/Vis detector (Agilent 1100 Series, USA) at a wavelength of 246 nm for quantification of erlotinib and 260 nm for genistein. A Synergi Polar-RP 80°A HPLC Column (250 x 4.6 mm x 4 μm) acquired from Phenomenex, Torrance, California, an ether-linked phenyl phase suitable for the separation of polar and aromatic components, was used as the stationary phase for separation in this study. As erlotinib and genistein have benzene rings in their main structures and different polarities, this column was considered appropriate for the separation of these two compounds, and also suitable for the isolation of these two drugs from other materials used in the formulations.

Isocratic elution was carried out with a mobile phase comprising a mixture of acetonitrile and 0.1 % v/v TFA in HPLC grade water (50:50 % v/v). The eluents were degassed before being pumped through the column at a flow rate of 1 mL/min. The column temperature was maintained at 25°C and the sample injection volume was 10 μL, with a run time of 10 min. The UV wavelength was set to shift from 246 nm to 260 nm after 5.2 min for simultaneous quantification

of the two drugs, while the wavelength for individual analyses remained fixed throughout the entire experiment.

HPLC chromatographic conditions of erlotinib and genistein for individual and co-quantification analysis are summarised in Table 4-1.

In order to ensure there was no interference between other components present in the liposomes preparation and the two drugs, empty liposomes (formulation without drug) comprising DPPC, cholesterol and DOPE (72:8:20 mol%) were studied using the same HPLC chromatographic systems.

Table 4-1 HPLC chromatographic conditions for assay of erlotinib and genistein using individual and simultaneous methods

Drug	**Erlotinib**	**Genistein**	**Simultaneous**
Injection volume (μL)	10	10	10
UV/Vis detector wavelength (nm)	246	260	246 and 260
Mobile phase (100% v/v acetronitrile : 0.1% TFA in HPLC grade water)	50:50	50:50	50:50
Column temperature (°C)	25	25	25
Flow rate (mL/min)	1	1	1
Run time (min)	10	10	10
Retention time (min)	4.6	5.8	4.6 (Erlo) 5.8 (Gen)

4.4.1.2 Preparation of standard solutions and calibration curves for erlotinib and genistein

Two standard stock solutions of erlotinib and genistein of 1000 μg/mL were individually prepared by dissolving 25 mg of erlotinib in 20 mL of DMSO and 25 mg of genistein in 20 mL of methanol in separate 25 mL volumetric flasks. The sample was bath-sonicated for a few minutes to ensure complete dissolution of

drug, and solutions made up to the final volume of 25 mL. After that, 0.35 mL of the stock solution was diluted to 5 mL in a 5 mL volumetric flask to obtain the highest concentration of 70 μg/mL. For the linearity study, serial dilutions of standard solutions were made in the range of 1 - 70 μg/mL; 1, 2, 3, 4, 5, 10, 20, 30, 40, 50, 60 and 70 μg/mL. Individual calibration curve for erlotinib and genistein were plotted, with taking peak area on the Y axis and analyte concentration on the X axis.

For simultaneous quantification of erlotinib and genistein, both stock solutions were prepared individually in DMSO before mixing to avoid potential chemical reaction between these two drugs at high concentrations. Subsequently, equal volumes of each stock solution were diluted with DMSO in the same volumetric flask, in order to make an equivalent series of concentrations ranging from 1 to 70 μg/mL for both drugs.

4.4.1.3 Analytical method validation

4.4.1.3.1 Linearity

Linearity in this study was performed by taking four samples of all serial dilutions of 1, 2, 3, 4, 5, 10, 20, 30, 40, 50, 60, 70 μg/mL from the stock solution and then injecting 10 μL of each concentration into the HPLC chromatographic system and recording the response. The degree of linearity was then determined by calculating the correlation coefficient. The slope, intercept and correlation coefficient of erlotinib, genistein and co-quantification were determined from the equation describing the response. It is noted that the ranges of tested concentrations for preparing individual and co-quantification HPLC analysis of erlotinib and genistein were the same.

4.4.1.3.2 Precision

Intraday precision was performed by injecting three concentrations (8, 35 and 55 μg/mL) in triplicate per concentration onto the chromatographic system on the same day. Inter-day precision was determined with those concentrations on three consecutive days. The repeatability study was undertaken by injecting the chosen

concentration of 35 μg/mL 9 times to obtain the relative standard deviation (%RSD) calculated as mentioned (Eq.3-1).

4.4.1.3.3 Accuracy

The accuracy was determined by the recovery method, using a series of concentrations between 3 and 70 μg/mL for erlotinib and between 2 and 70 μg/mL for genistein in triplicate for the quantification and co-quantification of erlotinib and genistein. The percentage recovery was calculated using as mentioned (Eq. 3-2).

4.4.1.3.4 Limit of detection

As mentioned in Section 3.4.1.5.4

4.4.1.3.5 Limit of quantification

As mentioned in Section 3.4.1.5.5

4.4.2 Preparation method for liposomes containing erlotinib or genistein and liposomes co-loaded with erlotinib and genistein

4.4.2.1 Effect of drug concentrations on the properties of DPPC liposomes

The aim of this study was to investigate the maximum drug loading into DPPC liposomes and to characterise the properties of co-loaded liposomes for mean size, particle size distribution, surface charge and encapsulation efficiency. Two stock solutions of erlotinib and genistein (each 1.25 mg/mL) were prepared individually by dissolving 25 mg of erlotinib and 25 mg of genistein in 20 mL of absolute ethanol in separate 28 mL glass vials. DPPC liposomes with incorporated drug were prepared by the thin-film hydration method. To prepare formulations of different initial drug/lipid concentrations (% w/w), 1 mL, 2 mL and 4 mL of drug solution was added to 50 mg of DPPC to obtain 2.5, 5 and 10% w/w drug in DPPC individually, respectively. The phospholipid (DPPC) and drug (erlotinib or genistein) were dissolved together in 30 mL of a mixture of absolute ethanol and chloroform (4:1 v/v) in a 250 mL round-bottomed flask. The mixture was then placed into a bath sonicator and sonicated to ensure the complete dissolution of

drug and lipid. Solvent was removed using a rotary vacuum evaporator (RC 900, Knf Neuberger GmbH, Germany) at 150 bars for 20 min at 60°C to acquire a thin film of drug and lipid. The dry thin film was flushed with nitrogen gas at ambient temperature for 5 min to remove residual solvent and then hydrated with 20 mL of HPLC water with vigorous hand-shaking, followed by gentle rotation on the rotary evaporation equipment at 200 rpm for 30 min at 60°C in a water bath to produce MLVs of 2.5 mg/mL lipid content.

For co-loaded formulations, erlotinib and genistein co-loaded liposomes were prepared using the thin-film hydration method as outlined above. 1 mL, 2 mL and 4 mL of stock solution of each drug (1.25 mg/mL in absolute ethanol) was added to 50 mg of DPPC, yielding a series of drug concentrations in lipid of approximately 2.5, 5 and 10% for each drug w/w.

Empty liposomes, without either drug, were also prepared using the same method. This was to compare and study the effect of drug incorporation on the properties of the liposomes.

Upon successful production of the MLVs, their sizes were reduced by probe sonication to achieve the required mean size of 100- 200 nm (Dandekar et al., 2010; Amini et al., 2014). Liposomes in this range can be readily into the droplets during nebulisation (Cipolla et al., 2016) with minimal drug waste as well as achieving greater avoidance of alveolar macrophage uptake within alveolar airspace compared with those larger than 200 nm (Kamali et al., 2016; Nakamura et al., 2016).

Non-incorporated drug was removed by syringe filtration. Each 2 mL of formulations was filtered through a 0.45-μm cellulose acetate membrane filter (Merck Millipore Ltd., UK) once, yielding a filtrate of drug-loaded liposomes.

4.4.2.2 Effect of cholesterol content on the properties of DPPC liposomes

Drug concentration was initially fixed at 5% w/w drug in total lipid, while the content of cholesterol in DPPC (mol%) for erlotinib or genistein liposomal formulations was varied as shown in Table 4-2. The range of these concentrations

was chosen based on values successfully employed in a previous study of genistein liposomes (Phan et al., 2013). 2mL of drug solutions (1.25 mg/mL from each stock solution in absolute ethanol) and lipid phase (50 mg in total, comprising DPPC and cholesterol) were dissolved in 30 mL of a mixture of absolute ethanol and chloroform (4:1 v/v). Liposomes were prepared, sonicated and characterised as described in Section 4.4.2.1. The results were reported as the mean and standard deviation (mean ± S.D.) of three separate experiments.

Table 4-2 The content of DPPC and cholesterol in erlotinib or genistein liposomal formulations

Composition	**Quantity (mg)**			
	F1 **0 mol% cholesterol**	**F2** **8 mol% cholesterol**	**F3** **15 mol% cholesterol**	**F4** **30 mol% cholesterol**
DPPC	100 mol% = 50 mg	92 mol% = 47.81 mg	85 mol% = 45.75 mg	70 mol% = 40.79 mg
Cholesterol	0 mol% = 0 mg	8 mol% = 2.19 mg	15 mol% = 4.25 mg	30 mol% = 9.21 mg

4.4.2.3 Effect of the addition of DOPE on the properties of liposomes

The aim of this study was to investigate the effect of the inclusion of 20 mol% DOPE (as previously successfully employed in a genistein liposome preparation (Phan et al., 2013)) on the properties of liposomes by comparing the liposomal formulation with and without DOPE. Drug-loaded liposomes (5% w/w erlotinib or 5% w/w genistein in total phospholipid) comprising 8 mol% of cholesterol (2.18 mg), 20 mol% of DOPE (10.51 mg) and 72 mol% of DPPC (37.31 mg) were prepared individually as described in Section 4.4.2.1.

For co-loaded preparations, erlotinib (2.5% w/w) and genistein (2.5% w/w), cholesterol (8% w/w) in total lipid were fixed (based on the results of individual formulations), whereas the concentrations of DOPE in total phospholipid (0, 10, 20, 30 and 40 mol% of lipid contents) and DPPC up to 100% w/w lipid were varied as shown in Table 4-3. All liposomal formulations were characterised as outlined in Section 4.4.3.

Table 4-3 The composition of DPPC: cholesterol: DOPE in erlotinib and genistein co-loaded liposomal formulations

Composition	**Quantity (mg)**				
	F1 = 0% DOPE	**F2 = 10% DOPE**	**F3 = 20% DOPE**	**F4 = 30% DOPE**	**F5 = 40% DOPE**
Erlotinib	1.25 mg	1.25 mg	1.25 mg	1.25 mg	1.25 mg
Genistein	1.25 mg	1.25 mg	1.25 mg	1.25 mg	1.25 mg
DPPC	47.81 mg	42.55 mg	37.31 mg	32.08 mg	26.87 mg
Cholesterol	2.18 mg	2.18 mg	2.18 mg	2.18 mg	2.18 mg
DOPE	0.00 mg	5.26 mg	10.51 mg	15.74 mg	20.95 mg

4.4.2.4 Effect of sonication time on liposome particle size distribution and drug entrapment

The purpose of this experiment was to study the influence of duration of probe-sonication on mean particle size, polydispersity index (PDI) and entrapment efficiency (%EE) of erlotinib and genistein individually. Optimised genistein or erlotinib-loaded MLVs liposomes, with lipid phase DPPC: cholesterol: DOPE (72:8:20 mol%), were prepared individually and their size reduced by 30 min probe-sonication. 20 mL of MLVs were placed in a 20 mL glass vial and kept in an ice bath throughout the size reduction. Probe sonication (MSE Soniprep 150, MSE, UK) was undertaken at a constant output of 12 watts (5 min/cycle and 1 min cooling at 4 ºC, to avoid overheating). The titanium probe (9.5 mm diameter) was immersed to a depth of 15 mm above the bottom of the glass vial. The time

for sonication (15, 30, 45 and 60 min) was varied to obtain a mean diameter of 100 to 200 nm. After that, optimal sonication time was fixed for the preparation of liposomes co-loaded with erlotinib and genistein.

4.4.3 Characterisation of liposomes

4.4.3.1 Particle size distribution measurement by dynamic light scattering

The mean hydrodynamic diameter and the particle size distribution were measured using the Malvern Nano ZS Zetasizer (Malvern Instruments, UK). 1.0 mL of liposomes was placed without further dilution into the zeta potential DTS 1070 folded capillary cell (Malvern instrument, UK). Three measurements were determined at 25 ºC. The data are expressed as mean Z-average particle diameter and polydispersity index (PDI).

4.4.3.2 Surface charge determination

For zeta potential measurements, the samples were prepared and assessed using the Malvern Nano ZS Zetasizer as described in Section 4.4.3.1. Three independent measurements based on electrophoretic mobility using the Helmholtz-Smoluchowski equation were determined and reported as mean values± S.D.

4.4.3.3 Transmission electron microscopy

The morphology and aggregation behaviour of co-loaded liposomes was studied following placement on a carbon grid and negative staining with one drop of uranyl acetate (1% w/v), and observation using a transmission electron microscope (Philips Electron Optics BV, Netherlands), as described in Section 3.4.4.4.

4.4.3.4 Drug-loading and entrapment efficiency

1 mL of each formulation was diluted with ethanol to a final volume of 5 mL prior to HPLC analysis. The entrapment efficiency (%EE) and drug loading

(%DL) of erlotinib and genistein were calculated using equations (Eq. 3-5 and Eq. 3-6) as outlined in Section 3.4.4.3.

4.4.4 Thermal analysis

Differential Scanning Calorimetry (DSC) has been extensively used as a highly sensitive technique for studying the interaction of biomolecules with phospholipid bilayers (Taylor and Morris, 1995; Elhissi et al., 2006b; Chiu and Prenner, 2011). In general, the incorporation of exogenous molecules into a lipid bilayer has more pronounced effect on the pre-transition than the main transition (Elhissi et al., 2006b; Saunders et al., 2007). Changes in the thermotropic behaviour of the main transition phase are dependent on the localisation of drug, with more obvious change when drug is located between C_1 and C_{10} of the hydrophobic hydrocarbon region (Saunders et al., 2007).

In recent times, DSC instrumentation with increased sensitivity or High Sensitivity DSC (HSDSC) has been employed in a number of studies to provide more accurate and reliable data, especially for small thermal events such as the pre-transition which are difficult to accurately measure by conventional DSC (Saunders et al., 2007). HSDSC was used for studying the interaction of hydrophobic drugs (erlotinib and genistein), cholesterol and DOPE with DPPC bilayer that may affect drug incorporation during pre-formulation studies.

4.4.4.1 Determining suitable lipid concentrations and scan rate for DSC analysis

DPPC liposomes were prepared by the lipid thin-film hydration method (Section 4.2.2.1) and sonicated for 30 min. To identify suitable lipid concentrations, DPPC concentrations of 2.5, 20 and 40 mg/mL were studied with the aim of achieving good resolution in the DSC thermogram at the minimum lipid concentration. The pre (T_{pre}) and main phase transition temperatures (T_m) and enthalpy of transition for DPPC-based liposomes (kJ/mol) were compared with previous reports.

For scan rate, 0.5 and 1 °C/min were studied for DPPC liposomes using a High Sensitivity Differential Scanning Calorimeter (HSDSC), a Multi cell DSC (TA instruments, Newcastle, UK).

4.4.4.2 Investigation of effect of drugs and helper lipids of different concentrations on DSC thermograms

1 mL of formulations having total lipid concentration 40 mg/mL were each placed into a DSC sample cell (TA Instruments, Newcastle, UK), which was sealed using a rubber O-ring and cell cap to ensure an airtight fit. The reference cell was empty. Nitrogen was supplied to prevent vapour condensation on the sample cells during cooling (Elhissi et al., 2006b; Saunders et al., 2007). Fifteen liposomal formulations characterised in this study were listed below:

- DPPC
- DPPC/Cholesterol
- DPPC/DOPE
- DPPC/Cholesterol/DOPE
- DPPC containing erlotinib at concentrations of 2.5, 5% and 10%
- DPPC containing genistein at concentrations of 2.5%, 5% and 10%
- DPPC containing both drugs at concentrations of 2.5% and 5%
- DPPC/Cholesterol/DOPE containing erlotinib at concentration of 2.5%
- DPPC/Cholesterol/DOPE containing genistein at concentration of 2.5%
- DPPC/Cholesterol/DOPE containing erlotinib and genistein at concentrations of 2.5%

All scans were undertaken at a rate of 0.5 °C/min from 15 to 70°C. The thermal behaviour of liposomes was evaluated based on the temperature of the pre-transition (T_{pre}), main phase transition temperature (T_m), enthalpy (ΔH) and half-height width (HHW) of the main endothermic peak using the instrument software. Three independent DSC measurements were determined and values are reported as mean ± SD.

4.4.5 Statistical analysis

All experiments were carried out in triplicate and results are present as the mean ± S.D. Data were statistically analysed using either Student's t-test or analysis of variance (ANOVA) and Tukey's post hoc test, using IBM SPSS Statistic 22 software. A p value < 0.05 was considered significant.

4.5 Results and discussion

4.5.1 Validation of HPLC analysis

4.5.1.1 HPLC chromatograms of erlotinib and genistein

The retention times for erlotinib and genistein were approximately 4.6 (Figure 4-3) and 5.8 min (Figure 4-4), respectively. In order to ensure there was no chemical reaction between two drugs prior to the pre-formulation studies of this combination, the retention times and the peak responses of HPLC methods for individual and simultaneous determination of erlotinib and genistein were assessed. Based on the comparison of chromatograms (Figure 4-3, Figure 4-4 and Figure 4-5), no difference in the retention times and the peak areas of both drugs individually and in combination was evident. This suggests no interaction between these two active ingredients impacting the HPLC analysis at the concentrations investigated.

Blank liposomes (formulation without any drugs) containing DPPC, cholesterol and DOPE were injected into the HPLC system, with only one chromatographic peak at 2.7 min as seen in Figure 4-6, Figure 4-7, Figure 4-8 and Figure 4-9. This observation indicates that the three components used in the formulation will not interfere in the quantitative of both drugs in the remaining studies.

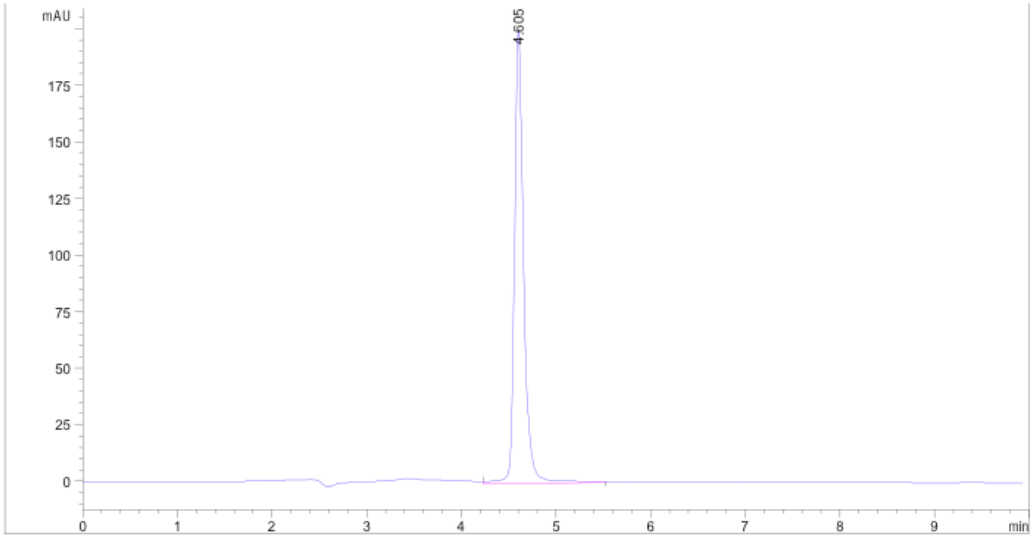

Figure 4-3 HPLC chromatogram of erlotinib (10 μg/mL)

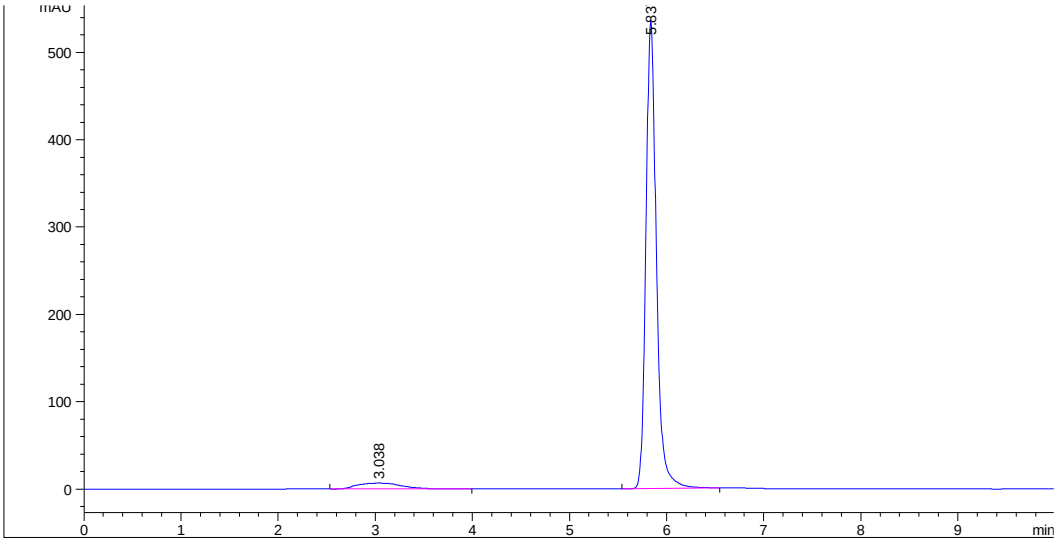

Figure 4-4 HPLC chromatogram of genistein (10 μg/mL)

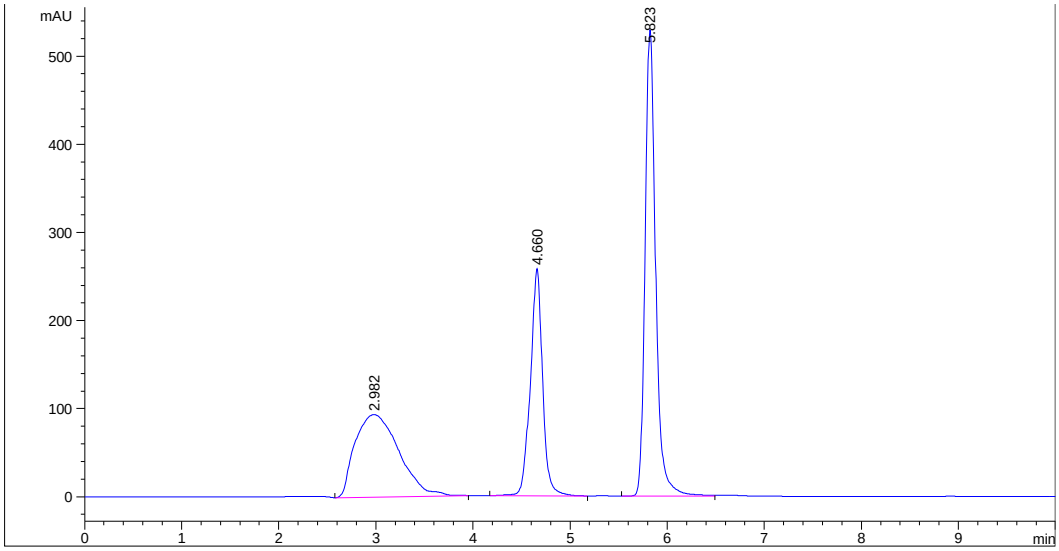

Figure 4-5 HPLC chromatogram of erlotinib (10 μg/mL) and genistein (10 μg/mL)

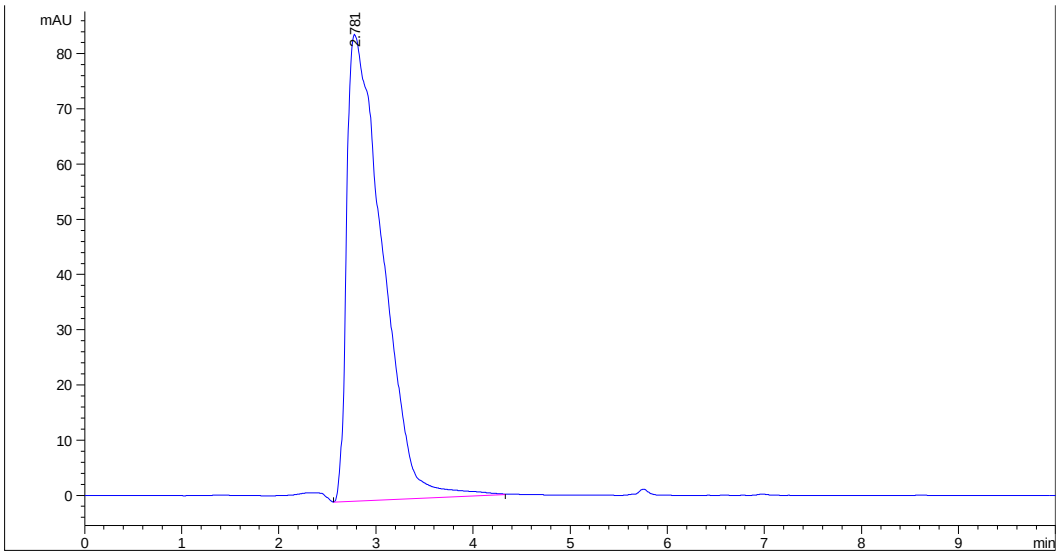

Figure 4-6 HPLC chromatogram of blank liposomes consisting of DPPC, cholesterol and DOPE

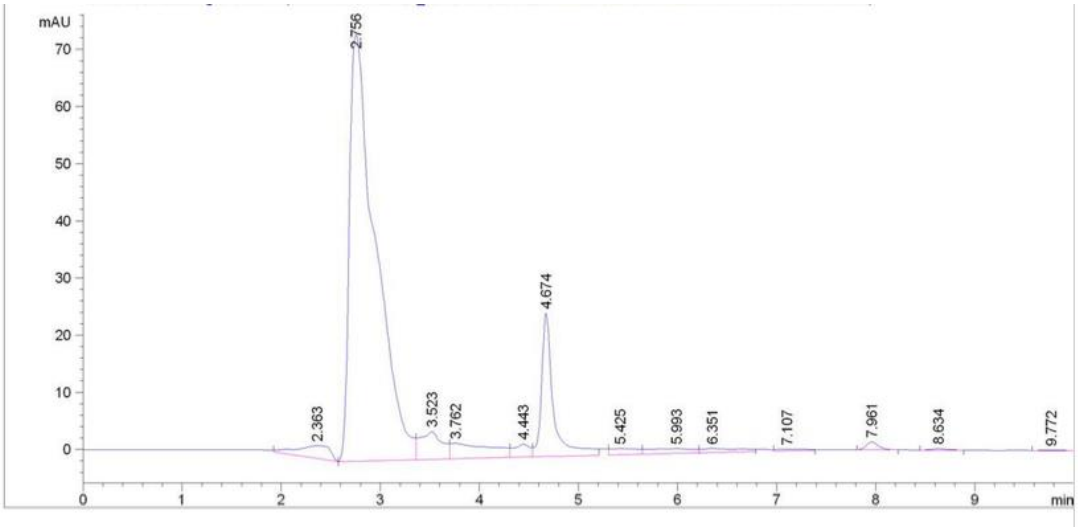

Figure 4-7 HPLC chromatogram of liposomes consisting of DPPC, cholesterol and DOPE containing erlotinib

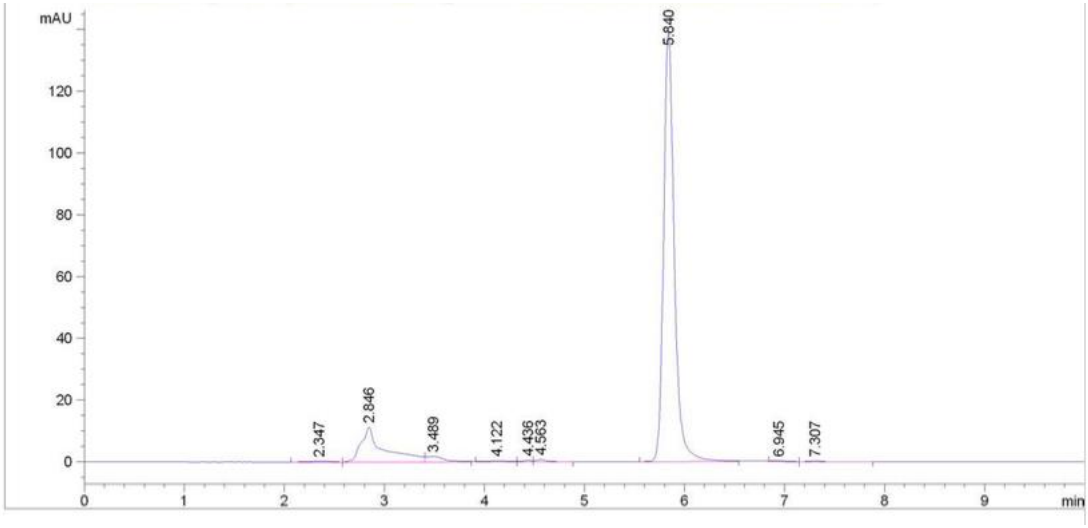

Figure 4-8 HPLC chromatogram of liposomes consisting of DPPC, cholesterol and DOPE containing genistein

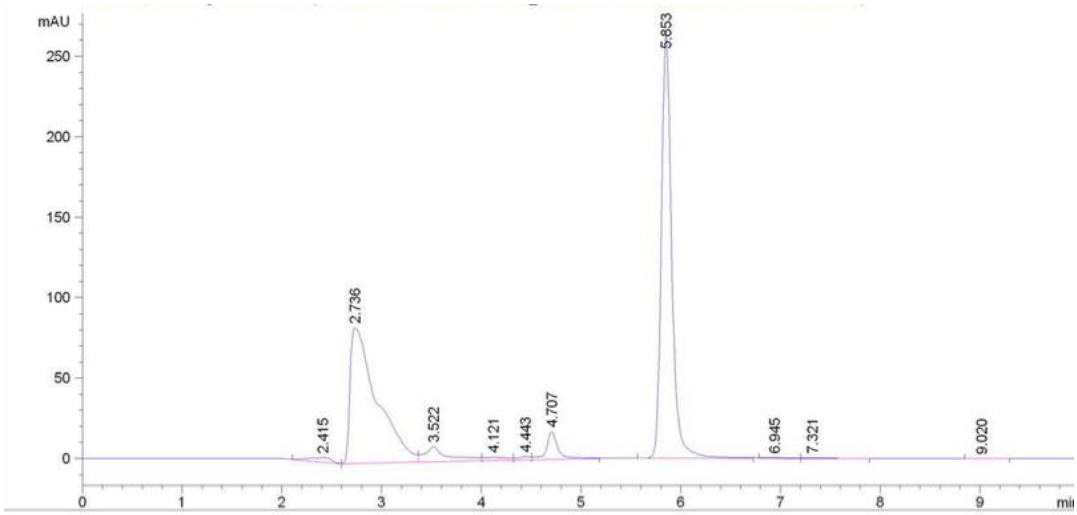

Figure 4-9 HPLC chromatogram of liposomes consisting of DPPC, cholesterol and DOPE containing erlotinib and genistein

4.5.1.2 Calibration curves for erlotinib, genistein and co-quantification of erlotinib and genistein

In order to examine the linearity of HPLC methods for quantification and co-quantification of erlotinib and genistein, serial dilutions of both standard solutions were prepared ranging from 1 to 70 µg/mL. Each graph was plotted as peak response (mAU) versus concentration of drug (µg/ mL), yielding an equation for the line as shown in Figure 4-10 to Figure 4-13. Based on the obtained analysis of the least-square regression, correlation coefficients that present the linear relationship between the peak areas of analyte and analyte concentrations were achieved with $R^2 > 0.999$ for the determined calibration curves. This represents good linearity for the analytical procedures over the drug concentration range investigated (Sistla et al., 2005; Faivre et al., 2011).

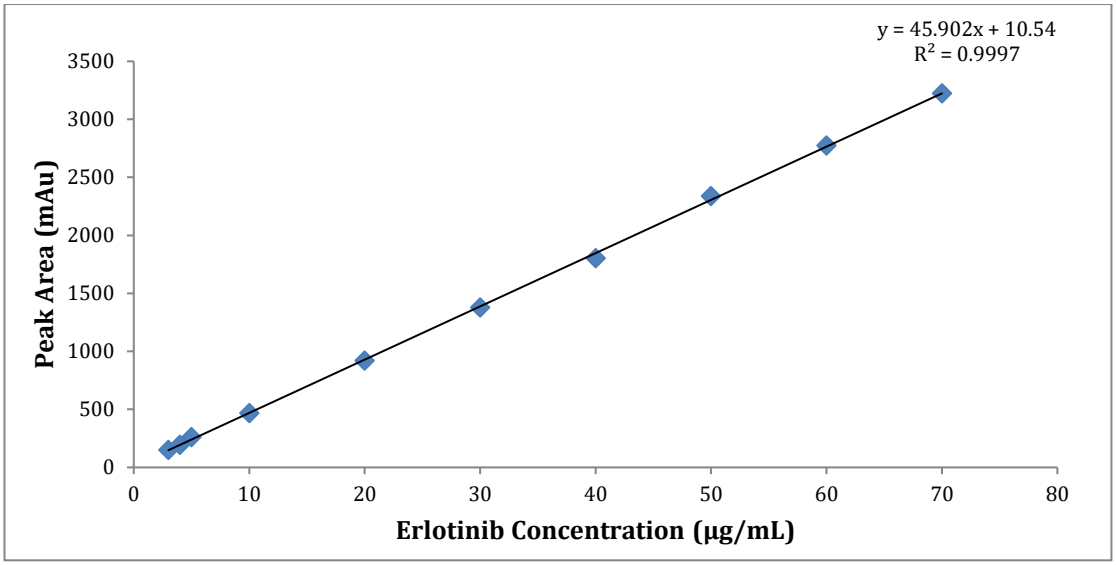

Figure 4-10 HPLC calibration curve of erlotinib (n= 3)

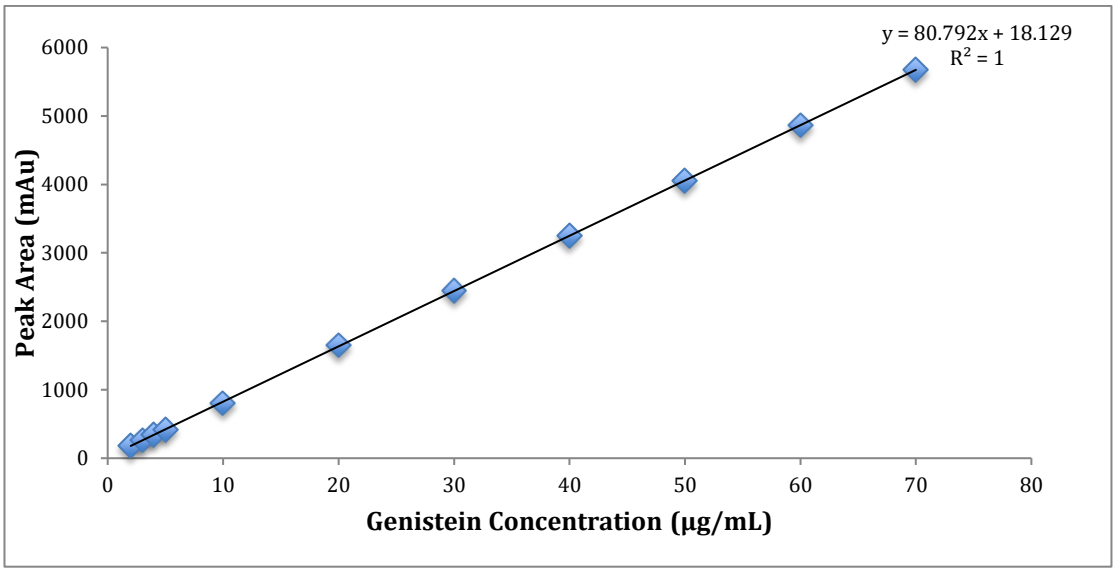

Figure 4-11 HPLC calibration curve of genistein (n=3)

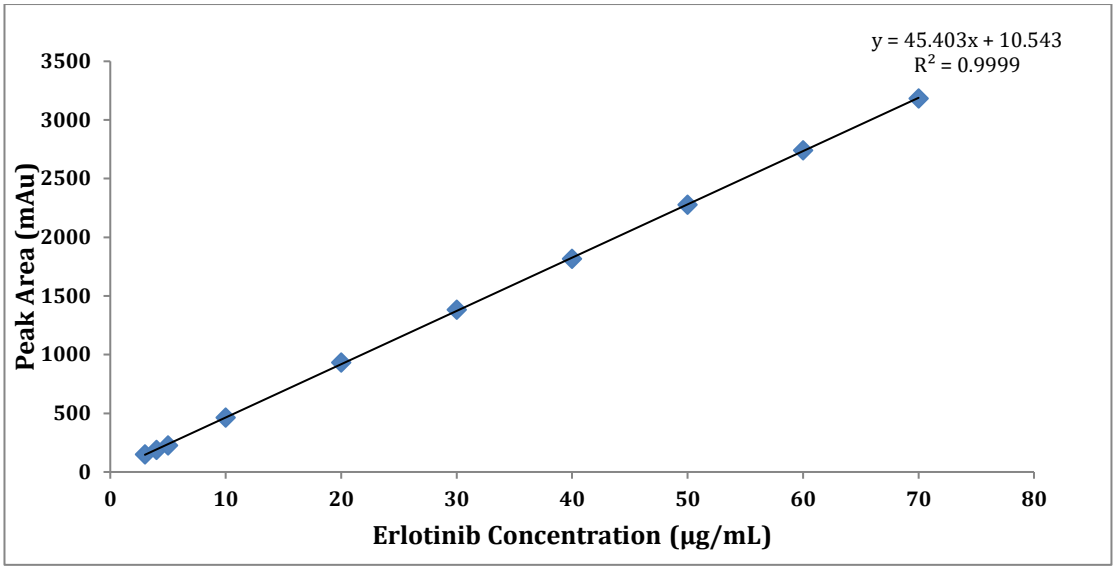

Figure 4-12 HPLC calibration curve of erlotinib (in presence of genistein) (n= 3)

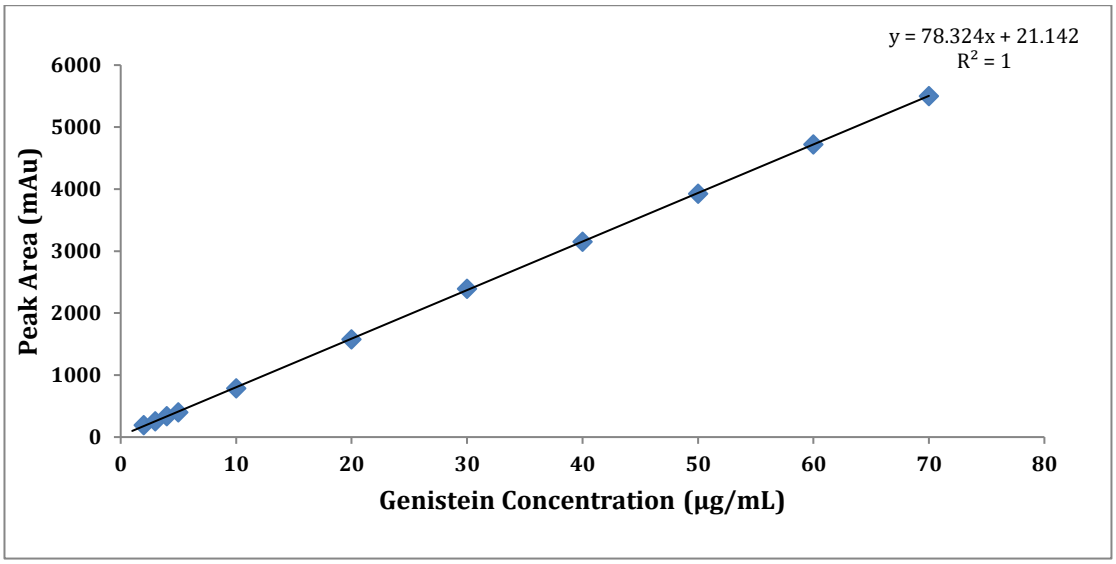

Figure 4-13 HPLC calibration curve of genistein (in presence of erlotinib) (n= 3)

4.5.1.3 **Analytical method validation**

The developed HPLC method for quantification of erlotinib and genistein did not require any buffer solutions throughout the analysis as compared to previous methods for erlotinib (Faivre et al., 2011; Bolandnazar et al., 2013; Latha et al., 2017) and genistein (Supko and Phillips, 1995; Da Costa César et al., 2006;

Pandit and Patravale, 2011). The results for analytical method validation, which included linearity, precision, accuracy, LOD and LOQ were achieved according to ICH guidelines with short analysis times (Table 4-4). The LOD and LOQ values were calculated based on the slope and standard deviation of the Y-intercept of the regression analysis of linear curves, as opposed to alternatives used to determine these critical values; for example, the signal to noise ratio (Latha et al., 2017).

Table 4-4 Regression characteristics, validation and system suitability for the analysis of erlotinib and genistein (n=4)

Parameters	**Individual HPLC analysis**		**Simultaneous HPLC analysis**	
	Erlotinib	**Genistein**	**Erlotinib**	**Genistein**
Retention time (min)	4.6	5.8	4.6	5.8
Linearity range (µg/mL)	3-70	2-70	3-70	2-70
Number of samples per curve	10	11	10	11
Limit of detection (µg/mL)	0.78	0.18	0.34	0.25
Limit of quantification (µg/mL)	3.00	2.00	3.00	2.00
Accuracy (% RE)	97.60–108.69	97.46-102.53	94.76–101.63	96.53-109.60
Precision (%RSD, n=3)	1.89- 7.52	0.55- 2.84	1.03- 9.86	1.26- 5.11
Repeatability (%RSD) at 35 µg/mL (n=9)	2.70	3.27	3.29	1.32

Table 4-5 shows that the intra-day and inter-day precisions determined by %RSD and the accuracy values (%RE) for individual and simultaneous HPLC analysis of erlotinib and genistein (8, 35 and 55 µg/mL), were within the acceptance criteria, being less than 5% SD (Sistla et al., 2005).

These HPLC methods show the similar retention time using a simpler composition of mobile phase compared with previous reports of the quantitative determination of erlotinib and genistein individually, providing a rapid, simple and cost-effective analytical method. Co-quantification of erlotinib and genistein has not been previously reported. This method can be used to simultaneously quantify erlotinib and genistein throughout the remaining studies.

Table 4-5 Inter-day and Intra-day variability of the HPLC method (n=4, mean± S.D)

Nominal concentration (μg/mL)	Intra-day			Inter-day			Intra-day			Inter-day		
	Measured concentration (μg/mL)	%RSD	%RE	Measured concentration (μg/mL)	%RSD	%RE	Measured concentration (μg/mL)	%RSD	%RE	Measured concentration (μg/mL)	%RSD	%RE
	Individual analysis of erlotinib						**Individual analysis of genistein**					
8	8.09± 0.10	1.19	-1.11	8.09± 0.24	2.94	-1.07	7.97± 0.09	1.19	0.32	7.93± 0.28	3.47	0.83
35	34.91± 0.17	0.49	0.27	34.44± 0.93	2.70	1.61	35.15± 0.26	0.73	-0.43	34.71± 1.13	3.27	0.82
55	54.09± 0.70	1.29	1.66	53.90± 1.27	2.36	2.00	55.16± 0.20	0.36	-0.29	54.05± 1.44	1.73	1.73
	Co-quantification analysis of erlotinib						**Co-quantification analysis of genistein**					
8	8.30± 0.18	2.11	-3.81	8.04± 0.28	3.50	-0.51	7.93± 0.08	0.97	0.89	7.89± 0.07	0.93	1.34
35	34.74± 0.22	0.63	0.73	34.28± 1.13	3.29	2.05	35.02± 0.12	0.35	-0.07	34.81± 0.46	1.32	0.55
55	54.30± 0.21	0.40	1.27	53.90± 1.26	2.34	2.01	54.55± 0.08	0.16	0.82	54.51± 0.62	1.14	0.89

4.5.2 Characterisation of drug-loaded liposomes

Saturated lipid hydrogenated soybean phosphatidylcholine (HSPC) and cholesterol have previously been used in the preparation of liposomes encapsulating either erlotinib or genistein (Phan et al., 2013; Mandal et al., 2016; Li et al., 2017; Zhou et al., 2018). However, co-encapsulation of erlotinib (log P=2.75) and genistein (log P=2.84) into liposomes has not yet been reported. This combination was studied as an interesting and rational challenge for pulmonary delivery.

Dipalmitoylphosphatidylcholine (DPPC), which contains two 16-carbon (palmitoyl) chains as compared to a mixture of 16 and 18–carbon chains for HSPC, was chosen as the main phospholipid component in the liposomal formulations studied here (Monteiro et al., 2014). DPPC and HSPC are not commercially available in inhalation products, though DPPC has been used for delivering ciprofloxacin in clinical trials. The use of DPPC as a major lipid in liposomes for the delivery of erlotinib and genistein individually and in combination was investigated since it was challenging for preparation, characterisation and optimisation. Secondly, the phase transition temperature of DPPC (41° C) is above 37° C, ensuring that there is no rapid loss of drug at body temperature (Chen et al., 2014). Importantly, DPPC is a major component of lung surfactant and may be more suitable for pulmonary delivery than HSPC (Kaviratna and Banerjee, 2012; Joshi et al., 2014).

4.5.2.1 Effect of cholesterol concentration on the properties of DPPC liposomes containing either erlotinib or genistein

A previous study demonstrated that the incorporations of cholesterol and DOPE into HSPC liposomes at the appropriate ratio improved the entrapment efficiency and stability of genistein-loaded liposomes compared with those of the HSPC alone (Phan et al., 2013). This was due to changes in the lipid packing and fluidity of the phospholipid bilayer (Phan et al., 2013). Initially in this study, 5% w/w

erlotinib or 5% w/w genistein in DPPC was fixed, and then cholesterol content was varied (ranging from 0 to 30 mol% of total lipid content), to study the effect of cholesterol concentrations on the properties of erlotinib or genistein-containing DPPC liposomes.

DPPC liposomes in the absence of cholesterol and those containing 8 mol% of cholesterol showed the similar encapsulation efficiency of genistein (Figure 4-14, respectively; 45% and 38.5% EE). This suggests that adding cholesterol content up to 8 mol% in the presence of genistein had no measurable impact on the packing of genistein within the saturated hydrocarbon chains of DPPC. As the inclusion of cholesterol was increased from 8% to 30%, a decrease in entrapment efficiency of genistein was seen ($p<0.05$). This may be because greater concentrations of cholesterol cause phase separation in the bilayer with a formation of cholesterol domain and/or a reduced free volume of the hydrocarbon chains, resulting in an exclusion of genistein from the liposomal bilayer and a decrease in genistein entrapment as described previously for other hydrophobic drugs (Elhissi et al., 2006b; Kępczyński et al., 2008). Cholesterol thus plays an important role in the molecular interaction of all other molecules present in the lipid bilayer, resulting in changes in bilayer properties and having a consequent effect on the incorporation of hydrophobic drugs (Chountoulesi et al., 2017).

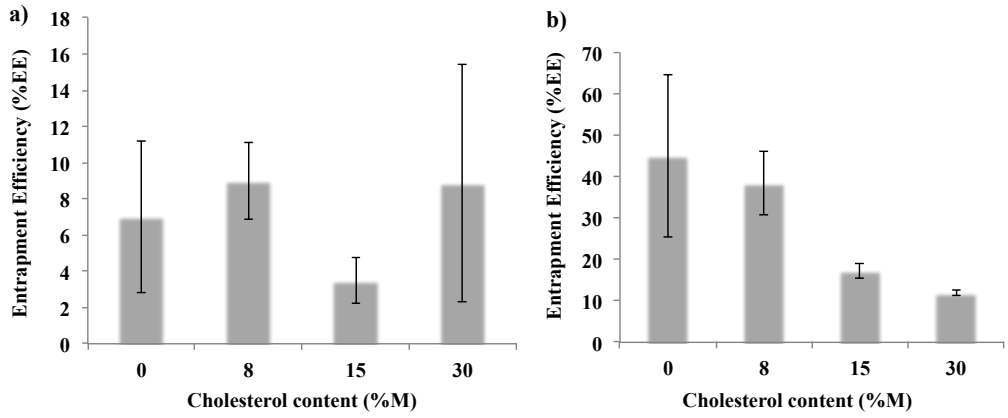

Figure 4-14 Effect of cholesterol content (mol%) on entrapment efficiency (%EE) of a) erlotinib and b) genistein in DPPC liposomes (n=3, mean ± S.D.)

The entrapment efficiency for erlotinib did not change with increasing cholesterol content (range 3.50 – 8.86 % EE), indicating no significant effect of cholesterol

on entrapment efficiency for erlotinib over the range investigated. This could be due to the differences in partitioning and orientation between erlotinib and cholesterol in the liposomal membrane (Zhao et al., 2007). Erlotinib may be predominantly located near the polar head groups of DPPC liposomes, whereas cholesterol was oriented within the bilayer (Monteiro et al., 2014). Moreover, entrapment efficiency of erlotinib was comparatively lower than genistein for all loading concentrations ($p<0.05$).

The incorporation of therapeutic agents into the liposomal bilayer depends on the nature of drugs (e.g. its molecular structure, polarity and oil/water partition coefficient) and the properties of lipid (hydrocarbon chain length, packing density and bilayer fluidity). These can all determine the localisation of drugs within the bilayer and their incorporation into liposomes, especially for hydrophobic drugs (Bozzuto and Molinari, 2015). This is because hydrophobic molecules tend to reside in the acyl chain regions within the bilayer rather than near the polar head groups of phospholipids in the liposomes (Bozzuto and Molinari, 2015). Cholesterol in DPPC bilayer modifies liposomal membrane properties particularly molecular packing and bilayer fluidity and consequently impacts drug incorporation into the bilayer especially for genistein. Differences in the molecular structures of erlotinib and genistein seem to affect the orientation of the drug molecules within the DPPC-based bilayer, reflected in differences in drug incorporation for the two drugs at the same cholesterol contents. Specifically, genistein appears to partition deeper than erlotinib within the bilayer in the hydrocarbon chain region, such that changes in packing order of the DPPC bilayer by cholesterol highly affected genistein incorporation.

Inclusion of 8 mol% cholesterol significantly reduced the variability in the entrapment efficiencies for both drugs, indicating a more reproducible and stable liposome production. Previously, research has shown cholesterol has a great effect on bilayer and thermal properties in a concentration dependent manner (Demetzos, 2008; Monteiro et al., 2014). Cholesterol increases the number of gauche configurations (kinks) in the phospholipid hydrocarbon chains at or below T_c (less rigid), which is associated with an increased lipid mobility and permeability in the gel phase compared to bilayers of the pure phospholipid (Cortijo and Chapman,

1981; Monteiro et al., 2014). By contrast, there is a decrease in the changes from trans to gauche configuration in lipids above the T_c, causing a reduction in bilayer fluidity and permeability in the fluid state (Cortijo and Chapman, 1981). The steroid rings of cholesterol are dense, and incorporation of cholesterol into the bilayer increases the density of hydrocarbon chains, decreases the fluidity, leading to higher rigidity of the liposomal bilayer (Monteiro et al., 2014). This effect was dependent on cholesterol concentration. At very high cholesterol concentration (i.e. 50 mol%) and greater, the phospholipid phase transition is effectively abolished (Cortijo and Chapman, 1981; Taylor and Morris, 1995).

4.5.2.2 Effect of cholesterol concentration on particle size distribution of liposomes containing either erlotinib or genistein

Mean particle size was not significant different for sonicated liposome formulations in the absence of cholesterol and those containing 8 mol% of cholesterol (Figure 4-15, $p>0.05$). However, there was an increase in mean size when cholesterol content was greater than 8 mol% for formulations containing either erlotinib or genistein ($p<0.05$). These findings were in accordance with previous reports of sonicated DPPC liposomes containing various cholesterol concentrations, indicating a concentration-dependent effect on mean size (Lopez-Pinto et al., 2005; Pattni et al., 2015). There was considerable variability in measurement of the hydrodynamic diameter for higher cholesterol contents (15% and 30% mole) particularly for erlotinib formulations. Moreover, some aggregation was apparent at ambient temperature for 30 mol% of cholesterol for both preparations, and also found for 15 mol% of cholesterol for erlotinib formulations within 5 min. These observations may suggest a phase separation, with a formation of cholesterol-rich domain. By contrast, there was no difference in PDI values ($p>0.05$). These results show that 8 mol% cholesterol in bilayer provides a restriction on the radius of vesicles that can be achieved by sonication.

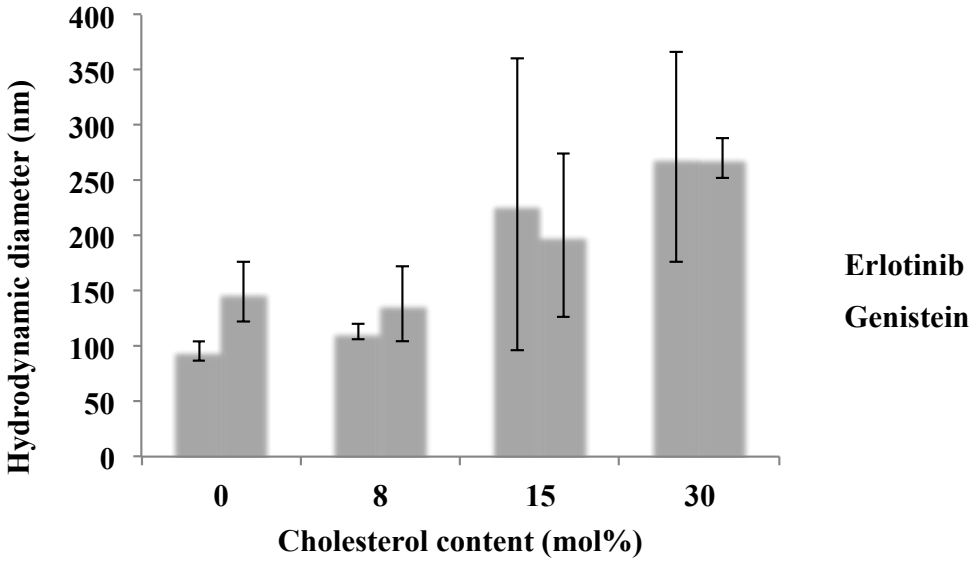

Figure 4-15 Effect of cholesterol concentration on mean hydrodynamic diameter (nm) of DPPC liposomes containing erlotinib or genistein after 30 min sonication (n=3, mean± S.D.)

Cholesterol is frequently included in liposome bilayers to control drug release or increase their in vivo and in vitro stability by stabilising the bioactive agent in the core of the liposome (Taylor and Morris, 1995; Monteiro et al., 2014)). Based on the findings for size stability and drug incorporation, a formulation including 8 mol% cholesterol was taken into further studies.

4.5.2.3 Effect of including DOPE on the properties of DPPC/Cholesterol liposomes loaded with either erlotinib or genistein

The degree of fatty acid saturation influences the permeability and packing of the phospholipid bilayer (Monteiro et al., 2014). Unsaturated lipids can have increased spaces between the tightly packed hydrocarbon tails within a bilayer. This may cause an increased bilayer fluidity and permeability compared with saturated hydrocarbon chains (Monteiro et al., 2014).

DOPE has previously been used as an unsaturated lipid to alter the bilayer packing and fluidity, thereby increasing the diffusivity and partitioning of exogenous compounds (Phan et al., 2013; Joshi et al., 2014). Formulations comprising DPPC and DOPE were not toxic upon inhalation, since DOPE acts as

a surfactant and is similar to the surfactant Protein-B (SP-B) present in endogenous lung surfactant (Joshi et al., 2014). Furthermore, fusogenic lipid like DOPE is usually used as a helper lipid in liposomes for enhancement of membrane permeability and improvement in intracellular drug delivery, due to its structural features. Consequently, DOPE, was considered in this study.

No studies have so far investigated the use of DPPC, cholesterol and DOPE for the incorporation of erlotinib and/or genistein into liposomes for delivery by pulmonary route. In this study, 20 mol% DOPE was initially studied based on a previous report of genistein incorporation (Phan et al., 2013). Encapsulation efficiency of erlotinib increased by approximately 16% ($p<0.05$) compared to those without DOPE (Figure 4-16). Differences in drug incorporation between the two drugs due to the inclusion of DOPE may be resulted from the orientation of drug molecules and DOPE, as found for inclusion of cholesterol. This suggests that the presence of 20% mole of this flexible unsaturated phospholipid (DOPE) enhanced incorporation of both drugs and would potentially be advantageous for the co-incorporation of erlotinib and genistein. However, the mole ratios between DPPC, cholesterol and DOPE should be further investigated to allow accommodation of both erlotinib and genistein molecules within the bilayer.

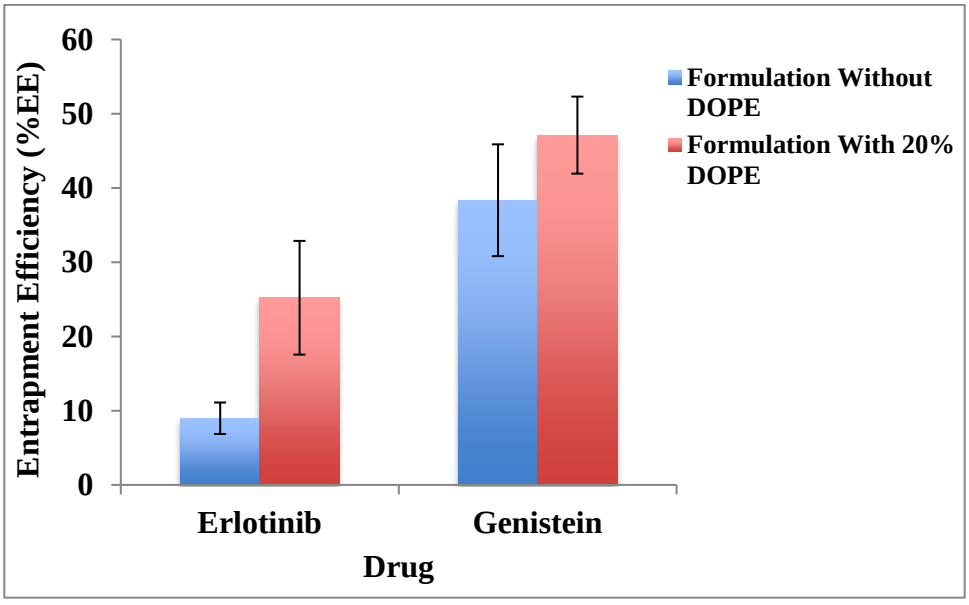

Figure 4-16 Effect of including DOPE on entrapment efficiency of 5% w/w erlotinib or 5% w/w genistein in DPPC: cholesterol (92:8) liposomes (n=3, mean ± S.D.)

4.5.2.4 Effect of sonication time on encapsulation efficiency of erlotinib or genistein in liposomes

The mean size of DPPC: cholesterol: DOPE (72:8:20) liposomes containing either erlotinib or genistein was reduced using probe-sonication from the initial size of approximately 7μm. From 15 min to 30 min sonication, encapsulation efficiencies of erlotinib and genistein evidently increased before remaining almost the same level (Figure 4-17). Consequently, 30 min sonication was chosen based on the high encapsulation efficiency of both drugs.

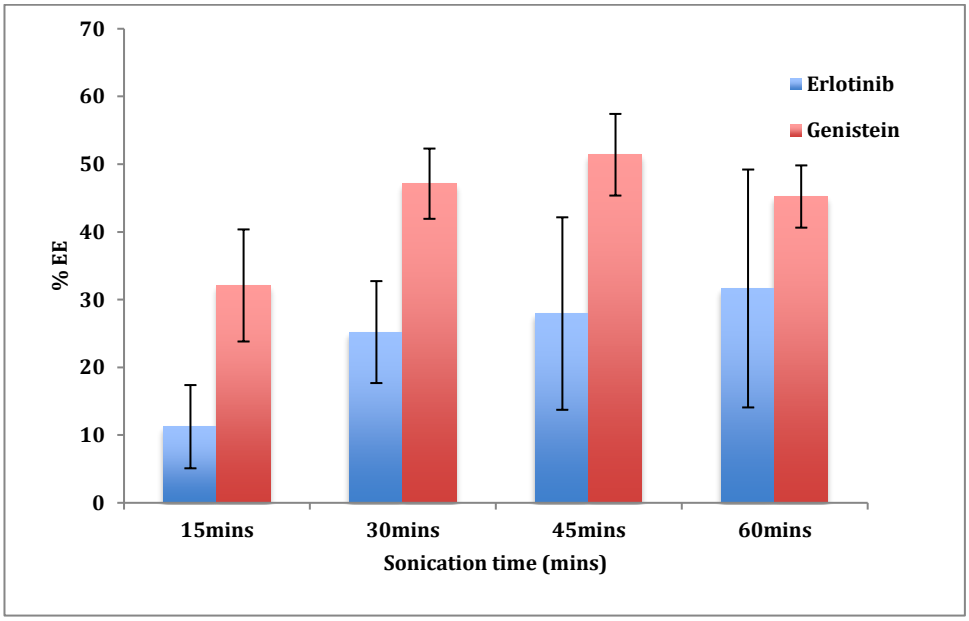

Figure 4-17 Effect of sonication time (min) on encapsulation efficiency (%EE) of 5% w/w erlotinib or 5% w/w genistein in DPPC: cholesterol: DOPE (72: 8: 20) liposomes (n=3, mean ± S.D.)

4.5.3 Characterisation of liposomes co-loaded with erlotinib and genistein

The inclusion of cholesterol (8 mol%) and DOPE (20 mol%) into DPPC bilayers gave improvements in drug entrapment for both drugs individually (5% w/w drug in total lipid). Since hydrophobic molecules are located within phospholipid bilayer, not only lipid composition but also the drug-to-lipid ratio will impact encapsulation efficiency (Bozzuto and Molinari, 2015; Chountoulesi et al., 2017). In this study, the weight ratio of total lipid: drug was investigated to identify the maximum drug incorporation for erlotinib and genistein when incorporated

individually or co-loaded into liposomes. Both individual and co-encapsulation formulations with the drug content of 2.5% w/w showed the highest entrapment efficiency of the three concentrations investigated ($p<0.05$, Table 4-6).

The encapsulation efficiencies of genistein in co-loaded DPPC formulations were the same as those for genistein alone ($p>0.05$), whereas the entrapment efficiency was lower for erlotinib in co-loaded liposomes. This may indicate drug-drug and/or drug-lipid interactions within phospholipid bilayers, resulting in the changes in the fluidity of phospholipid bilayers and physical drug entrapment, as previously described (Section 4.5.2.1).

The mean hydrodynamic diameter for all preparations was smaller than 200 nm except for 10% w/w co-loaded liposomes, while preparations were relatively polydispersed (PDI >0.3) except erlotinib-containing liposomes. The surface charge was in the range +0.66 to +4.78 mV. The formulation of erlotinib and genistein (2.5% w/w each drug in DPPC or 5% w/w total drug in DPPC) was further studied to identify the optimal DOPE content. It is noted that cholesterol content was maintained at 8 mol% and the drug concentration in total lipid was constant (5% w/w).

Table 4-6 Effect of drug-to-lipid ratio (%w/w) on the properties of DPPC liposomes (n=3, mean± S.D.)

Concentration (%w/w drug in lipid)	**Formulation**	**Entrapment Efficiency (EE; %)**	**Mean particle size (nm)**	**Polydispersity Index (PDI)**	**Zeta Potential (mV)**
2.5%	Erlo (Ind.)	32.53± 6.05	106.37± 1.84	0.25± 0.02	+4.78± 0.99
	Erlo (Comb.)	14.65± 3.42	159.22± 19.42	0.44± 0.09	+2.42± 1.82
	Gen (Ind.)	84.66± 2.70	139.03± 11.70	0.43± 0.02	+1.34± 0.77
	Gen (Comb.)	90.03± 10.99	159.22± 19.42	0.44± 0.09	+2.42± 1.82
5%	Erlo (Ind.)	13.20± 5.53	99.68± 2.18	0.22± 0.01	+4.78± 1.63
	Erlo (Comb.)	7.02 ±1.13	200.07± 45.81	0.50±0.12	+2.35± 0.43
	Gen (Ind.)	58.54± 8.06	158.17± 7.27	0.43± 0.05	+0.74± 0.46
	Gen (Comb.)	71.48± 9.03	200.07± 45.81	0.50±0.12	+2.35± 0.43
10%	Erlo (Ind.)	11.45± 10.70	106.67± 23.80	0.35± 0.17	+4.47± 2.09
	Erlo (Comb.)	3.09± 0.87	317.8± 57.06	0.86± 0.16	+3.54± 0.26
	Gen (Ind.)	24.05± 3.92	146.03± 16.49	0.51± 0.04	+0.66± 0.28
	Gen (Comb.)	41.24± 6.74	317.8± 57.06	0.86± 0.16	+3.54± 0.26

*Ind = Individual formulation and Comb= Combination formulation

Based on preliminary experiments, the incorporations of 20 mol% of DOPE and 8 mol% of cholesterol into DPPC liposomes improved the entrapment efficiency for erlotinib alone compared with the formulation without DOPE ($p<0.05$). Therefore, the content of DOPE (0-40 mol% of total lipid contents) was varied to determine the effect on co-loading of the two drugs. As seen in Table 4-7, there was no significant difference in encapsulation efficiency for genistein when DOPE was increased ($p>0.05$). By contrast, the highest drug entrapment ($p<0.05$) for erlotinib (23.16%) was achieved in the presence of 20 mol% DOPE before decreasing to approximately 12.5% EE ($p<0.05$). This may be because the inclusion of DOPE at lower contents increases the fluidity of the bilayer and consequently enhances drug incorporation. However, as higher concentrations of DOPE (>20 mol%), the internal volume to accommodate both drugs is reduced due to its localisation within bilayer. Hence, the formulation (DPPC: cholesterol: DOPE, 72:8:20) was considered optimal and used for further studies. In terms of mean hydrodynamic diameter, all formulations had mean size< 200 nm as desired.

Co-encapsulation of more than one drug into the same phospholipid bilayer may alter the liposome properties such as drug entrapment, mean size and the lipophilicity of membrane (Ingebrigtsen et al., 2017). There were significant increase in mean hydrodynamic diameter and particle size distribution when comparing liposomes co-loaded with erlotinib and genistein with those containing erlotinib ($p<0.05$). Considering drug entrapment, encapsulation efficiencies of erlotinib in co-loaded liposomes containing cholesterol (8 mol%) and DOPE (20 mol%) were significantly higher than co-loaded formulations without those two molecules ($p<0.05$), suggesting that the incorporation of genistein in the presence of cholesterol and DOPE into lipid bilayer may significantly alter the mobility and permeability of the lipids within bilayer (Table 4-6 and Table 4-7). Genistein and the other two molecules were expected to have a stronger association with the lipid bilayer than erlotinib and be localised within both superficial and deep layer of hydrocarbon chains. Hence, this effect may cause a change in membrane properties, causing an enhanced incorporation of erlotinib within the aqueous part and/or first few layers of fatty acyl chains of the liposomes.

To sum up, the co-delivery of erlotinib and genistein in liposomes comprising DPPC, cholesterol and DOPE (mole ratio of 72:8:20) would be beneficial to reduce the excipients used in individually prepared composition and potentially simplify administration. This co-loaded formulation was therefore considered appropriate for further studies.

Table 4-7 Effect of DOPE concentration (%w/w) on the properties of DPPC: cholesterol (92:8) liposomes co-loaded with 2.5% w/w erlotinib and 2.5% w/w genistein in total lipid (n=3, mean± S.D.)

Concentration of DOPE (%w/w drug in lipid)	**Drug**	**Entrapment Efficiency (EE; %)**	**Mean particle size (nm)**	**Polydispersity Index (PDI)**	**Zeta Potential (mV)**
0%	Erlotinib	12.87± 5.11	139.3± 16.18	0.42± 0.01	+1.88± 0.84
	Genistein	88.26± 7.15			
10 %	Erlotinib	11.96± 0.51	147.03± 38.41	0.52± 0.15	-2.18± 1.28
	Genistein	99.34± 0.47			
20%	Erlotinib	23.16± 2.08	128.00± 13.70	0.44± 0.05	-3.23± 0.05
	Genistein	101.58± 12.72			
30%	Erlotinib	16.67± 2.64	113.25± 7.58	0.37± 0.03	-7.31± 0.51
	Genistein	96.07± 2.51			
40%	Erlotinib	12.50± 0.76	102.69± 6.71	0.39± 0.02	-8.97± 0.54
	Genistein	98.22± 0.90			

4.5.4 Transmission electron microscopy

TEM images of co-loaded liposomes, size reduced by probe sonication, showed a population of small spherical liposomes between 100 and 200 nm in diameter (Figure 4-18). This was in good agreement with other previous reports of multilamellar vesicles (MLVs) prepared by thin-film hydration method and reduced size by probe-sonication (Bozzuto and Molinari, 2015; Pattni et al., 2015; Rudokas et al., 2016).

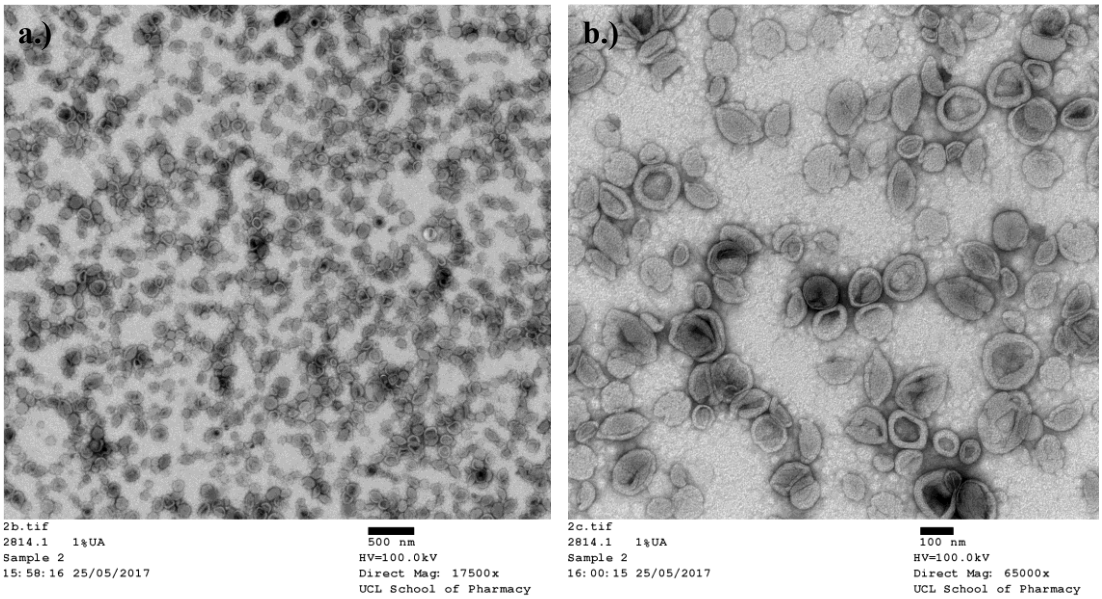

Figure 4-18 TEM images of erlotinib and genistein co-loaded liposomes (a.) 17500 x and (b.) 65000 x

4.5.5 Thermal analysis of liposomes

Differential Scanning Calorimetry (DSC), a highly sensitive thermal analytical technique, has been used extensively to study liposomal systems, giving information on drug-liposome interactions that may impact entrapment efficiency, stability and drug release (Taylor and Morris, 1995; Budai et al., 2003; Demetzos, 2008; Chen et al., 2014). DSC is a quick, simple and relatively low-cost technique compared with other thermoanalytical methods and provides accurate information about melting point and melting range, glass transitions, interactions, compatibility, decomposition, purity, and polymorphism based on changes on thermotropic properties (Demetzos, 2008). For liposomes, changes in the thermal

parameters of the lipid bilayers (i.e., T_m, HHW and ΔH) after incorporating drugs are associated with drug-lipid interactions, the stability of the formulation, and the percentage of active ingredient that can be incorporated into liposomal bilayer. This information allows for rational formulation design and development (Gardikis et al., 2006; Demetzos, 2008). In this study, calorimetric parameters, namely the pre-transition temperature (T_{pre}), main transition temperature (T_m), enthalpy (ΔH) and half height width (HHW) were investigated to determine drug-bilayer interactions and to determine the maximum drug incorporation into DPPC bilayers for both individual and co-loaded formulations.

4.5.5.1 **Effect of lipid concentrations on the DSC thermogram of liposomes**

The lipid concentration was investigated to determine the lowest concentration of DPPC yielding consistent and reproducible DSC results with good peak resolution. This is beneficial to minimise the waste and cost for formulations with a high content of expensive synthetic lipids. However, high concentrations of lipid may be necessary to give a clear pre- and/or main transition peaks with measureable enthalpies. DPPC liposomes were prepared (Section 4.4.2.1) and their reduced size by probe-sonication to achieve final DPPC concentrations of 2.5, 20 and 40 mg/mL. These were scanned in the DSC at a rate of 1ºC/min. There was no endothermic peak observed for the concentration of 2.5 mg/mL (data not shown). A main phase transition peak was evident at 20 mg/mL, though a clear pre-transition of DPPC was not present (data not shown).

Two different heating rates of 0.50 and 1.00°C/min with DPPC (40mg/mL) were employed to obtain high resolution of DSC thermograms to allow accurate calculation of T_{pre}, T_m, HHW and enthalpy. From previous reports, a slow scan rate is recommended for a highly purified phosphatidylcholines (PCs) as it yields high resolution and minimises broad and/or overlapping transitions (Sturtevant, 1987). Slower heating rates may however lead to low sensitivity, resulting in the requirements for higher instrumental sensitivity (Sturtevant, 1987; Chiu and Prenner, 2011). High Sensitivity Scanning Calorimeter (HSDSC) was thus performed in this study to overcome these problems. Based on a preliminary study, 0.5°C/min was determined to be a suitable scanning rate since it gave the

expected thermal events with peaks for the main and pre-transition evident (Figure 4-19), while there was no pre-transition apparent at 1.0 °C/min.

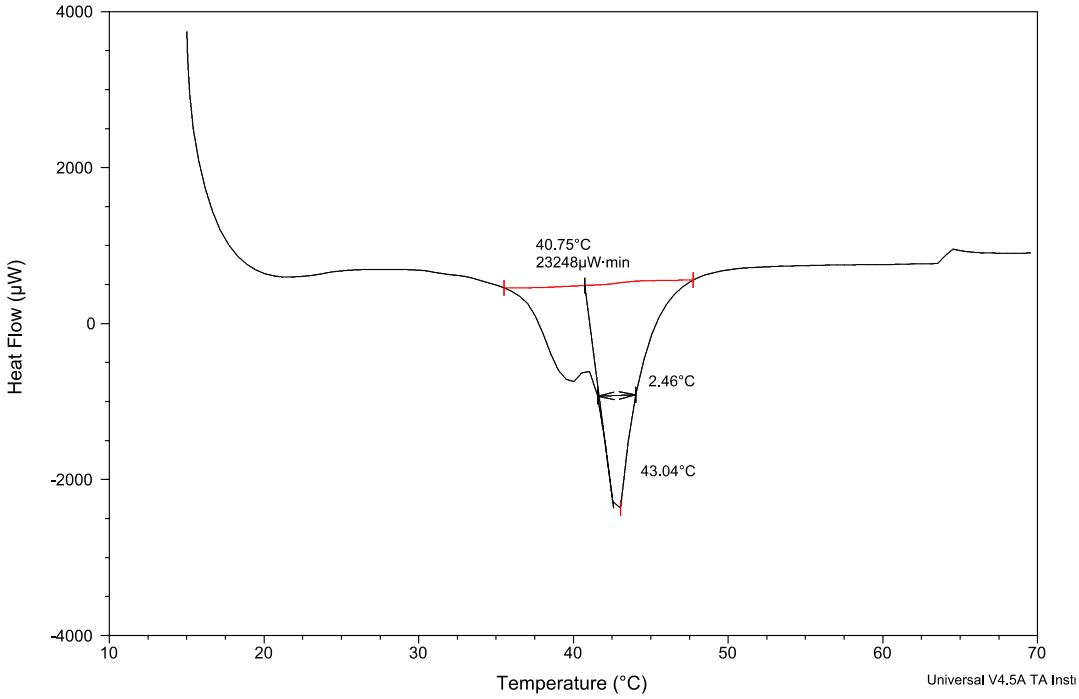

Figure 4-19 DSC thermogram of DPPC liposomes (40 mg/mL) scanned at 0.5 ºC/min

4.5.5.2 Thermal properties of DPPC liposomes reduced size by probe-sonication method

As DSC is very sensitive and able to detect slight changes in bilayer properties, DPPC liposomes (40 mg/mL) before and after size reduction were studied by HSDSC with a scan rate of 0.5°C/min (Chiu and Prenner, 2011). For non-sonicated DPPC liposomes, the values of thermal transitions such as a small broad pre-transition at 36 ºC and a sharp acyl chain melting transition at 41 ºC are in accordance with previous reports (Zhao et al., 2004; Wu et al., 2012; Hadian et al., 2014).

The pre-transition corresponds to a change in the orientation of the polar head groups of DPPC from a one-dimensional lamellar (Planar Gel Phase, $L_{\beta'}$) to a two-dimensional monoclinic lattice (Rippled Gel Phase, $P_{\beta'}$) (Taylor and Morris, 1995; Beni et al., 2006; Elhissi et al., 2006b). Probe sonication of DPPC

liposomes prepared by the thin-film hydration method, resulted in a decrease in the enthalpy of the pre-transition and main transition ($p<0.05$; Table 4-8). The pre-transition temperature significantly increased from 36.55ºC to 39.36 ºC for sonicated liposomes ($p<0.05$) as shown in Table 4-8, implying decreased mobility in the head group region of DPPC (Beni et al., 2006).

Table 4-8 Thermal properties of sonicated and unsonicated DPPC liposomes (n=3, mean± S.D.)

Preparation method	**Pre-transition**		**Main transition**			
	[1]T_{pre} (ºC)	[2]ΔH (KJ/mol)	[3]T_{onset} (ºC)	[4]T_m (ºC)	[5]HHW (ºC)	ΔH (KJ/mol)
Sonicated	39.36± 0.29	2.29± 0.66	41.36± 0.09	42.74± 0.28	1.68± 0.16	37.35± 3.05
Non-sonicated	36.55± 0.51	3.15± 1.28	41.54± 0.00	42.72± 0.27	1.62± 0.03	43.88± 0.89

[1]= The temperature of the pre-transition
[2]= Enthalpy
[3]= The onset temperature
[4]= The main temperature of the main transition
[5]= Half-height width

The onset temperature of the main transition (T_0) and the temperature at the peak (T_m), are commonly used to express the main lipid phase transition temperature (T_c) when carbon-carbon single bonds change from the gel phase (all-trans hydrocarbon chain configuration) to liquid-crystalline phase (some acyl chains present in the gauche (kinked) conformation) (Taylor and Morris, 1995; Elhissi et al., 2006b). In this study, T_0 significantly decreased for sonicated liposomes ($p<0.05$). Furthermore, the enthalpy values (main transition endotherm) significantly decreased for both pre- and main transition when the size of DPPC liposomes was reduced ($p<0.05$), suggesting the modifications to the ordered lipid structure of the DPPC bilayers. These observations are in agreement with previous reports for sonicated vesicles, indicating packing differences within the

hydrocarbon chains between the two preparations (Chiu and Prenner, 2011; Hadian et al., 2014).

The width at half-peak (HHW) of the main transition indicates the hydrophobic-hydrophobic interactions within hydrocarbon hydrophobic regions during the transition. The increase in HHW of the main transition represents a reduction in the packing order within the lipid chains, or an increase in the bilayer fluidity, leading to a decrease in the overall transition cooperativity (Budai et al., 2003; Saunders et al., 2007). HHW values for liposomes before and after sonication were similar ($p>0.05$), indicating no measurable impact on the co-operative movement of the rigid hydrocarbon chains.

Overall, liposomes reduced in size by probe-sonication showed some changes in the enthalpies of transition and the melting of the hydrocarbon chains. The data suggest that changes in thermal parameters result from the smaller radius of the sonicated liposomes and disrupted packing of the bilayers, given the highly curved membrane surface of the small sonicated liposomes. Changes in the intermolecular distance between carbon-carbon bonds may affect adjacent molecules, resulting in a reduction in main phase transition (Taylor and Morris, 1995; Beni et al., 2006).

4.5.5.3 Thermal properties of sonicated DPPC liposomes containing different concentrations of erlotinib

DSC thermograms of erotinib-loaded DPPC liposomes at various drug contents (2.5%, 5% and 10% w/w drug in lipid) and empty DPPC liposomes are shown in Figure 4-20, with calculated parameters in Table 4-9. Two thermal events; the pre-transition and main phase transition were measured for empty DPPC liposomes, at 39.36 ºC and 42.74 ºC, respectively. With 2.5% w/w erlotinib, thermograms still showed the pre-transition peak of DPPC liposomes at 39.21 ºC, whereas this transition disappeared at high contents of erlotinib. Since the pre-transition is particularly sensitive when additives are included, the loss of this peak cannot be attributed to any specific molecular changes (Budai et al., 2003; Elhissi et al., 2006b; Zhao et al., 2007). The disappearance of this peak at

concentrations higher than 2.5% implies the presence of erlotinib in the phospholipid head group interfacial region. This observation was previously reported for DPPC liposomes after incorporating hydrophobic and amphiphilic materials (Zhao et al., 2004; Elhissi et al., 2006b).

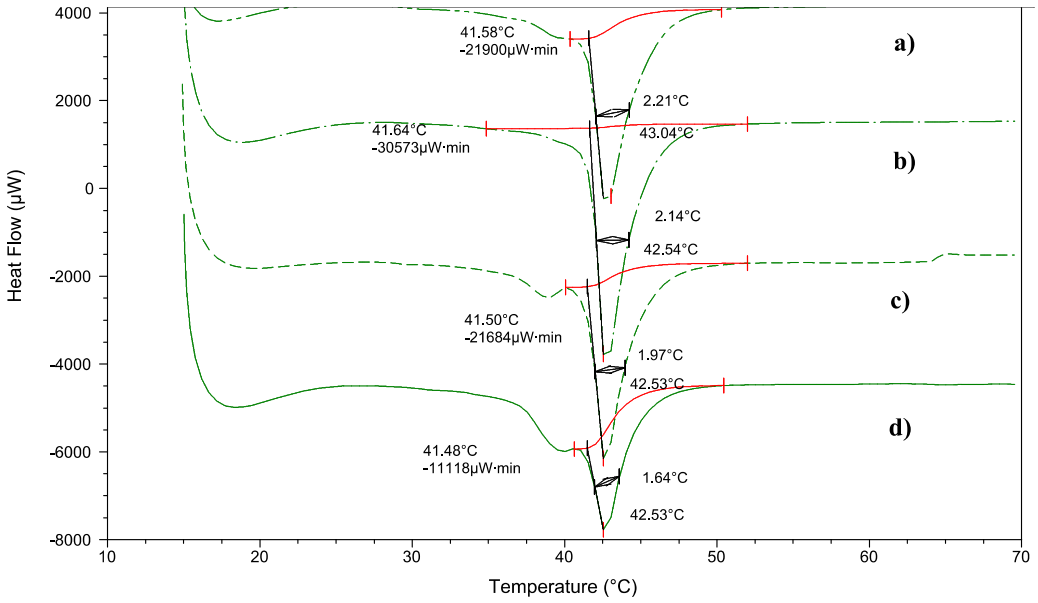

Figure 4-20 DSC thermograms of a) 10%, b) 5%, c) 2.5% erlotinib-incorporated into DPPC liposomes and d) DPPC liposomes

There was no significant change in T_c for all loadings of erotinib compared with DPPC liposomes (Table 4-9, $p>0.05$). The inclusion of erlotinib for the three concentrations investigated did not cause a change in enthalpy ($p>0.05$), indicating no significant impact on the main phase transition. The inclusion of 2.5%, 5% and 10% w/w erlotinib significantly increased the HHW values of DPPC liposomes ($p<0.05$), suggesting a reduction in the overall transition cooperativity, though there was no difference in HHW between the concentrations. This parameter can be used to estimate the maximum level of drug incorporation by either the concentration above which phase separation occurs, or at which no further changes in the main phase transition (Elhissi et al., 2006b). This data was not sufficient to define the precisely maximum erlotinib incorporation; concentrations lower than 2.5% w/w require further studies. Increasing the amount of erlotinib to 10% gave the lowest enthalpy ($p<0.05$), possibly due to phase separation and/or generation of an unstable formulation. Based on these

DSC results, it seems that erlotinib may be located in the upper region of hydrocarbon chains in the bilayer, close to the polar head groups (Beni et al., 2006).

Table 4-9 Thermal properties of erlotinib-loaded DPPC liposomes at concentrations between 2.5% and 10% w/w drug in total lipid (n=3, mean± S.D.)

Erlotinib content (%w/w)	**Pre-transition temperature (ºC)**	**Main transition**						
	T_{pre} (ºC)	T_{onset} (ºC)	T_m (ºC)	HHW (ºC)	ΔH (KJ/mol)	%EE	Mean particle size (nm)	PDI
DPPC	39.36± 0.29	41.36± 0.09	42.74± 0.28	1.68± 0.16	37.35± 3.06	-	109.05± 7.50	0.36± 0.03
2.5%	39.21± 0.28	41.50± 0.11	42.73± 0.27	2.26± 0.11	39.30± 1.50	32.53± 6.05	106.37± 1.84	0.25± 0.02
5%	-	41.43± 0.21	42.54± 0.01	2.27± 0.18	36.73± 2.61	13.20± 5.53	99.68± 2.18	0.22± 0.01
10%	-	41.25± 0.13	42.54± 0.01	2.39± 0.05	28.29± 2.06	2.23± 2.58	122.13± 15.35	0.37± 0.23

There were no differences in mean size or size distribution for all vesicles containing erlotinib compared with empty DPPC liposomes. However, 2.5%w/w showed a significantly higher drug entrapment efficiency compared to other contents ($p<0.05$).

Overall, it seems that erlotinib loaded in liposome bilayers may be predominantly located in the more polar region of the bilayer between C_1 and C_8 of the acyl chains with low interaction with the hydrocarbon chains of DPPC bilayer, and thus having a relatively minor effect on the main phase transition.

4.5.5.4 Thermal properties of sonicated DPPC liposomes containing different concentrations of genistein

No pre-transition peak was observed in the presence of genistein at any of concentrations investigated (Figure 4-21), suggesting the location of genistein near the polar head group region of DPPC bilayer. The T_c shifted to a lower temperature ($p<0.05$) and the main transition of the DPPC (HHW) was significantly broadened ($p<0.05$) for 2.5% w/w genistein-loaded DPPC liposomes. A decrease in the main phase transition temperature suggests incorporation of genistein into the hydrophobic hydrocarbon region of the DPPC bilayer, leading to an increased fluidity with a greater rotational freedom of phospholipid hydrocarbon chains. A broadening of the main phase transition (HHW) also indicates an increase in the fluidity of the liposome bilayer with a reduction in the order of packing within the chains. The presence of genistein may lead to changes in the phospholipid packing by steric restrictions, related to its structure comprising multiple benzene rings. As a consequence, the bilayer structure was disrupted and the membrane fluidity was increased, though the enthalpy was similar to that of DPPC bilayers ($p>0.05$). Increasing the content of genistein higher than 2.5% did not result in any further disruption to the DPPC bilayers, suggesting the highest drug incorporation had been established in the DPPC bilayer, as previously reported for paclitaxel (Zhao et al., 2007).

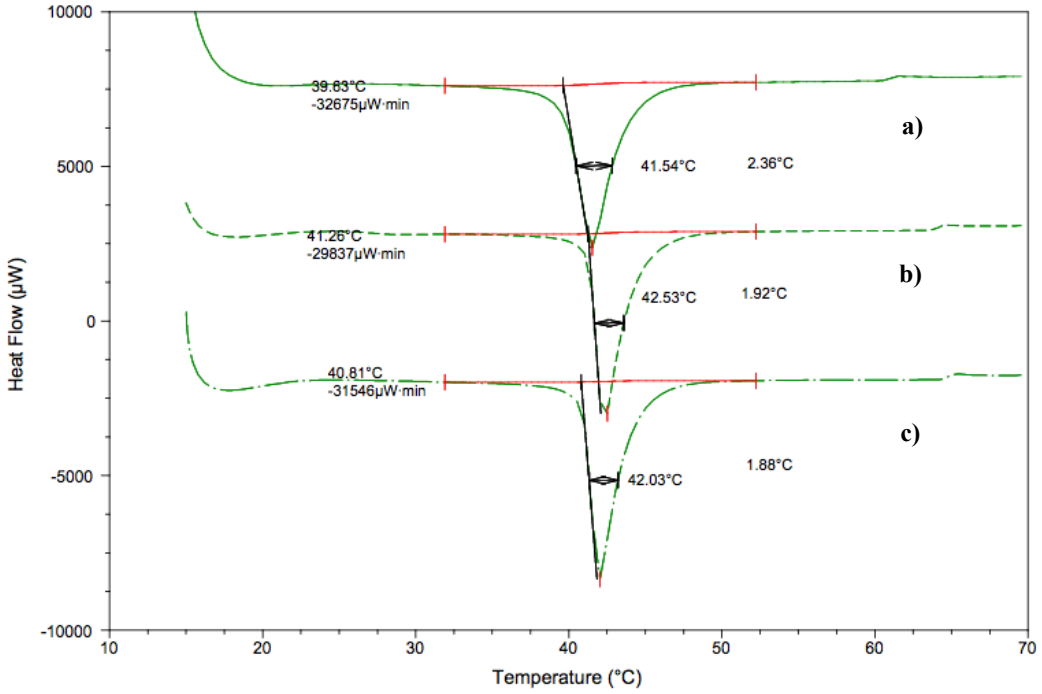

Figure 4-21 DSC thermograms of a) 10%, b) 5% and c) 2.5% genistein-loaded DPPC liposomes

Table 4-10 shows that the mean hydrodynamic diameter increased when genistein was incorporated into DPPC vesicles ($p<0.05$), suggesting that physically-encapsulated genistein could expand the space within the DPPC bilayer. However, there were no differences in particle size and size distribution between the three genistein formulations. A content of 2.5% w/w gave the highest genistein encapsulation efficiency ($p<0.05$) and this may explain why particle size and size distribution of formulations loading at higher contents of genistein were similar ($p>0.05$) to that at 2.5% w/w.

These DSC results suggest that the maximum drug incorporation into DPPC liposomes was 2.5% w/w. Furthermore, genistein is likely localised within hydrophobic interior of the lipid membrane and close to the polar head groups of DPPC since it significantly decreased the peak melting temperature of DPPC and the size of co-operative unit within bilayer and eliminated the pre-transition phase of DPPC vesicles.

Table 4-10 Thermal properties of genistein-loaded DPPC liposomes at concentrations between 2.5% and 10% w/w drug in total lipid (n=3, mean± S.D.)

Genistein-content (%w/w)	**Pre-transition (ºC)**	**Main transition**						
	T_{pre} (ºC)	T_{onset} (ºC)	T_m (ºC)	HHW (ºC)	ΔH (KJ/mol)	%EE	Mean particle size (nm)	PDI
DPPC	39.36± 0.29	41.36± 0.09	42.74± 0.28	1.68± 0.16	37.35± 3.06	-	109.05± 7.50	0.36± 0.03
2.5%	-	39.81± 0.34	41.63± 0.22	2.29± 0.11	40.53± 1.01	84.66± 2.70	139.03± 11.70	0.43± 0.02
5%	-	41.10± 0.22	42.34± 0.28	1.86± 0.08	41.68± 1.58	58.54± 8.06	158.17± 7.27	0.43± 0.05
10%	-	40.67± 0.18	41.83± 0.27	1.88± 0.04	40.30± 1.28	24.05± 3.92	146.03± 16.49	0.51± 0.04

4.5.5.5 Thermal properties of DPPC liposomes containing co-loaded erlotinib and genistein of different concentrations

No pre-transition peak was observed for formulations co-loaded with erlotinib and genistein investigated (2.5% and 5% of each), which may be attributed particularly to the inclusion of genistein (Figure 4-22). The onset and peak temperature of the main transition for 2.5% w/w co-loaded liposomes significantly decreased ($p<0.05$) compared with empty DPPC liposomes. A significant increase in HHW ($p<0.05$) was detected for the lower concentration of drugs. These suggest an increased fluidity of the DPPC bilayer with a reduction in the overall transition cooperativity. However, both concentrations of co-loaded DPPC liposomes had the same enthalpy for the main transition as DPPC ($p>0.05$). Including erlotinib and genistein beyond 2.5% w/w did not show any further changes in the main phase transition of DPPC vesicles, suggesting 2.5% w/w erlotinib and 2.5% w/w genistein were the maximum drug incorporations into the DPPC bilayer.

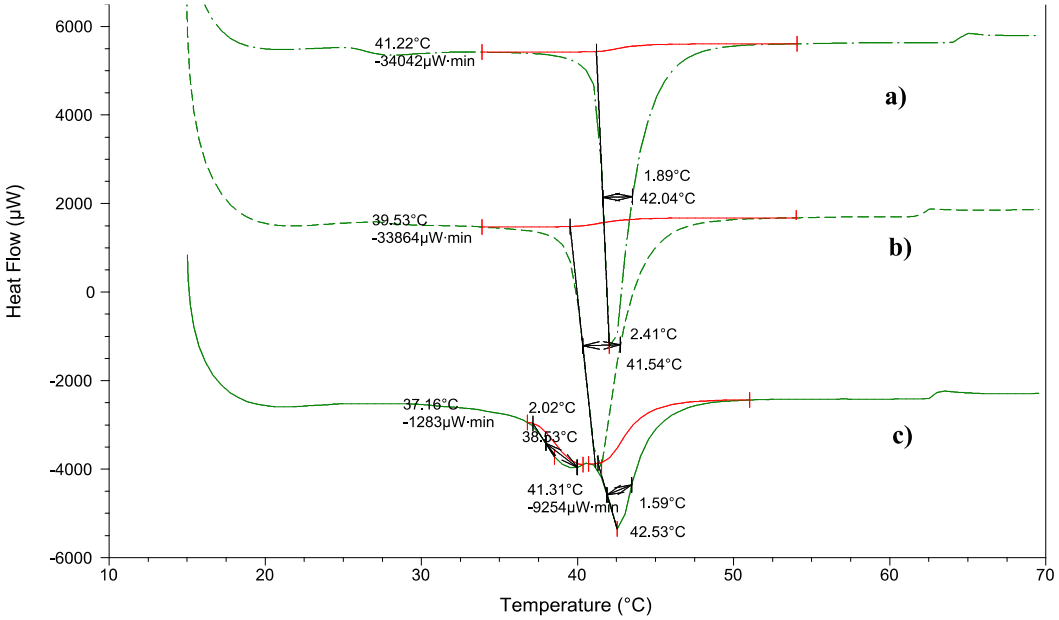

Figure 4-22 DSC thermograms of a) 5% erlotinib and 5% genistein and b) 2.5% erlotinib and 2.5% genistein co-loaded DPPC liposomes and c) DPPC liposomes

Loading drugs into DPPC liposomes increased their mean hydrodynamic diameter ($p<0.05$, Table 4-11); however, the mean size and size distribution of both co-loaded formulations were similar. These observations can be explained as for genistein-loaded DPPC formulations (Section 4.5.5.4). When considering drug entrapment, 2.5% of each drug showed greatest encapsulation efficiencies. These results suggest that 2.5% w/w each drug co-incorporated into DPPC was the maximum drug incorporation in the DPPC bilayer.

Table 4-11 Effect of erlotinib and genistein content (2.5% and 5% w/w each drug) on the thermal properties of co-loaded DPPC liposomes (n=3, mean± S.D.)

Combined drug content (%w/w)	**Pre-transition (ºC)**	**Main transition**						
	T_{pre} (ºC)	T_{onset}(ºC)	T_m (ºC)	HHW (ºC)	ΔH (KJ/mol)	%EE	Mean particle size (nm)	PDI
DPPC	39.36± 0.29	41.36± 0.09	42.74± 0.28	1.68± 0.16	37.35± 3.06	-	109.05± 7.50	0.36± 0.03
2.5%/ 2.5%	-	39.42± 0.14	41.34± 0.28	2.40± 0.07	40.02± 0.69	14.65± 3.42 (Erlo) 90.03± 10.99 (Gen)	159.22± 19.42	0.44± 0.09
5%/ 5%	-	41.10± 0.20	42.04± 0.00	1.86± 0.05	42.74± 1.58	7.02± 1.13 (Erlo) 71.48± 9.03 (Gen)	200.07± 45.81	0.50± 0.12

When the thermograms of DPPC liposomes containing erlotinib, genistein and co-loaded (2.5% each drug) were compared, the shape of the DSC curve and phase transition behaviour for genistein and co-loaded formulations were similar (Figure 4-23), suggesting that the inclusion of genistein had the more pronounced effect on the thermal properties of co-loaded liposomes.

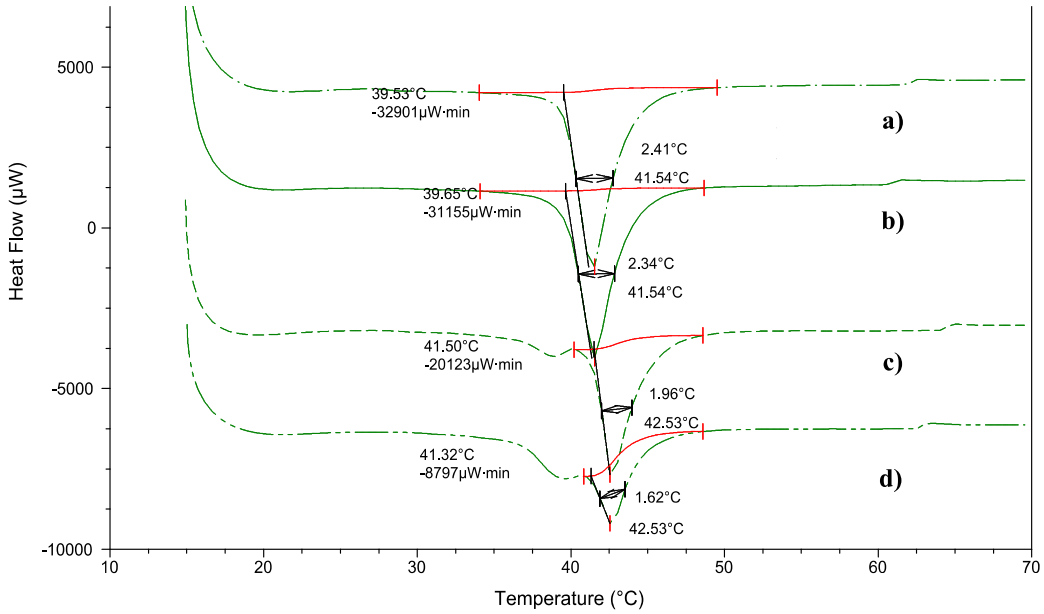

Figure 4-23 DSC thermogram of a) 2.5% erlotinib and 2.5% genistein co-loaded DPPC liposomes, b) 2.5% genistein-loaded DPPC liposomes, c) 2.5% erlotinib-loaded DPPC liposomes and d) DPPC liposomes

The mean hydrodynamic diameter and size distribution for genistein and co-loaded liposomes (2.5% w/w of each drug) were similar ($p>0.05$, Table 4-12). The encapsulation efficiencies of genistein in individual and co-incorporated formulations were very similar ($p>0.05$), whereas drug entrapment decreased approximately two- fold for erlotinib in combined liposomes, from approximately 33% to 15% EE ($p<0.05$).

Table 4-12 Effect of genistein and erlotinib alone or co-loaded at 2.5% w/w drug in lipid on the thermal properties of DPPC liposomes (n=3, mean± S.D.)

Drug-to-DPPC ratio (%w/w)	**Pre-transition (ºC)**	**Main transition**						
	T_{pre} (ºC)	T_{onset}(ºC)	T_m (ºC)	HHW (ºC)	ΔH (KJ/mol)	%EE	Mean particle size (nm)	PDI
2.5% Erlotinib	39.21± 0.28	41.50± 0.11	42.70± 0.26	2.27± 0.10	39.30± 1.50	32.53± 6.05	106.37± 1.84	0.25± 0.02
2.5% Genistein	-	39.81± 0.34	41.63± 0.22	2.29± 0.11	40.53± 1.01	84.66± 2.70	139.03± 11.70	0.43± 0.02
2.5% Co-loaded	-	39.42± 0.14	41.34± 0.28	2.40± 0.07	40.02± 0.69	14.65± 3.41 (Erlo) 90.03± 10.99 (Gen)	159.22± 19.42	0.44± 0.09

Due to the earlier findings that suggested genistein was localised both in the hydrophobic hydrocarbon chains of lipid bilayer and adjacent to the water-lipid interface (Section 4.5.5.4), this may limit penetration of erlotinib into the acyl chain region of the bilayer and/or the available polar head groups of DPPC. When the molecular structures of the two drugs are compared, the three –OH groups on the aromatic rings of genistein are easily protonated and will form a stronger ionic bonding with the amine and/or phosphate group of DPPC molecules, whereas the three nitrogen atoms and oxygen atom from quinazolinamine ring and methoxyethoxy chains of erlotinib will have weaker ionic interaction with the polar region of the phospholipids. These suggest the exclusion of erlotinib by the others.

4.5.5.6 Thermal properties of DPPC liposomes containing cholesterol and DOPE

No pre-transition phase was observed for DPPC liposomes containing cholesterol and/or DOPE, implying the presence of these molecules at the interfacial region. The phase transition temperature shifted to lower values when 8 mol% cholesterol, 20 mol% DOPE and 8 mol% cholesterol + 20 mol% DOPE were incorporated into DPPC liposomes (Figure 4-24), indicating greater freedom rotation of hydrocarbon chains within bilayer. The enthalpy decreased significantly and the main phase transition noticeably broadened (HHW) as reported in Table 4-13. This suggests that these molecules were inserted into the hydrophobic region of the DPPC bilayer. As cholesterol contains a tricyclic ring, hydrocarbon chains and hydroxyl group, the tricyclic ring was localised between the first few carbons of the fatty acyl chains into the hydrophobic core of DPPC bilayer and the hydrocarbon chains aligned parallel to acyl chains of DPPC phospholipid bilayer, while, its hydroxyl group orients towards the polar interface (Taylor and Morris, 1995; Bhattacharya and Haldar, 2000; Monteiro et al., 2014). For DOPE, this molecule comprises two longer hydrocarbon chains as compared to cholesterol. DOPE acyl chains (18-C) would be expected to align across the acyl chains of DPPC bilayer, while its phosphatidyl ethanolamine head group would orient towards the aqueous phase. Consequently, the inclusion of 20 mol% of DOPE seems have more pronounced effect on hydrophobic hydrocarbon chains of DPPC

bilayer than 8 mol% cholesterol, due to stronger hydrophobic-hydrophobic interaction associated with their structures.

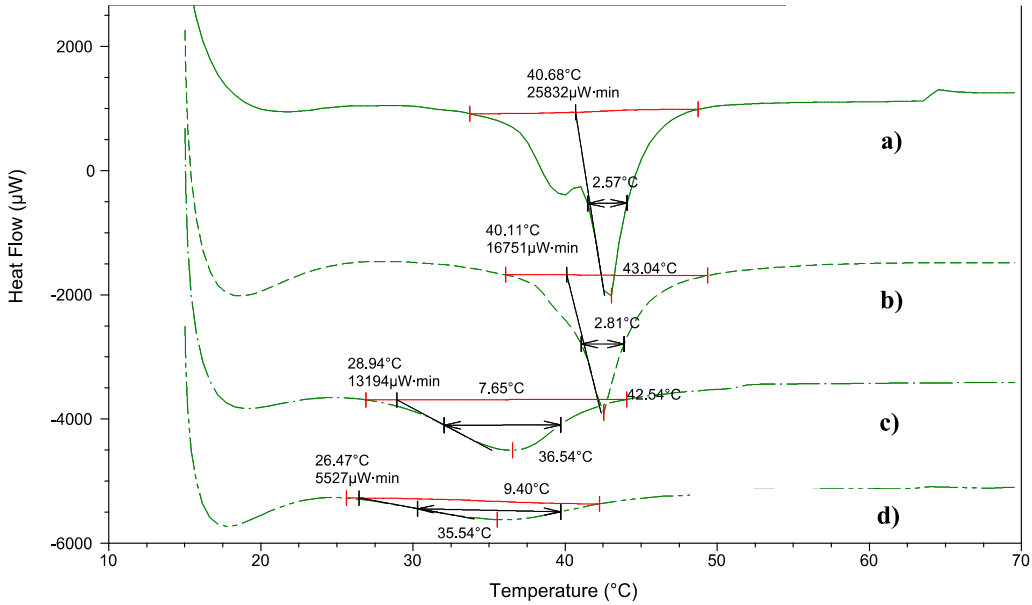

Figure 4-24 DSC thermogram of a) DPPC, b) DPPC with 8% cholesterol, c) DPPC with 20% DOPE and d) DPPC with 8% cholesterol and 20% DOPE

Table 4-13 Thermal properties of DPPC liposomes in the presence of cholesterol, DOPE, and cholesterol with DOPE (n=3, mean± S.D.)

Formulations	**Pre-transition (ºC)**	**Main transition**			
	T_{pre} (ºC)	T_{onset} (ºC)	T_m (ºC)	HHW (ºC)	ΔH (KJ/mol)
DPPC	39.36± 0.29	41.36± 0.09	42.74± 0.28	1.68± 0.16	37.35± 3.06
DPPC + 8% cholesterol	-	40.29± 0.23	42.54± 0.00	2.83± 0.35	27.93± 1.21
DPPC + 20% DOPE	-	28.63± 0.11	36.54± 0.00	8.09± 0.09	18.86± 0.62
DPPC + 8% cholesterol + 20% DOPE	-	26.48± 0.45	36.37± 0.58	10.87± 0.24	12.14± 1.42

4.5.5.7 Thermal properties of erlotinib-incorporated into DPPC liposomes with and without genistein, cholesterol and DOPE

A decrease in the main transition temperature and enthalpy was observed (Figure 4-25), while DSC endotherm broadened in the presence of genistein (2.5% erlotinib and 2.5% genistein co-loaded DPPC liposomes), 8 mol% cholesterol+ 20 mol% DOPE (2.5% erlotinib formulation) and genistein+ 8 mol% cholesterol+ 20 mol% DOPE (2.5% erlotinib and 2.5% genistein co-loaded formulation) within DPPC bilayer. These observations indicated modifications in the ordered lipid structure of the DPPC bilayer, which can result in the greater thermotropic changes in main transition phase. As the pre-transition phase was eliminated, these findings supported the molecular interactions of exogenous compounds with the DPPC head group. All combined results suggested that the inclusion of biomolecules into liposomes was located within hydrophobic hydrocarbon chains of the bilayer and/or adjacent to the interface of liposomes.

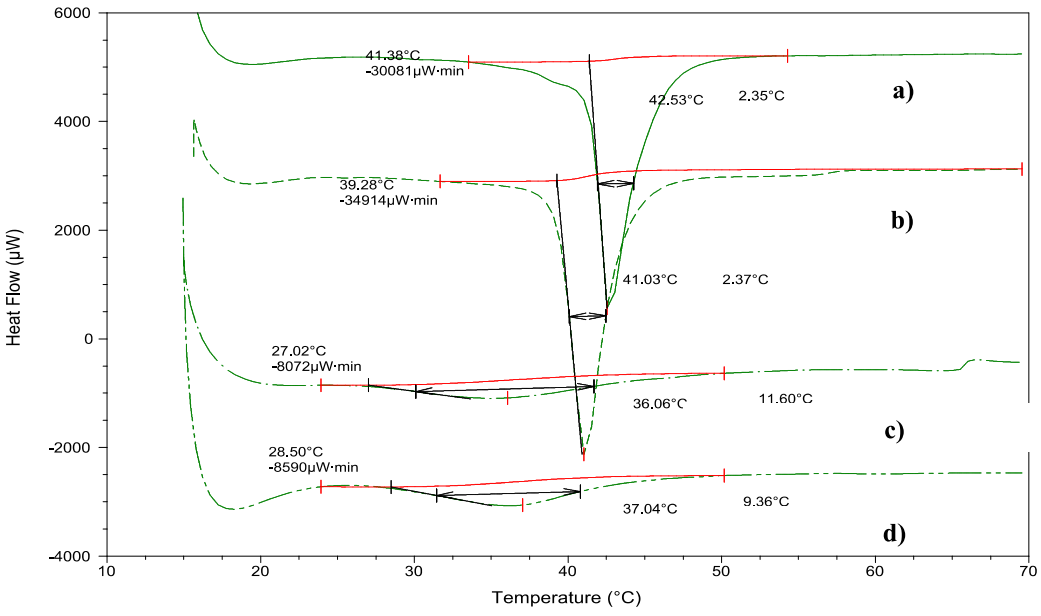

Figure 4-25 DSC thermograms of a) 2.5% erlotinib-loaded DPPC liposomes, b) 2.5% erlotinib and 2.5% genistein co-loaded DPPC liposomes, c) 2.5% erlotinib-loaded DPPC/cholesterol/DOPE liposomes and d) 2.5% erlotinib and 2.5% genistein co-loaded DPPC/cholesterol/DOPE liposomes

The mean particle size and polydispersity index increased for 2.5% erlotinib-loaded DPPC/cholesterol/DOPE liposomes, 2.5% erlotinib and 2.5% genistein co-

loaded DPPC liposomes, and 2.5% erotinib and 2.5% genistein co-loaded DPPC/cholesterol/DOPE liposomes as compared to 2.5% w/w erlotinib-loaded DPPC liposomes (Table 4-14), supporting the incorporation of these biomolecules into bilayer. The entrapment efficiency of erlotinib in DPPC formulations significantly decreased when cholesterol and DOPE were included ($p<0.05$). As cholesterol and DOPE were expected to orient parallel acyl chains of DPPC bilayer and towards the interfacial region, this may lead to a reduced space within the bilayer to accommodate erlotinib. Also, the addition of only genistein (2.5% erlotinib and 2.5% genistein co-loaded DPPC liposomes) decreased the encapsulation efficiency of erlotinib as that of cholesterol and DOPE.

By contrast, erlotinib incorporation noticeably increased when genistein, cholesterol and DOPE were included together ($p<0.05$). This observation suggests that genistein in the presence of cholesterol and DOPE had the greatest impact on bilayer properties in a fluid state ($T>T_m$), resulting in more mobile and flexible structure of acyl chains. This fluid state of lipid membrane appears to have allowed incorporation of erlotinib within bilayer to a greater extent during the formation of liposomes.

Table 4-14 Characteristics of erlotinib liposomal formulations at 2.5% w/w drug in total lipids (n=3, mean± S.D.)

Erlotinib in different formulations (2.5% w/w drug in lipids)	**Encapsulation Efficiency (% EE)**	**Mean particle size (nm)**	**PDI**
Erlotinib-loaded DPPC liposomes	32.53± 6.05	106.37± 1.84	0.25± 0.02
Erlotinib-loaded DPPC+cholesterol+DOPE liposomes	14.20± 5.44	150.77± 37.28	0.36± 0.08
Erlotinib and genistein co-loaded DPPC liposomes	14.65± 3.42	159.22± 19.42	0.44± 0.09
Erlotinib and genistein co-loaded DPPC+cholesterol+ DOPE liposomes	23.16± 2.08	128.00± 13.70	0.44± 0.05

4.5.5.8 Thermal properties of genistein-incorporated into DPPC liposomes with and without erlotinib, cholesterol and DOPE

For genistein, the trends in DSC endotherm were similar to those with erlotinib incorporation in DPPC/cholesterol/DOPE liposomes (Figure 4-26).

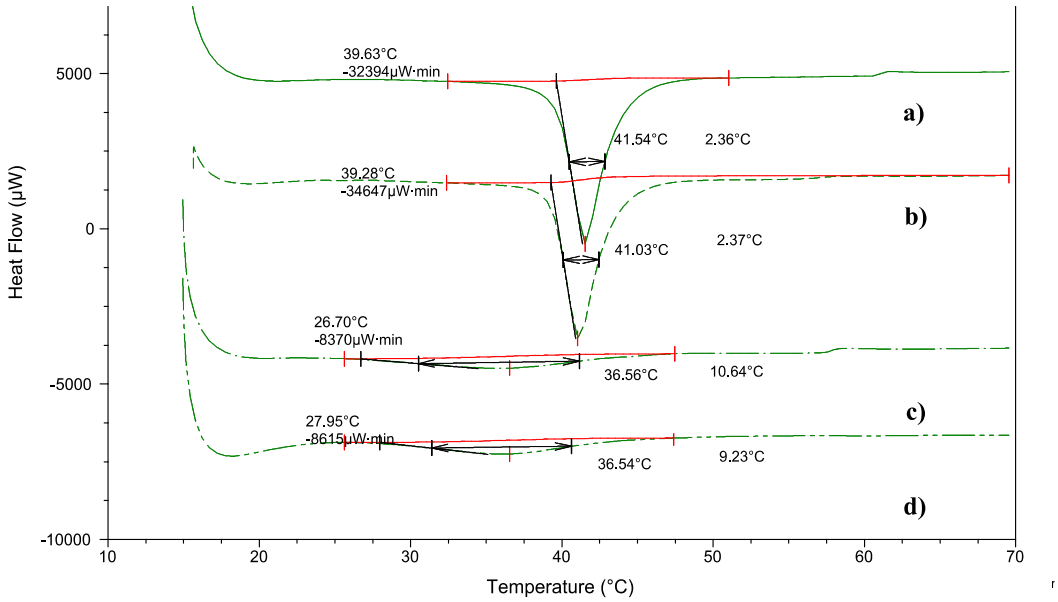

Figure 4-26 DSC thermograms of a) 2.5% genistein-loaded DPPC liposomes, b) 2.5% genistein and 2.5% erlotinib co-loaded DPPC liposomes, c) 2.5% genistein-loaded DPPC/cholesterol/DOPE liposomes and d) 2.5% genistein and 2.5% erlotinib co-loaded DPPC/cholesterol/DOPE liposomes

There was no significant difference in mean size, polydispersity index and encapsulation efficiency for all formulations shown in Table 4-15 ($p>0.05$). Encapsulation efficiency of genistein was similar for 2.5% genistein-loaded DPPC liposomes, 2.5% genistein-loaded DPPC/cholesterol/DOPE liposomes and 2.5% genistein and 2.5% erlotinib-loaded DPPC liposomes ($p>0.05$). However, genistein entrapment showed the highest value when erlotinib, cholesterol and DOPE were included.

.

Table 4-15 Characteristics of genistein-loaded liposomal formulations at 2.5% w/w drug in total lipids (n=3, mean± S.D.)

Genistein in different formulations (2.5% w/w drug in lipids)	**Encapsulation Efficiency (% EE)**	**Particle size (nm)**	**Polydispersity Index (PDI)**
Genistein-loaded DPPC liposomes	84.66± 2.70	139.03± 11.70	0.43± 0.02
Genistein-loaded DPPC+cholesterol+DOPE liposomes	83.78± 4.62	136.87± 13.19	0.45± 0.09
Erlotinib and genistein co-loaded DPPC liposomes	90.03± 10.99	159.22± 19.42	0.44± 0.09
Erlotinib and genistein co-loaded DPPC+cholesterol+ DOPE liposomes	101.58± 12.72	128.00± 13.70	0.44± 0.05

Thus, the DSC results suggest that the co-incorporation of erlotinib and genistein into DPPC bilayer disrupted the packing order of the acyl chain region and increased the bilayer fluidity resulting in changes in the main phase transition (T_m, HHW and ΔH). Also, cholesterol and DOPE were incorporated within hydrophobic hydrocarbon chains of DPPC bilayer and the polar regions of both molecules was oriented towards the water phase based on their structures. The properties of lipids in liposomes in terms of their T_m is a crucial parameter to consider for pre-formulation studies of these delivery systems. T_m for the optimised formulation was approximately body temperature and this can ensure that drug would not escape or leak out from bilayer before reaching the target site under physiological conditions (T ≈37ºC).

All the combined data confirm the successful co-incorporation of erlotinib and genistein into DPPC /cholesterol/DOPE liposomes up to approximately 10% for

erlotinib and 100% for genistein. This developed formulation would be advantageous for further formulation development since excipients quantities are less than for two individual formulations. Consequently, DPPC/cholesterol/DOPE co-loaded liposomes with erlotinib and genistein were considered for further investigations in the following chapter.

4.6 Conclusion

DPPC liposomes containing either erlotinib or genistein and in combination (2.5-10% w/w) were successfully prepared by thin-film hydration and size reduced by probe-sonication. A validated HPLC analysis for the co-quantification of this combination was achieved following ICH guideline. The HPLC results showed that the maximum incorporation of individual and co-loaded drugs in DPPC liposomes was 2.5% w/w.

DSC proved a valuable tool for understanding the interaction between formulation components in the liposome bilayers. The DSC thermograms of the drug-loaded liposomes showed changes in the main phase transition peak width, main transition and onset temperature, and the disappearance of the pre-transition peak compared to the empty liposomes. This suggests that both drug molecules were located close to the upper regions of the hydrophobic chains and polar head group of DPPC bilayers. Incorporation of 2.5% w/w drug individually and co-loaded into the liposomes resulted in higher HHW values and a decrease in phospholipid phase transition temperature. This suggests that the fluidity of bilayer was increased, caused by the reduced order of packing of phospholipid molecules in the presence of both drugs individually and in combination. Furthermore, genistein in the presence of cholesterol and DOPE have pronounced effects on bilayer fluidity and subsequently enhanced drug entrapment for erlotinib. Multichannel differential scanning calorimetry (MCDSC) was able to provide information for a better understanding of the molecular interactions between drugs and lipids within the phospholipid bilayer membrane. This analysis also helps to determine maximum drug incorporation for designing and optimising liposomal formulations.

Chapter 5 Aerosol properties of liposomes loaded with erlotinib and genistein

Chapter 5 Aerosol properties of liposomes loaded with erlotinib and genistein

5.1 Introduction

For delivery of liposomes, air-jet and vibrating-mesh nebulisers are considered more effective than ultrasonic devices, causing less disruption of the liposomal bilayers. (Elhissi et al., 2012; Elhissi et al., 2013). Air-jet nebulisers may result in significant leakage of entrapped hydrophilic drug from liposomes because of the shearing forces within the nebuliser, though drug losses can be reduced by incorporating cholesterol to make fluid-state bilayers more rigid, and by reducing the size of the liposomes being aerosolised (Bridges and Taylor, 2000; Cipolla et al., 2013; Lehofer et al., 2014). There are only minor losses of lipophilic drugs since hydrophobic materials remain incorporated within the liposome bilayer during air-jet nebulisation (Elhissi et al., 2011a; Cipolla et al., 2013; Elhissi et al., 2013). Vibrating-mesh nebulisers have been reported to minimise hydrophilic drug loss from liposomes compared to other nebulisers, and thus have been proposed as particularly suitable devices for liposome delivery (Elhissi et al., 2006a; Elhissi et al., 2012; Elhissi et al., 2013).

As outlined in Chapter 1, the Andersen Cascade Impactor (ACI), the Next Generation Impactor (NGI) and the Multistage liquid impinger (MSLI) are full cascade impactors comprising a series of stages that fractionate aerosolised sample based on the aerodynamic size distribution of aerosols delivered by pMDIs and DPIs, though only the NGI is routinely used for the determination of the aerosol properties of nebulised aerosols. However, low dose formulations including formulations with potent drugs are challenging for analytical quantification due to the small amounts of drug deposited across the eight stages of the NGI.

It has been proposed that the measurement of coarse and fine particle fractions obtained with an abbreviated impactor may be useful to describe the behaviour of aerosolised products, supplementing data from a full cascade impactor. Abbreviated Impactor Measurement (AIM) using an impactor with only 2 or 3 stages representing coarse and fine particle doses/fractions, has been proposed for routine quality control as well as for product development applications of orally inhaled products. However, removal of the stages may possibly affect the whole

particle size distribution of an aerosol cloud due to particle losses to internal surface of an abbreviated impactor (Mitchell et al., 2009a).

Three abbreviated impactors have been described (Figure 5-1); namely the Fast Screening Andersen (FSA), Reduced Next Generation Impactor (rNGI) and the Fast Screening Impactor (FSI).

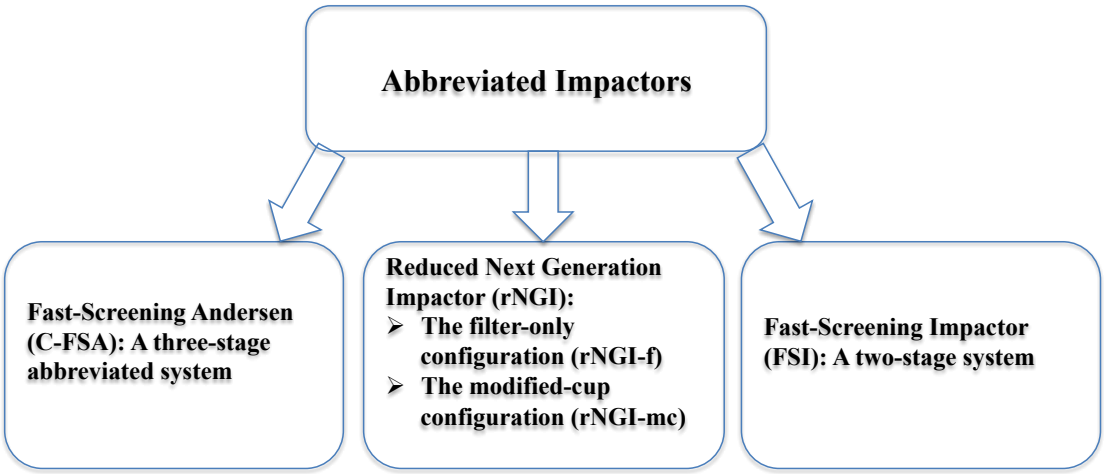

Figure 5-1 Commercially available abbreviated impactors

Of the three abbreviated impactors, the Fast Screening Impactor (FSI; Figure 1-15), which has been developed by Copley Instrument as a simple and labour-saving approach for the in-vitro characterisation of FPD/FPF for pMDIs and DPIs, was investigated with nebulisers in this study, for two main reasons. Firstly, the FSI has only two collecting stages with the cut-off diameter of 5 µm between upper and lower stages, and there was no modification of the internal surfaces of the impactor as required for the rNGI. However, the use of the FSI for aerosol characterisation has not been investigated widely and no abbreviated impactors are currently included in the European, United States or Japanese Pharmacopoeias.

5.2 Aims

1. To investigate the FSI as an alternative impactor to the NGI for aerosol characterisation of nebulised liposomes co-loaded with erlotinib and genistein using the same operating conditions.

2. To investigate the effects of the method for aerosolisation (nebuliser system, flow rates), impactor conditions (temperature) and properties of co-loaded liposomes (size reduction by either probe sonication or extrusion) on the aerosol properties determined using the FSI.

5.3 Materials

The materials used in the preparation of erlotinib and genistein co-loaded liposomes and for the reversed-phase HPLC method allowing simultaneous determination of this drug combination are outlined in Section 4.3.

5.4 Methods

5.4.1 Assessment of aerosol properties using the Next Generation Impactor (NGI)

5.4.1.1 Effect of lipid concentrations on measured aerosol properties

The aim of this study was to investigate the optimal drug and lipid concentrations to allow accurate quantification of low drug contents when characterising nebulised liposomes using a full cascade impactor. Liposomal preparations: 2.5% w/w erlotinib and 2.5% w/w genistein co-loaded into DPPC, cholesterol and DOPE (72:8:20 % mole ratio) liposomes, were prepared using the thin-film hydration method described in Section 4.4.2.1. In this study, drug and lipid concentrations were increased proportionately in comparison with the formulation described in chapter 4. The lipid concentration was increased from 2.5 mg/mL to 20 mg/mL, while the drug: lipid ratio was maintained (2.5% w/w erlotinib and 2.5% w/w genistein in lipids). To ensure that increased concentrations did not affect formulation properties, the following were determined: hydrodynamic diameter, surface charge and encapsulation efficiency (as described in Sections 4.4.3.1, 4.4.3.2 and 4.4.3.4, respectively).

5.4.1.2 Effect of nebuliser fill volume on measured aerosol properties

After cooling the NGI at 5± 3 °C for at least 90 min, 2 mL or 4 mL of the final liposome formulation (lipid concentration = 20 mg/mL) was added into Pari LC® Sprint air-jet nebuliser and nebulisation conducted for 5 and 10 min, respectively at a flow rate of 15 L/min generated by a Pari TurboBoy compressor (Section 3.4.6). The duration of aerosolisation was based on the time to nebulise to dryness this fill volume using water (Section 3.5.5). Deposited erlotinib and genistein were collected by rinsing with absolute ethanol including the nebuliser reservoir, induction port, NGI collection cups and back-up filter as outlined in Section 3.4.7 and then assayed by the simultaneous HPLC method as described in Section 4.4.1.1.

5.4.1.3 Optimal conditions for characterising nebulised liposomes using the NGI

The Pari LC® Sprint air-jet and Pari Velox® vibrating-mesh nebulisers were filled with 4 mL of liposomal suspension (containing 1.0 mg/mL erlotinib and 10 mg/mL genistein) which was nebulised into the NGI at an air flow rate of 15 L/min for 10 min, after cooling the impactor for at least 90 min at 5± 3 ºC. All collected samples from the induction port and collection cups across the impactor were made up to 5 mL with ethanol, whereas the volume of absolute ethanol for rinsing the nebuliser reservoir was 10 mL, prior to simultaneous HPLC assay. Aerosolisation parameters included mass balance, emitted dose (ED), Fine Particle Dose (FPD) and Fine Particle Fraction (FPF) were calculated as mentioned in Chapter 3.

5.4.2 Assessment of aerosol properties using the Fast Screening Impactor (FSI)

The Fast Screening Impactor (FSI; Copley Scientific, UK) was employed using the same operating conditions as for the NGI. The effect of air-flow rate, impactor temperatures and nebuliser types on aerosol properties were studied as outlined in Sections 5.4.2.1 to 5.4.2.3. Nebulisation of liposomes co-loaded with erlotinib and

genistein (4 mL) was conducted using an air-jet nebuliser into the cooled FSI, through the induction port, at a flow rate of 15 L/min for 10 min. After nebulisation, the FSI was dismantled and quantification of deposited drugs was determined by HPLC analysis from the nebuliser reservoir, mouthpiece, mouthpiece adapter, induction port, additional insert of the FSI housing and back-up filter together with the filter holder using appropriate volumes of absolute ethanol. 10 mL of absolute ethanol was used for rinsing nebulised liposomes in the nebuliser reservoir and the additional insert of the FSI, whereas the induction port and a back-up filter with filter holder required 5 mL of solvent. Fine Particle Dose (FPD) and Fine Particle Fraction (FPF) for the FSI were calculated as follows:

Fine Particle Dose (FPD) = Drug mass from lower stage of the FSI

$$\text{Fine Particle Fraction (FPF)} = \frac{\text{Mass of drug from stage 2}}{\text{Mass of drug from stage 1 and stage 2}} \times 100\ \% \qquad \text{Eq. 5-1}$$

5.4.2.1 Effect of flow rates on measured aerosol properties

The FSI contains an additional insert calibrated at 30 L/min to give a cut-off for 5 µm aerodynamic diameter. This insert was modified by alternately covering three of the six nozzles using wet glass microfiber filter when a flow rate of 15 L/min was employed (personal communication; Copley Instrument) as shown in Figure 5-2. A cut-off diameter of 5 µm is used for calculation of Fine Particle Fraction (FPF) and Fine Particle Dose (FPD) at this lower flow rate (Johal et al., 2013; Mohan et al., 2017). Each individual experiment was determined after the impactor was cooled at 5± 3°C for at least 90 min.

Figure 5-2 Modification of additional FSI insert utilised at flow rate of 15 L/min

5.4.2.2 Effect of impactor temperature on measured aerosol properties

The FSI was initially used in accordance with the European pharmacopoeia requirements for the NGI, i.e. cooling at 5± 3 °C for at least 90 min. In additional studies, a non-cooled FSI (at ambient temperature; 20 °C) was also employed. Both impactor temperatures were studied with the FSI operated at flow rates of 15 L/min and 30 L/min, and the aerosol properties of the nebulised liposomes were determined.

5.4.2.3 Effect of nebuliser system on measured aerosol properties

Experiments were conducted with an air-jet and vibrating-mesh nebulisers (respectively; Pari LC® Sprint and Pari Velox®, PARI Medical Ltd, Byfleet, UK) generating aerosols which were directed into the induction port of the FSI using a mouthpiece adaptor. The FSI measurements were undertaken after cooling the impactor at 5± 3°C for at least 90 min, at flow rates of 15 L/min and 30 L/min.

5.4.2.4 Size stability of liposomes before and after nebulisation

The aim of this experiment was to study the effects of nebulisation on the physical stability of liposomes. After nebulisation, nebulisers and FSI stages were rinsed with 1 mL of HPLC water for particle size analysis. The Z-average mean hydrodynamic diameter and Polydispersity Index (PDI) were measured in triplicate by dynamic light scattering (DLS) as described in Sections 4.4.4.1 for

liposomal formulations before and after nebulisation. The mean values and standard deviation are reported.

5.4.2.5 Transmission electron microscopy (TEM) of liposomes before and after nebulisation

The morphology and aggregation behaviour of freshly prepared liposomal formulations, liposomes remaining in air-jet and vibrating-mesh nebuliser reservoirs and those deposited on each stage of the FSI were determined by TEM. Samples were negatively stained with a drop of uranyl acetate (1% w/v) and observed using a transmission electron microscope (Philips Electron Optics BV, Netherlands) as described in Section 3.4.4.4.

5.4.3 Size reduction of liposomes co-loaded with erlotinib and genistein using membrane extrusion method

The MLVs were repeatedly extruded through a series of polycarbonate membrane filters of reducing pore sizes (Cyclopore®, Whatman, UK) using nitrogen gas. The dispersion was extruded through 3 µm and 1 µm polycarbonate membrane filters of 47 mm diameter held in a stainless-steel holder at 10 psi. Preparations were further extruded through a 100 nm pore filter at 120 psi (LiposoFast-LF50 extruder, Avestin, Ottawa, Canada). During extrusion the temperature was maintained at least 10°C above the main phase transition temperature of the mixture of phospholipids (i.e. at 50 ºC) (Hadian et al., 2014). The particle size distribution of extruded liposomes was measured using laser diffraction size analysis (Mastersizer 3000 laser diffraction particle size analyzer, Malvern Instrument Ltd, UK). The data are presented as volume median diameter (VMD) for micrometre-sized vesicles.

For nanometre-sized vesicles, dynamic light scattering (DLS) was employed and size expressed as Z-average hydrodynamic diameter and polydispersity index (PDI) as described in Section 4.4.4.1. A PDI < 0.1 is typically considered as representing a monodispersed system, < 0.3 is a relatively monodisperse system, while > 0.7 is classified as a polydispersed system (ISO-22412, 2008; Kannan et

al., 2015; Holmkvist et al., 2016). The pore size of membrane filters and number of extrusions were optimised to achieve a final mean particle size between 100 and 200 nm, with PDI <0.3.

The final formulation was also characterised for encapsulation efficiency (Section 4.4.4.4) using Eq. 3-5 and Eq. 3-6 (Section 3.4.4.3). The aerosol properties of extruded liposomes were characterised using the FSI under the same operating conditions as those for sonicated formulations (Section 5.4.2).

5.4.4 Statistical analysis

All experiments were carried out in triplicate and data are expressed as the mean ± standard deviation (SD). The data were statistically analyzed by either Student's t-test or analysis of variance (ANOVA) and Tukey's post hoc test, using IBM SPSS Statistic 22 software. A p value of < 0.05 was considered significant.

5.5 Results and discussion

5.5.1 Effect of drug and lipid concentrations on liposome properties for nebulisation

The final liposome preparation intended for nebuliser delivery was chosen based on optimal liposome size and high content of encapsulated erlotinib and genistein. Table 5-1 shows the characteristics of the 2.5% w/w erlotinib and 2.5% w/w genistein co-loaded liposomal formulation at different lipid concentrations. Drug and lipid concentrations (2.5% w/w each drug in total phospholipids) were increased in comparison with the optimised formulation (lipid concentration of 2.5 mg/mL) to enhance drug content (Section 5.4.1.1**)**. The 2.5% w/w erlotinib and 2.5% w/w genistein co-loaded liposomal formulation (50 mg of total lipid content in 20 mL of dispersion or lipid concentration of 2.5 mg/mL) for loading into nebuliser reservoir contained 0.25 mg of erlotinib and 1.25 mg of genistein, based on their encapsulation efficiencies. A fill volume of 4 mL contained 10 mg lipid (2.5 mg/mL) and 0.05 mg of erlotinib and 0.25 mg of genistein.

Increasing lipid concentration to 20 mg/mL did not affect the liposomal properties in terms of mean hydrodynamic diameter, polydispersity index, surface charge or encapsulation efficiency of genistein compared to the formulation having lipid concentration of 2.5 mg/mL ($p>0.05$). However, encapsulation efficiency of erlotinib significantly decreased ($p<0.05$), possibly due to changes in the bilayer. Genistein may adopt more tightly pack within DPPC bilayer than erlotinib (Chapter 4), therefore changes in a formation of lipid bilayer have a more pronounced effect on erlotinib entrapment.

Consequently, a lipid concentration of 20 mg/mL was chosen for further studies since it gave higher contents of both drugs than the previously optimal formulation, having the same mean size.

Table 5-1 Characterisation of liposomes co-loaded with 2.5% w/w erlotinib and 2.5% w/w genistein at different lipid concentrations (n=3, mean± S.D)

Lipid concentration (mg/mL)	**Mean hydrodynamic diameter (nm)**	**Polydispersity Index**	**Zeta Potential (mV)**	**Encapsulation Efficiency (%)**
2.5 (Section 4.4.2.1)	128.00± 13.70	0.44± 0.06	-3.23± 0.05	23.16± 2.08 (Erlo) 101.58± 12.72 (Gen)
20	139.30± 2.42	0.56± 0.03	0.27± 0.05	8.57± 1.06 (Erlo) 100.13± 1.15 (Gen)

In preliminary studies, 2 mL and 4 mL of the final formulation (lipid concentration = 20 mg/mL) as shown in Table 5-2 for nebulisation were nebulised for 5 and 10 min, respectively and drug deposited within the NGI assayed by HPLC. When a 2 mL fill volume was nebulised and characterised by the NGI, all

concentrations of both drugs were below the limit of quantification (LOQ). The genistein concentration was above the LOQ for the 4 mL fill volume, but erlotinib concentration was lower than the LOQ for all stages of the NGI. Consequently, 4 mL of liposomal formulation was used in further studies based on full quantification of genistein. 4 mL was nebulised for 10 min into the NGI and then deposited erlotinib and genistein were recovered from the NGI by rinsing with absolute ethanol prior to quantification by HPLC analysis.

Table 5-2 Content of erlotinib and genistein in co-loaded liposomes (lipid concentration 20 mg/mL)

Initial content of drug (2.5% w/w each drug in 400 mg lipids in 20 mL of preparation)	**Encapsulation efficiency (EE)**	**Content of drug in 20 mL of dispersion (mg)**	**Content of drug in 4 mL of dispersion (mg)**	**Content of drug in 2 mL of dispersion (mg)**
10 mg (Erlotinib)	8.57± 1.06	0.86	0.17	0.08
10 mg (Genistein)	100.13± 1.15	10	2	1

5.5.2 Comparison of aerosol properties of liposomal preparations delivered by an air-jet nebuliser determined using the Next Generation Impactor (NGI) and Fast Screening Impactor (FSI)

Erlotinib deposited on each of the eight impaction stages of the NGI could not be accurately quantified by the validated HPLC analysis as concentrations of solutions collected from some stages were below the limit of quantification (LOQ). The two-stage abbreviated impactor (FSI) was subsequently evaluated as an alternative to overcome this problem. Table 5-3 shows that the values of mass

balance for genistein with both the NGI and FSI were within European Pharmacopeia acceptance limits, being in the range of 75- 125%. There was no significant difference in emitted dose (%ED) ($p>0.05$) as determined using both impactors, being approximately 30%. These results are in agreement with previous reports of in vitro aerodynamic characterisation of the dose emitted using Pari LC®, where %ED was in the range 15-40% (Sahib et al., 2010; Zhang et al., 2014c; Mashat et al., 2016). The aerosol parameters for nebulised erlotinib could not be calculated due to the inability to quantify accurately drug deposition on each stage of the NGI. The aerosol parameters for genistein could be accurately calculated using both impactors and therefore, the performance of the NGI and FSI is best compared based on full quantification of genistein.

Table 5-3 Aerosol parameters of liposomal aerosols delivered from an air-jet nebuliser into the NGI and FSI determined by the quantification of genistein (n=3, mean ± S.D.)

Aerosol parameters	**NGI**	**FSI**
Mass balance (%)	85.44± 1.49	82.91± 2.28
ED[1] (%)	34.42± 0.92	34.31± 5.86
FPD[2] (µg)	328.33± 36.17	224.24± 10.14
FPF[3] (%)	58.33± 4.51	42.55± 6.28

[1] ED= Emitted dose
[2] FPD= Fine particle dose
[3] FPF= Fine particle fraction

The concentration of drug substance in the nebuliser chamber may increase during aerosolisation as a result of water evaporation (Pritchard et al., 2018), whilst disruption of liposomal bilayers may cause accumulation of large liposomes and/or aggregation of the vesicles, as discussed in Section 5.5.3.4. In addition, lipid composition may affect output. For example, beclometasone dipropionate-loaded liposomes prepared from lipids with a higher T_m (DPPC) gave lower drug outputs than those containing phospholipids with a lower T_m, possibly due to an increased rigidity of vesicles, resulting in greater resistance to delivery from nebulisers (Darwis and Kellaway, 2001; Sahib et al., 2010; Elhissi et al., 2011b). The remaining fluid in the reservoir represents drug wastage, which can be

proportionately reduced using a higher fill volume as well as by modifying nebuliser fluid properties.

There were differences in the calculated values of Fine Particle Fraction (FPF) and Fine Particle Dose (FPD) using the two impactors (Table 5-3). Using the NGI, the FPF and FPD for genistein was significantly higher than that obtained with the FSI ($p<0.05$). Differences in FPF and FPD values for the NGI and FSI may result from differences in the internal volume of the full cascade impactor and abbreviated impactor system. For the NGI, there is a longer distance and transit time as the aerosol passes through the impactor compared to the FSI. This allows an increase in heat-transfer related water evaporation from the nebulised droplets, resulting in the droplets shrinking (Dennis et al., 2008; Kuhli et al., 2009). Further, a difference in the internal volume of these two impactors could affect aerosol generation at the earliest stage of the evaluation when the air-flow rate quickly increased from zero to the constant value of 15 L/min. Another possible cause for differences in values is the method used for calculating FPF/FPD with the two impactors. For the NGI, values are determined by the interpolation of the plot of cumulative fraction or cumulative mass of active drug collected in all stages of the impactor versus cut-off diameter, whilst for the FSI the dose and fraction less than 5 µm are based on the mass of drug deposited on the lower stage of the impactor.

Under the same operating conditions, the two impactors produced different but comparable values for the key parameter of aerosolisation (FPF and FPD) with the same value for emitted dose (ED). Overall, the FSI had great utility as a relatively rapid method for formulation development and evaluation of nebulised liposomal formulations, and overcame the analytical quantification problems associated with erlotinib when using the full impactor.

As differences in tidal breathing patterns (tidal volumes and flow rates) between patients may affect the delivered dose of nebulised drug, the use of a breath simulator for in vitro aerosol analysis may be used with a cascade impactor. Recently, using cascade impactors with breathing simulators, the breathing profile of an adult; for example, tidal volume= 500 mL, 15 breaths per minute with the inhalation and exhalation ratio of 1:1 has been recommended for delivered dose

testing and evaluating nebuliser performance (Copley, 2014). In this study, the experiments were conducted without this additional step for characterising the nebulised liposomes in order to keep the process simple, and to follow the requirements of and EMA guidelines (EMA, 2006; Ph. Eur. 9.0, 2017).

5.5.3 Aerosol characterisation using the FSI; effect of impactor operating conditions and nebuliser system

Several factors such as air-flow rate through the FSI, impactor temperature and nebuliser systems were investigated to determine their influence on the measured aerosol properties.

5.5.3.1 The influence of flow rate through the FSI on measured aerosol properties

The additional insert (Stage 1) of the FSI calibrated at 30 L/min with six nozzles was used in these experiments. Additionally, a flow rate of 15 L/min, as recommended by the Ph. Eur. for the NGI was investigated, with three of the six nozzles covered with wet microglass filter as described in Section 5.4.2. When comparing the two impactor flow rates, FPF increased almost two-fold, from approximately 40% to 70% for both drugs when using a higher flow rate (30 L/min; Figure 5-3). As seen in Table 5-4, the FPD for both drugs delivered by the air-jet nebuliser through the FSI was higher at a flow rate of 30 L/min. This is because the higher flow rate can entrain relatively warmer air, causing enhanced evaporation effect and consequently droplet shrinkage prior to deposition within the impactor, as described in the previous studies of the NGI and Anderson Cascade Impactor (ACI) (Abdelrahim, 2011; Lewis et al., 2016). A decreased droplet size may yield higher values for FPF and FPD as shown in this study. A different value of FPD was observed for the nebulised aerosol of genistein ($p<0.05$), but not erlotinib, which demonstrated larger variability at the higher flow rate ($p>0.05$).

The explanation for the differences between these two drugs is unclear. A decrease in temperature of aerosol leaving the air-jet nebuliser ($T < T_c$ of

liposomes) during aerosolisation may not affect disruption of liposomal bilayers, causing no impact on drug solubility and loss of entrapped hydrophobic drug, since liposomal bilayers are rigid and stable when the temperature is lower than their T_c (36.37°C). However, the content of erlotinib on the lower stage of the FSI was slightly higher than the LOQ of the HPLC assay, though these values were in the middle concentration range of calibration curve for genistein. Accordingly, this may explain the differences between erlotinib and genistein for FPD values. However, both drugs showed the same trend in FPD and FPF when increasing air flow rate through the FSI.

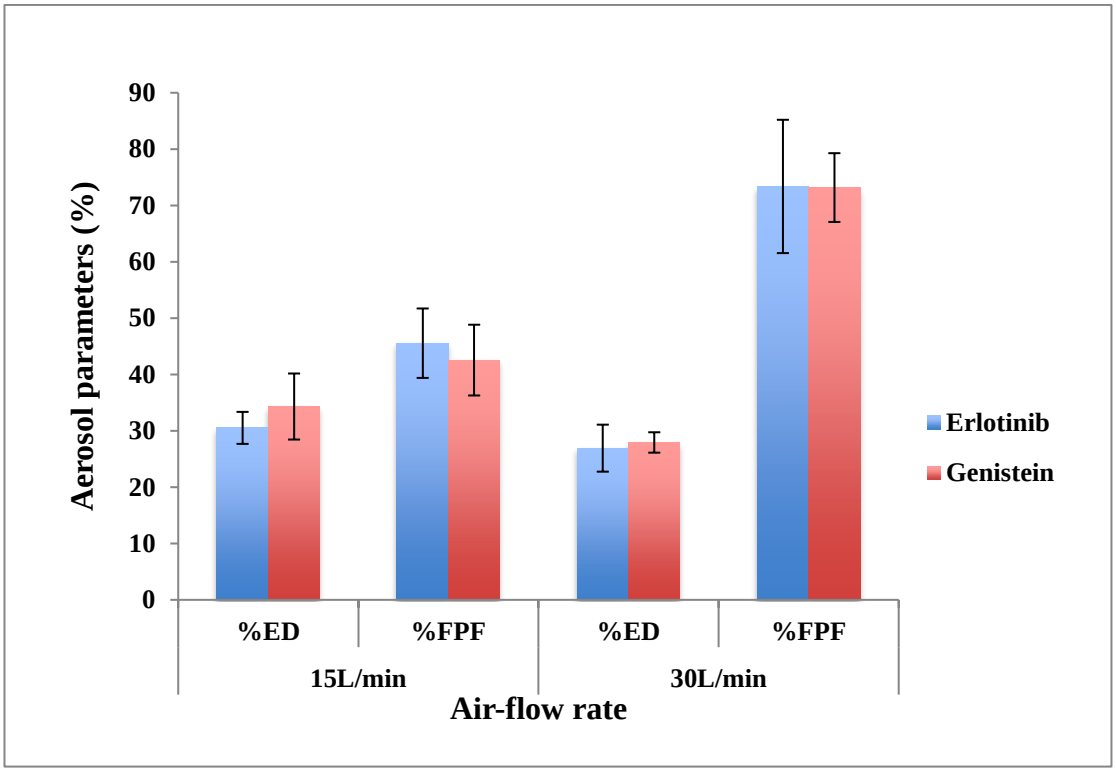

Figure 5-3 Aerosol parameters of co-loaded MLVs aerosols generated using an air-jet nebuliser measured using a cooled FSI at 15 and 30 L/min (n=3, mean ±S.D.).

Table 5-4 Fine particle dose for co-loaded liposomal aerosols delivered by the air-jet nebuliser operated at 15 L/min and 30 L/min, using the cooled FSI (n=3, mean ±S.D.)

Type of nebulisers	Air-flow rate (L/min)	Fine Particle Dose (µg)
Air-jet	15	18.02± 2.51 (Erlo) 224.24± 10.14 (Gen)
	30	25.93± 9.17 (Erlo) 326.87± 37.91 (Gen)

5.5.3.2 Effect of impactor temperature on measured aerosol parameters

The FSI was cooled at 5± 3ºC as this is recommended in the Ph. Eur. for the NGI. Experiments were also conducted with a non-cooled FSI (ambient temperature, 20 °C). The FPF values of erlotinib and genistein were not significantly different ($p>0.05$) at the two temperatures at a flow rate of 15 L/min (Table 5-5), whereas the measured FPD was relatively higher for both drugs at ambient temperature. At the flow rate of 30 L/min, a decrease in FPF for genistein was evident ($p<0.05$) when ambient temperature was employed, while the value of FPD was similar ($p>0.05$; Table 5-5). The FPD (which is a function of FPF and emitted dose) of erlotinib was comparatively higher for those collected from the non-cooled FSI at 30 L/min, while there was no significant difference in FPF as compared to the cooled FSI ($p>0.05$).

Table 5-5 Aerosol parameters for co-loaded liposomal aerosols delivered by the air-jet nebuliser at different FSI temperatures and flow rates (n=3, mean ±S.D.)

Initial Temperature of the FSI	**Air-flow rate (L/min)**	**Emitted Dose (%)**	**Fine Particle Fraction (%)**	**Fine Particle Dose (µg)**
5± 3°C	15	30.52±2.84 (Erlo) 34.31±5.86 (Gen)	45.55±6.16 (Erlo) 42.55±6.28 (Gen)	18.02±2.51 (Erlo) 224.24±10.14 (Gen)
Ambient temperature	15	53.23±4.37 (Erlo) 47.57±1.96 (Gen)	48.03±9.57 (Erlo) 42.97±10.50 (Gen)	38.19±2.76 (Erlo) 327.66±91.77 (Gen)
5± 3°C	30	26.92±4.17 (Erlo) 27.93±1.81 (Gen)	73.37±11.83 (Erlo) 73.17±6.10 (Gen)	25.93±9.17 (Erlo) 326.87±37.91 (Gen)
Ambient temperature	30	60.88±7.82 (Erlo) 56.99±7.16 (Gen)	55.17±7.15 (Erlo) 50.17±6.44 (Gen)	48.44±10.44 (Erlo) 420.74±101.61 (Gen)

The data revealed that the impactor temperature had less effect on the performance of the FSI, than the NGI which needs cooling as recommended by the Ph. Eur in order to avoid evaporation-related bias and to reduce the variability in the data when compared to use at ambient temperature (Dennis et al., 2008). Cascade impactor temperature has previously shown effects on heat transfer and droplet evaporation, especially for aqueous droplets produced by nebulisers (Bonam et al., 2008). Due to the latent heat associated with evaporation resulting from energy absorption, the temperature of nebulised aerosol is relatively cooler than the surrounding air (approximately 10°C) (Dennis et al., 2008). The cooled aerosol comes into contact with the warmer metal of the interior surfaces of the NGI. In order to maintain the moisture saturation, further evaporation takes place from the droplets, resulting in reduced droplet sizes throughout the non-cooled NGI (Dennis et al., 2008). However, omission of cooling nebulisers, air-stream

and the impactor at a fixed temperature would increase simplicity, be labour and time-saving for aerosol characterisation and beneficial for routine quality control.

Artefactual reduction in droplet size arising from thermal transfer-related evaporation may be less significant with the FSI since the FSI flight path is comparatively shorter than the NGI, causing a lower thermal capacity through the internal volume of the FSI; both impactors are made of stainless steel. By contrast, a larger headspace in the FSI may allow enhanced water evaporation when drawing nebulised liposomes through the cooled FSI using ambient air, leading to the similar results for nebulisation parameters at the two impactor temperatures (non-cooled and cooled FSI).

The magnitude of the trend to the finer droplets caused by heat transfer-related evaporation is dependent on nebuliser type. This is because surface area, concentration and size distribution of the droplets initially produced by inhaler devices have a significant impact on mass transfer from liquid to vapour state (Dennis et al., 2008). Consequently, further studies such as the use of different formulations having various physicochemical properties and other nebulisers are required. A vibrating-mesh nebuliser was subsequently investigated further to allow comparison with an air-jet nebuliser under the same operating conditions.

5.5.3.3 Aerosol properties of liposomal aerosols delivered from a vibrating-mesh nebuliser

The trends in measured aerosol properties of both drugs in the liposomal formulation delivered by air-jet and vibrating-mesh nebulisers were similar when determined using an FSI at two air-flow rates. Figure 5-4 shows the performance of a vibrating-mesh nebuliser for delivering liposomal aerosols at flow rates of 15 L/min and 30 L/min for a 10 min nebulisation period. When increasing the flow rate through the FSI from 15 L/min to 30 L/min, the FPF for erlotinib and genistein increased from approximately 20% to 40%, with the same emitted dose ($p>0.05$). Furthermore, FPD was higher for both drugs at the higher flow rate ($p<0.05$; Table 5-6). Thus overall, increasing the flow rate through the impactor using both types of nebuliser (air-jet and vibrating-mesh) affected measured

aerosol parameters, likely resulting from a decrease in droplet sizes, due to evaporative losses as outlined in Section 5.5.3.1.

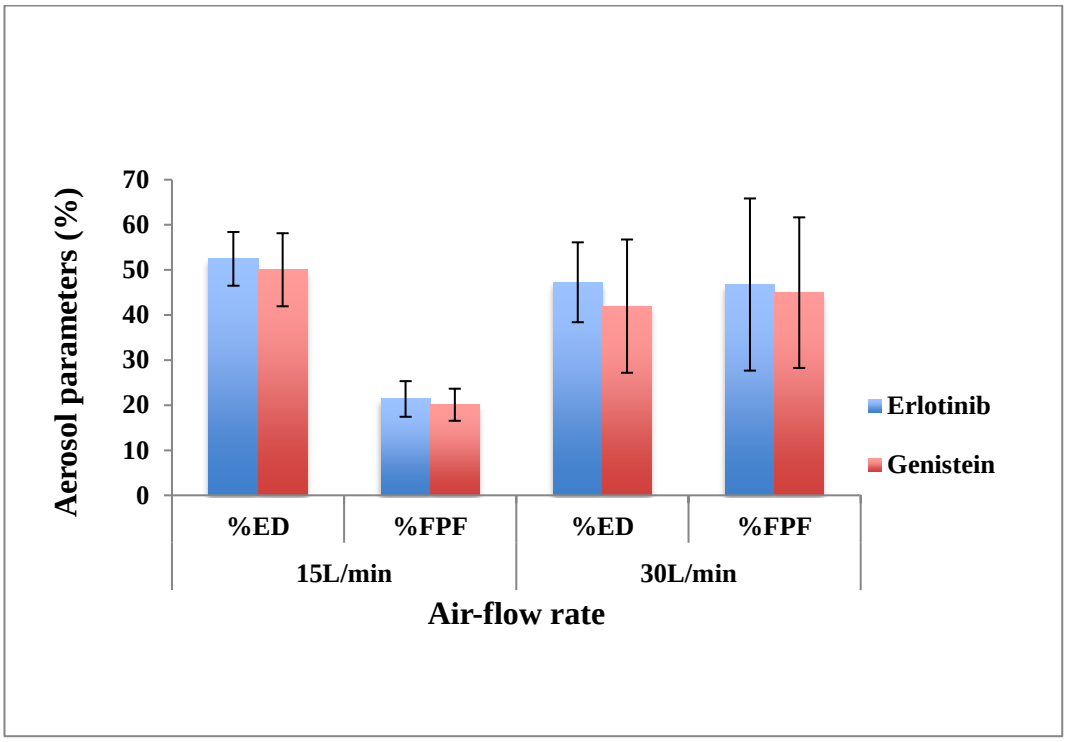

Figure 5-4 Aerosol parameters of co-loaded liposomes aerosols generated using a vibrating-mesh nebuliser determined using a cooled FSI at 15 and 30 L/min (n=3, mean ±S.D.).

Table 5-6 Fine particle dose for co-loaded liposomal aerosols delivered by a vibrating-mesh nebuliser operated at 15 L/min and 30 L/min, determined using the cooled FSI (n=3, mean ±S.D.)

Type of nebuliser	**Air-flow rate (L/min)**	**Fine Particle Dose (µg)**
Vibrating- mesh	15	17.25± 1.72 (Erlo) 149.14± 41.52 (Gen)
	30	32.83± 4.44 (Erlo) 269.83± 13.33 (Gen)

The air-jet nebuliser appears more appropriate for delivering liposomal aerosols than the vibrating-mesh nebuliser based on a two-fold higher FPF of both drugs at both flow rates (Figure 5-3 and Figure 5-4). The values of FPD, a critical parameter for medical aerosols reflected FPF, and were more similar for these two nebulisers. This was because the emitted dose was significantly higher with the vibrating-mesh nebuliser ($p<0.05$), in good agreement with previous studies (Lass et al., 2006; Pitance et al., 2010). For both flow rates, the air-jet nebuliser produced significantly higher FPD for genistein ($p<0.05$; Table 5-4 and Table 5-6), while there were no differences in FPD for erlotinib delivered using the two devices ($p>0.05$).

Previously, vibrating-mesh nebulisers have been reported to give higher aerosol mass and drug outputs compared to air-jet nebulisers (Ari, 2014). However, the air-jet devices appeared superior in this study, which may be specific for this particular liposomal formulation. The physicochemical properties of the formulation including viscosity and surface tension, particle size distribution and zeta potential of dispersed systems have an impact on nebuliser performance and aerosol characteristics, particularly for both active and passive vibrating-mesh nebulisers (Chan et al., 2011; Carvalho and McConville, 2016). The lower efficiency of the vibrating-mesh nebuliser for delivering this specific formulation may be due to the absence of an ionic component (particularly a halide) or surfactant in the formulation as reported for curcumin-loaded genistein-mPEG polymeric micelles (Chapter 3). The presence of ions is also crucial for providing an enhanced output rate and for less variable aerosol characteristics (Carvalho and McConville, 2016). Moreover, vibrating-mesh technology could possibly cause the generation of heat over a 10 min aerosolisation period, resulting in the aggregation/degradation of liposomes as reported for thermobile proteins (Hertel et al., 2014; Beck-Broichsitter and Oesterheld, 2017).

An additional concern is that the mesh aperture could possibly be blocked because of inappropriate properties of the liposomal formulation, drug crystallisation or repeated use, causing a decrease in the diameter of mesh pore and consequently higher resistance to aerosol generation (Chan et al., 2011; Manunta et al., 2011;

Carvalho and McConville, 2016). As a result of clogging, significant variations in output rate and delivered dose can be problematic.

To further investigate the implications of these findings, the physicochemical properties of fluids; for instance, viscosity and surface tension, along with the influence of fluid constituents including electrolytes/halides and surfactants in formulations during aerosolisation should be studied in the future in relation to the measured aerosol properties and nebuliser performance for liposomal aerosols.

5.5.3.4 Particle size distribution of liposomes before and after nebulisation

The particle size distribution of nebulised vesicles on individual stages of the impactor and in both nebuliser reservoirs was determined to evaluate liposomal size during aerosolisation. Table 5-7 shows the measured particle size of aerosolised liposomes delivered by air-jet and vibrating-mesh nebulisers. The mean size of sonicated liposomes remaining in the air-jet reservoir and on the additional insert (upper stage of the FSI) was approximately three-fold larger than the initial size ($p<0.05$), indicating liposome disruption, aggregation and/or fusion and consequent changes in the vesicle size (Manca et al., 2012). The PDI increased significantly ($p<0.05$), implying aggregation and/or fusion of the vesicles, broadening of the particle size distribution (Elhissi et al., 2012), which may be attributed to water evaporation during jet nebulisation, causing higher concentration of phospholipids and consequent vesicle aggregation within droplets (Elhissi et al., 2007). For the lower stage of the FSI (filter and filter holder), the measured mean size of liposomes was smaller than other regions but larger than those measured before aerosolisation ($p<0.05$).

Table 5-7 Mean hydrodynamic diameter (Z-ave) and Polydispersity Index (PDI) of nebulised sonicated co-loaded liposomes delivered to the FSI stages, and those remaining in the nebuliser reservoir (n=3, mean± S.D.)

Type of nebuliser	**Before nebulisation**		**After nebulisation**					
			Nebuliser reservoir		Upper stage of FSI		Lower stage of FSI	
	Z-ave (nm)	PDI	Z-ave (nm)	PDI	Z-ave (nm)	PDI	Z-ave (nm)	PDI
Air-jet	139.3± 2.42	0.56± 0.03	363.50± 31.05	0.75 ±0.14	258.40± 14.4	0.83± 0.19	172.50± 18.36	0.35± 0.08
Vibrating-mesh	146.2± 4.58	0.53± 0.01	210.90 ±22.78	0.77± 0.10	250.00± 88.02	0.72± 0.16	112.60± 13.51	0.37± 0.03

For the vibrating-mesh nebuliser, the mean particle size and PDI for nebulised liposomes remaining in the vibrating-mesh reservoir and on the upper stage of the FSI (stage 1 of the FSI housing) was significantly larger than the starting size ($p<0.05$), indicating that the accumulation of large liposomes and/or liposome aggregates can occur, which fail to pass through or be extruded through the mesh apertures during aerosolisation (Elhissi et al., 2011a; Carvalho and McConville, 2016). However, liposomes collected on the lower stage of the FSI showed the smallest vesicle size ($p<0.05$).

The mean size and size distribution of liposomes measured on the lower stage of the FSI was smaller than those remaining in both nebuliser reservoirs and on stage 1 of the impactor. This may be due to water loss when aerosol droplets pass through the impactor or liposome disruption after being emitted from the devices (Elhissi et al., 2007). For both nebulisers, further studies are required to determine whether a marked size reduction of liposomes collected on the lower stage of the impactor causes drug leakage, though drug losses on size reduction are not usually a major issue for hydrophobic drugs unlike hydrophilic materials (Desai et al., 2002). The impaction on metal surfaces and subsequent drying of the deposited droplets in the FSI may be a further possible reason leading to vesicle disruption and aggregation on the upper stage of the FSI. Overall, the physical stability of nebulised liposomal aerosols generated by air-jet and vibrating-mesh nebulisers was similar.

Based on these findings particularly for FPF, the air-jet nebuliser was considered the more appropriate delivery device for delivering the developed liposomal formulation. The morphology of liposomes delivered using the air-jet nebuliser was studied by TEM (Figure 5-5 a and 5-5 b), revealing a population of small relatively uniform spherical vesicles (50-250 nm) before and after nebulisation. This observation was in good agreement with previous reports of multilamellar vesicles (MLVs) reduced in size by probe-sonication and nebulised (Bozzuto and Molinari, 2015; Pattni et al., 2015; Rudokas et al., 2016). The lamellarity of the vesicles did not change during nebulisation (Figure 5-5 c and 5-5 d), suggesting that air-jet nebuliser is a suitable device for delivering aerosols of the freshly sonicated liposomes.

It was noted that sonicated liposomes became cloudy within 30 min after preparation, suggesting poor physical stability. It has been reported that extrusion of MLVs through 1-µm polycarbonate filter improved physical stability of liposomes during air-jet nebulisation and enhanced drug output for air-jet and vibrating-mesh nebulisers (Carvalho and McConville, 2016). Therefore, membrane extrusion was investigated as an alternative size reduction method.

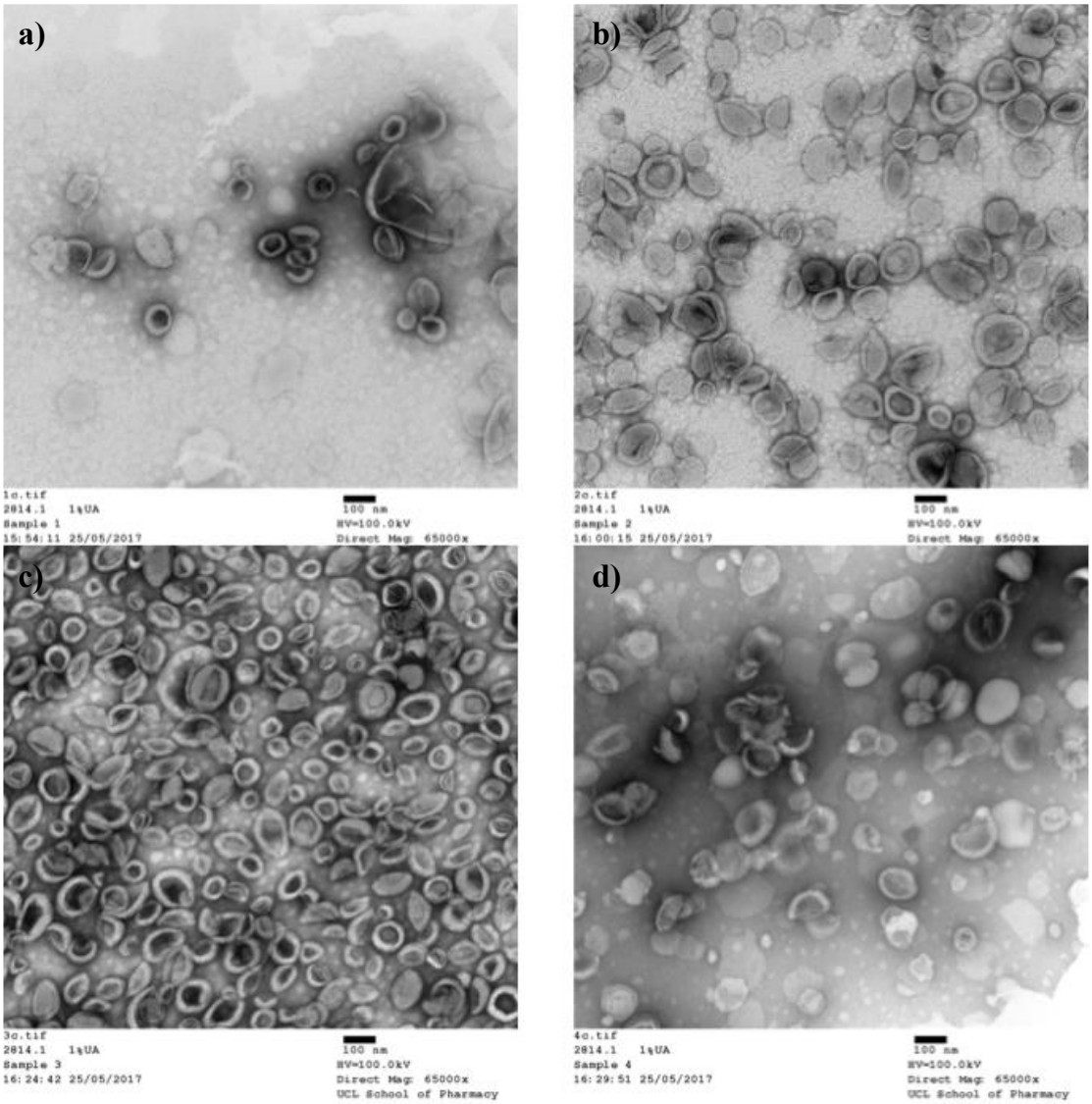

Figure 5-5 TEM images of co-loaded liposomes prepared by probe-sonication before and after air-jet nebulisation (a) freshly prepared formulation (b) vesicles remaining in air-jet reservoir following nebulisation (c) liposomes deposited on stage 1 of the FSI and (d) liposomes deposited on stage 2 of the FSI.

5.5.4 Optimisation of liposome extrusion

The composition of extruded co-loaded liposomes was the same as those previously size reduced by probe-sonication. The extrusion process would not be expected to affect drug encapsulation for both erlotinib and genistein since both drug molecules were incorporated within the liposome bilayers prior to this step (Morton et al., 2012). Consequently, optimisation of extrusion was initially aimed at improving the physical stability of liposomal formulations during their preparation.

The initial mean volume median diameter (VMD) of freshly prepared erlotinib and genistein co-loaded liposomes (lipid concentration of 20 mg/mL) before extrusion was 7.83± 0.40 µm. Figure 5-6 a shows an exponential decrease in mean VMD ($p<0.05$) on repeated extrusion cycles through a 3 µm pore membrane and that there was only a small further reduction in VMD after 5 extrusion passes. In this case, VMD was less than the pore size which is contrary to previous reports whereby mean vesicle size is normally larger than the pore size of the filter used, due to a reversible elastic deformation of the liposomes when passing through the filter pores (Hinna et al., 2015). In this study, it is possible that lipid bilayers 'squeezed off' during extrusion and reformed vesicles having mean diameter smaller than the pore size of membrane filter. Another feasible cause is that extruded liposomes have large particles of unentrapped drug removed, during the extrusion process. The co-loaded liposomal formulation extruded 5 times through a 3 µm pore polycarbonate filter was then extruded further, through a 1 µm pore filter. The trend for VMD was similar to that obtained with a 3 µm pore filter, 5 cycles was the optimal number of extrusion passes to reduce mean size to approximately 1 µm (Figure 5-6 b).

Figure 5-6 c shows that when further extruded through a 0.1µm filter, a final constant value of approximately 0.13 µm was achieved. This was in accordance with previous reports using pore size < 0.2 µm (Morton et al., 2012; Ong et al., 2016). Hence, 5 extrusion cycles using a polycarbonate filter with 0.1 µm pore size resulted in the desired mean size of 130 nm, when combined with the earlier extrusion steps at 3 and 1 µm.

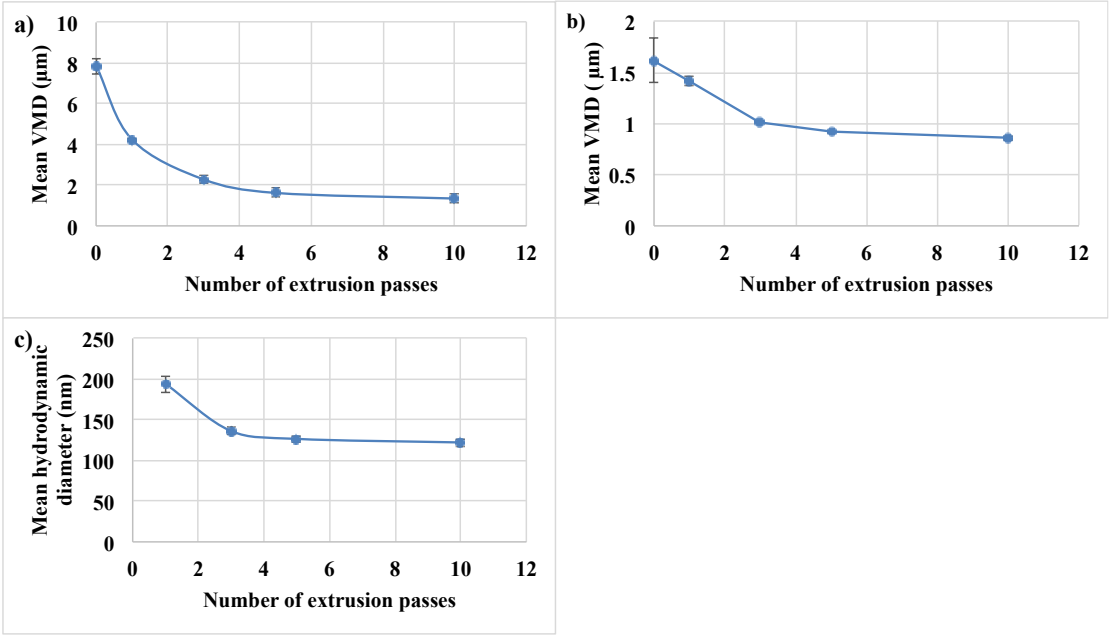

Figure 5-6 Mean VMD of liposomes extruded through: a) 3 µm pore polycarbonate membrane filter and b) further extruded through a 1 µm pore polycarbonate membrane filter, and c) mean hydrodynamic diameter of liposomes further extruded through a 0.1 µm pore polycarbonate membrane filter (n=3, mean± S.D.)

In summary, when membrane extrusion was used as a method of size reduction, the mean size decreased with an increasing number of extrusion cycles, as previously reported (Morton et al., 2012; Ong et al., 2016), reaching a size plateau after approximately 5 cycles for each membrane pore size (Figure 5-6 a, 5-6 b and 5-6 c). Low nitrogen pressure was required to extrude liposomes through large membrane pores, whereas a higher pressure was required for extrusion through the smallest pore sizes and to increase the homogeneity of liposomes (Morton et al., 2012). The mean diameter of extruded liposomes passing through larger membrane pore size (5 and 3 µm) was smaller than or approximated the pore size of filter, while that of liposomes passed through 100 nm pore membranes was slightly larger than the nominal pore size, due to the flexibility of liposomal membranes, in accordance with previous reports of the relationship between liposome particle size and extrusion membrane pore size (Mayer et al., 1986; Hunter and Frisken, 1998; Ong et al., 2016).

5.5.5 Comparison of the properties of liposomes, size reduced by probe-sonication and membrane-extrusion

In Chapter 4, size reduction of erlotinib and genistein co-loaded liposomes comprising DPPC, cholesterol and DOPE (72:8:20 mole %) was achieved using 30 min probe-sonication, giving a final mean size of approximately 130 nm after removing free drugs (Table 5-8). In this chapter, membrane extrusion was used as an alternative method of size reduction to achieve vesicles with a mean size in the same range.

Liposomes pre-filtration were cloudy and opalescent, due to non-incorporated drugs and/or liposome aggregates. Table 5-8 shows the mean particle size after passing sonicated or extruded liposomes through the cellulose acetate filters was smaller than the nominal pore size of 0.45 μm membrane filters, suggesting that only incorporated drugs in small liposomes remained in samples (Elhissi et al., 2013). The mean measured surface charge for all liposome preparations were not significantly different ($p>0.05$), the value being approximately neutral as expected based on the individual bilayer components. Commensurately, extruded liposomes had a relatively homogeneous size distribution, with small PDI value (PDI<0.03) indicative of a monodispersed population (Castile and Taylor, 1999; Hadian et al., 2014).

Table 5-8 The effect of size reduction method on mean hydrodynamic diameter, Polydispersity Index (PDI), zeta potential and drug encapsulation for co-loaded liposomes after removing non-incorporated drugs by filtration (n=3, mean± S.D.)

Size reduction method	**Hydrodynamic diameter (nm)**	**PDI**	**Zeta potential (mV)**	**Encapsulation Efficiency (%)**
Probe-sonication Post-filtration	139.30± 2.42	0.56± 0.03	+0.27± 0.05	10.65± 1.69 (Erlo) 98.69± 3.14 (Gen)
Extrusion Post-filtration	125.60± 2.15	0.13± 0.05	+0.43± 0.22	11.45± 1.13 (Erlo) 105.30± 4.24 (Gen)

Extrusion parameters were optimised using the chosen lipid composition, to generate liposomes in the desired size range with maximum incorporation of both drugs. The entrapment efficiencies of erlotinib and genistein-loaded liposomes prepared by probe-sonication and membrane extrusion were compared after removing unentrapped drugs using syringe-filtration. Previous research has demonstrated that the entrapment of sonicated hydrophobic steroid-containing liposomes was mainly dependent on lipid composition (Elhissi et al., 2013). The total content of erlotinib and genistein including free drug and drug-loaded liposomes for pre-filtered MLVs after 30 min probe-sonication compared with initial weight of drug in liposome preparation was 100%, indicating no drug was lost during preparation and sonication before non-incorporated drugs were removed by filtration. However, the total content of erlotinib and genistein including free drug and drug-incorporated liposomes after passing through a series of membrane filters was approximately 10% and 100% of initial weight of drug in formulations, respectively, indicating that unentrapped erlotinib was retained on the polycarbonate membrane filters during size reduction, while almost 100% of initial genistein was successfully incorporated into liposomes and

passed through the series of polycarbonate membranes. The entrapment efficiencies determined after separating non-incorporated drugs by passing through 0.45 μm cellulose acetate membrane filters did not show differences between sonicated and extruded liposomes for either drug ($p>0.05$). Thus, loading erlotinib and genistein (2.5% w/w each drug) into DPPC/cholesterol/DOPE liposomes (72:8:20 mol%) was not dependent on the method of size reduction since both encapsulated drugs were incorporated within the liposomal bilayer during preparation (Eckert et al., 2011; Rasti et al., 2012; Hadian et al., 2014).

Considering the physical stability of liposomal formulations, the aggregation of liposomes was clearly observed within 30 min at ambient temperature for sonicated liposomes, and therefore freshly prepared formulations were used for determining the properties of nebulised aerosol. By contrast, there was no change in mean particle size (approximately 125 nm), but slightly increase in PDI of extruded liposomes, from 0.13 to 0.26 after 1-day; storage at 4ºC. However, no liposomal aggregates were observed. These combined observations suggested that membrane extrusion produced a more stable co-loaded liposomal formulation than sonication.

Long-term stability studies are required; however, these findings support the development of liposomal formulation prepared by extrusion for enhanced stability.

Overall, extruded liposomes comprising DPPC, cholesterol and DOPE (72:8:20), prepared by thin-film hydration with size reduction using extrusion represented the best manufacturing and formulation approaches in terms of particle size distribution and co-loading of drugs.

5.5.6 Aerosol characterisation of extruded liposomes aerosolised using air-jet and vibrating-mesh nebulisers

Aerosol properties of nebulised extruded liposomes were studied using the cooled FSI, operated at the air-flow rate of 15 L/min for 10 min to investigate whether the method of size reduction affected aerosol properties. The air-jet nebuliser

generated significantly higher FPF and FPD than the vibrating-mesh nebulisers ($p<0.05$) after 10 min nebulisation (Figures 5-3 and Figure 5-4, Table 5-4 and Table 5-6). Comparing the findings for sonicated and extruded liposomes (Figures 5-3 and 5-4 for sonicated liposomes and Figure 5-7 for extruded liposomes), there were no significant differences in FPF for liposomes prepared by the different methods of size reduction using air-jet nebulisers ($p>0.05$), while vibrating-mesh nebulisers generated significantly higher FPF for extruded liposomes ($p<0.05$). However, the values of FPD of extruded erlotinib and genistein liposomes generated by both nebulisers were significantly higher than for sonicated liposomes ($p<0.05$) as seen in Tables 5-4, 5-6 and 5-9. This possibly resulted from the more monodispersed liposome population produced by membrane extrusion, passing more readily through the multiple aperture mesh of the nebulisers compared with those prepared by sonication.

From these findings, the air-jet device would appear superior to the vibrating-mesh device for delivering liposomes prepared by both methods of size reduction. Based on the combined results of FPD from Tables 5-4, 5-6 and 5-9, for the liposomal system, size reduction by extrusion, the air-jet nebuliser would appear preferable, with the aerosol properties less dependent on the properties of the liposomal formulations than the vibrating-mesh device.

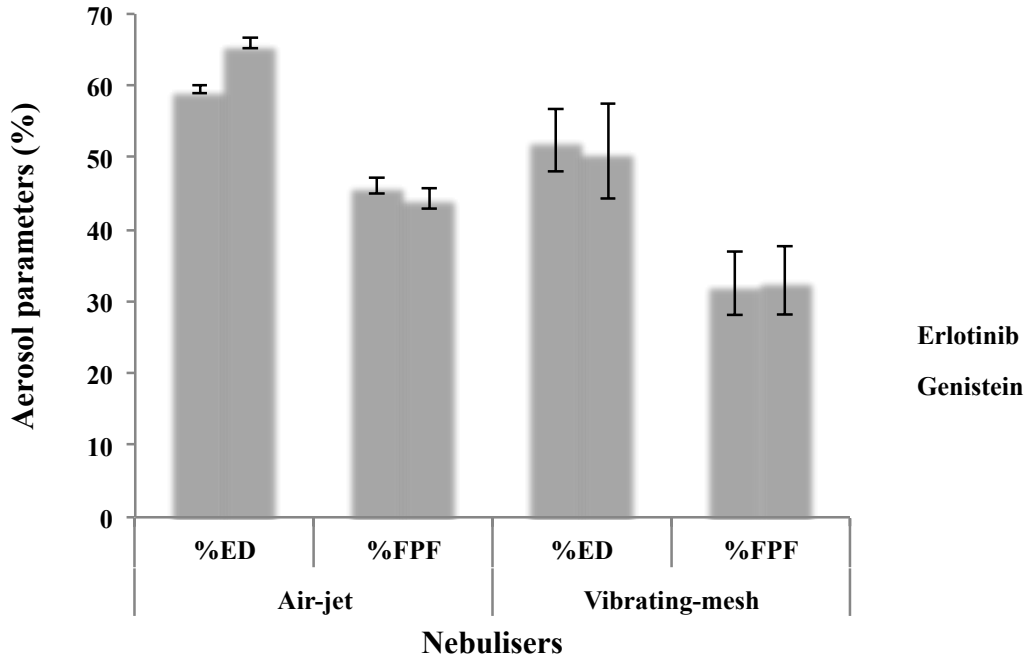

Figure 5-7 Aerosol parameters of extruded co-loaded liposomes delivered by air-jet and vibrating-mesh nebulisers with the cooled FSI at 15 L/min (n=3, mean ±S.D.)

Table 5-9 Fine particle dose for extruded co-loaded liposomal aerosols delivered by air-jet and vibrating-mesh nebulisers into the cooled FSI operated at 15 L/min (n=3, mean ±S.D.)

Type of nebuliser	**Fine Particle Dose (μg)**
Air-jet	49.43± 5.88 (Erlo) 480.36± 16.23 (Gen)
Vibrating-mesh	31.75± 5.05 (Erlo) 307.62± 87.49 (Gen)

5.5.7 Size stability of nebulised extruded liposome delivered by the air-jet and vibrating-mesh nebulisers

For liposomes prepared by extrusion, there was a very small increase in mean particle size and PDI of liposomes remaining in the main reservoir of the air-jet and vibrating-mesh devices, upper and lower stage of the FSI compared with freshly prepared formulations ($p<0.05$; Table 5-10).

When Table 5-7 and Table 5-10 are compared, liposomes sized reduced by extrusion process showed better size stability than those size-reduced by sonication during aerosolisation using both nebulisers in terms of changes in mean size after nebulisation, particularly for those remaining in the nebuliser reservoirs and deposited on stage 1 of the FSI. The mechanism underlying this is unclear and merits further investigation. In this study, liposomes were nebulised immediately after size reduction. Sonication is a physically much more disruptive and energy intensive process than extrusion, resulting in fracturing of vesicles and formation of new liposomes from bilayer fragments. With insufficient time for annealing of these newly formed structures, aggregation and fusion of vesicles may occur more readily than for extruded liposomes, which are size reduced by the relatively gentle process of squeezing through pores of defined size (Lawaczeck et al., 1976).

Table 5-10 Hydrodynamic diameter (Z-ave) and Polydispersity Index (PDI) of nebulised extruded co-loaded liposomal aerosols delivered to the FSI stages, and those remaining in the nebulizer reservoir (n=3, mean ±S.D.)

Type of nebuliser	**Before nebulisation**		**After nebulisation**					
			Nebuliser reservoir		**Upper stage of the impactor**		**Lower stage of the impactor**	
	Z-ave (nm)	PDI	Z-ave (nm)	PDI	Z-ave (nm)	PDI	Z-ave (nm)	PDI
Air-jet	117.9± 2.27	0.08± 0.02	129.90± 0.87	0.25± 0.01	139.50± 10.21	0.28± 0.00	125.40± 5.55	0.22± 0.03
Vibrating-mesh	115.4± 1.97	0.14± 0.09	116.10± 4.78	0.10± 0.03	138.70± 6.60	0.29± 0.03	113.60± 3.27	0.15± 0.04

5.6 Conclusions

Sonicated and extruded co-loaded liposomes with potential for pulmonary delivery were successfully prepared by the conventional thin-filmed hydration method, followed by probe-sonication or membrane extrusion to reduce the mean size. The effects of probe sonication and membrane extrusion methods on drug incorporation and size stability during aerosol generation using air-jet and vibrating-mesh nebulisers has been studied and shown that the performance of air-jet nebulisers was more effective than vibrating-mesh nebulisers for delivering liposomes reduced in size by both methods. The use of full impactors to characterise inhaler formulations may be limited by the need to accurately quantify deposited drug across multiple stages and they are labour intensive to use. The Fast Screening Impactor (FSI), comprising only two impaction stages with minor modifications, was found to be simple, labour and time-saving for aerosol characterisation, representing a useful alternative technique for characterising the aerosol properties of nebulised formulations, particularly when pre-cooled and used at 15 L/min. An air-jet nebuliser was found superior to a vibrating-mesh nebuliser, for delivering the co-loaded liposomes over a 10-min period, in terms of higher fine particle fraction. Extrusion was superior to probe sonication during preparation of formulations and aerosolisation process, giving greatest size stability of co-loaded liposomes as determined by size analysis before and after nebulisation.

Overall, liposomes co-loaded with erlotinib and genistein prepared by extrusion were effectively delivered using an air-jet nebuliser.

Chapter 6 General conclusion and future work

6.1 General discussion and conclusion

Non-small cell lung cancer (NSCLC) is the most common cause of cancer-related deaths worldwide (Zarogoulidis et al., 2013). Currently, oral and injected therapies for lung cancer are limited due to the systemic side effects and sub-therapeutic levels of chemotherapeutic agents at the target site (Hu et al., 2013; Rudokas et al., 2016). Pulmonary drug delivery is an attractive route of administration and has been used to deliver drugs for local treatment of respiratory diseases including asthma, COPD and cystic fibrosis (Pilcer and Amighi, 2010). Thus, this delivery route may achieve effective localised treatment for NSCLC.

Targeted therapy, one treatment approach in NSCLC, has been studied to treat specific molecular targets, including the epidermal growth factor receptor (EGFR) (Molina et al., 2008). Erlotinib, an epidermal growth factor receptor tyrosine kinase inhibitor (EGFR-TKIs), has been approved as 1st line treatment for patients who have EGFR mutations and as 2nd and 3rd line treatments for those with advanced-stage NSCLC. However, the toxicity of erlotinib is problematic (Thatcher et al., 2009; Zarogoulidis et al., 2013). Combinations of a phytochemical (e.g. genistein, curcumin, fisetin) and a chemotherapeutic agent have attracted a great deal of attention for reducing drug toxicity on normal cells and for their potentiation effects. Among a number of phytochemicals that have been studied on multiple targets in cancer cells, more than 60% are flavonoids, which can be found in fruits and vegetables. For example, the combination of erlotinib and genistein has shown synergistic anti tumour activity in three different NSCLC cell lines (Gadgeel et al., 2009).

One factor that can limit the bioavailability for NSCLC treatment is the low aqueous solubility of many hydrophobic anticancer agents. Formulation approaches using colloidal drug carriers (e.g. polymeric micelles, liposomes, cyclodextrin, dendrimer) have been proposed to improve water solubility, which when administered by the pulmonary route may achieve drug dose uniformity, decrease the frequency of drug dosing and reduce the incidence of potential systemic side effects (Mansour et al., 2009). This PhD research explores a

potential strategy to enhance the treatment of lung cancer, by using polymeric micelles or liposomes for co-delivery of hydrophobic anticancer agents by the pulmonary route. Polymeric- and lipid-based carriers may be particularly suitable for pulmonary delivery, due to their biocompatibility and reduced drug toxicity (Li et al., 2015).

For in-vitro aerosol characterisation of nebulised aerosols, the Next Generation Impactor (NGI) is routinely used. However, the quantification of nebulised low dose formulations is challenging, due to the small absolute amounts of drug deposited across many stages of a full impactor. Also, the use of full cascade impactors is time-consuming and labour intensive. Therefore, Abbreviated Impactor Measurement (AIM) using the Fast Screening Impactor (FSI), which yields limited information about the whole particle size distribution of an aerosol cloud was considered in this study. This was to investigate whether this faster method for aerosol analysis gave comparable results for key quality parameters for aerosolised drug carriers using medical nebulisers.

This PhD investigated whether a hydrophobic drug-hydrophilic polymer conjugate could self-assembly to form micelles for delivering hydrophobic anticancer agents. Secondly, whether nebulisation of micelles and liposomes for the co-delivery of hydrophobic drugs delivered by air-jet and vibrating-mesh nebulisers could produce desirable aerosol characteristics, with high drug output and fine particle dose. Thirdly, this thesis studied whether the FSI could be used as an alternative impactor to the NGI, giving comparable values for key parameters for inhaler products including emitted dose, mass balance, fine particle fraction and fine particle dose. The work in this thesis was divided into three main sections; 1) synthesis and characterisation of drug-polymer conjugate, 2) preparation and characterisation of hydrophobic drugs-loaded polymeric micelles and liposomes and 3) aerosol characterisation of nebulised aerosols determined by the NGI and the FSI.

The first part of this thesis studied a potential strategy for formulating hydrophobic drugs using hydrophilic polymer-hydrophobic drug conjugates. Drug-polymer conjugates have demonstrated a number of advantages including

enhancing the aqueous solubility of hydrophobic drugs (Hans et al., 2005; Khandare and Minko, 2006). In this approach, the drug-polymer conjugate forms micelles, encapsulating another drug for co-delivery. Recently, phytochemicals have received great attention as chemo-preventive agent. Genistein, one of the most extensively studied isoflavones, has shown synergistic anti-carcinogenic activities with both cytotoxic drug (i.e. erlotinib) and a herbal medicine (i.e. curcumin) against different cancer cell lines including lung, breast, ovarian and prostate cancer, without exerting toxic effects on normal cells (Liu et al., 2014b). Therefore, genistein was considered for co-delivery with a conventional cytotoxic drug; namely erlotinib in this study since co-delivery may allow the dose of cytotoxic drug to be reduced.

The hydrophilic polymer, methoxy poly (ethylene glycol) (mPEG) has been frequently used in hydrophilic drug carriers. mPEG has been used in approved PEGylated biopharmaceutical products for clinical use namely mPEG-epoetin beta and mPEG-filgrastim (Turecek et al., 2016, BNF, 2018). Thus, mPEG was chosen to form a genistein- mPEG conjugate as described in **Chapter 2** for producing drug carriers. Such carriers may retain the biological activity of genistein and be capable of delivering erlotinib or curcumin. The synthesis of amphiphilic genistein-mPEG conjugate involved two main steps: 1) oxidation and 2) esterification. The successful synthesis of genistein-mPEG conjugate yielded a pale yellow powder, with a yield of 43.7% was confirmed by FT-IR, ^{1}H-NMR and mass spectroscopy.

Initially, this drug-polymer conjugate was studied to determine whether it could self-assembly to form micelles. The critical micelle concentration (CMC), measured using DLS was 1.35 mg/mL (2.56 x 10^{-4} M) as outlined at the beginning of **Chapter 3,** indicating self-assembly into micelles. The main body of the experimental work described in this chapter investigated the preparation and characterisation of genistein-mPEG micelles loaded with hydrophobic drug (erlotinib or curcumin). The aerodynamic characteristics of micelles delivered in aerosol generated by air-jet and vibrating-mesh nebulisers were measured using the NGI.

A preliminary study of erlotinib loading into the synthesized conjugate, showed an encapsulation efficiency of approximately 3%, with the generation of a turbid white suspension during preparation. This indicated that this conjugate was not appropriate for the delivery of erlotinib. On the other hand, curcumin was successfully incorporated into genistein-mPEG micelles, giving a transparent yellow solution with no precipitation. These observations suggest that the polymer was not suitable for erlotinib, possibly due to its molecular structure which limited drug incorporation into the micelles. Nevertheless, this new amphiphilic compound was a suitable drug carrier for curcumin. Curcumin was incorporated into genistein-mPEG at a range of concentrations to identify the optimal drug concentration (% w/w drug in total polymer content) for further studies.

Based on effect of curcumin concentration on drug entrapment, surface charge, mean particle size and size distribution, 5% w/w drug in polymer was found to be the optimal content. This concentration gave the maximum solubilisation of curcumin, combined with other desirable properties; a high negative charge, mean size < 200 nm and PDI <0.3. Consequently, this final formulation was chosen for delivery by nebulisers.

The aerosol properties of curcumin-loaded micelles (5%w/w drug in conjugate) delivered from air-jet and vibrating-mesh nebulisers, were determined using the NGI. The air-jet nebuliser produced significantly higher fine particle dose (FPD) and fine particle fraction (FPF) compared with the vibrating-mesh nebuliser. The predominant reason for the unexpected relatively poor performance of the vibrating-mesh nebuliser may be the physicochemical properties of the formulation investigated. Thus, further investigation is required to improve understanding to develop appropriate formulation strategies as outlined in future work.

In summary, genistein-mPEG micelles incorporating curcumin at 5% w/w were successfully delivered using both nebulisers, with emitted dose greater than 50% (ED). The values of FPD and FPF for air-jet and vibrating-mesh nebulisers were in the range of 73-136 µg, and 33-48%, respectively. This indicates the potential of the micelle formulation approach for pulmonary co-delivery of anticancer

agents. Few studies of nebulised polymeric micelles have been previously reported; for instance, amphotericin B and budesonide micelles (Gilani et al., 2011; Sahib et al., 2011; Moazeni et al., 2012). The drug-polymer conjugate developed in this thesis may have application for nebulisation of other hydrophobic molecules, which have similar structural properties to genistein.

Since genistein-mPEG conjugate was not suitable for the delivery of erlotinib, another lipid-based formulation approach was explored for this drug in **Chapter 4**. Liposomes are lipid-based carriers used for various therapeutic applications including cancer treatment (Sercombe et al., 2015; Rudokas et al., 2016). These drug-carriers have more available space to accommodate exogenous compounds within different lipid bilayers compared to micelles, due to their size and lamellarity, and they are thermodynamically more stable than micelles following dilution (Bozzuto and Molinari, 2015), retaining incorporation and maintaining their size and structure better than micelles. Consequently, liposomes were considered for the co-delivery of erlotinib and genistein in **Chapter 4**.

Erlotinib and genistein co-loaded liposomes were prepared by the traditional thin-film hydration method, followed by probe-sonication. The in-vitro characterisation of the developed liposome formulation co-loaded with erlotinib and genistein was the major focus of this chapter. In order to develop formulations, an understanding of the effect of drugs and excipients on the properties of the lipid bilayer is important to optimise the quality attributes liposomal system especially entrapment efficiency, drug release and in-vitro stability (Demetzos, 2008; Chen et al., 2014). Thermal analysis using DSC, which is commonly employed to explore drug interactions with the phospholipid bilayer, is useful for liposomal formulation development. Two analytical methodologies (HPLC and DSC) were employed to study drug incorporation and the molecular interactions between drugs and lipids within the DPPC bilayer.

A new HPLC analytical method developed and validated according to ICH was used to show that the maximum incorporation of erlotinib and genistein individually and co-loaded in DPPC liposomes was 2.5% w/w. DSC thermograms showed that the incorporation of both drugs into DPPC liposomes reduced the

packing of the acyl chain domain observed by a broadening of the main phase transition, measured as an increase in the half-height width (HHW), with a significant decrease in the main transition temperature of DPPC. This indicates an increase in the fluidity of the hydrocarbon chains and a reduction of cooperative unit within the phospholipid bilayer, suggestive of incorporation of the hydrophobic drugs close to the upper regions of the bilayer and polar head group of DPPC liposomes. The pre-transition was abolished on incorporation of the drugs. These combined results confirm that erlotinib and genistein were successfully incorporated into DPPC liposomes.

The highest HHW value was found with 2.5% w/w erlotinib and 2.5% w/w genistein co-loaded liposomes, suggesting maximum drug incorporation. The final liposome formulation co-loaded with erlotinib and genistein in the presence of cholesterol (8 mol% of total lipid content) and DOPE (20 mol% of total lipid content) after 30 min sonication showed mean hydrodynamic diameter and PDI of approximately 136 nm and 0.45, respectively. The inclusion of cholesterol and DOPE caused a change in membrane properties, resulting in enhanced drug incorporation into the liposomes. The DSC data showed changes in the main phase transition (T_m, HHW and ΔH) as compared to formulations containing only drugs and DPPC, supporting that the incorporation of the two biomolecules into DPPC bilayer disrupted the packing order of the hydrophobic hydrocarbon chains and increased bilayer fluidity. The entrapment efficiency of genistein was 10 times higher than for erlotinib, being approximately 100% and 10%, respectively. Thermal analysis using DSC showed that genistein had a more pronounced effect on the bilayer properties than erlotinib. Specifically, it seems that the three hydroxyl groups on the benzene rings of genistein are easier to protonate and can form stronger ionic bonding with the phosphate and/or amine group of DPPC compared with oxygen from the methoxyethoxy chains and nitrogen atoms from the quinazolinamide ring of the erlotinib molecule. Moreover, the rigid structure of erlotinib containing three benzene rings attached to alkyne may limit the rotation and penetration of erlotinib molecules into the bilayer. From this, differences in their molecular structure may be the main reason for differences in partitioning into the bilayer and consequently encapsulation efficiency.

Since DSC can provide information about energetic properties, this method plays an important role in the development of drug delivery systems such as for prediction of maximum drug incorporation into membranes (Casado et al., 2016). 2.5% w/w erlotinib and 2.5% w/w genistein co-loaded liposomes were chosen for future studies based on these findings and optimal liposome size. In **Chapter 5**, nebulisation of 4 mL of this liposomal preparation for 10 min was considered optimal, to give high delivery of erlotinib and genistein.

At the same flow rate of 15 L/min, the FSI (cooled at 5 ºC for 90 min) with modifications was evaluated as an alternative to the NGI to overcome the analytical drawbacks associated with the NGI for evaluating erlotinib delivered by an air-jet nebuliser. An additional insert calibrated at 30 L/min of the FSI was modified by covering three of six nozzles alternately with wet glass microfiber filter to maintain a cut-off for 5 µm at the employed flow rate of 15 L/min. This two-stage abbreviated impactor was found to be simple to use and labour-saving for simple aerosol characterisation, with similar performance compared to the NGI. This suggests the FSI may have great utility as a relatively quick method for formulation development and evaluation of nebulised liposomal preparations. There were differences in absolute values for FPD and FPF calculated using the two impactors, but trends for both drugs were the same. The NGI gave higher values for FPD and FPF compared to FSI ($p<0.05$).

The differences in absolute values may result from the longer distance that the aerosol must pass as it travels through the full impactor, resulting in solvent loss from the nebulised droplets. There are also differences in the way FPF/FPD are calculated with the two impactors: by interpolation of cumulative fraction or cumulative mass of active substance versus cut-off diameter plot for the NGI, drug mass deposited on the lower stage for the FSI. The low absolute values for FPF and FPD reflect that large volumes of formulation were nebulised, not to dryness. Also, an internal dead space upstream of the FSI gives an internal geometry of the FSI dissimilar to that of the NGI, resulting in differences in particle deposition behaviour between the two impactors. Using the cooled FSI (5 ºC) at a flow rate of 15 L/min for 10 min demonstrated that for the developed

liposomal formulation the air-jet, rather than vibrating-mesh nebuliser, was the more appropriate delivery device, giving higher FPF and FPD.

Whilst the majority of studies reported were conducted with sonicated liposomes, the aerosol properties of nebulised extruded liposomes were also studied. Based on the results, the membrane extrusion method improved the size stability of liposomes during preparation and aerosolisation process as determined by particle size distribution before and after nebulisation.

To conclude, the vibrating-mesh nebuliser was efficient; reaching dryness in a short time (3-10 min) for both sonicated and extruded preparations under the same operating conditions (Ari, 2014; Pritchard et al., 2018). However, the performance of these devices is dependent on formulation physicochemical properties; for example, ionic content, viscosity, surfactant, and particle size for dispersed systems (Chan et al., 2011; Carvalho and McConville, 2016). The lower efficiency of the vibrating-mesh nebuliser for delivering this specific formulation may be due to the lower energy input for atomisation and absence of an ionic component (particularly halides) or surfactant (Ghazanfari et al., 2007; Beck-Broichsitter and Oesterheld, 2017). Pari GmbH has reported that nebulisation of 2.5 mL of salbutamol sulfate solutions in the presence of 0.9% w/v NaCl for 3 min using Pari Velox mesh nebuliser produced aerosol with MMAD and FPF, of 3.8 µm and 74%, respectively. Consequently, the inclusion of the appropriate type and concentration of ionic solutions (usually chloride) and/or viscosity reducing agent should be conducted in future work.

In terms of dose, formulations of curcumin, genistein and erlotinib for pulmonary delivery are not commercially available; therefore the appropriate local dose given via the pulmonary route should be evaluated. Clinical studies have suggested that 1500 mg daily is the recommended oral dose of curcumin for patients with lung cancer (Gupta et al., 2013; Fadus et al., 2017). The dose required for the oral treatment of NSCLC using erlotinib is 150 mg once daily (Yeo et al., 2010b, BNF, 2018). For genistein, an oral dose of 50 mg/kg body weight has been suggested based on in vivo studies (Spagnuolo et al., 2015). Based on the present findings of nebulised aerosols emitted from air-jet nebuliser, the fine particle doses of

curcumin in micelles, erlotinib and genistein in co-loaded liposomes are 123 mg, 49 mg, and 480 mg, respectively. Since a decrease in drug metabolised prior to reaching the target site (pre-systemic metabolism) is one of the main benefits of pulmonary delivery, a lower dose is often required for inhalation compared to oral delivery for local lung co-delivery. In order to increase aerosol dosing, preparation of formulations as a dry powder by spray-drying or freeze-drying process, followed by reconstitution in a small volume of water is suggested. This is to increase the concentration of drug in the final dispersion before nebulisation. Also, dosing can be adjusted by increasing nebulisation time or frequency of administration to achieve the desired dose of drug in the deep lung.

To sum up, all the findings of this thesis together support the development of two formulation approaches for the co-delivery of a herbal substance (genistein) and a cytotoxic drug (erlotinib) using liposomes and the combination of two herbal substances (genistein and curcumin) using micelles as suitable for delivery as an aerosol from a medical nebuliser. From previous reports of aerosol characterisation for DPIs and pMDIs, the utility of the FSI has shown equivalent performance to the NGI in terms of similar FPD and FPF (Mitchell and Nichols, 2011). In this study, the FSI was found to be a useful alternative to the NGI based on the nebulised liposomal formulation containing genistein. The FSI is not able to provide all the information that the NGI or other full cascade impactors do, such as MMAD and GSD since these require plotting of multiple data points and interpolation of data, which is not available with the FSI. This applies also to the other two abbreviated impactors, namely the Fast Screening Andersen (FSA) and Reduced Next Generation Impactor (rNGI), which employ two or three-sized fractionating stages. However, the data obtained with abbreviated impactor is sufficient and adequate for routine quality control and inhaler product development including using ‘Efficient Data Analysis (EDA)’. Consequently, it may be beneficial to use the FSI as an alternative impactor for quality control where the purpose is to check for batch-to-batch variation as well as product development applications of nebuliser formulations.

6.2 Future work

The findings presented in this thesis have demonstrated that the two studied formulation approaches; micelles and liposomes can be considered for the co-delivery of hydrophobic anticancer agents and their aerosol properties can be characterised by a full-cascade impactor or an abbreviated impactor, following nebulisation. There are four areas that future work could focus upon as listed below.

1) **Study of the biological activity of genistein in genistein-mPEG conjugate**

The aim of this study was to synthesize a new compound that may produce polymeric micelles, which retain the biological activity of genistein. The hydroxyl groups (-OH) attached to the benzene rings of genistein are responsible for its biological activities (Pavese et al., 2010; Rusin et al., 2010; Yoon and Park, 2014). For example, genistein can act as an antioxidant via protonation at –OH groups, thereby protecting against oxidative damage (Yoon and Park, 2014). The antiproliferative activity of genistein via inhibition of tyrosine kinase, topoisomerase II and G2/M block of the cell cycle is also related to the structural features of genistein. Consequently, the genistein-mPEG conjugate requires further investigation to determine whether the activity of genistein such as anticancer and antioxidant properties remain after being hydrolysed by carboxylesterase enzyme in bronchial epithelial cell (Mutch et al., 2007).

Many studies have been carried out on the antioxidant activity of compounds found in natural substances and medicinal herbs. In vitro studies, the antioxidant activity of genistein in soybean can be determined by DPPH radical-scavenging activity and ABTS radical-scavenging activity in future since these two methods are sensitive to detect antioxidant activity within a short time (Mihaylova and Schalow, 2013; Lee et al., 2015a).

To study the in vitro cytotoxic effect of genistein, A549 cells should be considered since this NSCLC cell line has been used to study the anticancer

activity of genistein in combination with erlotinib or curcumin. The assessment of cell viability can be determined using the 3-(4,5-dimethylthiazol-2-yl)-2,5-diphenyltetrazolium bromide (MTT assay) to reflect the inhibition of cell growth for human lung carcinoma cells (Liu et al., 2014b; Yang et al., 2016; Zhang et al., 2017). Moreover, other hydrophobic drugs for cancer-related diseases may be delivered using this conjugate.

2) **Study of the synergistic activity of curcumin-loaded genistein-mPEG polymeric micelles and liposomes co-loaded with erlotinib and genistein**

It should be noted that the genistein content in genistein-mPEG micelles could not be accurately determined in this study. This is because the ester bond of genistein and mPEG-COOH was not hydrolysed prior to HPLC determination. Further studies should consider the hydrolysis of genistein from genistein-mPEG (Qiu et al., 2010). Also, the potential synergistic anticancer activity in NSCLC may allow dose reduction in combinations of genistein and curcumin and for genistein and erlotinib. Therefore, a cell viability (A549 cell line) study should be carried out by MTT assay to determine the lowest dose needed in the two drug combinations. The data of in vitro cytotoxicity of combinations may suggest an appropriate formulation approach as well as suitable dosing and treatment durations for patients.

3) **Study of the effect of fluid properties on the discriminatory ability of the cascade impactors**

The concept of Abbreviated Impactor Measurement (AIM) has received attention from the pharmaceutical industry and instrument manufacturers as a quick method of measuring Aerodynamic Particle Size Distribution (ASPD) using a reduced number of stages in the impactor. The lower number of stages in the FSI as compared to a full cascade impactor makes it possible for higher accuracy due to low internal losses and less opportunity for analyst error, as well as for faster data acquisition (Mitchell et al., 2009b). Various studies have previously been conducted to compare the results obtained using the NGI or ACI and the FSI;

however, the use of FSI as an interchangeable impactor with the NGI for fluid nebuliser for routine quality control and product development has not been investigated widely.

In this work, liposomes were studied to explore the comparability of the full and abbreviated cascade impactor methods. Future work should evaluate the effect of changes in formulation properties (e.g. viscosity and surface tension) and formulation strategies (solution, complexation, dendrimer etc.) on the performance of the two cascade impactors with respect to critical quality attributes such as emitted dose and fine particle dose to explore the relative ability of full and abbreviated impactors to determine differences in aerosol properties resulting from changes in fluid properties. Also, variations from multiple operators should be tested for sensitivity of the NGI and the FSI.

4) **Study of the effect of fluid properties on the performance of air-jet and vibrating-mesh nebulisers**

Based on the studies in this thesis, the air-jet nebuliser was found to be more efficient than vibrating-mesh nebuliser, with significantly higher FPD and FPF for curcumin-loaded genistein-mPEG micelles and for extruded liposomes co-loaded with erlotinib and genistein. These findings were at variance with some previous reports.

There are a number of factors affecting the aerosolisation performance of vibrating-mesh devices. For example, components of the mesh itself (i.e. the size of pore, the mode of vibration, shape of mesh, material used and the aerosolisation mechanism) can vary widely between different manufacturers (Pritchard et al., 2018). Additionally, various physicochemical properties; for instance, surface tension, viscosity, salt and halide content and particle size in dispersed systems also have effects on drug output rate delivered by vibrating-mesh nebulisers (Ari, 2014; Pritchard et al., 2018). As stated in Chapter 3 and 5, HPLC grade water was used to prepare micelles and liposomes to keep formulations as simple as possible. For aerosol properties of nebulised droplet delivered by air-jet and vibrating-mesh nebulisers, both formulations showed the

same trends. This may be because the particle size of drug-carriers (micelles and liposomes) and fluid viscosity were similar.

The Velox mesh nebuliser used in this work, is based on the eFlow technology (active-mesh nebuliser) and was launched by Pari GmbH in 2015 (Pritchard et al., 2018). A further systematic investigation of various drug-carriers and fluid properties should be considered for a better understanding of the droplet size, the dose emitted from a particular device and the nebuliser output efficiency.

References

ABDELRAHIM, M. E. 2011. Aerodynamic characteristics of nebulized terbutaline sulphate using the Andersen Cascade Impactor compared to the Next Generation Impactor. *Pharm Dev Technol,* 16**,** 137-145.

ABDELRAHIM, M. E. & CHRYSTYN, H. 2009. Aerodynamic characteristics of nebulized terbutaline sulphate using the Next Generation Impactor (NGI) and CEN method. *J Aerosol Med Pulm Drug Deliv,* 22**,** 19-28.

ABDELRAHIM, M. E., PLANT, P. & CHRYSTYN, H. 2010. In-vitro characterisation of the nebulised dose during non-invasive ventilation. *J Pharm Pharmacol,* 62**,** 966-972.

ADITYA, N. P., SHIM, M., LEE, I., LEE, Y., IM, M. H. & KO, S. 2013. Curcumin and genistein coloaded nanostructured lipid carriers: in vitro digestion and antiprostate cancer activity. *J Agric Food Chem,* 61**,** 1878-1883.

AHMAD, Z., SHAH, A., SIDDIQ, M. & KRAATZ, H. B. 2014. Polymeric micelles as drug delivery vehicles. *RSC Advances,* 4**,** 17028-17038.

AJAZUDDIN, A., ALEXANDER, A., AMARJI, B. & KANAUJIA, P. 2013. Synthesis, characterization and in vitro studies of pegylated melphalan conjugates. *Drug Dev Ind Pharm,* 39**,** 1053-1062.

ALI, A. A., HSU, F. T., HSIEH, C. L., SHIAU, C. Y., CHIANG, C. H., WEI, Z. H., CHEN, C. Y. & HUANG, H. S. 2016. Erlotinib-conjugated iron oxide nanoparticles as a smart cancer-targeted theranostic probe for MRI. *Sci Rep,* 6**,** 1-16.

ALMAHY, H. & ALHASSAN, N. 2011. Studies on the chemical constituents of the leaves of ficus bengalensis and their antimicrobial activity. *J Sci Technol,* 12**,** 118-124.

AMANI, A., YORK, P., CHRYSTYN, H. & CLARK, B. J. 2010. Evaluation of a nanoemulsion-based formulation for respiratory delivery of budesonide by nebulizers. *AAPS PharmSciTech,* 11**,** 1147-1151.

AMINI, M. A., FARAMARZI, M. A., GILANI, K., MOAZENI, E., ESMAEILZADEH-GHAREHDAGHI, E. & AMANI, A. 2014. Production, characterisation, and in vitro nebulisation performance of budesonide-loaded PLA nanoparticles. *J Microencapsul,* 31**,** 422-429.

ANAND, P., NAIR, H. B., SUNG, B., KUNNUMAKKARA, A. B., YADAV, V. R., TEKMAL, R. R. & AGGARWAL, B. B. 2010. Design of curcumin-loaded PLGA nanoparticles formulation with enhanced cellular uptake, and increased bioactivity in vitro and superior bioavailability in vivo. *Biochim Pharmacol,* 79**,** 330-338.

ANDRADE, L. M., DE FÁTIMA REIS, C., MAIONE-SILVA, L., ANJOS, J. L. V., ALONSO, A., SERPA, R. C., MARRETO, R. N., LIMA, E. M. & TAVEIRA, S. F. 2014. Impact of lipid dynamic behavior on physical stability, in vitro release and skin permeation of genistein-loaded lipid nanoparticles. *Eur J Pharm BioPharm,* 88**,** 40-47.

ANTONIO, P., RENATO, D., ANTONIO, D. N., MONICA, N., GIOVANNI, S. & ANTONIO, T. 2004. Erbium(III) triflate: a valuable catalyst for the rearrangement of epoxides to aldehydes and ketones. *Synlett,* 14**,** 2633-2635.

ARI, A. 2014. Jet, ultrasonic, and mesh nebulizers: an evaluation of nebulizers for better clinical outcomes. *Eurasian J Pulmonol,* 16**,** 1-7.

ARZHAVITINA, A. & STECKEL, H. 2010. Surface active drugs significantly alter the drug output rate from medical nebulizers. *Int J Pharm,* 384**,** 128-136.

ATKINS, P. J. 2005. Dry powder inhalers: an overview. *Respir Care,* 50**,** 1304-1312.

BABU, A., TEMPLETON, A. K., MUNSHI, A. & RAMESH, R. 2013. Nanoparticle-based drug delivery for therapy of lung cancer: progress and challenges. *J Nanomater,* 2013**,** 14-24.

BAKHTIARY, Z., BARAR, J., AGHANEJAD, A., SAEI, A. A., NEMATI, E., EZZATI NAZHAD DOLATABADI, J. & OMIDI, Y. 2017. Microparticles containing erlotinib-loaded solid lipid nanoparticles for treatment of non-small cell lung cancer. *Drug Dev Ind Pharm,* 43**,** 1244-1253.

BANERJEE, S. S., AHER, N., PATIL, R. & KHANDARE, J. 2012. Poly(ethylene glycol)-prodrug conjugates: concept, design, and applications. *J Drug Deliv,* 2012**,** 17-33.

BARGHI, L., ASGARI, D., BARAR, J., NAKHLBAND, A. & VALIZADEH, H. 2014. Synthesis, characterization and in vitro anti-tumoral evaluation of erlotinib-PCEC nanoparticles. *Asian Pac J Cancer Prev,* 15**,** 10281-10287.

BATRAKOVA, E., BRONICH, T., VETRO, J. & KABANOV, A. 2006. *Polymer micelles as drug carriers*. Imperial College Press, pp 1-51.

BEASLEY, R., RAFFERTY, P. & HOLGATE, S. T. 1988. Adverse reactions to the non-drug constituents of nebuliser solutions. *Br J Clin Pharmacol,* 25**,** 283-287.

BECK-BROICHSITTER, M. & OESTERHELD, N. 2017. Electrolyte type and nozzle composition affect the process of vibrating-membrane nebulization. *Eur J Pharm Biopharm,* 119, 11-16.

BENI, S., BUDAI, M., NOSZAL, B. & GROF, P. 2006. Molecular interactions in imatinib-DPPC liposomes. *Eur J Pharm Sci,* 27**,** 205-211.

BERG, E., LAMB, P., ALI, A., DENNIS, J., TSERVISTAS, M. & MITCHELL, J. 2008. Assessment of the need to coat particle collection cups of the NGI to mitigate droplet bounce when evaluating nebuliser-produced droplets. *Pharmeur Sci Notes,* 1**,** 21-25.

BERG, E., MITCHELL, J., DENNIS, J., KREHER, C., JAUERNIG, J., LAMB, P., KARLSSON, M., NIKANDER, K. & TSERVISTAS, M. 2007a. The Nebuliser sub-team of the European Pharmaceutical Aerosol Group (EPAG). *DDL 2007*, 1, 71-74.

BERG, E., SVENSSON, J. O. & ASKING, L. 2007b. Determination of nebulizer droplet size distribution: a method based on impactor refrigeration. *J Aerosol Med,* 20**,** 97-104.

BHATTACHARYA, S. & HALDAR, S. 2000. Interactions between cholesterol and lipids in bilayer membranes. Role of lipid headgroup and hydrocarbon chain–backbone linkage. *Biochim Biophys Acta,* 1467**,** 39-53.

BNF. 2018. British National Formulary 76th ed. London: BMJ Group and Pharmaceutical Press.

BOAKYE, C. H. A., PATEL, K., DODDAPANENI, R., BAGDE, A., MAREPALLY, S. & SINGH, M. 2017. Novel amphiphilic lipid augments

the co-delivery of erlotinib and IL36 siRNA into the skin for psoriasis treatment. *J Control Rel,* 246**,** 120-132.

BOHR, A. & BECK-BROICHSITTER, M. 2015. Generation of tailored aerosols for inhalative drug delivery employing recent vibrating-mesh nebulizer systems. *Ther Deliv,* 6**,** 621-636.

BOLANDNAZAR, S., DIVSALAR, A., VALIZADEH, H., KHODAEI, A. & ZAKERI-MILANI, P. 2013. Development and application of an HPLC method for erlotinib protein binding studies. *Adv Pharm Bull,* 3**,** 289-293.

BONAM, M., CHRISTOPHER, D., CIPOLLA, D., DONOVAN, B., GOODWIN, D., HOLMES, S., LYAPUSTINA, S., MITCHELL, J., NICHOLS, S., PETTERSSON, G., QUALE, C., RAO, N., SINGH, D., TOUGAS, T., OORT, M. V., WALTHER, B. & WYKA, B. 2008. Minimizing variability of cascade impaction measurements in inhalers and nebulizers. *AAPS PharmSciTech,* 9**,** 404-413.

BOZZUTO, G. & MOLINARI, A. 2015. Liposomes as nanomedical devices. *Int J Nanomedicine,* 10**,** 975-999.

BRIDGES, P. A. & TAYLOR, K. M. G. 2000. An investigation of some of the factors influencing the jet nebulisation of liposomes. *Int J Pharm,* 204**,** 69-79.

BUDAI, M., SZABÓ, Z., SZŐGYI, M. & GRÓF, P. 2003. Molecular interactions between DPPC and morphine derivatives: a DSC and EPR study. *Int J Pharm,* 250**,** 239-250.

CAI, L., YU, R., HAO, X. & DING, X. 2017. Folate receptor-targeted bioflavonoid genistein-loaded chitosan nanoparticles for enhanced anticancer effect in cervical cancers. *Nanoscale Res Lett,* 12**,** 509-517.

CARVALHO, T. C. & MCCONVILLE, J. T. 2016. The function and performance of aqueous aerosol devices for inhalation therapy. *J Pharm Pharmacol,* 68**,** 556-578.

CARVALHO, T. C., PETERS, J. I. & WILLIAMS, R. O. 2011. Influence of particle size on regional lung deposition – what evidence is there? *Int J Pharm,* 406**,** 1-10.

CASADO, A., GIUFFRIDA, M. C., SAGRISTA, M. L., CASTELLI, F., PUJOL, M., ALSINA, M. A. & MORA, M. 2016. Langmuir monolayers and differential scanning calorimetry for the study of the interactions between camptothecin drugs and biomembrane models. *Biochim Biophys Acta,* 1858**,** 422-433.

CASTILE, J. D. & TAYLOR, K. M. G. 1999. Factors affecting the size distribution of liposomes produced by freeze-thaw extrusion. *Int J Pharm,* 188**,** 87-95.

CASTILLO, P. M., DE LA MATA, M., CASULA, M. F., SÁNCHEZ-ALCÁZAR, J. A. & ZADERENKO, A. P. 2014. PEGylated versus non-PEGylated magnetic nanoparticles as camptothecin delivery system. *Beilstein J Nanotechnol,* 5**,** 1312-1319.

CÉSAR, I. C., BRAGA, F. C., SOARES, C. D. V., DE AGUIAR NUNAN, E., PIANETTI, G. A., CONDESSA, F. A., BARBOSA, T. A. F. & CAMPOS, L. M. M. 2006. Development and validation of a RP-HPLC method for quantification of isoflavone aglycones in hydrolyzed soy dry extracts. *J Chromatogr B,* 836**,** 74-78.

CHAN, J. G., KWOK, P. C., YOUNG, P. M., CHAN, H. K. & TRAINI, D. 2011. Mannitol delivery by vibrating mesh nebulisation for enhancing mucociliary clearance. *J Pharm Sci,* 100**,** 2693-2702.

CHANG, C. H., LEE, C. H., KO, J. C., CHANG, L. Y., LEE, M. C., WANG, J. Y. & YU, C. J. 2017. Gefitinib or erlotinib in previously treated non-small-cell lung cancer patients: a cohort study in Taiwan. *Cancer Med,* 6**,** 1563-1572.

CHATBURN, R. L. & MCPECK, M. 2007. A new system for understanding nebulizer performance. *Respir Care,* 52**,** 1037-1050.

CHEN, F., PENG, J., LEI, D., LIU, J. & ZHAO, G. 2013. Optimization of genistein solubilization by κ-carrageenan hydrogel using response surface methodology. *Food Science and Human Wellness,* 2**,** 124-131.

CHEN, H., CHEN, L., WANG, L., ZHOU, X., CHAN, J. Y., LI, J., CUI, G. & LEE, S. M. 2016a. Synergistic effect of fenretinide and curcumin for treatment of non-small cell lung cancer. *Cancer Biol Ther***,** 1-8.

CHEN, J., HE, C. Q., LIN, A. H., XU, F., WANG, F., ZHAO, B., LIU, X., CHEN, Z. P. & CAI, B. C. 2014. Brucine-loaded liposomes composed of HSPC and DPPC at different ratios: in vitro and in vivo evaluation. *Drug Dev Ind Pharm,* 40**,** 244-251.

CHEN, P., ZHANG, H., CHENG, S., ZHAI, G. & SHEN, C. 2016b. Development of curcumin loaded nanostructured lipid carrier based thermosensitive in situ gel for dermal delivery. *Colloids Surf A Physicochem Eng Asp,* 506**,** 356-362.

CHEN, S. C., WU, G., SHI, J. & WANG, Y. Z. 2011. Novel "star anise"-like nano aggregate prepared by self-assembling of preformed microcrystals from branched crystalline-coil alternating multi-block copolymer. *Chem Commun,* 47**,** 4198-4200.

CHEN, S. F., LU, W. F., WEN, Z. Y., LI, Q. & CHEN, J. H. 2012. Preparation, characterization and anticancer activity of norcantharidin-loaded poly(ethylene glycol)-poly(caprolactone) amphiphilic block copolymer micelles. *Pharmazie,* 67**,** 781-788.

CHENG, Y. S. 2014. Mechanisms of pharmaceutical aerosol deposition in the respiratory tract. *AAPS PharmSciTech,* 15**,** 630-640.

CHIU, M. H. & PRENNER, E. J. 2011. Differential scanning calorimetry: an invaluable tool for a detailed thermodynamic characterization of macromolecules and their interactions. *J Pharm Bioallied Sci,* 3**,** 39-59.

CHOI, K. H., MOON, S. H., PARK, S. K., CHO, G., NAM, K. & PARK, B. 2018. Fabrication and characterization of medical mesh-nebulizer for aerosol drug delivery. *Appl Sci,* 8**,** 604-616.

CHOLKAR, K., TRINH, H. M., VADLAPUDI, A. D. & MITRA, A. K. 2014. Synthesis and characterization of ganciclovir long chain lipid prodrugs. *Adv Ophthalmol Vis Syst,* 1-14.

CHOUNTOULESI, M., NAZIRIS, N., PIPPA, N. & DEMETZOS, C. 2017. The significance of drug-to-lipid ratio to the development of optimized liposomal formulation. *J Liposome Res***,** 1-10.

CHOW, A. H., TONG, H. H., CHATTOPADHYAY, P. & SHEKUNOV, B. Y. 2007. Particle engineering for pulmonary drug delivery. *Pharm Res,* 24**,** 411-437.

CIPOLLA, D., BLANCHARD, J. & GONDA, I. 2016. Development of liposomal ciprofloxacin to treat lung infections. *Pharmaceutics,* 8-39.

CIPOLLA, D., GONDA, I. & CHAN, H. K. 2013. Liposomal formulations for inhalation. *Ther Deliv,* 4**,** 1047-1072.

CLARK, A. R. 1995. The use of laser diffraction for the evaluation of the aerosol clouds generated by medical nebulizers. *Int J Pharm,* 115**,** 69-78.

CLAY, M. M., PAVIA, D., NEWMAN, S. P., LENNARD-JONES, T. & CLARKE, S. W. 1983. Assessment of jet nebulisers for lung aerosol therapy. *Lancet,* 2**,** 592-594.

CLAYTON, K. N., SALAMEH, J. W., WERELEY, S. T. & KINZER-URSEM, T. L. 2016. Physical characterization of nanoparticle size and surface modification using particle scattering diffusometry. *Biomicrofluidics,* 10**,** 1-14.

COATES, A. L. & HO, S. L. 1998. Drug administration by jet nebulization. *Pediatr Pulmonol,* 26**,** 412-423.

COLOMBO, P., TRAINI, D. & BUTTINI, F. 2013. Aerodynamic assessment for inhalation products: fundamentals and current pharmacopoeial methods. IN COLOMBO, P. (Eds.) *Inhalation drug delivery: techniques and products.* John Willey & Sons, Ltd.

CORTIJO, M. & CHAPMAN, D. 1981. A comparison of the interactions of cholesterol and gramicidin a with lipid bilayers using an infrared data station. *FEBS Lett,* 131**,** 245-248.

COUNCIL OF EUROPE. 2017. *European Pharmacopoeia.* Strasbourg: Council of Europe.

COPLEY, M. 2014. Using breathing simulators to enhance inhaled product testing. [online]. [Accessed 5th July 2018]. Available at http://www.copleyscientific.com/files/ww/news/COP%20JOB%20251_Using%20breathing%20simulators%20to%20enhance%20inhaled%20product%20testing.pdf.

COPLEY, M. 2008. Cascade impactors: theory, design, and practical information for optimal testing. [Online]. [Accessed 18th June 2018]. Available at http://www.copleyscientific.com/files/ww/articles/Cascade%20Impactors.pdf.

CRUPI, V., FICARRA, R., GUARDO, M., MAJOLINO, D., STANCANELLI, R. & VENUTI, V. 2007. UV–vis and FTIR–ATR spectroscopic techniques to study the inclusion complexes of genistein with β-cyclodextrins. *J Pharm Biomed Anal,* 44**,** 110-117.

CUI, T., ZHANG, S. & SUN, H. 2017. Co-delivery of doxorubicin and pH-sensitive curcumin prodrug by transferrin-targeted nanoparticles for breast cancer treatment. *Oncol Rep,* 37**,** 1253-1260.

DAILEY, L. A., SCHMEHL, T., GESSLER, T., WITTMAR, M., GRIMMINGER, F., SEEGER, W. & KISSEL, T. 2003. Nebulization of biodegradable nanoparticles: impact of nebulizer technology and nanoparticle characteristics on aerosol features. *J Control Rel,* 86**,** 131-144.

DALBY, R., SPALLEK, M. & VOSHAAR, T. 2004. A review of the development of Respimat® Soft Mist™ Inhaler. *Int J Pharm,* 283**,** 1-9.

DALBY, R., EICHER, J. & ZIERENBERG, B. 2011. Development of Respimat(®) Soft Mist™ Inhaler and its clinical utility in respiratory disorders. *Med Devices (Auckl),* 4**,** 145-155.

DANAFAR, H., DAVARAN, S., ROSTAMIZADEH, K., VALIZADEH, H. & HAMIDI, M. 2014. Biodegradable m-PEG/PCL core-shell micelles:

preparation and characterization as a sustained release formulation for curcumin. *Adv Pharm Bull,* 4**,** 501-510.

DANAFAR, H., ROSTAMIZADEH, K., DAVARAN, S. & HAMIDI, M. 2017. Co-delivery of hydrophilic and hydrophobic drugs by micelles: a new approach using drug conjugated PEG-PCLNanoparticles. *Drug Dev Ind Pharm,* 43**,** 1908-1918.

DANCIU, C., SOICA, C., CSANYI, E., AMBRUS, R., FEFLEA, S., PEEV, C. & DEHELEAN, C. 2012. Changes in the anti-inflammatory activity of soy isoflavonoid genistein versus genistein incorporated in two types of cyclodextrin derivatives. *Chem Cent J,* 6**,** 58-69.

DANDEKAR, P., VENKATARAMAN, C. & MEHRA, A. 2010. Pulmonary targeting of nanoparticle drug matrices. *J Aerosol Med Pulm Drug Deliv,* 23**,** 343-353.

DARWIS, Y. & KELLAWAY, I. W. 2001. Nebulisation of rehydrated freeze-dried beclomethasone dipropionate liposomes. *Int J Pharm,* 215**,** 113-121.

DAVIES, L. A., NUNEZ-ALONSO, G. A., MCLACHLAN, G., HYDE, S. & Gill, H. 2014. Aerosol delivery of DNA/liposomes to the lung for cystic fibrosis gene therapy. *Hum Gene Ther Clin Dev,* 25, 97-107.

DAVIS, B. M., RICHENS, J. L. & O'SHEA, P. 2011. Label-free critical micelle concentration determination of bacterial quorum sensing molecules. *Biophys J,* 101**,** 245-254.

DE BOER, A. H., GJALTEMA, D., HAGEDOORN, P. & FRIJLINK, H. W. 2002. Characterization of inhalation aerosols: a critical evaluation of cascade impactor analysis and laser diffraction technique. *Int J Pharm,* 249**,** 219-231.

DE PABLO, E., FERNÁNDEZ-GARCÍA, R., BALLESTEROS, M. P., TORRADO, J. J. & SERRANO, D. R. 2017. Nebulised antibiotherapy: conventional versus nanotechnology-based approaches, is targeting at a nano scale a difficult subject? *Ann Transl Med,* 5**,** 448-464.

DEMETZOS, C. 2008. Differential Scanning Calorimetry (DSC): a tool to study the thermal behavior of lipid bilayers and liposomal stability. *J Liposome Res,* 18**,** 159-173.

DENNIS, J., BERG, E., SANDELL, D., ALI, A., LAMB, P., TSERVISTAS, M., KARLSSON, M. & MITCHELL, J. 2008. Cooling the NGI - an approach to size a nebulised aerosol more accurately. *Pharmeur Sci Notes,* 2008**,** 27-30.

DENYER, J. & DYCHE, T. 2010. The Adaptive Aerosol Delivery (AAD) technology: past, present, and future. *J Aerosol Med Pulm Drug Deliv,* 23**,** 1-10.

DESAI, T. R., HANCOCK, R. E. & FINLAY, W. H. 2002. A facile method of delivery of liposomes by nebulization. *J Control Rel,* 84**,** 69-78.

DESHPANDE, D., BLANCHARD, J., SRINIVASAN, S., FAIRBANKS, D., FUJIMOTO, J., SAWA, T., WIENER-KRONISH, J., SCHREIER, H. & GONDA, I. 2002. Aerosolization of lipoplexes using AERx® pulmonary delivery system. *AAPS PharmSci,* 4**,** 12-21.

DHAND, R. 2010. Intelligent nebulizers in the age of the internet: the I-neb Adaptive Aerosol Delivery (AAD) system. *J Aerosol Med Pulm Drug Deliv,* 23**,** 3-5.

DOLOVICH, M. B. & DHAND, R. 2011. Aerosol drug delivery: developments in device design and clinical use. *Lancet,* 377**,** 1032-1045.

DORA, C. P., TROTTA, F., KUSHWAH, V., DEVASARI, N., SINGH, C., SURESH, S. & JAIN, S. 2016. Potential of erlotinib cyclodextrin nanosponge complex to enhance solubility, dissolution rate, in vitro cytotoxicity and oral bioavailability. *Carbohydr Polym,* 137**,** 339-349.

DU, J. Z., LONG, H. Y., YUAN, Y. Y., SONG, M. M., CHEN, L., BI, H. & WANG, J. 2012. Micelle-to-vesicle morphological transition via light-induced rapid hydrophilic arm detachment from a star polymer. *Chem Commun,* 48**,** 1257-1259.

DUNBAR, C. & MITCHELL, J. 2005. Analysis of cascade impactor mass distributions. *J Aerosol Med,* 18**,** 439-451.

DUST, J. M., FANG, Z. H. & HARRIS, J. M. 1990. Proton NMR characterization of poly(ethylene glycols) and derivatives. *Macromolecules,* 23**,** 3742-3746.

ECKERT, G. P., CHANG, S., ECKMANN, J., COPANAKI, E., HAGL, S., HENER, U., MULLER, W. E. & KOGEL, D. 2011. Liposome-incorporated DHA increases neuronal survival by enhancing non-amyloidogenic APP processing. *Biochim Biophys Acta,* 1808**,** 236-243.

EDWARDS, D. A., HANES, J., CAPONETTI, G., HRKACH, J., BEN-JEBRIA, A., ESKEW, M. L., MINTZES, J., DEAVER, D., LOTAN, N. & LANGER, R. 1997. Large porous particles for pulmonary drug delivery. *Science,* 276**,** 1868-1872.

EL-GENDY, N., SELVAM, P., SONI, P. & BERKLAND, C. 2012. Development of budesonide nanocluster dry powder aerosols: processing. *J Pharm Sci,* 101**,** 3425-3433.

ELHISSI, A. M. A., FAIZI, M., NAJI, W. F., GILL, H. S. & TAYLOR, K. M. G. 2007. Physical stability and aerosol properties of liposomes delivered using an air-jet nebulizer and a novel micropump device with large mesh apertures. *Int J Pharm,* 334**,** 62-70.

ELHISSI, A. M. A., GIEBULTOWICZ, J., STEC, A. A., WROCZYNSKI, P., AHMED, W., ALHNAN, M. A., PHOENIX, D. A. & TAYLOR, K. M. G. 2012. Nebulization of ultradeformable liposomes: the influence of aerosolization mechanism and formulation excipients. *Int J Pharm,* 436**,** 519-526.

ELHISSI, A. M. A., GILL, H. S., AHMED, W. & TAYLOR, K. M. G. 2011a. Vibrating-mesh nebulization of liposomes generated using an ethanol-based proliposome technology. *J Liposome Res,* 21**,** 173-180.

ELHISSI, A. M. A., HIDAYAT, K., PHOENIX, D. A., MWESIGWA, E., CREAN, S., AHMED, W., FAHEEM, A. & TAYLOR, K. M. G. 2013. Air-jet and vibrating-mesh nebulization of niosomes generated using a particulate-based proniosome technology. *Int J Pharm,* 444**,** 193-199.

ELHISSI, A. M. A., KARNAM, K. K., DANESH-AZARI, M. R., GILL, H. S. & TAYLOR, K. M. G. 2006a. Formulations generated from ethanol-based proliposomes for delivery via medical nebulizers. *J Pharm Pharmacol,* 58**,** 887-894.

ELHISSI, A. M. A., O' NEILL, M. A., AHMED, W. & TAYLOR, K. M. G. 2011b. High-sensitivity differential scanning calorimetry for measurement of steroid entrapment in nebulised liposomes generated from proliposomes. *IET Micro & Nano Letters,* 6**,** 694-697.

ELHISSI, A. M. A., O'NEILL, M. A., ROBERTS, S. A. & TAYLOR, K. M. G. 2006b. A calorimetric study of dimyristoylphosphatidylcholine phase

transitions and steroid–liposome interactions for liposomes prepared by thin film and proliposome methods. *Int J Pharm,* 320**,** 124-130.

EMA. 2006. Guideline on the pharmaceutical quality of inhalation and nasal products. *Committee for medicinal products for human use (CHMP)*. [online]. [accessed 14th July 2017]. Available at http://www.ema.europa.eu/ema/

FADUS, M. C., LAU, C., BIKHCHANDANI, J. & LYNCH, H. T. 2017. Curcumin: an age-old anti-inflammatory and anti-neoplastic agent. *J Tradit Complement Med,* 7**,** 339-346.

FAIVRE, L., GOMO, C., MIR, O., TAIEB, F., SCHOEMANN-THOMAS, A., ROPERT, S., VIDAL, M., DUSSER, D., DAUPHIN, A., GOLDWASSER, F. & BLANCHET, B. 2011. A simple HPLC-UV method for the simultaneous quantification of gefitinib and erlotinib in human plasma. *J Chromatogr B,* 879**,** 2345-2350.

FINLAY, W. H. & STAPLETON, K. W. 1999. Undersizing of droplets from a vented nebulizer caused by aerosol heating during transit through an anderson impactor. *J Aerosol Sci,* 30**,** 105-109.

FISHLER, R. & SZNITMAN, J. 2017. A novel aerodynamic sizing method for pharmaceutical aerosols using image-based analysis of settling velocities. *Inhalation,* 11**,** 21-25.

FONSECA-SANTOS, B., GREMIÃO, M. P. D. & CHORILLI, M. 2016. A simple reversed phase high-performance liquid chromatography (HPLC) method for determination of in situ gelling curcumin-loaded liquid crystals in in vitro performance tests. *Arab J Chem,* 10, 1029-1037.

FU, J., CAI, Z., GONG, Y., O'REILLY, S. E., HAO, X. & ZHAO, D. 2015. A new technique for determining critical micelle concentrations of surfactants and oil dispersants via UV absorbance of pyrene. *Colloids Surf A Physicochem Eng Asp,* 484**,** 1-8.

GADGEEL, S. M., ALI, S., PHILIP, P. A., WOZNIAK, A. & SARKAR, F. H. 2009. Genistein enhances the effect of epidermal growth factor receptor tyrosine kinase inhibitors and inhibits nuclear factor kappa B in nonsmall cell lung cancer cell lines. *Cancer,* 115**,** 2165-2176.

GAO, M., CHEN, C., FAN, A., ZHANG, J., KONG, D., WANG, Z. & ZHAO, Y. 2015. Covalent and non-covalent curcumin loading in acid-responsive polymeric micellar nanocarriers. *Nanotechnology,* 26**,** 1-7.

GAO, P., ZHANG, X., WANG, H., ZHANG, Q., LI, H., LI, Y. & DUAN, Y. 2016. Biocompatible and colloidally stabilized mPEG-PE/calcium phosphate hybrid nanoparticles loaded with siRNAs targeting tumors. *Oncotarget,* 7**,** 2855-2866.

GAO, X., WANG, B., WEI, X., RAO, W., AI, F., ZHAO, F., MEN, K., YANG, B., LIU, X., HUANG, M., GOU, M., QIAN, Z., HUANG, N. & WEI, Y. 2013. Preparation, characterization and application of star-shaped PCL/PEG micelles for the delivery of doxorubicin in the treatment of colon cancer. *Int J Nanomedicine,* 8**,** 971-982.

GARBUZENKO, O. B., MAINELIS, G., TARATULA, O. & MINKO, T. 2014. Inhalation treatment of lung cancer: the influence of composition, size and shape of nanocarriers on their lung accumulation and retention. *Cancer Biol Med,* 11**,** 44-55.

GARDIKIS, K., HATZIANTONIOU, S., VIRAS, K., WAGNER, M. & DEMETZOS, C. 2006. A DSC and Raman spectroscopy study on the

effect of PAMAM dendrimer on DPPC model lipid membranes. *Int J Pharm,* 318**,** 118-123.

GAZDAR, A., LINNOILA, L., KURITA, Y., OIE, H., MULSHINE., J., CLARK, J. & WHITSETT, J. 1990. Peripheral airway cell differentation in human lung cancer cell lines. *Cancer Res,* 50, 5481-5487.

GHARSE, S. & FIEGEL, J. 2016. Large porous hollow particles: lightweight champions of pulmonary drug delivery. *Curr Pharm Des,* 22**,** 2463-2469.

GHAZANFARI, T., ELHISSI, A. M. A., DING, Z. & TAYLOR, K. M. G. 2007. The influence of fluid physicochemical properties on vibrating-mesh nebulization. *Int J Pharm,* 339**,** 103-111.

GILANI, K., MOAZENI, E., RAMEZANLI, T., AMINI, M., FAZELI, M. R. & JAMALIFAR, H. 2011. Development of respirable nanomicelle carriers for delivery of amphotericin B by jet nebulization. *J Pharm Sci,* 100**,** 252-259.

GELLER, D. & KESSER, K. 2010. The I-neb adaptive aerosol delivery system enhances delivery of α 1- antitrypsin with controlled inhalation. *J Aerosol Med Pulm Drug Deliv,* 23, 55-59.

GILLES, V., VIEIRA, M. A., LACERDA, J. R., V., CASTRO, E. V. R., SANTOS, R. B., ORESTES, E., CARNEIRO, J. W. M. & GRECO, S. J. 2015. A new, simple and efficient method of steglich esterification of juglone with long-chain fatty acids: synthesis of a new class of non-polymeric wax deposition inhibitors for crude oil. *J Brazil Chem Soc,* 26**,** 74-83.

GOEL, A., BABOOTA, S., SAHNI, J. K. & ALI, J. 2013. Exploring targeted pulmonary delivery for treatment of lung cancer. *Int J Pharm Investig,* 3**,** 8-14.

GONG, F., CHEN, D., TENG, X., GE, J., NING, X., SHEN, Y. L., LI, J. & WANG, S. 2017. Curcumin-loaded blood-stable polymeric micelles for enhancing therapeutic effect on erythroleukemia. *Mol Pharm,* 14**,** 2585-2594.

GRAPATSAS, K., LEIVADITIS, V., TSILOGIANNI, Z., HAUSSMANN, E., KAPLUNOV, V., DAHM, M., ZAROGOULIDIS, P., HOHENFORST-SCHMIDT, W., TSAKIRIDIS, K., FOROULIS, C., PALIOURAS, D., BARBETAKIS, N. & KOSAN, B. 2017. Epidermology, risk factors, symptomatology, TNM classification of non small cell lung cnacer. An overview while waiting the 8th TNM classification. *Oncomedicine,* 2, 14-23.

GUO, C., NGO, D., AHADI, S. & DOUB, W. H. 2013. Evaluation of an abbreviated impactor for Fine Particle Fraction (FPF) determination of Metered Dose Inhalers (MDI). *AAPS PharmSciTech,* 14**,** 1004-1011.

GUPTA, S. C., PATCHVA, S. & AGGARWAL, B. B. 2013. Therapeutic roles of curcumin: lessons learned from clinical trials. *AAPS J,* 15**,** 195-218.

HADIAN, Z., SAHARI, M. A., MOGHIMI, H. R. & BARZEGAR, M. 2014. Formulation, characterization and optimization of liposomes containing eicosapentaenoic and docosahexaenoic acids; a methodology approach. *Iran J Pharm Res,* 13**,** 393-404.

HALLWORTH, G. W. & WESTMORELAND, D. G. 1987. The twin impinger: a simple device for assessing the delivery of drugs from metered dose pressurized aerosol inhalers. *J Pharm Pharmacol,* 39**,** 966-972.

HAMMERMAN, P. S., JÄNNE, P. A. & JOHNSON, B. E. 2009. Resistance to epidermal growth factor receptor tyrosine kinase inhibitors in non–small cell lung cancer. *Clin Cancer Res,* 15**,** 7502-7509.

HANS, M., SHIMONI, K., DANINO, D., SIEGEL, S. J. & LOWMAN, A. 2005. Synthesis and characterization of mPEG−PLA prodrug micelles. *Biomacromolecules,* 6**,** 2708-2717.

HASSAN, A. & NAFISA, A. 2011. Studies on the chemical constituents of the leaves of ficus bengalensis and their antimicrobial activity. *J Sci Tech,* 12, 118-124.

HASSAN, M. S. & LAU, R. W. M. 2009. Effect of particle shape on dry particle inhalation: study of flowability, aerosolization, and deposition properties. *AAPS PharmSciTech,* 10**,** 1252-1262.

HASSANZADEH, F., FARZAN, M., VARSHOSAZ, J., KHODARAHMI, G. A., MAALEKI, S. & ROSTAMI, M. 2017. Poly (ethylene-co-vinyl alcohol)-based polymeric thermo-responsive nanocarriers for controlled delivery of epirubicin to hepatocellular carcinoma. *Res Pharml Sci,* 12**,** 107-118.

HEATH, F., NEWMAN, A., CLEMENTI, C., PASUT, G., LIN, H., STEPHENS, G., WHALLEY, B., OSBORN, H. & GRECO, F. 2016. A novel PEG–haloperidol conjugate with a non-degradable linker shows the feasibility of using polymer–drug conjugates in a non-prodrug fashion. *Polym Chem,* 7**,** 7204-7210.

HERRERA C., URANGA, J. G., NARDI, M., PROCOPIO, A., WUNDERLIN, D. A. & SANTIAGO, A. N. 2016. Selective and eco-friendly procedures for the synthesis of benzimidazole derivatives. The role of the Er(OTf)(3) catalyst in the reaction selectivity. *Beilstein J Org Chem,* 12**,** 2410-2419.

HERTEL, S., POHL, T., FRIESS, W. & WINTER, G. 2014. That's cool! – nebulization of thermolabile proteins with a cooled vibrating mesh nebulizer. *Eur J Pharm Biopharm,* 87**,** 357-365.

HERTEL, S., WINTER, G. & FRIESS, W. 2015. Protein stability in pulmonary drug delivery via nebulization. *Adv Drug Deliv Rev,* 93**,** 79-94.

HESS, D. 2008. Aerosol delivery devices in the treatment of asthma. *Respir Care,* 53, 699-723.

HESS, D. 2000. Nebulizers: principles and performance. *Respir Care,* 45**,** 609-622.

HINNA, A., STEINIGER, F., HUPFELD, S., STEIN, P., KUNTSCHE, J. & BRANDL, M. 2015. Filter-extruded liposomes revisited: a study into size distributions and morphologies in relation to lipid-composition and process parameters. *J Liposome Res,* 26, 11-20.

HIRA, D., KOIDE, H., NAKAMURA, S., OKADA, T., ISHIZEKI, K., YAMAGUCHI, M., KOSHIYAMA, S., OGUMA, T., ITO, K., FUNAYAMA, S., KOMASE, Y., MORITA, S. Y., NISHIGUCHI, K., NAKANO, Y. & TERADA, T. 2018. Assessment of inhalation flow patterns of soft mist inhaler co-prescribed with dry powder inhaler using inspiratory flow meter for multi inhalation devices. *Plus One,* 13**,** 1-12.

HO, S. L., KWONG, W. T., O'DROWSKY, L. & COATES, A. L. 2001. Evaluation of four breath-enhanced nebulizers for home use. *J Aerosol Med,* 14**,** 467-475.

HOLMKVIST, A. D., FRIBERG, A., NILSSON, U. J. & SCHOUENBORG, J. 2016. Hydrophobic ion pairing of a minocycline/Ca2+/AOT complex for

preparation of drug-loaded PLGA nanoparticles with improved sustained release. *Int J Pharm,* 499**,** 351-357.

HOLZNER, P. M. & MÜLLER, B. W. 1995. Particle size determination of metered dose inhalers with inertial separation methods: apparatus A and B (BP), four stage impinger and andersen mark II cascade impactor. *Int J Pharm,* 116**,** 11-18.

HU, L., LIANG, G., YULIANG, W., BINGJING, Z., XIANGDONG, Z. & RUFU, X. 2013. Assessing the effectiveness and safety of liposomal paclitaxel in combination with cisplatin as first-line chemotherapy for patients with advanced NSCLC with regional lymph-node metastasis: study protocol for a randomized controlled trial (PLC-GC trial). *Trials,* 14-45.

HU, L., SHI, Y., LI, J. H., GAO, N., JI, J., NIU, F., CHEN, Q., YANG, X. & WANG, S. 2015. Enhancement of oral bioavailability of curcumin by a novel solid dispersion system. *AAPS PharmSciTech,* 16**,** 1327-1334.

HUNTER, D. G. & FRISKEN, B. J. 1998. Effect of extrusion pressure and lipid properties on the size and polydispersity of lipid vesicles. *Biophys J,* 74**,** 2996-3002.

IBRAHIM, M., VERMA, R. & GARCIA-CONTRERAS, L. 2015. Inhalation drug delivery devices: technology update. *Med Devices (Auckl),* 8**,** 131-139.

ICH. 2005. Validation of analytical procedures: text and methodology Q2 (R1). *ICH harmonised tripartile guideline.* [online]. [Accessed 22nd November 2015]. Available at http://www.ich.org.

INGEBRIGTSEN, S. G., SKALKO-BASNET, N., DE ALBUQUERQUE CAVALCANTI JACOBSEN, C. & HOLSAETER, A. M. 2017. Successful co-encapsulation of benzoyl peroxide and chloramphenicol in liposomes by a novel manufacturing method - dual asymmetric centrifugation. *Eur J Pharm Sci,* 97**,** 192-199.

ISHII, T., YAMADA, M., HIRASE, T. & NAGASAKI, Y. 2005. New synthesis of heterobifunctional poly(ethylene glycol) possessing a pyridyl disulfide at one end and a carboxylic acid at the other end. *Polym J,* 37**,** 221-228.

ISO-22412. 2008. Particle Size Analysis, Dynamic Light Scattering (DLS). International Organization for Standardization.

IYER, R., HSIA, C. C. & NGUYEN, K. T. 2015. Nano-therapeutics for the lung: state-of-the-art and future perspectives. *Curr Pharm Des,* 21**,** 5233-5244.

JABBAL, S., POLI, G. & LIPWORTH, B. 2017. Does size really matter?: relationship of particle size to lung deposition and exhaled fraction. *J Allergy Clin Immunol,* 139**,** 2013-2014.

JEON, O., LEE, S. H., KIM, S. H., LEE, Y. M. & KIM, Y. H. 2003. Synthesis and characterization of poly(l-lactide)−poly(ε-caprolactone) multiblock copolymers. *Macromolecules,* 36**,** 5585-5592.

JEONG, Y. I., KIM, D. G., JANG, M. K. & NAH, J. W. 2008. Preparation and spectroscopic characterization of methoxy poly(ethylene glycol)-grafted water-soluble chitosan. *Carbohydr Res,* 343**,** 282-289.

JEVON, P. & EWENS, B. 2001. Assessment of a breathless patient. *Nurs Stand,* 15**,** 48-53.

JIANG, S., ZHU, R., HE, X., WANG, J., WANG, M., QIAN, Y. & WANG, S. 2017. Enhanced photocytotoxicity of curcumin delivered by solid lipid nanoparticles. *Int J Nanomedicine,* 12**,** 167-178.

JIANG, Y. & KUANG, C. 2009. Novel one-pot synthesis of functionalized (Z)-2-arylvinyl bromides. *Synth Commun,* 39**,** 4298-4308.

JIN, H., QIAO, F., WANG, Y., XU, Y. & SHANG, Y. 2015. Curcumin inhibits cell proliferation and induces apoptosis of human non-small cell lung cancer cells through the upregulation of miR-192-5p and suppression of PI3K/Akt signaling pathway. *Oncol Rep,* 34**,** 2782-2789.

JOHAL, B., HOWALD, M., FISCHER, M., MARSHALL, J. & VENTHOYE, G. 2013. Fine particle profile of fluticasone propionate/formoterol fumarate versus other combination products: the DIFFUSE study. *Comb Prod Ther,* 3**,** 39-51.

JOHNSON, K. R., ELLIS, G. & TOOTHILL, C. 1977. The sulfophosphovanillin reaction for serum lipids: a reappraisal. *Clin Chem,* 23**,** 1669-1678.

JOSHI, N., SHIRSATH, N., SINGH, A., JOSHI, K. S. & BANERJEE, R. 2014. Endogenous lung surfactant inspired pH responsive nanovesicle aerosols: pulmonary compatible and site-specific drug delivery in lung metastases. *Sci Rep,* 4**,** 1-11.

KAMALI, H., ABBASI, S., AMINI, M. A. & AMANI, A. 2016. Investigation of factors affecting aerodynamic performance of nebulized nanoemulsion. *Iran J Pharm Res,* 15**,** 687-693.

KANNAN, V., BALABATHULA, P., DIVI, M. K., THOMA, L. A. & WOOD, G. C. 2015. Optimization of drug loading to improve physical stability of paclitaxel-loaded long-circulating liposomes. *J Liposome Res,* 25**,** 308-315.

KARAMI, Z., SADIGHIAN, S., ROSTAMIZADEH, K., PARSA, M. & REZAEE, S. 2016. Naproxen conjugated mPEG-PCL micelles for dual triggered drug delivery. *Mater Sci Eng C Mater Biol Appl,* 61**,** 665-673.

KAROLINA, A. W., Stumbe J. F. & Rainer, H. 2016. Polyester-based, biodegradable core-multishell nanocarriers for the transport of hydrophobic drugs. *Polymers,* 8, 1-24.

KAVIRATNA, A. S. & BANERJEE, R. 2012. Nanovesicle aerosols as surfactant therapy in lung injury. *Nanomedicine,* 8**,** 665-672.

KAYSER, C. H., CHARLES, B. & VACHANI, C. 2017. All about non-small cell lung cancer. *OncoLink,* [online]. [Accessed 16th January 2019]. Available at https://www.oncolink.org/cancers/lung/non-small-cell-lung-cancer-nsclc/all-about-non-small-cell-lung-cancer.

KENDRICK, A. H., SMITH, E. C. & WILSON, R. S. 1997. Selecting and using nebuliser equipment. *Thorax,* 52**,** 92-101.

KĘPCZYŃSKI, M., NAWALANY, K., KUMOREK, M., KOBIERSKA, A., JACHIMSKA, B. & NOWAKOWSKA, M. 2008. Which physical and structural factors of liposome carriers control their drug-loading efficiency? *Chem Phys Lipids,* 155**,** 7-15.

KHALE, A. & Bele, A. A. 2010. An overview onthin layer chromatography. *Int J Pharm Sci Res***,** 256-257.

KHAN, N. & MUKHTAR, H. 2015. Dietary agents for prevention and treatment of lung cancer. *Cancer Lett,* 359**,** 155-164.

KHANDARE, J. & MINKO, T. 2006. Polymer–drug conjugates: progress in polymeric prodrugs. *Prog Polym Sci,* 31**,** 359-397.

KHUROO, T., VERMA, D., KHUROO, A., ALI, A. & IQBAL, Z. 2018. Simultaneous delivery of paclitaxel and erlotinib from dual drug loaded PLGA nanoparticles: formulation development, thorough optimization and in vitro release. *J Mol Liq,* 257**,** 52-68.

KIM, J. T., BARUA, S., KIM, H., HONG, S. C., YOO, S. Y., JEON, H., CHO, Y., GIL, S., OH, K. & LEE, J. 2017. Absorption study of genistein using solid lipid microparticles and nanoparticles: control of oral bioavailability by particle sizes. *Biomol Ther,* 25**,** 452-459.

KLEINSTREUER, C. & ZHANG, Z. 2010. Airflow and particle transport in the human respiratory system. *Annu Rev Fluid Mech,* 42**,** 301-334.

KUHLI, M., WEISS, M. & STECKEL, H. 2009. A sampling and dilution system for droplet aerosols from medical nebulisers developed for use with an optical particle counter. *J Aerosol Sci,* 40**,** 523-533.

KUMAR, A., AHUJA, A., ALI, J. & BABOOTA, S. 2016. Curcumin-loaded lipid nanocarrier for improving bioavailability, stability and cytotoxicity against malignant glioma cells. *Drug Deliv,* 23**,** 214-229.

KUMI, D. J., MERCHANT, K., HACES, A., HORMANN, V. & JOHNSON, M. 2010. Genistein-selenium combination induces growth arrest in prostate cancer cells. *J Med Food,* 13**,** 842-850.

KWON, S., KIM, S., HA, K., KANG, M., HUH, J., JONG, I., KIM, Y., PARK, Y., KANG, K., LEE, S., CHANG, J., LEE, J. & CHOI, Y. 2007. Pharmaceutical evaluation of genistein-loaded pluronic micelles for oral delivery. *Arch Pharmacal Res,* 30**,** 1138-1143.

KWONG, T., TOWN, I., WINDOM, H. & BEASLEY, R. 1990. The use of water as a diluent for bronchodilator nebuliser solutions. *N Z Med J,* 103**,** 290-291.

LABIRIS, N. R. & DOLOVICH, M. B. 2003. Pulmonary drug delivery. Part I: physiological factors affecting therapeutic effectiveness of aerosolized medications. *Br J Clin Pharmacol,* 56**,** 588-599.

LARSON, N. & GHANDEHARI, H. 2012. Polymeric conjugates for drug delivery. *Chem Mater,* 24**,** 840-853.

LASS, J. S., SANT, A. & KNOCH, M. 2006. New advances in aerosolised drug delivery: vibrating membrane nebuliser technology. *Expert Opin Drug Deliv,* 3**,** 693-702.

LATHA, S. T., ANANDA, S., JAMBULINGAM, M., SEREYA, K., KAMALAKANNAN, D. & ANILKUMAR, M. 2017. Development and validation of RP-HPLC method for the estimation of erlotinib in pharmaceutical formulation. *Arab J Chem*, 10, 1138-1144

LAVORINI, F. 2013. The challenge of delivering therapeutic aerosols to asthma patients. *ISRN Allergy*, 2013**,** 1-17.

LAVORINI, F., PISTOLESI, M. & USMANI, O. S. 2017. Recent advances in capsule-based dry powder inhaler technology. *Multidiscip Respir Med,* 12**,** 1-7.

LAWACZECK, R., KAINOSHO, M. & CHAN, S. I. 1976. The formation and annealing of structural defects in lipid bilayer vesicles. *Biochim Biophys Acta,* 443**,** 313-330.

LE BRUN, P. P., DE BOER, A. H., HEIJERMAN, H. G. & FRIJLINK, H. W. 2000. A review of the technical aspects of drug nebulization. *Pharm World Sci,* 22**,** 75-81.

LEE, K. J., OH, Y. C., CHO, W. K. & MA, J. Y. 2015a. Antioxidant and anti-inflammatory activity determination of one hundred kinds of pure chemical compounds using offline and online screening HPLC assay. *Evid Based Complement Alternat Med,* 2015**,** 1-13.

LEE, W. H., LOO, C. Y., TRAINI, D. & YOUNG, P. M. 2015b. Inhalation of nanoparticle-based drug for lung cancer treatment: advantages and challenges. *Asian J Pharm Sci,* 10**,** 481-489.

LEHOFER, B., BLODER, F., JAIN, P. P., MARSH, L. M., LEITINGER, G., OLSCHEWSKI, H., LEBER, R., OLSCHEWSKI, A. & PRASSL, R. 2014. Impact of atomization technique on the stability and transport efficiency of nebulized liposomes harboring different surface characteristics. *Eur J Pharm Biopharm,* 88**,** 1076-1085.

LEUNG, K., LOUCA, E. & COATES, A. L. 2004. Comparison of breath-enhanced to breath-actuated nebulizers for rate, consistency, and efficiency. *Chest,* 126**,** 1619-1627.

LEWIS, D. A., O'SHEA, H., CHURCH, T. K., BRAMBILLA, G., TRAINI, D. & YOUNG, P. M. 2016. Exploring the impact of sample flowrate on in vitro measurements of metered dose inhaler performance. *Int J Pharm,* 514**,** 420-427.

LI, C., SHEN, Y., SUN, C., NIHAD, C. & TU, J. 2016. Immunosafety and chronic toxicity evaluation of monomethoxypoly(ethylene glycol)-b-poly(lactic acid) polymer micelles for paclitaxel delivery. *Drug Deliv,* 23**,** 888-895.

LI, H. Q., LUO, Y. & QIAO, C. H. 2012a. The mechanisms of anticancer agents by genistein and synthetic derivatives of isoflavone. *Mini Rev Med Chem,* 12**,** 350-362.

LI, J., WANG, X., ZHANG, T., WANG, C., HUANG, Z., LUO, X. & DENG, Y. 2015. A review on phospholipids and their main applications in drug delivery systems. *Asian J Pharm Sci,* 10**,** 81-98.

LI, Q., CAI, T., HUANG, Y., XIA, X., COLE, S. P. C. & CAI, Y. 2017. A review of the structure, preparation, and application of NLCs, PNPs, and PLNs. *Nanomaterials (Basel),* 7, 1-25.

LI, Q. S., LI, C. Y., LI, Z. L. & ZHU, H. L. 2012b. Genistein and its synthetic analogs as anticancer agents. *Anticancer Agents Med Chem,* 12**,** 271-281.

LIAO, B. C., LIN, C. C., LEE, J. H. & YANG, C. H. 2017. Optimal management of EGFR-mutant non-small cell lung cancer with disease progression on first-line tyrosine kinase inhibitor therapy. *Lung Cancer,* 110**,** 7-13.

LIU, C. L., WU, G., CHEN, S. C., YOU, J. & WANG, Y. Z. 2014a. Crystallization induced micellization of poly(p-dioxanone)-block-polyethylene glycol diblock copolymer functionalized with pyrene moiety. *Chin Chem Lett,* 25**,** 1311-1317.

LIU, D., YAN, L., WANG, L. A. N., TAI, W., WANG, W. & YANG, C. 2014b. Genistein enhances the effect of cisplatin on the inhibition of non-small cell lung cancer A549 cell growth in vitro and in vivo. *Oncol Lett,* 8**,** 2806-2810.

LOPEZ-PINTO, J. M., GONZALEZ-RODRIGUEZ, M. L. & RABASCO, A. M. 2005. Effect of cholesterol and ethanol on dermal delivery from DPPC liposomes. *Int J Pharm,* 298**,** 1-12.

LU, X., ZHU, T., CHEN, C. & LIU, Y. 2014. Right or left: the role of nanoparticles in pulmonary diseases. *Int J Mol Sci,* 15**,** 17577-17600.

MAHAJAN, H. S. & MAHAJAN, P. R. 2016. Development of grafted xyloglucan micelles for pulmonary delivery of curcumin: in vitro and in vivo studies. *Int J Biol Macromol,* 82**,** 621-627.

MAJORAL, C., PAPE, A. L., DIOT, P. & VECELLIO, L. 2006. Comparison of various methods for processing cascade impactor data. *Aerosol Sci Technol,* 40**,** 672-682.

MANCA, M. L., SINICO, C., MACCIONI, A. M., DIEZ, O., FADDA, A. M. & MANCONI, M. 2012. Composition influence on pulmonary delivery of rifampicin liposomes. *Pharmaceutics,* 4**,** 590-606.

MANDAL, B., MITTAL, N. K., BALABATHULA, P., THOMA, L. A. & WOOD, G. C. 2016. Development and in vitro evaluation of core–shell type lipid–polymer hybrid nanoparticles for the delivery of erlotinib in non-small cell lung cancer. *Eur J Pharm Sci,* 81**,** 162-171.

MANSOUR, H. M., RHEE, Y. S. & WU, X. 2009. Nanomedicine in pulmonary delivery. *Int J Nanomedicine,* 4**,** 299-319.

MANUNTA, M. D., MCANULTY, R. J., TAGALAKIS, A. D., BOTTOMS, S. E., CAMPBELL, F., HAILES, H. C., TABOR, A. B., LAURENT, G. J., O'CALLAGHAN, C. & HART, S. L. 2011. Nebulisation of receptor-targeted nanocomplexes for gene delivery to the airway epithelium. *PLoS One,* 6**,** 1-13.

MARPLE, V. A., ROBERTS, D. L., ROMAY, F. J., MILLER, N. C., TRUMAN, K. G., VAN OORT, M., OLSSON, B., HOLROYD, M. J., MITCHELL, J. P. & HOCHRAINER, D. 2003. Next generation pharmaceutical impactor (a new impactor for pharmaceutical inhaler testing). Part I: design. *J Aerosol Med,* 16**,** 283-299.

MARTIN, G. P., MACRITCHIE, H. B., MARRIOTT, C. & ZENG, X. M. 2006. Characterisation of a carrier-free dry powder aerosol formulation using inertial impaction and laser diffraction. *Pharm Res,* 23**,** 2210-2219.

MASARUDIN, M. J., CUTTS, S. M., EVISON, B. J., PHILLIPS, D. R. & PIGRAM, P. J. 2015. Factors determining the stability, size distribution, and cellular accumulation of small, monodisperse chitosan nanoparticles as candidate vectors for anticancer drug delivery: application to the passive encapsulation of [(14)C]-doxorubicin. *Nanotechnol Sci Appl,* 8**,** 67-80.

MASHAT, M., CLARK, B. J., ASSI, K. H. & CHRYSTYN, H. 2016. In vitro aerodynamic characterization of the dose emitted during nebulization of tobramycin high strength solution by novel and jet nebulizer delivery systems. *Pulm Pharmacol Ther,* 37**,** 37-42.

MAYER, L. D., HOPE, M. J. & CULLIS, P. R. 1986. Vesicles of variable sizes produced by a rapid extrusion procedure. *Biochim Biophys Acta,* 858**,** 161-168.

MCCALLION, O. N., TAYLOR, K. M. G., THOMAS, M. & TAYLOR, A. J. 1995. Nebulization of fluids of different physicochemical properties with air-jet and ultrasonic nebulizers. *Pharm Res,* 12**,** 1682-1688.

MENON, J. U., RAVIKUMAR, P., PISE, A., GYAWALI, D., HSIA, C. C. W. & NGUYEN, K. T. 2014. Polymeric nanoparticles for pulmonary protein and DNA delivery. *Acta Biomater,* 10**,** 2643-2652.

MERCHANT, Z. 2017. DELIVERY OF NANOCARRIER-LOADED HYDROPHOBIC DRUGS VIA THE AIRWAYS. *High-performance liquid chromatography (HPLC) and analytical method validation for determination of CNB001 and curcumin.* University College London.

MEYERS, C. L. F. & MEYERS, D. J. 2001. Thin-Layer Chromatography. *Curr Protoc Nucleic Acid Chem*, 34, 1-13.

MIHAYLOVA, D. & SCHALOW, S. 2013. Antioxidant and stabilization activity of a quercetin-containing flavonoid extract obtained from Bulgarian sophora japonica L. *Braz Arch Biol Technol,* 56**,** 431-438.

MILLER, N. C., MARPLE, V. A., SCHULTZ, R. K. & POON, W. S. 1992. Assessment of the twin impinger for size measurement of metered-dose inhaler sprays. *Pharm Res,* 9**,** 1123-1127.

MITCHELL, J. P., COPLEY, M., SIZER, Y., RUSSELL, T. & SOLOMON, D. 2012a. Adapting the Abbreviated Impactor Measurement (AIM) concept to make appropriate inhaler aerosol measurements to compare with clinical data: a scoping study with the "Alberta" idealized throat (AIT) inlet. *J Aerosol Med Pulm Drug Deliv,* 25**,** 188-197.

MITCHELL, J. P., MACKAY, H., AVVAKOUMOVA, V., ALI, R. & NAGEL, M. 2008. The Abbreviated Impactor Measurement (AIM) concept: influence of particle bounce and re-entrainment – application to the Copley Fast Screening Andersen Impactor (C-FSA), *DDL* 2008, 2, 30-33.

MITCHELL, J. P,, TOUGAS, T. & LYAPUSTINA, S. 2012b. The Abbreviated Impactor Measurement (AIM) and Effective Data Analysis (EDA) Concepts: why they are important and how to go about working with them. [Online]. [Accessed 12nd August 2018]. Available at https://www.researchgate.net/profile/Jolyon_Mitchell/publication/274065063_The_Abbreviated_Impactor_Measurement_AIM_and_Effective_Data_Analysis_EDA_Concepts_Why_They_are_Important_and_How_to_Go_About_Working_with_Them/links/551349020cf23203199bb435/The-Abbreviated-Impactor-Measurement-AIM-and-Effective-Data-Analysis-EDA-Concepts-Why-They-are-Important-and-How-to-Go-About-Working-with-Them.pdf.

MITCHELL, J. P,, NAGEL, M. W., AVVAKOUMOVA, V., MACKAY, H. & ALI, R. 2009a. The abbreviated impactor measurement (AIM) concept: part 1—influence of particle bounce and re-entrainment—evaluation with a “Dry” Pressurized Metered Dose Inhaler (pMDI)-based formulation. *AAPS PharmSciTech,* 10**,** 243-251.

MITCHELL, J. P., NAGEL, M. W., AVVAKOUMOVA, V., MACKAY, H. & ALI, R. 2009b. The abbreviated impactor measurement (AIM) concept: part 2-influence of evaporation of a volatile component-evaluation with a "droplet-producing" pressurized metered dose inhaler (pMDI)-based formulation containing ethanol as cosolvent. *AAPS PharmSciTech,* 10**,** 252-257.

MITCHELL, J. P., NAGEL, M. W., DOYLE, C. C., ALI, R., AVVAKOUMOVA, V., CHRISTOPHER, J. D., QUIROZ, J., STRICKLAND, H., TOUGAS, T. & LYAPUSTINA, S. 2010. Relative precision of inhaler Aerodynamic Particle Size Distribution (APSD) metrics by full resolution and abbreviated Andersen Cascade Impactors (ACIs): part 1. *AAPS PharmSciTech,* 11**,** 843-851.

MITCHELL, J. P. & NICHOLS, S. C. 2011. Summary of abbreviated impactor measurement workshop organized by the European Pharmaceutical Aerosol Group. *Ther Deliv,* 2**,** 307-310.

MOAZENI, E., GILANI, K., NAJAFABADI, A. R., REZA-ROUINI, M., MOHAJEL, N., AMINI, M. & BARGHI, M. A. 2012. Preparation and evaluation of inhalable itraconazole chitosan based polymeric micelles. *J Pharm Sci,* 20**,** 85-85.

MOHAN, M., LEE, S., GUO, C., PERI, S. P. & DOUB, W. H. 2017. Evaluation of Abbreviated Impactor Measurements (AIM) and Efficient Data Analysis (EDA) for Dry Powder Inhalers (DPIs) against the full-resolution Next Generation Impactor (NGI). *AAPS PharmSciTech,* 18**,** 1585-1594.

MOLINA, J. R., YANG, P., CASSIVI, S. D., SCHILD, S. E. & ADJEI, A. A. 2008. Non–small cell lung cancer: epidemiology, risk factors, treatment, and survivorship. *Mayo Clin Proc,* 83**,** 584-594.

MOLLAEI, S., TAMHIDI, S., HASHEMPOUR, H. & GHASSEMPOUR, A. 2013. Recycling preparative high performance liquid chromatography for the separation of curcumin from curcuminoids in Curcuma Longa L. A*cta Chromatogr*, 27, 387-398.

MONTEIRO, N., MARTINS, A., REIS, R. L. & NEVES, N. M. 2014. Liposomes in tissue engineering and regenerative medicine. *J R Soc Interface,* 11, 1-24.

MORTON, L. A., SALUDES, J. P. & YIN, H. 2012. Constant pressure-controlled extrusion method for the preparation of nano-sized lipid vesicles. *J Vis Exp,* 64, 1-6.

MORTON, S. W., LEE, M. J., DENG, Z. J., DREADEN, E. C., SIOUVE, E., SHOPSOWITZ, K. E., SHAH, N. J., YAFFE, M. B. & HAMMOND, P. T. 2014. A nanoparticle-based combination chemotherapy delivery system for enhanced tumor killing by dynamic rewiring of signaling pathways. *Sci Signal,* 7**,** 1-27.

MOSSMAN, B. T., LIPPMANN, M., HESTERBERG, T. W., KELSEY, K. T., BARCHOWSKY, A. & BONNER, J. C. 2011. Pulmonary endpoints (lung carcinomas and asbestosis) following inhalation exposure to asbestos. *J Toxicol Environ Health B Crit Rev,* 14**,** 76-121.

MUCHAO, F. P. & FILHO, L. V. 2010. Advances in inhalation therapy in pediatrics. *J Pediatr,* 86**,** 367-376.

MUTCH, E., NAVE, R., MCCRACKEN, N., ZECH, K. & WILLIAMS, F. M. 2007. The role of esterases in the metabolism of ciclesonide to desisobutyryl-ciclesonide in human tissue. *Biochem Pharmacol,* 73**,** 1657-1664.

NAJLAH, M., VALI, A., TAYLOR, M., ARAFAT, B. T., AHMED, W., PHOENIX, D. A., TAYLOR, K. M. G. & ELHISSI, A. M. A. 2013. A study of the effects of sodium halides on the performance of air-jet and vibrating-mesh nebulizers. *Int J Pharm,* 456**,** 520-527.

NAKAMURA, Y., MOCHIDA, A., CHOYKE, P. L. & KOBAYASHI, H. 2016. Nanodrug delivery: is the enhanced permeability and retention effect sufficient for curing cancer? *Bioconjug Chem,* 27**,** 2225-2238.

NASERI, N., ZAKERI-MILANI, P., HAMISHEHKAR, H., PILEHVAR-SOLTANAHMADI, Y. & VALIZADEH, H. 2017. Development, in vitro characterization, antitumor and aerosol performance evaluation of respirable prepared by self-nanoemulsification method. *Drug Res,* 67**,** 343-348.

NEWMAN, S. 2014. Improving inhaler technique, adherence to therapy and the precision of dosing: major challenges for pulmonary drug delivery. *Expert Opin Drug Deliv,* 11**,** 365-378.

NEWMAN, S. 2005. Principles of metered-dose inhaler design. *Respir Care,* 50**,** 1177-1190.

NG, Z. Y., WONG, J. Y., PANNEERSELVAM, J., MADHESWARAN, T., KUMAR, P., PILLAY, V., HSU, A., HANSBRO, N., BEBAWY, M., WARK, P., HANSBRO, P., DUA, K. & CHELLAPPAN, D. K. 2018. Assessing the potential of liposomes loaded with curcumin as a therapeutic intervention in asthma. *Colloids Surf B,* 172**,** 51-59.

NICHOLS, S. C., MITCHELL, J. P., SANDELL, D., ANDERSSON, P. U., FISCHER, M., HOWALD, M., PENGILLEY, R. & KRÜGER, P. 2016. A multi-laboratory in vitro study to compare data from abbreviated and pharmacopeial impactor measurements for orally inhaled products: a report of the European Aerosol Group (EPAG). *AAPS PharmSciTech,* 17**,** 1383-1392.

NIERO, E. L., ROCHA-SALES, B., LAUAND, C., CORTEZ, B. A., DE SOUZA, M. M., REZENDE-TEIXEIRA, P., URABAYASHI, M. S., MARTENS, A. A., NEVES, J. H. & MACHADO-SANTELLI, G. M. 2014. The multiple facets of drug resistance: one history, different approaches. *J Exp Clin Cancer Res,* 33**,** 1-14.

NIKANDER, K., PRINCE, I., COUGHLIN, S., WARREN, S., & TAYLOR, G. 2010. Mode of breathing- tidal or slow and deep- through the I- neb adaptive aerosol delivery (AAD) system affects lung deposition of ^{99m}Tc-DTPA. *J Aerosol Med Pulm Drug Deliv,* 1, 37- 43.

NIVEN, R. W., PRESTRELSKI, S. J., TREUHEIT, M. J., IP, A. Y. & ARAKAWA, T. 1996. Protein nebulization II. Stabilization of G-CSF to air-jet nebulization and the role of protectants. *Int J Pharm,* 127**,** 191-201.

NOORZIDAH, M. S., ABU, N., MASTOR, A., HISHAM, S. & NOORSAL, K. 2012. Preparation and characterization of conjugated polyamidoamine-mPEG-methotrexate for potential drug delivery system, AIP Conf Proc , 1455, 70-82.

NURWIDYA, F., TAKAHASHI, F. & TAKAHASHI, K. 2016. Gefitinib in the treatment of nonsmall cell lung cancer with activating epidermal growth factor receptor mutation. *J Nat Sc Biol Med,* 7**,** 119-123.

O'CALLAGHAN, C. & BARRY, P. W. 1997. The science of nebulised drug delivery. *Thorax,* 52**,** 31-44.

OGINO, K., KUBOTA, T., UCHIYAMA, H. & ABE, M. 1988. Micelle formation and micellar size by a light scattering technique. *J Oleo Sci,* 37**,** 588-591.

ONG, S. G. M., CHITNENI, M., LEE, K. S., MING, L. C. & YUEN, K. H. 2016. Evaluation of extrusion technique for nanosizing liposomes. *Pharmaceutics,* 8, 1-12.

OWEN, S. C., CHAN, D. P. Y. & SHOICHET, M. S. 2012. Polymeric micelle stability. *Nano Today,* 7**,** 53-65.

PANDEY, R., SHARMA, A., ZAHOOR, A., SHARMA, S., KHULLER, G. K. & PRASAD, B. 2003. Poly (DL-lactide-co-glycolide) nanoparticle-based inhalable sustained drug delivery system for experimental tuberculosis. *J Antimicrob Chemother,* 52**,** 981-986.

PANDIT, N. T. & PATRAVALE, V. B. 2011. Design and optimization of a novel method for extraction of genistein. *Indian J Pharm Sci,* 73**,** 184-192.

PARANJPE, M. & MÜLLER-GOYMANN, C. C. 2014. Nanoparticle-mediated pulmonary drug delivery: a review. *Int J Mol Sci,* 15**,** 5852-5873.

PARDEIKE, J., WEBER, S., HABER, T., WAGNER, J., ZARFL, H. P., PLANK, H. & ZIMMER, A. 2011. Development of an itraconazole-loaded

nanostructured lipid carrier (NLC) formulation for pulmonary application. *Int J Pharm,* 419**,** 329-338.

PATIL, J. S. & SARASIJA, S. 2012. Pulmonary drug delivery strategies: a concise, systematic review. *Lung India,* 29**,** 44-49.

PATTNI, B. S., CHUPIN, V. V. & TORCHILIN, V. P. 2015. New developments in liposomal drug delivery. *Chem Rev,* 115**,** 10938-10966.

PAVESE, J. M., FARMER, R. L. & BERGAN, R. C. 2010. Inhibition of cancer cell invasion and metastasis by genistein. *Cancer Metast Rev,* 29**,** 465-482.

PHAN, V., WALTERS, J., BROWNLOW, B. & ELBAYOUMI, T. 2013. Enhanced cytotoxicity of optimized liposomal genistein via specific induction of apoptosis in breast, ovarian and prostate carcinomas. *J Drug Target,* 21**,** 1001-1111.

PILCER, G. & AMIGHI, K. 2010. Formulation strategy and use of excipients in pulmonary drug delivery. *Int J Pharm,* 392**,** 1-19.

PILCER, G., VANDERBIST, F. & AMIGHI, K. 2008. Correlations between cascade impactor analysis and laser diffraction techniques for the determination of the particle size of aerosolised powder formulations. *Int J Pharm,* 358**,** 75-81.

PITANCE, L., VECELLIO, L., LEAL, T., REYCHLER, G., REYCHLER, H. & LIISTRO, G. 2010. Delivery efficacy of a vibrating mesh nebulizer and a jet nebulizer under different configurations. *J Aerosol Med Pulm Drug Deliv,* 23**,** 389-396.

PRITCHARD, J. N., HATLEY, R. H., DENYER, J. & HOLLEN, D. V. 2018. Mesh nebulizers have become the first choice for new nebulized pharmaceutical drug developments. *Ther Deliv,* 9**,** 121-136.

PYKA, A. 2014. Detection progress of selected drugs in TLC. *BioMed Res Int,* 2014**,** 1-19.

QIU, F., FENG, J., WU, D. Q., ZHANG, X. Z. & ZHUO, R. X. 2009. Nanosized micelles self-assembled from amphiphilic dextran-graft-methoxypolyethylene glycol/poly(ε-caprolactone) copolymers. *Eur Polym J,* 45**,** 1024-1031.

QIU, N., CAI, L. L., XIE, D., WANG, G., WU, W., ZHANG, Y., SONG, H., YIN, H. & CHEN, L. 2010. Synthesis, structural and in vitro studies of well-dispersed monomethoxy-poly(ethylene glycol)-honokiol conjugate micelles. *Biomed Mater,* 5**,** 1-6.

RAO, D. A., NGUYEN, D. X., MISHRA, G. P., DODDAPANENI, B. S. & ALANI, A. W. 2015. Preparation and characterization of individual and multi-drug loaded physically entrapped polymeric micelles. *J Vis Exp***,** 102, 1-5.

RAU, J. L., ARI, A. & RESTREPO, R. 2004. Performance comparison of nebulizer designs: constant-output, breath-enhanced, and dosimetric. Respir Care, 49, 174-179.

RASTI, B., JINAP, S., MOZAFARI, M. R. & YAZID, A. M. 2012. Comparative study of the oxidative and physical stability of liposomal and nanoliposomal polyunsaturated fatty acids prepared with conventional and Mozafari methods. *Food Chem,* 135**,** 2761-2170.

RAVAL, A., PARMAR, A., RAVAL, A. & BAHADUR, P. 2012. Preparation and optimization of media using Pluronic® micelles for solubilization of sirolimus and release from the drug eluting stents. *Colloids Surf B,* 93**,** 180-187.

RECK, M., HEIGENER, D. F., MOK, T., SORIA, J. C. & RABE, K. F. 2013. Management of non-small-cell lung cancer: recent developments. *Lancet,* 382**,** 709-719.

RENATO, D., MONICA, N., MANUELA, O., ROSINA, P. & ANTONIO, P. 2009. Erbium(III) triflate is a highly efficient catalyst for the synthesis of b-alkoxy alcohols, 1,2-diols and b-hydroxy sulfides by ring opening of epoxides. *Synthesis,* 20**,** 3433-3438.

RESPAUD, R., MARCHAND, D., PARENT, C., PELAT, T., THULLIER, P., TOURNAMILLE, J. F., VIAUD-MASSUARD, M. C., DIOT, P., SI-TAHAR, M., VECELLIO, L. & HEUZÉ-VOURC'H, N. 2014. Effect of formulation on the stability and aerosol performance of a nebulized antibody. *mAbs,* 6**,** 1347-1355.

RIEBESEEL, K., BIEDERMANN, E., LOSER, R., BREITER, N., HANSELMANN, R., MULHAUPT, R., UNGER, C. & KRATZ, F. 2002. Polyethylene glycol conjugates of methotrexate varying in their molecular weight from MW 750 to MW 40000: synthesis, characterization, and structure-activity relationships in vitro and in vivo. *Bioconjug Chem,* 13**,** 773-785.

RIELY, G. J. & LADANYI, M. 2008. KRAS mutations: an old oncogene becomes a new predictive biomarker. *J Mol Diagn,* 10**,** 493-495.

ROA, W. H., AZARMI, S., AL-HALLAK, M. H., FINLAY, W. H., MAGLIOCCO, A. M. & LOBENBERG, R. 2011. Inhalable nanoparticles, a non-invasive approach to treat lung cancer in a mouse model. *J Control Rel,* 150**,** 49-55.

ROCKS, N., BEKAERT, S., COIA, I., PAULISSEN, G., GUEDERS, M., EVRARD, B., VAN-HEUGEN, J. C., CHIAP, P., FOIDART, J. M., NOEL, A. & CATALDO, D. 2012. Curcumin-cyclodextrin complexes potentiate gemcitabine effects in an orthotopic mouse model of lung cancer. *Br J Cancer,* 107**,** 1083-1092.

RUBIN, B. K. & WILLIAMS, R. W. 2014. Emerging aerosol drug delivery strategies: from bench to clinic. *Adv Drug Deliv Rev,* 75**,** 141-148.

RUDOKAS, M., NAJLAH, M., ALHNAN, M. A. & ELHISSI, A. M. A. 2016. Liposome delivery systems for Inhalation: a critical review highlighting formulation issues and anticancer applications. *Med Princ Pract,* 25**,** 60-72.

RUSIN, A., KRAWCZYK, Z., GRYNKIEWICZ, G., GOGLER, A., ZAWISZA-PUCHALKA, J. & SZEJA, W. 2010. Synthetic derivatives of genistein, their properties and possible applications. *Acta Biochim Pol,* 57**,** 23-34.

RUSSO, M., SPAGNUOLO, C., TEDESCO, I. & RUSSO, G. L. 2010. Phytochemicals in cancer prevention and therapy: truth or dare? *Toxins,* 2**,** 517-551.

SAEED, H., ELBERRY, A., SALAH, A., HAGAG, H. & ABDELRAHIM, M. 2017. Effect of nebulizer designs on aerosol delivery during non-invasive mechanical ventilation: a modeling study of in vitro data, *Pulm Ther,* 3, 233-241.

SAHIB, M., DARWIS, Y., KOK-KHIANG, P. & TAN, Y. 2010. Aerodynamic characterization of marketed inhaler dosage forms: High performance liquid chromatography assay method for the determination of budesonide, *Afr J Pharm Pharmacol,* 4, 878-884.

SAHIB, M., DARWIS, Y., PEH, K. K., ABDULAMEER, S. A. & TAN, Y. 2011. Rehydrated sterically stabilized phospholipid nanomicelles of budesonide for nebulization: physicochemical characterization and in vitro, in vivo evaluations. *Int J Nanomedicine,* 6**,** 2351-2366.

SANGHA, R., PRICE, J. & BUTTS, C. A. 2010. Adjuvant therapy in non-small cell lung cancer: current and future directions. *The Oncologist,* 15**,** 862-872.

SANT, V. P. & NAGARSENKER, M. S. 2011. Synthesis of monomethoxypolyethyleneglycol-cholesteryl ester and effect of its incorporation in liposomes. *AAPS PharmSciTech,* 12**,** 1056-1063.

SAUNDERS, M., TAYLOR, K. M. G., CRAIG, D. Q., PALIN, K. & ROBSON, H. 2007. High sensitivity differential scanning calorimetry study of DNA-cationic liposome complexes. *Pharm Res,* 24**,** 1954-1961.

SCARANO, W., DE SOUZA, P. & STENZEL, M. 2014. Dual-drug delivery of curcumin and platinum drugs in polymeric micelles enhances the synergistic effects: a double act for the treatment of multidrug-resistant cancer, *Biomater Sci,* 3, 163-174.

SCHETTINO, C., BARESCHINO, M. A., RICCI, V. & CIARDIELLO, F. 2008. Erlotinib: an EGF receptor tyrosine kinase inhibitor in non-small-cell lung cancer treatment. *Expert Rev Respir Med,* 2**,** 167-178.

SERCOMBE, L., VEERATI, T., MOHEIMANI, F., WU, S. Y., SOOD, A. K. & HUA, S. 2015. Advances and challenges of liposome assisted drug delivery. *Front Pharmacol,* 6**,** 1-13.

SHARMA, R. A., GESCHER, A. J. & STEWARD, W. P. 2005. Curcumin: the story so far. *Eur J Cancer,* 41**,** 1955-1968.

SHIN, G. H., LI, J., CHO, J. H., KIM, J. T. & PARK, H. J. 2016. Enhancement of curcumin solubility by phase change from crystalline to amorphous in cur-TPGS nanosuspension. *J Food Sci,* 81**,** 494-501.

SHINDIKAR, A., SINGH, A., NOBRE, M. & KIROLIKAR, S. 2016. Curcumin and resveratrol as promising natural remedies with nanomedicine approach for the effective treatment of triple negative breast cancer. *J Oncol,* 2016**,** 1-13.

SHUKLA, V., CHANDRA, V., SANKHWAR, P., POPLI, P., KAUSHAL, J. B., SIROHI, V. K. & DWIVEDI, A. 2015. Phytoestrogen genistein inhibits EGFR/PI3K/NF-kB activation and induces apoptosis in human endometrial hyperplasial cells. *RSC Advances,* 5**,** 56075-56085.

SIEGEL, R., MA, J., ZOU, Z. & JEMAL, A. 2014. Cancer statistics, 2014. *CA Cancer J Clin,* 64**,** 9-29.

SISTLA, R., TATA, V. S., KASHYAP, Y. V., CHANDRASEKAR, D. & DIWAN, P. V. 2005. Development and validation of a reversed-phase HPLC method for the determination of ezetimibe in pharmaceutical dosage forms. *J Pharm Biomed Anal,* 39**,** 517-522.

SOJITRA, P., RAVAL, A., KOTHWALA, D., KOTADIA, H. & ADESHARA, S. 2010. Covalently conjugation of genistein with biodegradable poly l-lactide. *Trends Biomater Artif Organs,* 23**,** 144-148.

SONG, Z., ZHU, W., LIU, N., YANG, F. & FENG, R. 2014. Linolenic acid-modified PEG-PCL micelles for curcumin delivery. *Int J Pharm,* 471**,** 312-321.

SOTO-CASTRO, D., CRUZ-MORALES, J. A., RAMIREZ-APAN, M. T. & GUADARRAMA, P. 2010. Synthesis of non-cytotoxic poly(ester-amine)

dendrimers as potential solubility enhancers for drugs: methotrexate as a case study. *Molecules,* 15**,** 8082-8097.

SPAGNUOLO, C., RUSSO, G. L., ORHAN, I. E., HABTEMARIAM, S., DAGLIA, M., SUREDA, A., NABAVI, S. F., DEVI, K. P., LOIZZO, M. R., TUNDIS, R. & NABAVI, S. M. 2015. Genistein and cancer: current status, challenges, and future directions. *Adv Nutr,* 6**,** 408-419.

STAHLHOFEN, W., RUDOLF, G. & JAMES, A. C. 1989. Intercomparison of experimental regional aerosol deposition data. *J Aerosol Med,* 2**,** 285-308.

STEIN, S. W., SHETH, P., HODSON, P. D. & MYRDAL, P. B. 2014. Advances in metered dose inhaler technology: hardware development. *AAPS PharmSciTech,* 15**,** 326-338.

STOLARCZYK, E. U., STOLARCZYK, K., LASZCZ, M., KUBISZEWSKI, M., MARUSZAK, W., OLEJARZ, W. & BRYK, D. 2017. Synthesis and characterization of genistein conjugated with gold nanoparticles and the study of their cytotoxic properties. *Eur J Pharm Sci,* 96**,** 176-185.

STURTEVANT, J. M. 1987. Biochemical applications of differential scanning calorimetry. *Annu Rev Phys Chem,* 38**,** 463-488.

SUPKO, J. G. & PHILLIPS, L. R. 1995. High-performance liquid chromatographic assay for genistein in biological fluids. *J Chromatogr B Biomed Appl,* 666**,** 157-167.

TADROS, M. I. 2008. The influence of sodium hyaluronate, L-leucine and sodium taurocholate on the nebulization of aqueous betamethasone-17-valerate suspensions. *AAPS PharmSciTech,* 9**,** 243-249.

TAKAHASHI, A., OZAKI, Y., KUZUYA, A. & OHYA, Y. 2014. Impact of core-forming segment structure on drug loading in biodegradable polymeric micelles using pEG-b-poly(lactide-co-depsipeptide) block copolymers. *BioMed Res Int,* 2014**,** 1-10.

TANG, J., XU, N., JI, H., LIU, H., WANG, Z. & WU, L. 2011. Eudragit nanoparticles containing genistein: formulation, development, and bioavailability assessment. *Int J Nanomedicine,* 6**,** 2429-2435.

TAYLOR, K. M. G. & MCCALLION, O. N. M. 1997. Ultrasonic nebulisers for pulmonary drug delivery. *Int J Pharm,* 153**,** 93-104.

TAYLOR, K. M. G. & MORRIS, R. M. 1995. Thermal analysis of phase transition behaviour in liposomes. *Thermochim Acta,* 248**,** 289-301.

TAYLOR, K. M. G. 2018. Pulmonary drug delivery. IN AULTON, M.E. & TAYLOR, K. M. G. (Eds.) *Aulton's pharmaceutics: the design and manufacture of medicines.* 5 ed. London, Elsevier Ltd., pp 653-670.

THATCHER, N., NICOLSON, M., GROVES, R. W., STEELE, J., EABY, B., DUNLOP, J., MCPHELIM, J., NIJJAR, R. & UKACHUKWU, I. 2009. Expert consensus on the management of erlotinib-associated cutaneous toxicity in the u.k. *Oncologist,* 14**,** 840-847.

TIMSINA, M. P., MARTIN, G. P., MARRIOTT, C., GANDERTON, D. & YIANNESKIS, M. 1994. Drug delivery to the respiratory tract using dry powder inhalers. *Int J Pharm,* 101**,** 1-13.

TOPEL, Ö., ÇAKIR, B. A., BUDAMA, L. & HODA, N. 2013. Determination of critical micelle concentration of polybutadiene-block-poly(ethyleneoxide) diblock copolymer by fluorescence spectroscopy and dynamic light scattering. *J Mol Liq,* 177**,** 40-43.

TORCHILIN, V. P. 2001. Structure and design of polymeric surfactant-based drug delivery systems. *J Control Rel,* 73**,** 137-172.

TÓTH, G., JÁNOSKA, Á., SZABÓ, Z. I., VÖLGYI, G., ORGOVÁN, G., SZENTE, L. & NOSZÁL, B. 2016. Physicochemical characterisation and cyclodextrin complexation of erlotinib. *Supramol Chem,* 28**,** 656-664.

TOUGAS, T., CHRISTOPHER, D., MITCHELL, J., LYAPUSTINA, S., VAN OORT, M., BAUER, R. & GLAAB, V. 2011a. Introduction. IN TOUGAS, T., CHRISTOPHER, D., MITCHELL, J. (Eds). *Good cascade impactor practices, AIM and EDA for orally inhaled products,* Springer US. 1-15.

TOUGAS, T., CHRISTOPHER, D., MITCHELL, J., LYAPUSTINA, S., VAN OORT, M., BAUER, R. & GLAAB, V. 2011b. Product lifecycle approach to cascade impaction measurements. *AAPS PharmSciTech,* 12**,** 312-322.

TRAN, P. H., HANSEN, P. E., NGUYEN, H. T. & LE, T. N. 2015. Erbium trifluoromethanesulfonate catalyzed friedel–crafts acylation using aromatic carboxylic acids as acylating agents under monomode-microwave irradiation. *Tetrahedron Lett,* 56**,** 612-618.

TRUONG, D. H., TRAN, T. H., RAMASAMY, T., CHOI, J. Y., LEE, H. H., MOON, C., CHOI, H. G., YONG, C. S. & KIM, J. O. 2016. Development of solid self-emulsifying formulation for improving the oral bioavailability of erlotinib. *AAPS PharmSciTech,* 17**,** 466-473.

TSAI, J. R., LIU, P. L., CHEN, Y. H., CHOU, S. H., CHENG, Y. J., HWANG, J. J. & CHONG, I. W. 2015. Curcumin inhibits non-small cell lung cancer cells metastasis through the adiponectin/NF-kappab/MMPs signaling pathway. *PLoS One,* 10**,** 1-19**.**

TURECEK, P. L., BOSSARD, M. J., SCHOETENS, F. & IVENS, I. A. 2016. PEGylation of biopharmaceuticals: a review of chemistry and nonclinical safety information of approved drugs. *J Pharm Sci,* 105**,** 460-475.

UNITED STATES PHARMACOPEIAL CONVENTION. 2005. *The United States Pharmacopeia: USP 29: the National Formulary: NF 24.* Rockville, Md.

USHA, S., JOHNSON, I. M. & MALATHI, R. 2005. Interaction of resveratrol and genistein with nucleic acids. *J Biochem Mol Biol,* 38**,** 198-205.

VAN-DYKE, R. E. & NIKANDER, K. 2007. Delivery of iloprost inhalation solution with the HaloLite, prodose, and I-neb adaptive aerosol delivery systems: an in vitro study. *Respir Care,* 52**,** 184-190.

VIDEIRA, M. A., BOTELHO, M. F., SANTOS, A. C., GOUVEIA, L. F., DE LIMA, J. J. & ALMEIDA, A. J. 2002. Lymphatic uptake of pulmonary delivered radiolabelled solid lipid nanoparticles. *J Drug Target,* 10**,** 607-613.

VRIGNAUD, S., HUREAUX, J., WACK, S., BENOIT, J.-P. & SAULNIER, P. 2012. Design, optimization and in vitro evaluation of reverse micelle-loaded lipid nanocarriers containing erlotinib hydrochloride. *Int J Pharm,* 436**,** 194-200.

WALDREP, J. C. & DHAND, R. 2008. Advanced nebulizer designs employing vibrating mesh/aperture plate technologies for aerosol generation. *Curr Drug Deliv,* 5**,** 114-119.

WANG, C. H. & HSIUE, G. H. 2005. Polymer-DNA hybrid nanoparticles based on folate-polyethylenimine-block-poly(L-lactide). *Bioconjug Chem,* 16**,** 391-396.

WANG, J., BYRNE, J. D., NAPIER, M. E. & DESIMONE, J. M. 2011. More effective nanomedicines through particle design. *Small,* 7**,** 1919-1931.

WANG, L., XU, X., ZHANG, Y., ZHU, Y., SHI, J., SUN, Y. & HUANG, Q. 2013. Encapsulation of curcumin within poly(amidoamine) dendrimers for delivery to cancer cells. *J Mater Sci Mater Med,* 24**,** 2137-2144.

WANG, Y., SCHMID-BINDERT, G. & ZHOU, C. 2012. Erlotinib in the treatment of advanced non-small cell lung cancer: an update for clinicians. *Ther Adv Med Oncol,* 4**,** 19-29.

WATTS, A. B., MCCONVILLE, J. T. & WILLIAMS, R. O. 2008. Current therapies and technological advances in aqueous aerosol drug delivery. *Drug Dev Ind Pharm,* 34**,** 913-922.

WU, R. G., WANG, Y. R., WU, F. G., ZHOU, H. W., ZHANG, X. H. & HOU, J. L. 2012. A DSC study of paeonol-encapsulated liposomes, comparison the effect of cholesterol and stigmasterol on the thermotropic phase behavior of liposomes. *J Therm Anal Calorim,* 109**,** 311-316.

WU, Y., WANG, W., CHEN, Y., HUANG, K., SHUAI, X., CHEN, Q., LI, X. & LIAN, G. 2010. The investigation of polymer-siRNA nanoparticle for gene therapy of gastric cancer in vitro. *Int J Nanomedicine,* 5**,** 129-136.

XIANG, L., SHEN, L. J., LONG, F., YANG, K., FAN, J. B., LI, Y. J., XIANG, J. & ZHU, M. Q. 2011. A convenient method for the synthesis of the amphiphilic triblock copolymer poly(L-lactic acid)-block-poly(l-lysine)-block-poly(ethylene glycol) monomethyl ether. *Macromol Chem Phys,* 212**,** 563-573.

XIE, Z., LU, T., CHEN, X., ZHENG, Y. & JING, X. 2009. Synthesis, self-assembly in water, and cytotoxicity of MPEG-block-PLLA/DX conjugates. *J Biomed Mater Res A,* 88**,** 238-245.

XU, H., HE, C., LIU, Y., JIANG, J. & MA, T. 2017. Novel therapeutic modalities and drug delivery - erlotinib liposomes modified with galactosylated lipid: in vitro and in vivo investigations. *Artif Cells Nanomed Biotechnol***,** 1-6.

YANG, C. J., TSAI, M. J., HUNG, J. Y., LEE, M. H., TSAI, Y. M., TSAI, Y. C., HSU, J. F., LIU, T. C., HUANG, M. S. & CHONG, I. W. 2017a. The clinical efficacy of afatinib 30 mg daily as starting dose may not be inferior to afatinib 40 mg daily in patients with stage IV lung adenocarcinoma harboring exon 19 or exon 21 mutations. *BMC Pharmacol Toxicol,* 18**,** 1-8.

YANG, K. M., SHIN, I. C., PARK, J. W., KIM, K. S., KIM, D. K., PARK, K. & KIM, K. 2017b. Nanoparticulation improves bioavailability of erlotinib. *Drug Dev Ind Pharm,* 43**,** 1557-1565.

YANG, X., LI, Z., WANG, N., LI, L., SONG, L., HE, T., SUN, L., WANG, Z., WU, Q., LUO, N., YI, C. & GONG, C. 2015. Curcumin-encapsulated polymeric micelles suppress the development of colon cancer in vitro and in vivo. *Sci Rep,* 5**,** 1-15.

YANG, Y., ZANG, A., JIA, Y., SHANG, Y., ZHANG, Z., GE, K., ZHANG, J., FAN, W. & WANG, B. 2016. Genistein inhibits A549 human lung cancer cell proliferation via miR-27a and MET signaling. *Oncol Lett,* 12**,** 2189-2193.

YAO, H., XU, W., SHI, X. & ZHANG, Z. 2011. Dietary flavonoids as cancer prevention agents. *J Environ Sci Health Environ Carcinog Ecotoxicol Rev,* 29**,** 1-31.

YEAP, G. Y., ALSHARGABI, A., ITO, M. M., MAHMOOD, W. A. K. & TAKEUCHI, D. 2012. Synthesis and anisotropic properties of azo-bridged benzothiazole-phenyl esters. *Mol Cryst Liq Cryst,* 557**,** 126-133.

YEO, L. Y., FRIEND, J. R., MCINTOSH, M. P., MEEUSEN, E. N. & MORTON, D. A. 2010a. Ultrasonic nebulization platforms for pulmonary drug delivery. *Expert Opin Drug Deliv,* 7**,** 663-679.

YEO, W. L., RIELY, G. J., YEAP, B. Y., LAU, M. W., WARNER, J. L., BODIO, K., HUBERMAN, M. S., KRIS, M. G., TENEN, D. G., PAO, W., KOBAYASHI, S. & COSTA, D. B. 2010b. Erlotinib at a dose of 25 mg daily for non-small cell lung cancers with EGFR mutations. *J Thorac Oncol,* 5**,** 1048-1053.

YIN, H., ZHANG, H. & LIU, B. 2013. Superior anticancer efficacy of curcumin-loaded nanoparticles against lung cancer. *Acta Biochim Biophys Sin,* 45**,** 634-640.

YOON, G. A. & PARK, S. 2014. Antioxidant action of soy isoflavones on oxidative stress and antioxidant enzyme activities in exercised rats. *Nutr Res Pract,* 8**,** 618-624.

ZAPPA, C. & MOUSA, S. A. 2016. Non-small cell lung cancer: current treatment and future advances. *Transl Lung Cancer Res,* 5**,** 288-300.

ZAROGOULIDIS, K., ZAROGOULIDIS, P., DARWICHE, K., BOUTSIKOU, E., MACHAIRIOTIS, N., TSAKIRIDIS, K., KATSIKOGIANNIS, N., KOUGIOUMTZI, I., KARAPANTZOS, I., HUANG, H. & SPYRATOS, D. 2013. Treatment of non-small cell lung cancer (NSCLC). *J Thorac Dis,* 5**,** 389-396.

ZHANG, C. Y., XIONG, D., SUN, Y., ZHAO, B., LIN, W. J. & ZHANG, L. J. 2014a. Self-assembled micelles based on pH-sensitive PAE-g-MPEG-cholesterol block copolymer for anticancer drug delivery. *Int J Nanomedicine,* 9**,** 4923-4933.

ZHANG, G., DAVID, A. & WIEDMANN, T. S. 2007a. Performance of the vibrating membrane aerosol generation device: aeroneb micropump nebulizer. *J Aerosol Med,* 20**,** 408-416.

ZHANG, J., SU, H., LI, Q., LI, J. & ZHAO, Q. 2017. Genistein decreases A549 cell viability via inhibition of the PI3K/AKT/HIF1alpha/VEGF and NFkappaB/COX2 signaling pathways. *Mol Med Rep,* 15**,** 2296-2302.

ZHANG, J., ZHAO, Y. J., SU, Z. G. & MA, G. H. 2007b. Synthesis of monomethoxy poly(ethylene glycol) without diol poly(ethylene glycol). *J Appl Polym Sci,* 105**,** 3782-3786.

ZHANG, T., CHEN, Y., GE, Y., HU, Y., LI, M. & JIN, Y. 2018. Inhalation treatment of primary lung cancer using liposomal curcumin dry powder inhalers. *Acta Pharm Sin B,* 8**,** 440-448.

ZHANG, W., LI, X., YE, T., CHEN, F., YU, S., CHEN, J., YANG, X., YANG, N., ZHANG, J., LIU, J., PAN, W. & KONG, J. 2014b. Nanostructured lipid carrier surface modified with eudragit RS 100 and its potential ophthalmic functions. *Int J Nanomedicine,* 9**,** 4305-4315.

ZHANG, X., LIU, Q., HU, J., XU, L. & TAN, W. 2014c. An aerosol formulation of R-salbutamol sulfate for pulmonary inhalation. *Acta Pharm Sin B,* 4**,** 79-85.

ZHANG, X., SHEN, Z., FENG, C., YANG, D., LI, Y., HU, J., LU, G. & HUANG, X. 2009. PMHDO-g-PEG double-bond-based amphiphilic graft copolymer: synthesis and diverse self-assembled nanostructures. *Macromolecules,* 42**,** 4249-4256.

ZHANG, Y., HUANG, Y. & LI, S. 2014d. Polymeric micelles: nanocarriers for cancer-targeted drug delivery. *AAPS PharmSciTech,* 15**,** 862-781.

ZHAO, L., FENG, S. S. & GO, M. L. 2004. Investigation of molecular interactions between paclitaxel and DPPC by langmuir film balance and differential scanning calorimetry. *J Pharm Sci,* 93**,** 86-98.

ZHAO, L., FENG, S. S., KOCHERGINSKY, N. & KOSTETSKI, I. 2007. DSC and EPR investigations on effects of cholesterol component on molecular interactions between paclitaxel and phospholipid within lipid bilayer membrane. *Int J Pharm,* 338**,** 258-266.

ZHOU, X., TAO, H. & SHI, K. H. 2018. Development of a nanoliposomal formulation of erlotinib for lung cancer and in vitro/in vivo antitumoral evaluation. *Drug Des Devl Ther,* 12**,** 1-8.

ZHOU, Y., AHUJA, A., IRVIN, C. M., KRACKO, D. A., MCDONALD, J. D. & CHENG, Y. S. 2005. Medical nebulizer performance: effects of cascade impactor temperature. *Respir Care,* 50**,** 1077-1082.

ZHU, W. T., LIU, S. Y., WU, L., XU, H. L., WANG, J., NI, G. X. & ZENG, Q. B. 2017. Delivery of curcumin by directed self-assembled micelles enhances therapeutic treatment of non-small-cell lung cancer. *Int J Nanomedicine,* 12**,** 2621-2634.

ZIEGLER, J. & WACHTEL, H. 2005. Comparison of cascade impaction and laser diffraction for particle size distribution measurements, *J Aerosol Med*, 18, 311-324.

Publication and presentations

Publication

NIMMANO, N., TAYLOR, K. M. G., SOMAVARAPU, S. 2018. Aerosol characterisation of nebulised liposomes co-loaded with erlotinib and genistein using an abbreviated cascade impactor method. *Int J Pharm,* 542, 8-17.

Poster presentations

NIMMANO, N., TAYLOR, K. M. G., SOMAVARAPU, S. 2016. Novel curcumin-loaded nanocarrier for pulmonary delivery. Annual Meeting-Controlled Release Society 2016, Washington (U.S.A), 17- 20 July 2016.

NIMMANO, N., TAYLOR, K. M. G., SOMAVARAPU, S. 2017. Aerosol characterisation of nebulised liposomes co-loaded with erlotinib and genistein. Drug Delivery to the Lungs 2017, Edinburgh (UK), 6- 8 December 2017.

Internal UCL Presentations

NIMMANO, N., TAYLOR, K. M. G., SOMAVARAPU, S. 2016. A thermal analysis investigation of erlotinib and genistein-loaded liposome. UCL School of Pharmacy PhD Research Day, London (UK), September 2016. Poster presentation.

NIMMANO, N., TAYLOR, K. M. G., SOMAVARAPU, S. 2017. Aerosol characterisation of nebulised liposomes co-loaded with erlotinib and genistein. UCL School of Pharmacy PhD Research Day, London (UK), April 2017. Oral presentation.